

FORN INFORMATION

DOE/ET/10145-74

Vol. 2 of 2

**DATA REQUIREMENTS FOR EOR SURFACTANT-POLYMER
PROCESS SIMULATION AND ANALYSIS OF EL DORADO
PILOT PROJECT SIMULATION, BUTLER COUNTY, KANSAS**

Vol. II: Appendices

Work Performed for the Department of Energy
Under Contract No. DE-AC01-78ET10145

Date Published—January 1983

Gulf Universities Research Consortium
Bellaire, Texas

U. S. DEPARTMENT OF ENERGY



DISCLAIMER

This report was prepared as an account of work sponsored by an agency of the United States Government. Neither the United States Government nor any agency thereof, nor any of their employees, makes any warranty, express or implied, or assumes any legal liability or responsibility for the accuracy, completeness, or usefulness of any information, apparatus, product, or process disclosed, or represents that its use would not infringe privately owned rights. Reference herein to any specific commercial product, process, or service by trade name, trademark, manufacturer, or otherwise, does not necessarily constitute or imply its endorsement, recommendation, or favoring by the United States Government or any agency thereof. The views and opinions of authors expressed herein do not necessarily state or reflect those of the United States Government or any agency thereof.

Printed in the United States of America. Available from:
National Technical Information Service
U.S. Department of Commerce
5285 Port Royal Road
Springfield, VA 22161

NTIS price codes

Paper copy: \$19.50
Microfiche copy: \$4.00

**DATA REQUIREMENTS FOR EOR SURFACTANT-POLYMER
PROCESS SIMULATION AND ANALYSIS OF EL DORADO
PILOT PROJECT SIMULATION, BUTLER COUNTY, KANSAS**

Vol. II: Appendices

By

E. L. Claridge and A. Lohse

James L. Gumnick, *Principal Investigator*
Gulf Universities Research Consortium
5909 West Loop South, Suite 600
Bellaire, Texas 77401

Fred W. Burtch, *Technical Project Officer*
Bartlesville Energy Technology Center
P.O. Box 1398
Bartlesville, Oklahoma 74005

Work Performed for the Department of Energy
Under Contract No. DE-AC01-78ET10145

Date Published—January 1983

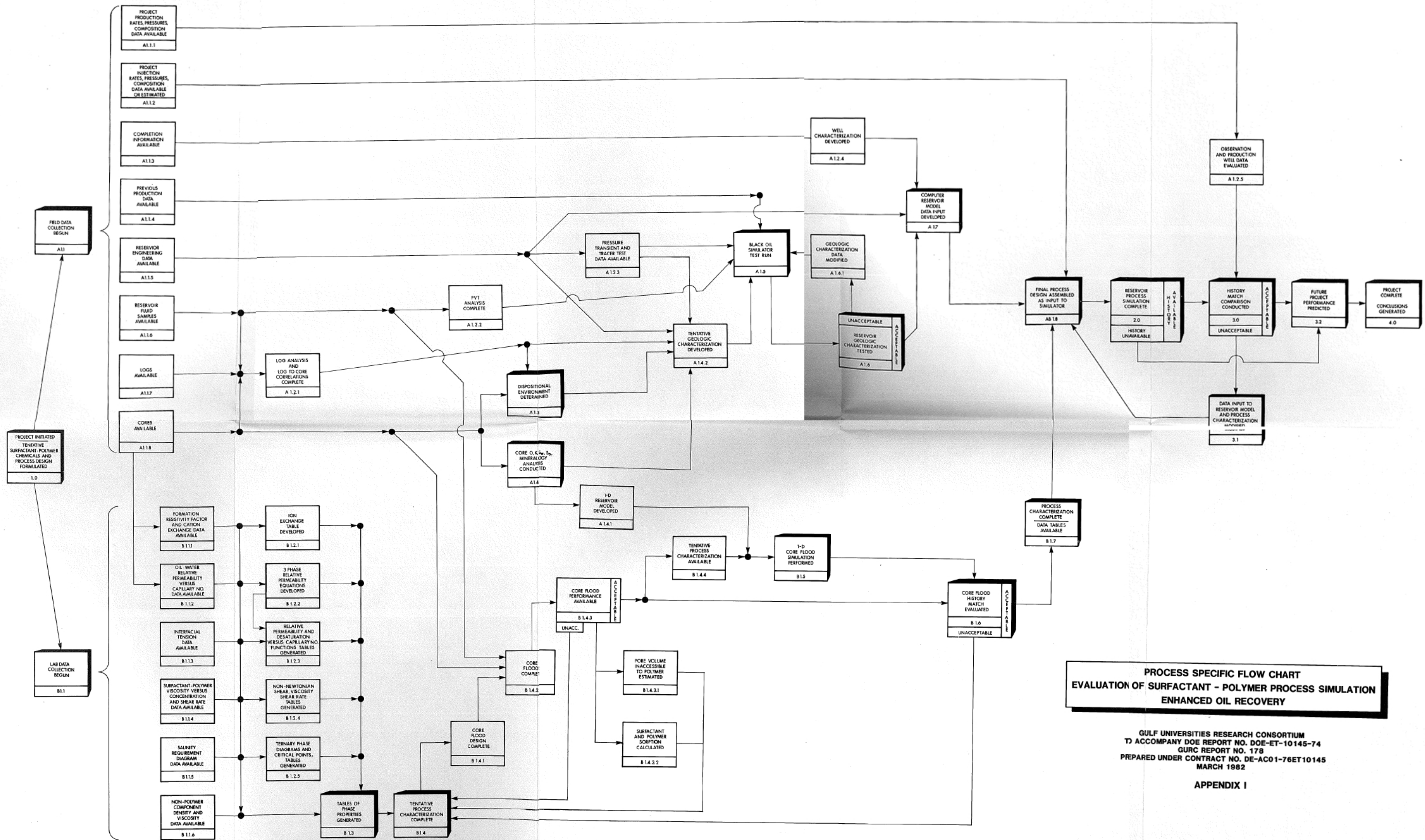
UNITED STATES DEPARTMENT OF ENERGY

TABLE OF CONTENTS

APPENDIX I	1
APPENDIX II	3
SUMMARY	3
TASK OBJECTIVES AND APPROACH	6
TASK OBJECTIVES	6
APPROACH	7
EL DORADO MICELLAR-POLYMER DEMONSTRATION PROJECT	8
DATA ASSESSMENT AND ANALYSIS	9
RESERVOIR ROCK AND FLUID DATA	9
Geologic Data	9
Residual Oil Saturation and Saturation Distribution	10
Oil-Water Relative Permeability	10
Capillary Desaturation Curves	11
Oil-Water Capillary Pressure	11
Fluid Densities and Viscosities	11
Salinity of Formation and Injection (Make-Up) Water	12
Cation Exchange Capacity	12
PROCESS DESCRIPTION DATA	12
Phase Equilibria	12
Surfactant Sorption	17
Polymer Data	18
Cation Exchange	18
Interfacial Tension	19
Viscosity	20
Dispersion	22
High-Capillary-Number Three-Phase Relative Permeability	23
Coreflood Data	26
Field Data	27

NUMERICAL SIMULATION	30
COREFLOOD SIMULATIONS	30
History Matching	30
Coreflood Sensitivity Simulations	31
RESERVOIR DESCRIPTION	32
Element for Simulation	32
Asymmetric Grid	32
Geologic Model for Asymmetric Grid	33
Allocation of Injected Fluids for Asymmetric Grid	33
Symmetric Grid	34
Injection Rates and Volumes	34
FIELD SIMULATIONS	35
Field Data	35
Simulation of Laboratory-Derived Process in Center Streamtube (Two Layers)	35
Simulation of Adjusted Process in Center Streamtube (Two Layers)	37
Simulation of Adjusted Process in Center Streamtube (One Layer)	39
Simulation of Preflush in Full Grids (One Layer)	40
Performance Prediction in Center Streamtube (One Layer)	40
Performance Prediction in Center Streamtube (Two Layers)	42
Sensitivity Simulations in Center Streamtube	42
Performance Prediction in Asymmetric Grid	44
Performance Prediction in Symmetric Grid	45
APPLICATION OF RESULTS	47
REFERENCES	49
TABLES	54-88
FIGURES	89-141

APPENDIX III	142
A. CHEMICAL FLOOD MODEL DESCRIPTION	142
FIGURE	148
B. DETAILS OF GRID CONSTRUCTION	149
FIGURES	157-168
C. TERNARY PHASE EQUILIBRIA MODEL	169
FIGURES	186-203
D. DESCRIPTION OF HIGH-CAPILLARY-NUMBER RELATIVE PERMEABILITY MODEL	204
FIGURES	213-221
E. CORRESPONDENCE PERTAINING TO REQUESTS FOR DATA	222



**PROCESS SPECIFIC FLOW CHART
EVALUATION OF SURFACTANT - POLYMER PROCESS SIMULATION
ENHANCED OIL RECOVERY**

GULF UNIVERSITIES RESEARCH CONSORTIUM
TO ACCOMPANY DOE REPORT NO. DOE-ET-10145-74
GURC REPORT NO. 178
PREPARED UNDER CONTRACT NO. DE-AC01-76ET10145
MARCH 1982

APPENDIX I

APPENDIX II

SUMMARY

Data for the high-water-content process portion of the El Dorado Micellar-Polymer Demonstration Project were assessed relevant to evaluation of the project by numerical simulation. The data adequacy was measured against the data requirements for INTERCOMP's Chemical Flooding Ternary Equilibrium simulator.

The data available in the public domain were found to be inadequate to characterize the chemical flooding process. In particular, phase equilibria and capillary desaturation data were not available, and phase viscosity, interfacial tension, and coreflood data were incomplete. Some phase behavior data were measured during the course of the study, but other data had to be estimated or assumed to perform the simulations. Accordingly, the process characterization which resulted from coreflood history matching was only partially complete.

For the field simulations, an isolated asymmetrical grid system was constructed from streamline modeling results. A heterogeneous, two-layer reservoir description was utilized within the asymmetric grid to predict the performance of the process at MP-131, an observation well in the isolated element. When the process characterization obtained from coreflood matching was incorporated with the asymmetrical grid, the simulated results matched poorly with the performance observed at MP-131.

The match was somewhat improved by a downward adjustment of the value of the optimal salinity used in the coreflood process description. Although this adjustment was based on concentration data from wellhead samples, the resulting process characterization represents only one scenario which might be used to explain the project's performance at MP-131. Even with the adjusted process, however, the match of the simulated results with data from a second observation well, MP-132, was not good.

Performance predictions were made using the adjusted process characterization in a one-layer reservoir description for both the asymmetric grid incorporating areal

heterogeneity, and a symmetric grid representing a one-eighth of a five-spot in a homogeneous, isotropic reservoir. The simulator predicted that 24.3% and 13.4% of the oil-in-place after waterflooding will be produced for the asymmetric and symmetric grids, respectively, after one cumulative pore volume of chemical slug and polymer drive injection.

The primary reasons for the predicted low oil recovery are the trapping of surfactant in an immobile phase, brought about by the lower optimal salinity used to adjust the process characterization, and the relatively small size of the surfactant slug which was injected.

Sensitivity simulations in the central portion of the asymmetric grid showed that fractional oil recovery was strongly influenced by the surfactant slug size and the salinity of the polymer drive; whereas the effects of preflush injection, gross layering, and waterflood residual saturation were relatively small.

The conclusions of this study are:

1. Data in the public domain were not extensive enough to characterize the El Dorado high-water-content chemical flooding process with a high degree of confidence.
2. The question as to whether or not a micellar-polymer process characterized by simulation of coreflood data can be used to predict performance in the field could not be definitively answered.
3. The accuracy of the available data could not be judged, as measures of statistical significance of the data were in general not reported.
4. The process characterization suggested from the best simulated match obtained of the field data, while only one possible explanation of project performance, revealed process phenomena which might warrant further investigation in the laboratory.
5. Analyses of fluid samples from observation wells are essential toward the understanding of the chemical flooding process in a reservoir environment.

It is worth noting that at the time the El Dorado micellar-polymer project was designed, neither reservoir simulators of the type used in this study nor important theoretical developments had been publicly documented. Thus, the importance of many of the data requirements was simply not known or appreciated. One purpose of this report is to set forth the data requirements and the reasons why the data are important, vis-a-vis the current state-of-the-art of chemical flooding technology.

TASK OBJECTIVES AND APPROACH

TASK OBJECTIVES

Gulf Universities Research Consortium (GURC) is prime contractor to the United States Department of Energy (DOE) on a study involving the collection, collation, and analysis of data generated from demonstration projects sponsored by the DOE to help stimulate the economic development of enhanced oil recovery (EOR) within the U. S. One important goal of the DOE demonstration projects is to place necessary and sufficient information into the public domain so that a third party, with proper engineering evaluation of data from a particular test, can assess the economic feasibility of initiating EOR operations in a different section of the same field or in another similar field. Thus, GURC and the DOE seek to develop and transfer guidelines for a methodology comprising analytical and interpretive procedures for the intra- and inter-field analysis of DOE cost-shared field tests. These guidelines are to include the data and reporting required to support the methodology.

Because of the complex interaction of micellar-polymer process variables and reservoir characteristics, GURC decided that numerical simulation would best serve to help develop the desired guidelines. Data available from the Cities Service Company/DOE cost-shared El Dorado Micellar-Polymer Demonstration Project were selected for use in the simulations.

INTERCOMP was selected by GURC to assess the data in the public domain from the El Dorado North (Chesney) lease project and to determine whether or not this data is extensive and/or accurate enough to evaluate the project.

APPROACH

To accomplish the study objectives, the following approach was proposed:

1. Gather, analyze, and develop data for input to INTERCOMP's Chemical Flooding Ternary Equilibrium (CFTE) simulator.
2. Characterize the chemical process by history matching the results of laboratory corefloods.
3. Select and develop for simulation an isolated element of the North lease, using a geologic model for the element to be supplied by GURC.
4. Combine the process characterization with the reservoir description of the isolated element and predict the performance of the process in the field.
5. Establish the numerical model as a predictive tool by comparison of model-predicted results with observed data from the field.
6. Determine the sensitivity of performance to process and reservoir parameters based on various numerical simulations.
7. Illustrate the application of the results of simulation to intra- and inter-field analysis with a performance prediction of one-eighth of a five-spot element of symmetry.

INTERCOMP's CFTE finite-difference reservoir simulator was used in this study. A description of the CFTE model is given in Appendix A.

EL DORADO MICELLAR-POLYMER DEMONSTRATION PROJECT

The Cities Service Company/DOE El Dorado Micellar-Polymer Demonstration Project is being conducted in the 650-ft Admire sand of the El Dorado field, Butler County, Kansas. The target sand was first produced when the field was discovered in 1915, and has an area of about 6,200 acres and an estimated original oil-in-place of 108 million barrels. During primary and air-drive operation of the field, 23 million barrels of oil were produced, and waterflooding recovered an additional 13.5 million barrels of oil before water injection was terminated in February 1971.

The 25.6-acre North lease consists of four 6.4-acre five-spots in which a high-water-content (HWC) micellar process developed by Cities Service Company is being pilot-tested. A soluble oil process developed by Union Oil Company of California is being tested in the South (Hegberg) lease.

DATA ASSESSMENT AND ANALYSIS

This section of the report discusses the type of data required for simulation with the CFTE model, reference to the data source, if available, and the data input to the model. Although much of the required data or parameters for the generation of simulator input were available in the public domain, some key data were incomplete or missing altogether. These data, therefore, had to be estimated or assumptions made in order to perform the simulations. The details of handling the data input and the basis for estimates or assumptions for data which were incomplete or not reported are discussed in the sections to follow. In addition, as a guideline to future work, suggestions are made regarding the importance and accuracy of data required for evaluation and simulation of the micellar-polymer process.

RESERVOIR ROCK AND FLUID DATA

Geologic Data

The CFTE simulator provides a means to describe reservoir heterogeneity in considerable detail. This includes the distribution of permeability (horizontal and vertical) and porosity, areally and by layer, and net pay thickness by layer.

Geologic data for the Admire (Chesney) sand were used by GURC to prepare a two-layered heterogeneous model of the reservoir element to be simulated. The geologic model and the details of the grid construction for the simulation element are presented in the section on Reservoir Simulation and in Appendix B.

A discussion of either the adequacy of the geologic data or the methods used to prepare the geologic model is beyond the scope of this report. A complete discussion will be presented in GURC's El Dorado task report. While the reservoir characterization was not one of INTERCOMP's tasks, we would like to comment that it is at least as important as the process characterization, if not more so, to the overall understanding and interpretation of a field test.

Residual Oil Saturation and Saturation Distribution

Residual oil saturation (S_{or}) is defined as the oil saturation that would be left behind by a piston-like water front in the regions contacted by water. Residual oil saturation is the single most important determinant of the micellar-polymer target oil and also greatly affects volumetric displacement efficiency. The most reliable values for S_{or} are derived from cores, laboratory displacements, or the Exxon tracer test. A "best case" parameter set would include some indication of saturation distribution as the possibility exists that high-permeability zones contain low residual oil saturations.

On the recommendation of Cities Service Company, a residual oil saturation of 0.33, uniformly distributed, was used in the field simulations. This value of S_{or} presumably was based on material balance calculations. However, well logs indicate that S_{or} 's as low as 0.23 may exist in the central portion of the simulated element.¹ Some simulations were done with this lower value to determine the sensitivity of predicted performance to S_{or} .

Oil-Water Relative Permeability

Relative permeability is by far the most important rock property since it is a measure of rock wettability and affects mobility requirements nearly as much as crude oil viscosity.

Adequate relative permeability data were available in the El Dorado annual reports with data reported from measurements on core plugs from wells MP-104, MP-124, and MP-217. As discussed later the data from MP-124,² a production well in the simulation element, were used as input to the high-capillary-number relative permeability model.

Capillary Desaturation Curves

As discussed in Appendix A, the CFTE simulator requires as input the relationship between capillary number and the wetting and nonwetting phase residual saturations to the micellar slug. This relationship is the link between in-situ physical properties and the oil displacement efficiency of the slug, and represents the most important information toward assessment of the viability of chemical flooding for a given rock type.

Preferably, desaturation data should be obtained from laboratory displacements with field cores. However, the methods involved are somewhat beyond those usually encountered in routine coreflood work. An excellent example of the required laboratory procedures is given by Gupta and Trushenski,³ who determined capillary desaturation curves for Berea rock.

Data of these type or data to allow computation of desaturation behavior from theory⁴ were not available for Admire sandstone. Therefore, the capillary desaturation curves had to be estimated. As discussed in the section on Process Description and in Appendix D, this was done by shifting Berea curves to account for the more oil-wet nature of Admire rock.

Oil-Water Capillary Pressure

Data on capillary pressure from cores from wells MP-106, MP-110, and MP-122⁵ were averaged and used in some of the preliminary simulations, but did not affect the results. Accordingly, capillary pressure was not accounted for in any of the simulations discussed in this report. Capillary forces are generally not important unless the reservoir is highly fractured or highly stratified.

Fluid Densities and Viscosities

The most important quantity in this group is crude viscosity at reservoir temperature and pressure as it affects design mobilities. Based on a gravity of 37.4⁰ API for El Dorado crude oil,⁶ oil viscosity and density of 5.2 cp and 52.2 lb/ft³, respectively, were used in all simulations. Polymer-free brine viscosity was assigned a value of

1.07 cp⁷ and the density of all brines was assumed as 62.4 lb/ft³. Density of the high-water-content surfactant slug was assumed to be 60.0 lb/ft³.

Salinity of Formation and Injection (Make-up) Water

Adequate data on major anions and cations were reported⁸ for both formation and make-up water. It should be pointed out that total dissolved solids, which are reported by many operators, convey little useful information toward screening or design of a micellar-polymer flood.

Cation Exchange Capacity

CEC is a rock property which determines the salinity environment and thus is important to the design requirements for the preflush and micellar slug salinity. The CEC used in the cation exchange model, discussed below, was the average of 0.044 mg Ca⁺⁺/gm rock reported for well MP-130 and 0.071 mg Ca⁺⁺/gm rock reported for well MP-110.⁹ These data were judged adequate for purposes of simulation.

PROCESS DESCRIPTION DATA

Phase Equilibria

During the data assessment portion of the work, it was determined that there were neither data available on the phase equilibria per se, (e.g., K-values) nor data from which to estimate the phase behavior. In order to perform the simulations, INTERCOMP then requested that Cities Service Company obtain phase volume data for the HWC surfactant-oil-brine system.

These data were reported¹⁰ in tabular form and are presented in Appendix E, along with the associated correspondence. The phase volume data were obtained at several surfactant concentrations and a 1:1 brine/oil ratio as a function of salinity (NaCl). Examination of the data tables shows that if enough surfactant is present, the phase behavior moves from a "lower" two-phase region through a "middle" or three-phase region and finally to an "upper" two-phase environment as salinity increases.

The phase volume data are plotted in Figures 1 - 4 as phase volume diagrams. These diagrams were used to estimate some of the parameters for input to the phase equilibria model. Before considering these diagrams, the phase equilibria model will be discussed.

Any model employed to estimate phase behavior of the type represented in Figures 1 - 4 must account for the transition between phase regions as a function of salinity, and must generate data over the entire range of concentrations using only a few actual data points for initialization. Furthermore, for input to the CFTE simulator, the model must compute the phase data in the form of pseudo-ternary phase diagrams with associated equilibrium tie-lines. One model which satisfies these requirements is the one developed at The University of Texas at Austin based on the work of Nelson and Pope¹¹ and Pope and Nelson¹².

The theory, assumptions, and results for this model are presented in Appendix C. A qualitative representation of the ternary diagrams computed by the model is depicted in Figure 5. Notice that all features vary in a continuous way as the phase diagrams are swept out as a function of effective ionic strength (salinity), CSE. For $CSE < CSEL$, the phase behavior is "lower" (surfactant favors water), and since the slope of the tie-lines is negative, is denoted by type II(-). For $CSEL \leq CSE \leq CSEU$, the phase behavior is "middle," or type III, in which three phases may exist in equilibrium. The composition of the middle phase is invariant at the point "M" in Figure 5. The composition of the other two "excess" phases in equilibrium with the middle or microemulsion phase are 100% oil and 100% brine. Two-phase regions, either type II(-) or type II(+), may also exist within the type III region. For $CSE > CSEU$, the phase behavior is "upper" (surfactant favors oil) and since the slope of the tie-lines is positive, is denoted as type II(+). Thus, CSEU and CSEL are the salinities at which the phase behavior switches from type II(+) to type III and from III to II(-), respectively. The optimal salinity, CSEOP, the salinity at which either phase swelling or interfacial tension is a minimum,¹³ is well approximated by the midpoint salinity $(CSEU + CSEL)/2$. The optimal salinity, then, occurs in the type III region.

As discussed in Appendix C, seven input parameters are required for the phase equilibria model:

1. Maximum height of binodal curve in type II(-), C3MAX0
2. Maximum height of binodal curve in type III, C3MAX1
3. Maximum height of binodal curve in type II(+), C3MAX2
4. Oil coordinate of plait point in type II(-), C2PR
5. Oil coordinate of plait point in type II(-), C2PL
6. CSEL
7. CSEU

For the HWC system designed for use at El Dorado, C3MAX0, C3MAX1, and C3MAX2 were estimated as 0.3, 0.1, and 0.3, respectively; C2PR and C2PL were estimated as 0.95 and 0.05, respectively. Experience with the phase equilibria model and the CFTE simulator has shown that, among the five parameters C3MAX0, C3MAX1, C3MAX2, C2PR, and C2PL, the simulated oil recovery is by far the most sensitive to C3MAX1. This parameter was, therefore, also estimated by material balance from the phase volume data, assuming that all of the surfactant was in the middle phase when three phases exist. The value of C3MAX1 came out to be about 0.1, corroborating the earlier estimate.

CSEL and CSEU were estimated from the phase volume diagrams, Figures 1 and 2. The selection of CSEL in particular from these diagrams is not clear-cut. For example, Figure 2, which represents a surfactant solution with injection concentrations of surfactant (0.075 meq/ml) and polymer (900 ppm), shows what appears to be two distinct phase transitions at salinities of about 0.35 wt. % NaCl and about 1.0%. Some of the uncertainty as to which of these values represents a true CSEL could be reduced if the concentration of surfactant in the various phases in equilibrium had been reported. Even without polymer (Figure 1), the system shows similar behavior.

Phase volume data were also measured at other values of surfactant concentration (Figures 3 and 4), and in the presence of calcium, with the results provided by Cities Service Company in the form of salinity requirement diagrams (SRD), shown in Figure 6. Whereas a phase volume diagram tracks phase behavior as a function of CSE at a given surfactant concentration, an SRD tracks this behavior for all CSE and all surfactant concentrations.

The upper SRD of Figure 6, for $\text{Ca}^{++}/\text{Na}^+ = 0$, however, is not consistent with the tabular data from which Figures 1 - 4 were constructed. It is clear from this SRD that CSEL (and CSEU) decreases as surfactant concentration decreases. But comparison of Figure 1 with Figure 3 (for $\text{Ca}^{++}/\text{Na}^+ = 0$) shows that as surfactant concentration decreases from 0.075 to 0.0375 meq/ml, CSEL increases, not decreases as in the SRD. It would appear that the upper SRD was constructed from data other than that reported in Appendix E. In addition, the tabular data reported for $\text{Ca}^{++}/\text{Na}^+ = 0.22$ (mass ratio) were insufficient to construct the lower SRD of Figure 6.

The interfacial tension (IFT) data were examined to resolve this apparent inconsistency. The IFT data, discussed in a subsequent section, showed that the (optimal) salinity at which the minimum IFT occurred fell with decreasing surfactant concentration. Therefore, it was assumed that the SRD's have a positive slope, as shown in Figure 6. With this assumption that the SRD's are correct, two important trends in the data may be noted: (1) optimal salinity falls as surfactant concentration decreases, and (2) the presence of calcium narrows the optimal salinity (type III) region and greatly reduces the absolute value of CSEOP over the entire range of surfactant concentration. As pointed out by Nelson,^{14,15} both trends are key to the design of a successful chemical flood. As the highest oil recoveries are achieved with a salinity of the polymer drive below optimal, these trends thus lower the "salinity requirement" of the drive.

The $\text{Ca}^{++}/\text{Na}^+$ ratio (0.22) reported for the lower SRD of Figure 6 is somewhat greater than the maximum ratio, about 0.15, observed in samples from observation well MP-131 during the course of the flood. This being the case, the true path of optimal salinity in the field lies between the upper and lower SRD's of Figure 6. Because the exact path of optimal salinity is not known, and because the CFTE

simulator did not allow CSEL and CSEU to vary with surfactant concentration (SRD slope of zero) when the simulations were performed, CSEL was used as the matching parameter for both the coreflood and field data. The rationale for the selection of CSEL is discussed in subsequent sections.

To illustrate the use of the phase equilibria model, in Table 1 are listed six sets of output data generated by the model: one type II(-), four type III, and one type II(+). The data are output as plait point, invariant point, and tie-line compositions. Concentrations are designated as C1 (water), C2 (oil), and C3 (surfactant). As previously discussed, the input parameters were $C3MAX0 = 0.3$, $C3MAX1 = 0.1$, $C3MAX2 = 0.3$, $C2PR = 0.95$, and $C2PL = 0.05$. The six salinities, one for each data set, range from $CSEL = 0.0042$ wt. fr. Na^+ ($= 4200$ ppm $Na^+ = 10,700$ ppm NaCl) to $CSEU = 0.0168$ Na^+ . As discussed later, these values of CSEL and CSEU resulted in the best history match obtained on the coreflood data.

For a given $C3MAX0$, etc., changing CSEL and CSEU merely shifts the diagrams in salinity space (Figure 5); all features of the diagrams remain constant. This is shown by the set of diagrams in Appendix C, again generated using El Dorado input parameters, as a function of normalized optimal salinity.

Table 2 shows the output of Table 1 reformatted as K-values and binodal curves for entry into the CFTE simulator.

The phase behavior representation is pseudo-ternary in that the "surfactant" component in the reported phase volume data includes two sulfonates and an alcohol ethoxysulfate, but not the secondary butyl alcohol injected with the surfactant slug. It is not implied that alcohol is unimportant to phase behavior; rather, the representation is the most complete one that could be rendered with the available data.

The use of minimal laboratory data to estimate the HWC system phase behavior can only be described as partially successful. Too many assumptions had to be made regarding the input parameters for the phase equilibria model. It is suggested that these assumptions could be somewhat relaxed, and the phase volume data made more useful if in future studies the laboratory data included:

1. Concentration of active surfactant in all phases
2. Repeat tests, particularly when CSEL and CSEU are not well defined, so that some statistical significance could be assigned to the data
3. Data at several brine/oil and $\text{Ca}^{++}/\text{Na}^{+}$ ratios
4. Tabular data to support salinity requirement diagrams.

Work by INTERCOMP on the DOE's Nowata micellar-polymer project, for which extensive data of the type just described were obtained, validated the phase equilibria model as a means to predict laboratory data.

The other alternative to any "model" to predict the phase behavior is to obtain by experiment n-dimensional equilibrium diagrams and tie-lines. Such an endeavor, however, represents a quantum jump in time and expense over the method outlined here.

Surfactant Sorption

As determined from dynamic Admire coreflood experiments, surfactant retention (adsorption and trapping) was 0.10 - 0.12 meq surfactant/100 gm rock.¹⁶ Static adsorption data were not reported so the contribution of adsorption alone could not be determined. However, because the surfactant retention was independent of the salinity of the polymer drive in the corefloods, trapping was assumed nil, leaving sorption accountable for all of the retention. To check this assumption, Lake and Pope's 100% clay curve¹⁷ was used to estimate the sorption on Admire (15 - 21% clay¹⁸) rock. This correlation gives a value of about 0.11 meq/100 gm, so the assumption that trapping was very low in the corefloods seems reasonable.

The value used in all simulations for the sorption isotherm plateau (Figure 7) was 0.104 meq/100 gm rock (0.0036 ft³/ft³ pv, 1.21 lb/bbl pv). Sorption was assumed irreversible for all surfactant concentrations. Some coreflood sensitivity simulations were made with partially reversible sorption. The surfactant concentration of 10⁻⁴

(vol. fr. in micellar phase) at which the isotherm breaks over was arbitrarily selected to reflect a low critical micelle concentration (CMC) for the mixed surfactant system employed. Thus, the isotherm is steep enough to preclude any sorption of unassociated molecules at concentrations greater than 10^{-4} . The CMC may be estimated quite easily from the break in the surfactant solution / air surface tension concentration curve, but these data were not reported.

Polymer Data

Polymer sorption was not accounted for in the coreflood simulations since there was no polymer effluent data reported. For the field simulations, 100 lb/acre ft (0.052 lb/bbl pv) was assumed for irreversible polymer sorption, and the inaccessible pore volume to polymer was assumed to be 0.1. Since the polymer employed was a biopolymer, a polymer residual resistance factor of unity was used in all simulations.

Cation Exchange

Cation exchange was simulated assuming the equilibrium relationship for mass action¹⁹

$$(C_r^+)^2 / C_r^{++} = K (C^+)^2 / C^{++} \quad (1)$$

between solution concentrations (eq/l) of Na^+ , denoted by C^+ , and calcium + magnesium = M^{++} , denoted by C^{++} , and the rock concentrations (subscript r, eq/l pv). The value of the coefficient K was estimated as 0.01.¹⁹ The cation exchange capacity, Q_v , was assumed constant:

$$Q_v = C_r^+ + C_r^{++} \quad (2)$$

As discussed previously, Q_v was taken as the average of 0.044 and 0.071 mg Ca^{++} /gm rock. Expressing sorption (totally reversible) of Na^+ and M^{++} as

$$\Gamma_i = w^i C_r^i \quad (3)$$

with $i = +$ or $++$ and $w^i =$ equivalent wt. of species i , Equations (1) and (2) yield

$$(\Gamma_{++}/w^{++})^2 = (\Gamma_{++}/w^{++}) K (C^+)^2/C^{++} + 2Q_V - Q_V^2 \quad (4)$$

and

$$\Gamma_+ = (Q_V - \Gamma_{++}/w^{++}) w^+ \quad (5)$$

from which two-dimensional sorption tables $\Gamma_+(C^+, C^{++})$ and $\Gamma_{++}(C^+, C^{++})$ were constructed for input to the simulator. The sorption isotherms are given in Figures 8 and 9.

Interfacial Tension

As discussed in Appendix A, IFT data are extremely important to the CFTE simulator as these data are used in the computation of capillary number. IFT data are reported in the Third Annual Report,²⁰ but these data are of limited utility because the associated concentration data are incomplete.

For example, the data were limited to a 1:1 brine/oil ratio and a constant Ca^{++}/Na^+ ratio, so it was not possible to ascertain IFT as a function of oil concentration or to separate the dependence of IFT on either Na^+ or Ca^{++} concentration alone. Moreover, IFT's in the type III region, which according to the phase volume data was traversed for the range of salinity studied, were not distinguished as either aqueous-microemulsion or microemulsion-oleic. The most serious omissions, however, were that neither the phase concentrations of surfactant nor the dependence of IFT on alcohol concentration were reported.

In order to honor as much of the data as possible, these data limitations were handled as follows. IFT was read in the simulator as a function of total surfactant concentration, and Na^+ and Ca^{++} concentration in the water. The dependence of IFT on the concentration of Na^+ and Ca^{++} was separated for the individual species by invoking a form of the Schultz-Hardy rule for which $1/Ca^{++} = \beta/Na^+$, with $\beta = 10$. As may be calculated from the SRD's in Figure 6, β varies from about 7 to about 14, so $\beta = 10$ is a reasonable estimate. Any effect of alcohol on IFT was not simulated.

For purposes of presentation only, IFT is shown in Figures 10 and 11 as a function of surfactant concentration in the total fluid and equivalent Na^+ ($= \text{Na}^+ + 10 \text{Ca}^{++}$). The bottom two rows in Figure 11 were not included in the Third Annual Report data but were reported separately.²¹ The value for brine-oil IFT (30 dynes/cm) was furnished at INTERCOMP's request (Appendix E). Figure 10 clearly shows that the optimal salinity, as reflected by minimum IFT, falls as surfactant concentration decreases.

One problem with the IFT data is that no measure of statistical significance (standard deviation, standard error, etc.) was reported. This is particularly important for the one low value, 0.0001 dyne/cm, which had a major impact on the results of the simulations. Since measurements of IFT's of this order may scatter several hundred percent around the mean value, they should always be checked for reproducibility.

In retrospect, it would have been preferable to use the correlation of Healy, et al,²² to estimate IFT rather than the data which were reported. This correlation, as shown on p. C-16, relates the ratios in the micellar phase of oil/surfactant or water/surfactant to the IFT's at the respective interfaces micellar-oleic or micellar-aqueous. The data usually correlate rather well on semi-log plots of the type shown on p. C-35.²³ This particular plot was generated by the phase equilibria program using the correlation coefficients as indicated but was not used in the simulations.

Viscosity

Viscosity of the Abbot biopolymer in 1.0% NaCl as a function of polymer concentration and shear rate was used as reported.²⁴ The data are plotted in Figure 12. The polymer injected both with and after the micellar slug was considered as a trace component which partitioned into the water-rich phase only.²⁵ This partitioning allows polymer to remain in the same phase as surfactant in a type II(-) phase environment, and to separate from surfactant in type III regions.

Viscous shear was included in the calculation of viscosity in phases which contained polymer by correlating shear rate to Darcy velocity between grid blocks. The equation used for the correlation was²⁶

$$v = 9.55 \times 10^{-3} \dot{\gamma} (k\phi)^{\frac{1}{2}} \quad (6)$$

where

- v = Darcy velocity, ft/day
- $\dot{\gamma}$ = shear rate, sec^{-1}
- k = permeability, md
- ϕ = porosity, fraction

Average North lease properties were used in Equation (6) to compensate for shear in interblock calculations. The wellbore model in the CFTE simulator does not include the effects of shear. Also, the simulator does not extrapolate beyond the limits of tables input for viscosity (or any) data. Thus for computed shear rates below 3.7 sec^{-1} (Figure 12), the simulator uses the viscosity at 3.7 sec^{-1} and similarly for high shear rates.

The viscosities of the aqueous, micellar, and oleic phases as a function of oil and surfactant concentration were not reported, and this severely compromised the ability to correctly simulate fluid mobilities. These viscosities were estimated in the simulator by using the computed phase compositions of surfactant, oil, brine, and polymer, and shear when appropriate. For these calculations, brine was assigned a viscosity of 1.07 cp, and oil viscosity was a constant 5.2 cp. The presence of surfactant at injection concentration was reported to add 2 - 4 cp to the viscosity of the aqueous and micellar phases (Appendix E). A value of 3 cp was used for this difference. Linear interpolation was used to calculate the viscosity of phases of compositions intermediate between injection concentrations and pure oil or brine. The effect of this linear interpolation was to mitigate any effects of high in-situ viscosities which may result from surfactant-oil complexing in type II(+) or type III regions.

Again, as with the IFT data, it would appear that use of a correlation for the phase viscosities based on literature data would have been preferable to use of data as reported. The middle phase viscosities are very important to the phase mobility, but these viscosities are rarely measured. For consistency and expediency, it is suggested that the phase volume data, viscosity, and IFT data could be taken on the same equilibrium mixtures as a function of concentration for all major components in all phases. This lack of phase concentrations, particularly for surfactant and oil, was the most serious shortcoming of the physical property data which were reported.

Dispersion

As discussed in Appendix A, a longitudinal dispersivity, α_L , is used in the CFTE simulator as a multiplier on phase velocity to account for convective flux. Salinity samples from the observation wells were used to estimate a characteristic α_L for field-scale dispersion.²⁷ The values obtained were 6.2 and 8.1 ft for wells MP-131 and MP-132, respectively. However, because the effect of heterogeneity was not considered in the analysis, α_L was reduced to 4.0 ft for all field simulations. This value was chosen to yield about the same inverse Peclet number (α_L/L) as was used in the one-foot coreflood history match with $\alpha_L = 0.01$ ft. The value of 0.01 ft is within the range (0.004 - 0.016 ft) reported²⁸ for α_L from laboratory displacements and compares favorably to the value of 0.006 ft ($D_e = \alpha_L v = 0.093 \text{ ft}^2/\text{day}$ for $v = 15 \text{ ft/day}$) reported for stacked Admire cores.²⁹

Laboratory scale measurements of α_t , the transverse dispersivity, are much less common than α_L , but they indicate²⁸ $\alpha_t \simeq \alpha_L/30$. No reliable measurements for field scale α_t were found in the literature. Because the two-layer geologic model indicated that the permeability contrast between the layers was, on the average, 2.0 or less, α_t for the two-layer cross section field simulations was arbitrarily set at the low value of 0.005 ft. This value was chosen to avoid any washing out of the effect of layering that may result from high transverse dispersion,³⁰ even when heterogeneity is considerably greater than at El Dorado.

The estimation of α_t could have been made less arbitrary by a numerical experiment to determine a value for the Peclet number for transverse dispersion, $h^2 \alpha_t/L$, below which the assumption of a homogeneous reservoir for purposes of modeling dispersive flow is valid. Sensitivity work with the CFTE simulator³⁰ indicates that the value for α_t of 0.005 ft used here may be about an order of magnitude too low. This is supported by recent unpublished results of L. W. Lake and co-workers, who found $\alpha_t = 0.03$ ft at El Dorado based on an analysis of field data. This value of α_t would tend to diminish the effects of an already moderate permeability contrast between layers as evidenced by the geologic model. Until experimental methods for field-scale dispersivities can be worked out, best educated guesses will have to be used for these parameters.

Any finite-difference simulator results in numerical truncation errors which have the effect of a physical dispersion. In order to judge the influence of the imposed α_L of 4.0 ft, numerical dispersion was calculated for a linear, 1-D, 20-grid-block system with a characteristic length of 384 ft. These values correspond to the number of grid blocks in the direction of flow and the injector-producer distance in the element selected for simulation. The simulated flood was run at a rate of 0.42 ft/day, which corresponds to the velocity averaged over the period of injection of preflush I and II in the Chesney pilot.

The numerical dispersion was calculated by examination of the effluent concentration profile of a nonadsorbing tracer in single-phase flow. Using the approximate solution of the convection-diffusion equation for a step change in concentration at the inlet face³¹, the following expression for the effective dispersion coefficient may be derived:

$$D_e = \frac{1}{t} \left[\frac{x_{90} - x_{10}}{3.625} \right]^2 \quad (7)$$

where x_{90} and x_{10} are coordinates of the 90 and 10 percent concentration values. For zero specified physical dispersion, a D_e of 0.48 ft²/day ($\alpha_L = 1.1$ ft) was obtained from the concentration profile predicted by the simulator. For a system length of 182 ft (10 grid blocks between injector and sampling point), α_L was calculated as 2.5 ft. It is not surprising that the numerical dispersion, which reflects numerical truncation error, is not constant. If the grid spacing was 5 ft rather than 19.2 ft, the corresponding α_L at $L = 384$ ft would be about 0.07 ft. The conclusion drawn from these results is that the numerical dispersion was somewhat less than, but of the same order of magnitude as, the imposed physical dispersion in the simulations performed.

High-Capillary-Number Three-Phase Relative Permeability

As there were no capillary desaturation curves measured for Admire sandstone, the relationship between capillary number (N_{cap}) and phase saturations had to be estimated, as did the relative permeabilities for three-phase flow conditions. The

relative permeability model used was proposed by Lake and is presented in Appendix D. This model allows for trapping of the aqueous, oleic, and micellar phases, and ensures continuity in relative permeability among phase types and across phase boundaries within a given phase environment. As required by the CFTE simulator, all phases have residual saturations calculated as a function of N_{cap} and end-points and curvatures which approach complete miscibility at high N_{cap} .

The major difference between this relative permeability model and that of Hirasaki, et al³² is the allowance in Lake's model of a trapped micellar phase saturation in the three-phase region at all possible oleic/aqueous phase saturations. If micellar phase trapping occurs at low oleic phase saturations, as proved to be the case in the El Dorado simulations, then the two relative permeability models should give essentially similar results.

The input required for Lake's relative permeability model are equations obtained by fitting drainage oil-water rock data. Drainage data are used since they best represent the formation of an oil bank in a chemical flood, with increasing saturation of the nonwetting phase. Data from core plugs from well MP-124 were taken as representative of the element for simulation and were fitted to the following equations:

$$k_{rw} = 0.194 \left[\frac{S_w - 0.238}{1 - 0.238 - 0.33} \right]^{2.568} \quad (8)$$

$$k_{ro} = 0.481 \left[\frac{1 - S_w - 0.33}{1 - 0.238 - 0.33} \right]^{1.942} \quad (9)$$

where $S_{or} = 0.33$ is the field-wide average, and $S_{wr} = 0.238$ was obtained from core analysis. The curves represented by Equations (8) and (9) and the data points used are shown in Figures 13 and 14.

The coefficients of Equations (8) and (9) were used to estimate the capillary desaturation curves for Admire rock. The ratio of end-point relative permeabilities $R = k_{rw}(S_w = 1 - S_{or}) / k_{ro}(S_w = S_{wr})$ was used as an index of rock wettability. With

R, estimates were then made for the critical capillary numbers, the N_{cap} at which the residual for a phase begins to decrease from its waterflood value. Berea was assumed as a standard for strongly water-wet rock with $R = 0.1$; $R = 10$ was assumed for a strongly oil-wet rock. As R varies from 0.1 to 10, the desaturation behavior of oil changes from that of the nonwetting phase in Berea to that of the wetting phase. It was also assumed that the slopes of the desaturation curves for Admire rock were the same as those for Berea; and further that the shift in the desaturation curve for the wetting phase is equal to but in opposite direction from the nonwetting phase curve shift. As a result of this shift, the Admire curves lie between the Berea curves. Were this not the case, a rock would become more oil-wet and more water-wet at the same time, a situation which on physical grounds seems highly unlikely.

From Equations (8) and (9), $R = 0.194/0.481 \approx 0.4$, which indicates the Admire is of intermediate wettability. Using critical N_{cap} of 10^{-5} and 10^{-4} for water- and oil-wet reservoirs, and 10^{-5} (oil) and 6×10^{-5} (water) for Berea, an interpolation on $\log N_{cap}$ produced the desaturation curves shown in Figure 15. In Figure 15, the primed variables refer to the waterflood values. For example, $S_{nwr}' = 0.33$, $n' = 1.942$, etc. Also included in Figure 15 are the Gupta-Trushenski³ laboratory-derived Berea desaturation curves. The desaturation curves are presented as straight lines. This was done because it was assumed that the slight "S" shape, typical of laboratory-derived curves, represents at most a second-order effect.

Figure 15 shows that for $N_{cap} \leq 2 \times 10^{-5}$ in Admire rock, waterflood conditions prevail. For $N_{cap} > 2 \times 10^{-5}$, the residuals first to oil and then to water begin to decrease as the curvature exponents tend to unity. At complete miscibility, the residual saturations of all phases are zero and relative permeability is identical to saturation.

Following the example given in Appendix D (which is for Bell Creek rock), Equations (8) and (9) and the desaturation curves were used to generate the relative permeabilities for the aqueous, oleic, and micellar phases in Admire rock. Relative permeabilities were computed at five capillary numbers for entry into the simulator, and results are shown in Table 3. Values in Table 3 were used without adjustment in all field simulations, except for a sensitivity run with $S_{or} = 0.23$. For purposes of simulation, the oleic phase relative permeability data contained negative values to

allow for correct interpolation of residual oil saturation between points in the tables. These negative relative permeabilities were set equal to zero if they appeared in the flow calculations. The calculations also account for the possibility that three-phase flow can exist at waterflood N_{cap} . This might be true in regions of the flood such as the outer streamtubes where velocity is low; thus, $N_{cap} = \mu v / \sigma$ could be small even though IFT was low.

Coreflood Data

A considerable effort was expended in coreflood experiments in support of the El Dorado project.³³ While a number of important process variables such as the salinity of the polymer drive and micellar slug size were studied, the results which were reported were generally limited to the amount of oil produced. As discussed in the section on coreflood history matching, the lack of data on the core effluent precluded a complete characterization of the process by simulation.

Concentration profiles of surfactant and polymer, the number of phases, and the phase compositions on the effluent would have been useful in tracking phase behavior and physical properties. Also, pressure-drop measurements across the cores could have been used to estimate in-situ phase viscosities.

In addition to all of the data requirements previously discussed, the type of experiments and data required for process characterization by coreflood simulation with the CFTE model might consist of the following (all on field cores):

1. Dynamic surfactant sorption isotherms, with and without crude oil present. When combined with the data from static sorption tests, these experiments can be used to estimate phase trapping of the surfactant.
2. Relative oil and water permeability data should be calculated throughout the waterflood history. Relative permeability data at saturation conditions intermediate between those of initial water and residual oil may be computed by the method of Johnson, et al.³⁴
3. Cation exchange capacities on representative core plugs.

4. Number and volumes of phases in effluent.
5. Phase compositions of all major ions and components (oil, surfactant, polymer, cosurfactant) in effluent.
6. Interfacial tension between all produced phase pairs and viscosity of produced phases.
7. Pressure measurements at core inlet, outlet, and several points in between.
8. In a few corefloods, residual oil saturation to the chemical slug as a function of distance along the core. This is an extremely important experiment to check whether the simulator is properly characterizing the in-situ process and to suggest possible process mechanisms. One way to make the measurements may be the microwave absorption technique developed to monitor in-situ oil/water saturations during caustic floods.³⁵
9. Among the most important process variables to study are sensitivity to rate, salinity gradient, and chemical slug size.
10. Corefloods should be repeated to obtain an estimate of the statistical significance of the data. Confidence in the methodology may be best obtained on Berea or similar cores. When dealing with field cores, the larger the sample population, the more meaningful the data are likely to be.

Field Data

One of the commendable facets of the El Dorado project are the analytical data reported from observation well samples. This includes concentration of surfactant, polymer, alcohol, and sodium, calcium, and magnesium ions. Although these data are not, in the strict sense, required for simulation, they proved to be very useful to this study because of the aforementioned paucity of data with which to characterize the process by coreflood history matching.

However, field samples should not be viewed as a substitute for laboratory data. Rather, the field data are valuable to track the field process and may be used, as was the case here, to infer modifications to the process characterization. This is particularly important if the field process does not appear to reflect the laboratory-derived process.

The following field data gathering program is intended as a guide to assist the monitoring and understanding of the process in a reservoir environment. Some of the suggested procedures supplement those performed for the El Dorado project. Also, data as may be required for reservoir characterization by black-oil simulation are not considered in this report.

1. Well Tests

- a. Interwell pressure tests prior to start of project.
- b. Single-well pressure tests used to monitor changes in fluid characteristics, injectivity, or productivity, or formation damage caused by fluid interactions, degradation, etc.
- c. Tracer tests used to monitor arrival of fronts or detect changes in flow paths in reservoir.
- d. Fluid injection and production wellbore surveys to determine which layers or zones are receiving/producing fluids, and detect changes with time.
- e. Periodic well logs to detect tracers and fluid saturations.

2. Injection Wells

- a. Rates and cumulative volumes of all chemical slugs, preflush, etc.
- b. Quantity and time of tracer injection.
- c. Samples of injected fluids, obtained periodically. Equipment should be available on-site to assay quality of injection fluids (composition, viscosity, salinity, etc.).
- d. Bottomhole pressure and temperature. Routine periodic measurements.
- e. Stimulation fluids. Stimulations of a chemical nature should be avoided. Compatibility of well treating chemicals and injected fluids should be tested prior to treatment.

3. Observation Wells

- a. Periodic fluid samples. Well should be pumped-off prior to sampling. A bottomhole sample should be obtained occasionally to check representivity of surface samples. If possible, on-site tests should be made for number of phases, volume fraction of phases, estimated composition, and salinity of phases.
- b. Sealed, unaltered samples should be sent to the laboratory for subsequent analyses.
- c. Emulsion-breaking chemicals. To be avoided at all costs prior to on-site or lab testing.
- d. Periodic well logs. Logs should be designed to detect tracers in addition to salinity and fluid saturations.

4. Production Wells

- a. Periodic fluid sample for each well. In addition to test procedures for observation wells stated above, sampling should be conducted to detect presence and activity of wellbore treatment chemicals.
- b. Cumulative volumes and rates of produced fluids.
- c. Bottomhole pressure and temperature.

5. Laboratory Support Data

- a. Quality control on injection wellhead samples.
- b. Observation and production well samples. Assay number of phases, phase volume fraction, phase composition, salinity, tracers, etc. Sample data may suggest phase behavior occurring in the field.
- c. Viscosities of and interfacial tensions between all phases.

NUMERICAL SIMULATION

COREFLOOD SIMULATIONS

History Matching

The idea of coreflood history matching is, with the process as described from laboratory data, to fine-tune the process characterization so as to allow the simulator to predict coreflood performance. This tuned process is then combined with the reservoir description and field simulations performed.

Coreflood 53 (six Admire core plugs from well MP-106) as documented by Kellerhals³³ was selected for matching because the sequence and compositions of the various fluids injected were similar to those used in the field. Pertinent data for coreflood 53 are presented in Table 4. 55.1% of the waterflood residual oil was recovered in this test. The process parameters were exactly as previously described, with a three-phase relative permeability table constructed for $S_{or} = 0.376$ and $S_{wr} = 0.238$. S_{wr} was estimated from relative permeability data on core plugs from well MP-124.

The primary data to be matched consisted of an oil fraction curve and the amount of surfactant produced (about 11% of the amount injected). No surfactant or polymer profiles in the effluent were reported. The coreflood was simulated in a 1-D, 20-grid-block model of uniform permeability. All fluids were injected at a rate of 6 ml/hr (frontal advance rate of 1 ft/day).

As discussed previously, CSEL was used as the matching parameter. A CSEL of about 1.0 wt. % NaCl may be estimated from either Figure 1 or Figure 2. Since the concentration of divalent ions in the micellar slug was nil, and since polymer was thought to be of minor importance to the phase behavior, initial estimates of $CSEL = 0.95$ and $CSEU = 3.8\%$ were made from Figure 1. The choice of CSEL is critical to the predicted results since the salinity of the polymer drive, CSEP, is 1.0%. If $CSEP > CSEL$, then because of the phase behavior model, a type III flood

dominates. Consequently, because of the relative permeability model, surfactant trapping may be significant. This is exactly what happened in the simulation with CSEL = 0.95. No surfactant was produced and tertiary oil recovery was only 32.9%.

To "untrap" the surfactant and thus increase the predicted oil recovery, the process was tuned by raising CSEL to 1.07% (midpoint salinity 2.7%), slightly above CSEP. As the salinity of the polymer drive now results in type II(-) phase behavior, surfactant will move through the core in the high-permeability aqueous phase. This simulation resulted in an acceptable match on oil cut, oil recovery, and overall surfactant production (Figure 16). It is emphasized, however, that this match does not necessarily reflect an accurate and complete process characterization, inasmuch as data on the distribution of surfactant and polymer in the produced fluids were not available for matching. At this point in the study, it was therefore reasoned that further simulations of off-design corefloods would not be productive, and that efforts to characterize the process by simulation would be better served by focusing on observation well MP-131, where produced samples were analyzed for chemicals.

Coreflood Sensitivity Simulations

Only a few sensitivity simulations were run in the coreflood environment and these were limited to the effects of surfactant sorption. (Sensitivity to preflush, residual oil saturation, surfactant slug size, and phase behavior were simulated in the reservoir model and are presented in the next section.)

Excepting sorption, the simulations were run with the coreflood 53 history match data intact (CSEL = 1.07%, etc.). Surfactant sorption was varied by increasing the isotherm plateau and/or the amount of reversibility. The results are presented in Table 5. When complete reversibility was allowed, a doubling of surfactant adsorption did not significantly reduce oil recovery. Although salinity-dependent sorption was not a part of the process description, reversible adsorption illustrates one of the effects of a lower salinity polymer drive, surfactant remobilization, which has been observed in laboratory coreflood experiments.^{36,37} Oil recovery dropped sharply when surfactant sorption was increased to 3X the base case value (Table 5), even though 100% reversibility was allowed. 3X sorption is so high relative to the amount of surfactant injected that low IFT's are not realized.

RESERVOIR DESCRIPTION

Element for Simulation

The portion of the element selected for simulation relative to the North lease is shown in Figure 17. This element includes the two observation wells MP-131 and MP-132, located between the injector MP-118 and producer MP-124. Since tertiary oil has not been produced at any of the pattern producing wells, the only history available are the samples and logs taken at MP-131 and MP-132, 90 and 187 ft, respectively, from the injection well. The rationale behind the element selection was to make use of the data on oil cut and surfactant and polymer concentration from samples from the observation wells as an aid in verifying the laboratory process characterization. The injection well is located in the center of the pilot area and should be the well least affected by the fluid drift which has been observed in the pilot area.

Two grid systems were used to approximate the element for purposes of numerical simulation. The first was constructed to conform to the geometry of the isolated element. This resulted in an asymmetric grid. The second grid was an idealized symmetric one-eighth of a five-spot.

Asymmetric Grid

The details of the construction of the asymmetric grid, the effects of rate imbalance on the construction, and the possible impact of fluid drift are presented in Appendix B. A generalized reservoir grid containing the four wells was generated from streamtube maps provided by Cities Service Company (Appendix B). The map used was calculated using a homogeneous, isotropic reservoir description, average flow rates, and a unit mobility ratio between displaced and displacing fluids. The 5 x 20 reservoir grid, shown in Figure 18, was created from flow and isopotential lines derived from the streamtube data. Figure 18 shows that the flow paths at the top of the element are distorted because of poor production rates in the producer immediately above the element. The converging streamtubes at MP-124 accelerate the times of arrival of fluid fronts at the producing well, while grid effects only slightly influence the performance of the second observation well and do not disturb performance at MP-131.

Despite these drawbacks and the fact that the asymmetric grid is not necessarily representative of the average pattern performance, it is without question the best grid possible to model the selected element. If average pattern performance is desired, then a representative one-eighth of a five-spot can be chosen which is homogeneous and symmetric. However, if a specific area of the reservoir is to be modeled, as was the case in this project, the most economical way to accomplish this is to generate an asymmetric grid which is parallel and perpendicular to the isopotential lines for this region.

Geologic Model for Asymmetric Grid

The geologic model imposed on the asymmetric grid was developed by GURC from log and core data. A two-layer model was described for the simulation element (Tables 6 and 7). This description shows the reservoir is of generally poorer quality in the vicinity of MP-132 and MP-123 (an inactive well south of MP-118). This two-layer description was used for cross-section simulations in the center streamtube of the asymmetric grid. For the areal simulations, a one-layer reservoir description (Table 8) was constructed from the two-layer model.

Allocation of Injected Fluids for Asymmetric Grid

In Appendix B are also presented the details of the calculations for the allocation of preflush and chemical slug among the five streamtubes of the asymmetric grid. Briefly, along each of the streamlines created between wells MP-118 and MP-124, a pressure gradient was calculated at a distance roughly 50 ft from the injection well. Application of Darcy's Law led to estimates of the relative volumes of fluid in each streamtube. The total element receives 28.1% of the injection volume in MP-118, with the distribution in each streamtube being 6.4%, 25.8%, 23.3%, 23.8%, and 20.8% of the fluid injected into the element for streamtubes 1 through 5, respectively. These fractions were used to divide the flow into each streamtube for the preflush simulations, during which no crossflow was allowed between streamtubes. Simulations with the more viscous surfactant slug and polymer drive were not restricted in this manner. In addition, during the injection of more viscous materials into MP-118, the portion of the injection stream entering the total pattern was increased to 36% because of a lesser deviation from radial flow paths for the low-mobility fluids.

Symmetric Grid

The one-eighth of a five-spot element (Figure 19) used to predict the North lease performance employed a homogeneous and isotropic reservoir description. The grid block boundaries in this grid system are similar to streamtubes in appearance, but do not represent internal no-flow boundaries. The average North lease reservoir properties used were permeability, porosity, and net thickness of 265 md, 24.3%, and 18 ft, respectively.³⁸ The distance between the injection and production wells was 380 ft, and two observation wells at 96 ft and 196 ft were included. The injection volumes used were one-eighth of the volumes injected into MP-118, and the rates used were the overall average rates for each fluid type.

The purpose of the symmetric grid was to provide a representation of the behavior, on the average, of an element of the field having average formation properties. Then a third party could, using the results of the simulations done for this grid, assess performance of the given micellar-polymer process in a field with similar average properties. Thus, the location of the wells in the symmetric grid was not intended to duplicate the exact interwell distances in the El Dorado field.

Injection Rates and Volumes

Volumes and average rates for all fluids for the North lease, MP-118, and both grid systems are given in Table 9. Because of the calculated nonuniform distribution of fluids which created the asymmetric element, the pore volumes of preflush and slug injected into each grid system were not constant. With respect to the surfactant slug, the center streamtube of the asymmetric grid received 16.4% pore volume, the entire asymmetric grid 10.6%, and the entire symmetric grid 6.1%. The entire confined North pattern received 5.2% pore volume of surfactant slug if uniform radial flow is assumed in the vicinity of each injection well, as only 47.3% of the injected slug would enter the project area. The symmetric grid, therefore, should provide the better estimation of overall North lease performance.

FIELD SIMULATIONS

Field Data

As presented in the First through Fifth Annual Reports, fluid samples were collected from the injection wells, both observation wells, and the production wells in the North pattern. Injection well samples showed that the compositions of the micellar slug and polymer drive were fairly constant except for the deletion of secondary butyl alcohol from the polymer drive between May and December of 1979.

Sample data from the observation wells constitute the major portion of the data from which to verify the chemical process description, since the oil bank or chemicals have not yet reached any producing well. Observation well samples were obtained from 1-ft intervals of the top layer only in both wells, with well logs taken periodically to augment the sample data. The initial simulations were therefore made with the two-layer reservoir description, with the observation wells completed only in the top layer.

Simulation of Laboratory-Derived Process in Center Streamtube (Two Layers)

The center streamtube of the asymmetric grid was simulated in x-z cross section with two layers. Fluid injection duplicated field operations for the two preflushes, the micellar slug, and the polymer drive, and is summarized in Table 9. Using the volume fractions computed for the center streamtube (see Appendix B), injection rates were calculated as bimonthly averages.

The salinities of the produced fluids were computed by the model at each of the wells until the end of history at August 31, 1979. The calculated monovalent (Na^+) and divalent ($\text{Ca}^{++} + \text{Mg}^{++}$) cation concentrations, represented by sodium and calcium as trace components in the water, compare very well with the salinities measured in the field for MP-131, but not for MP-132 or MP-124 (Figures 20 - 22). The favorable salinity match at MP-131 indicates that preflush injection rates, flood-front velocities, and grid geometry in the model are representative up to 90 ft. The computed salinity at MP-132 predicts flood fronts arriving earlier than was observed in the field. The discrepancy may be due to a number of things, such as the grid geometry,

fluid drift occurring in the field, or a flow restriction near MP-132. (The salinity match at MP-132 was improved using the one-eighth of a five-spot grid with crossflow, dashed line, Figure 21, as discussed later.) The salinity match at MP-124 is poor for both sodium and divalent cations, with good agreement only on the time of arrival for the first preflush. The match of arrival time, however, does not necessarily indicate a match on fluid velocities in the field because the preflush at MP-124 may be from other injection wells besides MP-118. If the arrival of preflush at MP-124 is not from injection at MP-118, the calculated velocities between the first observation well and the producer are too high, and the grid system calculated from streamline calculations will introduce some additional truncation error. The salinity match at MP-124 was improved with a one-layer simulation in the full asymmetric grid (Figure 23).

The simulation of the micellar-polymer process was performed using the same data input as for the coreflood match with one exception: because residual oil saturation was different in the field (0.33) than in the core (.376), a new three-phase relative permeability table was constructed (Table 3). The data input are summarized in Table 10.

The comparison of the computed with the observed performance at MP-131 is shown in Figures 24 and 25. Both the magnitude and duration of the predicted oil fraction curve are significantly higher than observed at MP-131. The computed polymer profile compares favorably with the observed samples, but the predicted surfactant breakthrough is about six months late and the predicted surfactant concentration is significantly higher than what was observed in the field. The phase equilibria model with CSEL = 1.07% allows the surfactant and polymer to exist in the same (aqueous) phase, and viscosity-concentration data cause the surfactant-rich polymer drive to have a higher viscosity than the surfactant-poor polymer drive. The resultant viscous instability allowed polymer to move ahead of the surfactant slug, the reverse of what was observed, and the predicted arrival of surfactant is late.

There are many possible reasons why the simulated results using the laboratory process characterization do not compare very well with the observed data. These reasons may be classified as due to inadequacies in the reservoir and/or process characterizations. Both are equally important to numerical modeling, but the scope

of this study was focused on the process. Thus, even though "history matching" was not an objective of this study, it was felt at this point in the project that some further tuning of the process characterization was justified. The basis of this reasoning was a lack of confidence in the completeness and accuracy of the coreflood-derived process characterization.

Simulation of Adjusted Process in Center Streamtube (Two Layers)

As evidenced by Figures 24 and 25, the goals of the process tuning were to reduce the predicted level of produced surfactant concomitantly with earlier surfactant breakthrough, and to reduce the amount of oil mobilized. Toward these ends, a number of adjustments to the laboratory data could be made:

1. Increasing the singular low IFT of 0.0001 dyne/cm (Figure 10), which appears to be anomalous.
2. Changing the fit of the oil relative permeability data in Figure 13 to allow for a closer match on the highest data points. This would result in shifting the Admire nonwetting desaturation curve to the right, thereby reducing both oil cut and recovery.
3. Including the effects of surfactant and oil concentration to increase microemulsion phase viscosity, thus lowering the mobility of that phase.
4. Altering the cation exchange capacity to produce a better salinity match at MP-132 and MP-124.
5. Including an assumed dependence of surfactant sorption on salinity.

Because this investigation was to stress the use of basic laboratory data in simulating field performance, none of the adjustments listed above were made. Rather, the value of CSEL was adjusted based on an interpretation of both laboratory and field data.

Because the polymer injected with the surfactant slug appeared to produce a three-phase region at the lower salinities, Figure 2 was used to estimate CSEL = 0.35 wt. % NaCl. In addition, samples from MP-131³⁹ showed a high ratio of surfactant in the oil phase to surfactant in the aqueous phase shortly after oil breakthrough. As discussed previously, "surfactant favoring oil" indicates that the phase behavior is in a type II(+) environment: either the II(+) region or the II(+) node of the type III region. One way to satisfy this behavior is to drop the CSEL from the coreflood match to a value somewhat below the salinity of the micellar slug and polymer drive.

Cities Service Company, upon reviewing the first draft of this report, noted that the procedures used to analyze the field samples for surfactant may tend to drive surfactant into the oil phase. This was not known at the time the simulations were performed. However, even if the claim that the data showing "surfactant favoring oil" are suspect is true, the lowering of CSEL may still be justified. Phase behavior in the type II(-) node of the type III region, where surfactant favors water, also implies that the system salinity is above CSEL.

The results of the simulation with CSEL = 0.35% are shown in Figures 26 and 27. These results were judged to be an improved representation of the field behavior as the predicted surfactant concentration and breakthrough and oil cut are shifted in the right direction. This process characterization is of course not unique and may not even be the correct one, but the midpoint salinity of 0.875% NaCl does fall, as might be expected from the argument on p. 13, between the SRD's of Figure 6.

It is not surprising that the apparent optimal salinity may be lower in the field than in a short core test. The separation of alcohol from the surfactant which was reported to have occurred in the field,⁴⁰ unfavorable ion exchange resulting in a higher $\text{Ca}^{++}/\text{Na}^{+}$ ratio, and more fully developed mixing zones in the field would all tend to drop optimal salinity faster than indicated by an SRD based on laboratory data.

Two distinct peaks are present in both the oil and surfactant as predicted at MP-131 by the model. These peaks are not numerical effects in the simulator, but are due to the change in IFT predicted between the injection well and MP-131. The path of computed IFT midway between the injection well and MP-131 (grid block 3) is shown in Figures 11 and 28. As the slug enters the block, surfactant concentration

increases, salinity drops from preflush values to the salinity of the slug, IFT drops to about 0.028 dynes/cm, and the first oil bank was created. With time, the surfactant concentration declined slowly with the salinity remaining fairly constant, and the flood began moving toward a very low IFT at 0.018 volume fraction surfactant. As the minimum IFT is approached, the capillary number becomes very large and a second oil bank is formed.

Both the measured and predicted surfactant concentrations reaching MP-131 are significantly lower than anticipated based on laboratory work conducted by Cities Service Company. In the model, the reason for the reduced level of surfactant is the formation of a third, surfactant-rich phase of intermediate wettability, which becomes trapped along with the remaining oil. The relative permeability model used allows this microemulsion phase to have a residual saturation between that of oil and water. Low IFT's are required to mobilize the microemulsion phase, since it generally is volumetrically small. During the course of the flood charted in Figure 28, much of the surfactant is held in the third phase until the IFT begins to decline, and the second surfactant peak on Figure 27 is created. A second surfactant peak was not observed in the field, although a very slight second oil peak was observed.

Even with the adjusted process, the predicted oil cut is larger than the oil cut measured in the field. The difference may be due to sampling errors either at bottomhole or at the surface, or by the limited area perforated in the wellbore. A more likely explanation is that the two-layer description is inadequate at well MP-131, as well logs show more than a one-layer response in each geologic layer.⁴¹ Tuning the reservoir characterization, for example by multilayer analyses to evaluate the effects of gravity and relative permeability at MP-131, might have resulted in a more favorable comparison between the predicted and observed data.

Simulation of Adjusted Process in Center Steamtube (One Layer)

The simulation with the adjusted process was repeated in the center steamtube of the asymmetric grid with a one-layer reservoir description (Table 8). The results (Figures 29 and 30) show that oil and surfactant fronts arrive later and with higher cuts than in the two-layer simulation. The representation of the observed data was

not as good when layering was neglected, primarily because the observation wells were completed originally in only the upper zone. The computed salinity at the producing well was not affected by layering, however, indicating that a one-layer model may be adequate to accurately predict overall pattern performance.

Simulation of Preflush in Full Grids (One Layer)

The full five-streamtube asymmetric grid was simulated during preflush injection with the one-layer reservoir description. No crossflow was allowed between streamtubes during the injection of preflush since a unit mobility ratio was assumed in the grid construction. The computed salinities at the observation wells were identical to those in the two-layer center streamtube simulation (Figures 20 and 21). The computed salinity at the producing well (Figure 23) represents a more gradual change in salinity than from the simulation in the center streamtube alone because the outer streamtubes were only partially contacted by preflush.

To illustrate grid effects on the simulated results for the salinities at MP-132 (Figure 21, dashed lines), a simulation was performed in the single-layer one-eighth of a five-spot symmetric element with average formation properties. The predicted arrival of preflush is only a few months earlier than observed at MP-132. This early arrival time is supported by well logs which indicate that preflush may have reached MP-132 a few months before the drop in sample salinity⁴¹. The return of salinity to original formation levels could not be matched with either the asymmetric or symmetric grid representations.

Performance Prediction in Center Streamtube (One Layer)

To investigate the effects of operational changes in the field beyond August 31, 1979, predictions were made with polymer drive injection continued at a constant, average rate until at least one pore volume injected after preflush. The simulations also included the reported drop in polymer salinity from 10,000 to 250 ppm NaCl in four stages from mid-December 1979 to mid-February 1980,⁴² but not the reported loss of polymer viscosity due to bacterial activity.⁴³

The following results should be viewed with the understanding that the process characterization used for the predictions represents only one possible explanation of the field behavior, and that a different process characterization or different input data might strongly affect the predicted results.

During simulation of the one-layer center streamtube beyond history, several changes in the character of the process were noted. The interaction between the surfactant and polymer, as discussed earlier, plays an important role in simulating performance at the first observation well. As the micellar slug is injected, with CSEL below the slug salinity, a third surfactant-rich phase forms and the surfactant separates from the polymer. The surfactant-rich phase quickly becomes trapped, however, and the polymer-rich aqueous phase begins to flow past the surfactant. Changes in the relative positions of surfactant and polymer before oil breakthrough at the producer are shown in Figures 31 and 32. An oil bank is created by the surfactant but is subsequently pushed ahead by polymer as surfactant is trapped.

A second change in the behavior of the flood occurs as the salinity of the polymer drive drops to 250 ppm NaCl (0.025 wt. %). The surfactant-rich third phase disappears as the drive salinity drops below CSEL = 0.35 wt. % NaCl, and the surfactant is no longer trapped. The flood progresses in a type II(-) phase regime with the surfactant mobile but far behind the polymer front, as depicted in Figure 33. Surfactant continues to reduce the residual oil saturation but not as efficiently as in type III phase behavior. At polymer breakthrough, 0.85 pv injected after preflush, the surfactant has only moved about one-half the distance between the injection well and the production well. The distribution of surfactant and oil after polymer breakthrough is shown in Figure 34.

The production of oil from MP-124 begins at 38.1% pore volume injected after preflush (Figure 35). Oil is produced at an average cut of 34.2% until polymer breakthrough at the producing well. At one pore volume injected after preflush, oil recovery was 39.5% of waterflood residual. A second oil bank freed by mobilized surfactant occurs at 105% pore volume injected after preflush at an average cut of 15.6%. Oil production ceases at about 140% pore volume injected after preflush, with ultimate oil recovery 52.8% of the waterflood residual. The final distribution of oil saturation is shown in Figure 36. The highest oil saturation is midway between the

injector and producer, near the point where all of the surfactant entered the type II(-) phase region. The oil saturation declined as the producing well was approached because of increased fluid velocity caused by viscous shear and converging flow. The velocity increase in the presence of surfactant increased capillary number, which in turn allowed the oil saturation to decrease.

Performance Prediction in Center Steamtube (Two Layers)

The performance of the two-layer description was essentially identical to that for one layer since both zones were swept by preflush, micellar slug, and polymer drive. The two-layer model did show earlier breakthrough of fronts at all sampling points, but the oil recoveries at later times, shown in Figure 37, are the same. For the reservoir description employed, the properties of the two layers were not dissimilar enough to significantly reduce sweep in the tight layer and thereby alter oil recovery. In addition, reduced communication ($k_v / k_x \approx 0$) between layers in the two-layer system was found to be unimportant to performance as long as communication between layers was assumed at the injection wellbore. The production history for oil and polymer from wells MP-132 and MP-124 is shown in Figures 38 and 39. Surfactant production was insignificant prior to the injection of one cumulative pore volume and consequently is not shown on either figure.

Sensitivity Simulations in Center Streamtube

Sensitivity simulations were run in the center streamtube of the asymmetric grid with the one-layer reservoir description to determine the effect of phase behavior, preflush, micellar slug size, and residual oil saturation on predicted performance. In addition, the two-layer simulation at well MP-131 was rerun with a lower residual oil saturation to waterflooding. The results are summarized in Table 11 and Figures 40 - 45.

1. Sensitivity to Phase Behavior

The phase data used to match coreflood 53 with CSEL = 1.07 wt. % NaCl was run in the center streamtube. The behavior of the flood is quite different than in the base-case (CSEL = 0.35) simulation. No middle phase

forms to trap surfactant, although the surfactant is still bypassed by polymer. Surfactant moves through the reservoir much more rapidly, and although generally higher oil saturations are left behind the surfactant (Figure 40), more oil is recovered at one pore volume injected after preflush (54.5% of waterflood residual versus 39.5% for the base case).

2. Sensitivity to Preflush

A simulation was made with CSEL = 0.35 wt. % NaCl in which the center streamtube was not first preflushed by lower-salinity water. Fractional oil recovery curves with and without preflush are shown in Figure 41. The only slightly poorer recovery without preflush resulted from the bypassing of surfactant by polymer, which created an in-situ preflush of polymer-thickened water at the (lowered) salinity of the polymer drive. The movement of surfactant, polymer, and oil is very similar to that for the preflush case (compare Figures 33 and 42), except that the type III phase region is smaller.

3. Sensitivity to Slug Size

The process was simulated with both 2X and 0.5X the base-case micellar slug size (16.4% pv) received by the center streamtube. The oil recoveries with 2X and 0.5X are contrasted with the base case in Figure 43. Oil recovery at one pore volume after preflush was 69.6% and 15.4% for the 2X and 0.5X slugs, respectively. The results indicate that for the range of slug size studied, oil recovery is roughly proportional to slug size. The 0.5X slug traveled as far as the base-case slug, but at a reduced level of surfactant concentration. The 2X slug traveled about twice as far at a slightly higher surfactant concentration. The distribution of remaining oil saturation for the three slug sizes is shown in Figure 44.

4. Sensitivity to Residual Oil Saturation

The effect of reducing the residual oil saturation to waterflooding from 0.33 to 0.23 was studied in 1- and 2-D in the center streamtube. The lower value represents a minimum for residual oil saturation in the part of the reservoir defined by the center streamtube, as shown by well log analysis.¹ The results of the one-layer simulation showed that oil breakthrough

occurred slightly later and oil recovery as a percent of S_{or} was slightly lower than for $S_{or} = 0.33$ (Table 11).

A two-layer center streamtube simulation of MP-131 was also run with $S_{or} = 0.23$. Figure 45 shows much better agreement with field samples for both oil cut and surfactant cut than in the match with $S_{or} = 0.33$. It appears from this result that $S_{or} = 0.23$ may have been a more appropriate base case for sensitivity work.

Performance Prediction in Asymmetric Grid

Performance after August 31, 1979 was predicted in two single-layer areal grids: The asymmetric grid and, as discussed below, the generalized one-eighth of a five-spot element of symmetry. The process description with CSEL = 0.35% NaCl was again employed. These predictions do not consider the effects of bacteria on biopolymer concentration and the resulting viscosity drop measured on samples from MP-131 beginning in September 1979.⁴³

The reservoir description supplied by GURC for the asymmetric grid allowed for heterogeneities which can in general be described as poorer reservoir in the vicinity of MP-132. Although an oil cut of about 1.0% was observed at the second observation well in December 1979, a significant oil bank was predicted to arrive there in June 1979, and predicted oil cuts at MP-132 averaged 35%. The most up-to-date information from the field indicates that an oil bank reached MP-132 in September 1980, with a sustained cut of about 6%.⁴⁴ Besides possible communication problems around MP-132, there are other reasons for the predicted early arrival of oil at MP-132 that are not accounted for in the simulation. These include the formation of a highly viscous, low-mobility emulsion phase and fluid drift. As discussed in Appendix B, the latter can be particularly significant at MP-132.

The oil bank was predicted to reach MP-124 in March 1980. Oil was produced at an average cut of 11.8% until polymer breakthrough in February 1983, at which time 22.7% of the waterflood residual oil had been produced. At one pore volume injected after preflush, 24.2% of the oil was recovered. Cumulative oil recovery as a function of time up to one pore volume of chemical slug and drive injection is shown in Figure 46.

The simulation results were overlaid on a map of the element to show the location of oil, surfactant, and polymer fronts at polymer breakthrough. Figures 47 and 48 show that oil saturation increases nonlinearly away from the injection well until the surfactant bank is reached, just before the second observation well. Polymer has moved far ahead of the surfactant front and has swept most of the oil bank to the producing well. A radially symmetrical shape has been created by the high-viscosity fluids to a distance where the streamtubes begin to converge beyond MP-132. This pattern of radial flow indicates that the degree of areal heterogeneity incorporated in the reservoir description does not have a significant effect on the flood performance. The nonradial contour lines along the bottom of Figure 48, which suggest heterogeneity effects, are more likely due to the asymmetrical shape of the grid boundaries, as the lower boundary of the grid is farthest from the injection well.

Performance Prediction in Symmetric Grid

The one-eighth of five-spot element employed a homogeneous reservoir description representing average North pattern properties. The performance of two observation wells and a producing well in the symmetrical grid are given in Figures 49 - 51.

An observation well located 96 ft from the injector shows two oil banks beginning in July 1978 (Figure 49). The two oil banks are accompanied by two surfactant peaks, as discussed earlier. As low-salinity polymer drive reaches the well, a third surfactant peak is seen as surfactant is remobilized. A second observation well at 196 ft shows an oil bank in December 1979 through September 1981 (Figure 50). A second oil bank is again produced after polymer breakthrough but before surfactant reaches the well in April 1984. The second oil bank was created by remobilized surfactant.

An oil bank was observed at a production well, 380 ft from the injection well in late 1982, approximately four years after the initiation of micellar slug injection (Figure 51). Oil cuts ranged between 7 and 19% prior to polymer breakthrough. Figure 52 shows the distribution of oil, polymer, and surfactant during oil bank production. Once polymer reached the production well, only 10.3% of the oil in the pattern had been produced. After one pore volume of slug and drive injection, the surfactant traversed about two-thirds of the distance to the production well as shown in Figure 53, and 13.4% of the oil was produced. Cumulative oil production is shown in Figure 46.

The one-eighth five-spot grid is likely to be more representative of average North pattern performance for several reasons. The asymmetric grid developed from streamline data can distort the predicted performance of the flood by misrepresenting the area swept by the injected fluids, and by unrealistically increasing the fluid viscosities in the vicinity of the producing well. The symmetric element, however, represents the idealized behavior of a confined rate-balanced five-spot that does not alter sweep areas or fluid velocities. The higher oil recovery from the asymmetric pattern is primarily due to the larger pore volume of slug (10.6%) injected into the pattern. This increased slug volume resulted from the distorted flow paths calculated from the streamline model. The average pore volume of slug which enters the pilot area (5.2%) is more closely represented by that entering the symmetric grid (6.1%).

**APPLICATION OF SIMULATION RESULTS
TO THE MICELLAR-POLYMER PROCESS
IN SIMILAR RESERVOIRS**

One important goal of DOE-supported demonstration projects is to place necessary and sufficient information into the public domain so that a third party, with proper evaluation of a particular test, can assess the technical and economic feasibility of initiating EOR operations in a different section of the same field or in another similar field. An important objective of this study was to show how the results of simulation might be used for such an assessment. However, because there were so many gaps in the data that the simulations could not be adequately performed, use of these results is not recommended for application to other micellar-polymer projects. However, one way to fulfill the DOE's objectives would be to reevaluate the project based upon considerable new and supplemental data. This course is suggested because the incremental time and expense involved, relative to what has been previously invested, is small, particularly in light of what could be learned. Having reevaluated the project, the following prescription could be used to assess other projects.

Reservoir simulation results from the El Dorado project may be used to estimate the performance of similar HWC micellar-polymer processes in other oil fields only if comparable reservoir fluids and rock are present. The validity of these estimates must be supported by the laboratory and field work described previously, particularly with respect to the chemical slug, drive fluid, and reservoir fluids, as minor variations often greatly influence the process performance. Variations of residual oil saturation, gross layering, and areal heterogeneities should also be considered.

The simulation of the one-eighth of a five-spot symmetry element is the base case from which predictions may be made. Process sensitivity simulations in the center streamtube or core can be used to estimate the effect, for example, of changes in residual oil saturation, preflush volume, slug size, polymer-drive salinity, and surfactant adsorption. The influence of areal and vertical heterogeneities can be estimated from previously published work,⁴⁵ but it is preferable if this is done with the aid of simulation as a function of layering and areal heterogeneity.

Adjustment of fractional oil recovery due to all of the above factors should be made for the base case. These adjustments might be, for example, increasing oil recovery by injecting a larger volume of slug or a different preflush, or accounting for better sweep efficiency. With estimated fractional reduction in overall residual oil saturation, a field-wide capillary number can be identified from the Admire desaturation curve for the nonwetting phase as presented in Figure 15. A desaturation curve for the prospect field must then be developed from relative permeability measurements, or (preferably) from laboratory coreflood data, and the reduction in residual oil at the same capillary number as identified for the Admire sand will approximate the recovery for the prospect field. A check on the approximated field capillary number can be made with the method developed by Lake and Pope⁴⁶ in which capillary number is estimated with data on absolute permeability, depth, and well spacing.

REFERENCES

1. "El Dorado Micellar-Polymer Demonstration Project - First Annual Report," BERC/TPR-75/1, U. S. Energy Research & Development Administration (October 1975) II-144.
2. First Annual Report, p. II-107.
3. "El Dorado Micellar-Polymer Demonstration Project - Second Annual Report," BERC/TPR-76/4, U. S. Department of Energy (November 1976) II-23, -24, -25.
4. Gupta, S. P. and S. P. Trushenski: "Micellar Flooding - Compositional Effects on Oil Displacement," Society of Petroleum Engineers Journal, (April 1979) 116-128.
5. Stegemeier, G. L.: "Mechanisms of Entrapment and Mobilization of Oil in Porous Media," Improved Oil Recovery by Surfactant and Polymer Flooding, D. O. Shah and R. S. Schechter, eds., Academic Press, New York (1977) 55-91.
6. "El Dorado Micellar-Polymer Demonstration Project - Third Annual Report," BERC/TPR-77/2, U. S. Department of Energy (February 1978) II-43, -44, -45.
7. First Annual Report, p. I-13.
8. First Annual Report, p. II-273.
9. First Annual Report, pp. II-9, -10.
10. Second Annual Report, p. I-7.
11. "El Dorado Micellar-Polymer Project - Monthly Technical Report for the Period September 1979," Cities Service Company, DOE/ET/13070-50 (November 1979).

11. Nelson, R. C. and G. A. Pope: "Phase Relationships in Chemical Flooding," Society of Petroleum Engineers Journal (October 1978) 325-338.
12. Pope, G. A. and R. C. Nelson: "A Chemical Flooding Compositional Simulator," Society of Petroleum Engineers Journal (October 1978) 339-354.
13. Reed, R. L. and R. N. Healy: "Some Physicochemical Aspects of Microemulsion Flooding - A Review," Improved Oil Recovery by Surfactant and Polymer Flooding, D. O. Shah and R. S. Schechter, eds., Academic Press, New York (1977) 383-437.
14. Nelson, R. C.: "Further Studies on Phase Relationships in Chemical Flooding," paper presented at the Third International Conference on Surface and Colloid Science, Stockholm, August 1979.
15. Nelson, R. C.: "The Salinity Requirement Diagram - A Useful Tool in Chemical Flooding Research and Development," paper SPE 8824 presented at the First Joint SPE/DOE Symposium on Enhanced Oil Recovery, Tulsa, Oklahoma, April 1980.
16. "Enhanced Oil Recovery and Improved Drilling Technology," Progress Review Number 17, DOE/BETC-79/1 (December 31, 1978) 48.
17. Lake, L. W. and G. A. Pope: "Selection of Reservoirs Amenable to Micellar Flooding," First Annual Report, Appendix I, "Identification of Micellar-Polymer Candidate Reservoirs," U. S. Department of Energy (in press) pp. 3-6.
18. First Annual Report, p. I-29.
19. Hill, H. J. and L. W. Lake: "Cation Exchange in Chemical Flooding," Society of Petroleum Engineers Journal (December 1978) 445-456.
20. Third Annual Report, p. II-5.
21. J. Vairogs (Cities Service Company), personal communication.

22. Healy, R. N., R. L. Reed, and D. G. Stenmark: "Multiphase Microemulsion Systems," Society of Petroleum Engineers Journal (March 1976) 147-160.
23. Glinsmann, G. R.: "Surfactant Flooding with Microemulsions Formed In Situ - Effect of Oil Characteristics," paper SPE 8326 presented at SPE 54th Annual Fall Meeting, Las Vegas, Nevada, September 1979.
24. Third Annual Report, p. II-7.
25. Pope, G. A., K. Tsaur, R. S. Schechter, and B. Wang: "The Effect of Several Polymers on the Phase Behavior of Micellar Fluids," paper SPE 8826 presented at the First Joint SPE/DOE Symposium on Enhanced Oil Recovery, Tulsa, Oklahoma, April 1980.
26. Odeh, A. S. and H. T. Yang: "Flow of Non-Newtonian Power-Law Fluids Through Porous Media," Society of Petroleum Engineers Journal (June 1979) 155-163.
27. Third Annual Report, p. I-56.
28. Lake, L. W. and G. J. Hirasaki: "Taylor's Dispersion in Stratified Porous Media," paper SPE 8436 presented at SPE 54th Annual Fall Meeting, Las Vegas, Nevada, September 1979.
29. Second Annual Report, p. I-8.
30. Todd, M. R. and C. A. Chase: "A Numerical Simulator for Predicting Chemical Flood Performance," paper SPE 7691 presented at SPE 52nd Annual Fall Meeting, Denver, Colorado, September 1977.
31. Brigham, W. E., P. W. Reed, and J. N. Dew: "Experiments on Mixing During Miscible Displacement in Porous Media," Society of Petroleum Engineers Journal (March 1961).

32. Hirasaki, G. J., H. R. van Domselarr, and R. C. Nelson: "Evaluation of the Salinity Gradient Concept in Surfactant Flooding," paper SPE 8825 presented at the First Joint SPE/DOE Symposium on Enhanced Oil Recovery, Tulsa, Oklahoma, April 1980.
33. Kellerhals, G. E.: "Laboratory Core Floods to Support the El Dorado Micellar-Polymer Project," paper SPE 8197 presented at SPE 54th Annual Fall Meeting, Las Vegas, Nevada, September 1979.
34. Johnson, E. F., D. P. Bossler, and V. O. Naumann: "Calculation of Relative Permeability from Displacement Experiments," Transactions, AIME (1959) Vol. 216, 370-372.
35. Pasquarelli, C. H., P. R. Brauer, D. T. Wasan, M. Ciempil, and J. P. Perl: "The Role of Acidic, High Molecular Weight Crude Components in Enhanced Oil Recovery," paper SPE 8895 presented at SPE 50th Annual California Regional Meeting, Los Angeles, California, April 1980.
36. Trushenski, S. P., D. L. Dauben, and D. R. Parrish: "Micellar Flooding - Fluid Propagation, Interaction and Mobility," Society of Petroleum Engineers Journal (November 1974) 633-645.
37. Glover, C. J., M. C. Puerto, J. M. Maerker, and E. L. Sandvik: "Surfactant Phase Behavior and Retention in Porous Media," Society of Petroleum Engineers Journal (June 1979) 183-193.
38. Miller, R. J. and G. W. Rosenwald: "Progress Report for the El Dorado Micellar-Polymer Project, El Dorado, Kansas," paper A-13 presented at the Fifth DOE EOR Symposium, Tulsa, Oklahoma, August 1979.
39. "El Dorado Micellar-Polymer Demonstration Project - Fifth Annual Report," DOE/ET/10370-53, U. S. Department of Energy (February 1980) I-17.
40. "Data for Fluid Samples from El Dorado Micellar-Polymer Demonstration Project Production and Observation Wells," Cities Service Company (March 1980) 25.

41. Third Annual Report, pp. II-49, -80.
42. Rosenwald, G. W. (Cities Service Company), personal communication.
43. "Enhanced Oil Recovery and Improved Drilling Technology," Progress Review No. 21, DOE/BETC-8011 (December 1979) 31.
44. J. Jensen (GURC), personal communication.
45. Craig, F. F. Jr.: "The Reservoir Engineering Aspects of Waterflooding," SPE Monograph No. 3, Dallas, Texas (1971).
46. Lake, L. W. and G. A. Pope: "Status of Micellar-Polymer Field Tests," Petroleum Engineer International (November 1979) 38-60.

TABLE 1

 * INTERCOMP *
 * TERNARY EQUILIBRIUM PHASE DATA *
 * GENERATION AND ANALYSIS MODEL *
 * TEPDATA - RELEASE 1.0.0 *

REMARKS ON TEPDATA INPUT AND OUTPUT

1. THE MAXIMUM NUMBER OF PHASES THAT CAN OCCUR IS TWO WHEN SALINITY VALUE IS EITHER BELOW 'CSUT2M' OR ABOVE 'CSLT2P'. IF SALINITY VALUE IS BETWEEN 'CSUT2M' AND 'CSLT2P', THEN THE MAXIMUM NUMBER OF PHASES THAT CAN OCCUR IS THREE.
2. PHASES OCCURRING AT SALINITIES BELOW 'CSUT2M' VALUE ARE CLASSIFIED AS TYPE II(-). PHASES OCCURRING AT SALINITIES ABOVE THE 'CSLT2P' VALUE ARE CLASSIFIED AS TYPE II(+). PHASES OCCURRING AT SALINITIES BETWEEN 'CSUT2M' AND 'CSLT2P' ARE CLASSIFIED AS TYPE III.
3. THE OPTIMUM SALINITY 'CSOPT' IS THE VALUE OF SALT CONCENTRATION AT WHICH MAXIMUM PHASE MISCIBILITY OCCURS. THUS THE LOWEST HEIGHT 'C3MAX1' (PEAK SURFACTANT CONCENTRATION) OF BINODAL CURVE OCCURS AT OPTIMUM SALINITY 'CSOPT'. THE HEIGHTS OF BINODAL CURVE 'C3MAX0' AND 'C3MAX2' ARE GREATER (HIGHER PEAK SURFACTANT CONCENTRATIONS) THAN 'C3MAX1' AT ZERO SALINITY AND AT TWICE THE OPTIMUM SALINITY.
4. THE INVARIANT POINT IN TYPE III PHASE IS THE POINT ON THE BINODAL CURVE AT WHICH THE RIGHT AND LEFT NODES MERGE.
5. THE PLAIT POINT (ON EITHER THE RIGHT OR LEFT NODE) IS THE POINT ON THE BINODAL CURVE AT WHICH TWO PHASES HAVE IDENTICAL COMPOSITION.
6. THE COMPONENTS WATER, OIL AND SURFACTANT ARE DENOTED AS COMPONENTS C1, C2 AND C3, RESPECTIVELY IN THIS PROGRAM OUTPUT.

 * INTERCOMP *
 * TERNARY EQUILIBRIUM PHASE DATA *
 * GENERATION AND ANALYSIS MODEL *
 * TEPDATA - RELEASE 1.0.0 *

INPUT DATA

EL DORADO PHASE DATA (BNC=.30,.10,.30,PP=.95,.05)

NUMBER OF TYPE II(-) PHASE DIAGRAMS, NDT2M	1
NUMBER OF TYPE III PHASE DIAGRAMS, NDT3	4
NUMBER OF TYPE II(+) PHASE DIAGRAMS, NDT2P	1
NUMBER OF TIE-LINES IN EACH RIGHT NODE, NTRN	10
NUMBER OF TIE-LINES IN EACH LEFT NODE, NTLN	10
FLAG FOR SPECIFICATION OF SALINITIES, ICSE	1
FLAG FOR SAVING PHASE DATA ON DISC FILE (UNIT 10), IGEN	1
FLAG FOR READING PHASE DATA FROM UNIT 10, ICALC	0

LOWER SALINITY FOR TYPE II(-) PHASE DIAGRAMS, CSLI2M	0.004
UPPER SALINITY FOR TYPE II(-) PHASE DIAGRAMS, CSUI2M	0.004
LOWER SALINITY FOR TYPE II(+) PHASE DIAGRAMS, CSLI2P	0.017
UPPER SALINITY FOR TYPE II(+) PHASE DIAGRAMS, CSUI2P	0.017
OPTIMUM SALINITY FOR ALL PHASE DIAGRAMS, CSOPT	0.010

USER-SPECIFIED SALINITIES AT WHICH PHASE DIAGRAMS WILL BE GENERATED:

1. 0.420E-02	2. 0.508E-02	3. 0.777E-02	4. 0.105E-01
5. 0.150E-01	6. 0.168E-01		

PEAK C3 VALUE ON BINODAL CURVE AT SALINITY=0, C3MAX0	0.300
PEAK C3 VALUE ON BINODAL CURVE AT SALINITY=CSOPT, C3MAX1	0.100
PEAK C3 VALUE ON BINODAL CURVE AT SALINITY=2*CSOPT, C3MAX2 ..	0.300
C2 VALUE AT PLAIT POINT IN TYPE II(-) PHASE DIAGRAMS, C2PSR ..	0.950
C2 VALUE AT PLAIT POINT IN TYPE II(+) PHASE DIAGRAMS, C2PSL ..	0.050

NUMBER OF COMPONENTS WHICH DEFINE EFFECTIVE SALINITY, NDCSE . 1

COMPONENT NUMBERS WHICH DEFINE EFFECTIVE SALINITY, IDCSE:

5

COEFFICIENTS OF COMPONENTS WHICH DEFINE EFFECTIVE SALINITY, COCSE:

1.00000

NOTE ON DEFINITION OF EFFECTIVE SALINITY, CSE:

CSE = SUM OF (COEFFICIENT*CONCENTRATION OF COMPONENT I) WHERE I=1, NDCSE

TABLE SHOWING VALUES OF LOWER SALINITY LIMIT FOR TYPE III PHASE ENVIRONMENT

NUMBER OF INDEPENDENT VARIABLES = 0

TABLE 1.(continued)

PAGE 3

 * INTERCOMP *
 * TERNARY EQUILIBRIUM PHASE DATA *
 * GENERATION AND ANALYSIS MODEL *
 * TEPDATA - RELEASE 1.0.0 *

TABLE SHOWING VALUES OF UPPER SALINITY LIMIT FOR TYPE III PHASE ENVIRONMENT

NUMBER OF INDEPENDENT VARIABLES = 0

PAGE 4

 * INTERCOMP *
 * TERNARY EQUILIBRIUM PHASE DATA *
 * GENERATION AND ANALYSIS MODEL *
 * TEPDATA - RELEASE 1.0.0 *

PHASE DIAGRAM NUMBER 1 GENERATED AT SALINITY = 0.420E-02

TYPE II(-) PHASE ENVIRONMENT

INVARIANT POINT COMPOSITION

C1 CONCENTRATION 1.00000
 C2 CONCENTRATION 0.00000
 C3 CONCENTRATION 0.00000

PLAIT POINT COMPOSITION

C1 CONCENTRATION 0.00469
 C2 CONCENTRATION 0.95000
 C3 CONCENTRATION 0.04531

TIE-LINE COMPOSITIONS

OLEIC PHASE COMPOSITION

MICELLAR PHASE COMPOSITION

C1	C2	C3	C1	C2	C3
0.00000	1.00000	0.00000	1.00000	0.00000	0.00000
0.00000	0.99950	0.00050	0.88941	0.02002	0.09057
0.00000	0.99902	0.00098	0.77882	0.06661	0.15457
0.00000	0.99851	0.00148	0.66823	0.13099	0.20078
0.00001	0.99794	0.00205	0.55764	0.21008	0.23228
0.00002	0.99723	0.00275	0.44705	0.30312	0.24983
0.00003	0.99628	0.00369	0.33646	0.41113	0.25241
0.00006	0.99480	0.00514	0.22587	0.53763	0.23649
0.00015	0.99171	0.00815	0.11528	0.69291	0.19181
0.00469	0.95000	0.04531	0.00469	0.95000	0.04531

TABLE 1 (continued)

 * INTERCOMP *
 * TERNARY EQUILIBRIUM PHASE DATA *
 * GENERATION AND ANALYSIS MODEL *
 * TEPCDATA - RELEASE 1.0.0 *

PHASE DIAGRAM NUMBER 2 GENERATED AT SALINITY = 0.508E-02

 TYPE III PHASE ENVIRONMENT

INVARIANT POINT COMPOSITION

 C1 CONCENTRATION 0.78180
 C2 CONCENTRATION 0.06984
 C3 CONCENTRATION 0.14836

PLAIT POINT COMPOSITIONS

 RIGHT NODE LEFT NODE

 C1 CONCENTRATION 0.00457 0.95975
 C2 CONCENTRATION 0.95349 0.00349
 C3 CONCENTRATION 0.04193 0.03676

RIGHT NODE TIE-LINE COMPOSITIONS

OLEIC PHASE COMPOSITION

MICELLAR PHASE COMPOSITION

C1	C2	C3	C1	C2	C3
0.00000	1.00000	0.00000	0.78180	0.06984	0.14836
0.00000	0.99964	0.00036	0.69544	0.12065	0.18391
0.00000	0.99925	0.00075	0.60908	0.18044	0.21049
0.00000	0.99881	0.00119	0.52272	0.24846	0.22882
0.00001	0.99828	0.00171	0.43636	0.32466	0.23898
0.00001	0.99761	0.00238	0.35001	0.40959	0.24040
0.00003	0.99668	0.00330	0.26365	0.50474	0.23162
0.00006	0.99520	0.00474	0.17729	0.61334	0.20937
0.00015	0.99209	0.00776	0.09093	0.74393	0.16514
0.00457	0.95349	0.04193	0.00457	0.95349	0.04193

LEFT NODE TIE-LINE COMPOSITIONS

AQUEOUS PHASE COMPOSITION

MICELLAR PHASE COMPOSITION

C1	C2	C3	C1	C2	C3
1.00000	0.00000	0.00000	0.78180	0.06984	0.14836
0.99948	0.00000	0.00052	0.79595	0.06247	0.14158
0.99886	0.00000	0.00113	0.81071	0.05510	0.13419
0.99810	0.00001	0.00189	0.82620	0.04772	0.12608
0.99713	0.00002	0.00285	0.84257	0.04035	0.11708
0.99583	0.00004	0.00413	0.86008	0.03298	0.10694
0.99397	0.00009	0.00594	0.87912	0.02561	0.09527
0.99099	0.00019	0.00882	0.90040	0.01824	0.08136
0.98499	0.00053	0.01448	0.92547	0.01086	0.06367
0.95975	0.00349	0.03676	0.95975	0.00349	0.03676

TABLE 1 (continued)

 * INTERCOMP *
 * TERNARY EQUILIBRIUM PHASE DATA *
 * GENERATION AND ANALYSIS MODEL *
 * TEPDATA - RELEASE 1.0.0 *

PHASE DIAGRAM NUMBER 3 GENERATED AT SALINITY = 0.777E-02

 TYPE III PHASE ENVIRONMENT

INVARIANT POINT COMPOSITION

 C1 CONCENTRATION 0.53154
 C2 CONCENTRATION 0.28333
 C3 CONCENTRATION 0.18513

PLAIT POINT COMPOSITIONS

 RIGHT NODE LEFT NODE

 C1 CONCENTRATION 0.00448 0.93105
 C2 CONCENTRATION 0.96417 0.01417
 C3 CONCENTRATION 0.03135 0.05479

RIGHT NODE TIE-LINE COMPOSITIONS

OLEIC PHASE COMPOSITION			MICELLAR PHASE COMPOSITION		
C1	C2	C3	C1	C2	C3
0.00000	1.00000	0.00000	0.53154	0.28333	0.18513
0.00000	0.99975	0.00025	0.47298	0.33666	0.19036
0.00000	0.99946	0.00054	0.41442	0.39306	0.19253
0.00000	0.99912	0.00088	0.35585	0.45268	0.19146
0.00001	0.99869	0.00130	0.29729	0.51589	0.18682
0.00001	0.99814	0.00185	0.23873	0.58326	0.17801
0.00003	0.99736	0.00261	0.18017	0.65585	0.16398
0.00006	0.99610	0.00384	0.12160	0.73571	0.14269
0.00018	0.99339	0.00643	0.06304	0.82797	0.10899
0.00448	0.96417	0.03135	0.00448	0.96417	0.03135

LEFT NODE TIE-LINE COMPOSITIONS

AQUEOUS PHASE COMPOSITION			MICELLAR PHASE COMPOSITION		
C1	C2	C3	C1	C2	C3
1.00000	0.00000	0.00000	0.53154	0.28333	0.18513
0.99910	0.00000	0.00090	0.56592	0.25343	0.18066
0.99802	0.00002	0.00196	0.60156	0.22352	0.17492
0.99672	0.00005	0.00324	0.63865	0.19361	0.16774
0.99506	0.00010	0.00483	0.67744	0.16370	0.15886
0.99287	0.00021	0.00692	0.71832	0.13380	0.14789
0.98974	0.00043	0.00963	0.76190	0.10389	0.13421
0.98472	0.00092	0.01436	0.80929	0.07398	0.11673
0.97455	0.00240	0.02305	0.86290	0.04407	0.09303
0.93105	0.01417	0.05479	0.93105	0.01417	0.05479

TABLE 1 (continued)

 * INTERCOMP *
 * TERNARY EQUILIBRIUM PHASE DATA *
 * GENERATION AND ANALYSIS MODEL *
 * TEPDATA - RELEASE 1.0.0 *

PHASE DIAGRAM NUMBER 4 GENERATED AT SALINITY = 0.105E-01

 TYPE III PHASE ENVIRONMENT

INVARIANT POINT COMPOSITION

C1 CONCENTRATION 0.39919
 C2 CONCENTRATION 0.50079
 C3 CONCENTRATION 0.10001

PLAIT POINT COMPOSITIONS

	RIGHT NODE	LEFT NODE
C1 CONCENTRATION	0.00678	0.94063
C2 CONCENTRATION	0.97504	0.02504
C3 CONCENTRATION	0.01818	0.03433

RIGHT NODE TIE-LINE COMPOSITIONS

GLEIC PHASE COMPOSITION

MICELLAR PHASE COMPOSITION

C1	C2	C3	C1	C2	C3
0.00000	1.00000	0.00000	0.39919	0.50079	0.10001
0.00000	0.99981	0.00018	0.35559	0.54586	0.09855
0.00000	0.99960	0.00040	0.31199	0.59189	0.09612
0.00001	0.99933	0.00066	0.26839	0.63898	0.09263
0.00002	0.99900	0.00098	0.22479	0.68729	0.08792
0.00004	0.99856	0.00140	0.18118	0.73707	0.08174
0.00008	0.99793	0.00199	0.13758	0.78873	0.07369
0.00017	0.99688	0.00295	0.09398	0.84306	0.06296
0.00049	0.99459	0.00493	0.05038	0.90194	0.04768
0.00678	0.97504	0.01818	0.00678	0.97504	0.01818

LEFT NODE TIE-LINE COMPOSITIONS

AQUEOUS PHASE COMPOSITION

MICELLAR PHASE COMPOSITION

C1	C2	C3	C1	C2	C3
1.00000	0.00000	0.00000	0.39919	0.50079	0.10001
0.99933	0.00001	0.00066	0.45148	0.44793	0.10059
0.99854	0.00004	0.00142	0.50502	0.39507	0.09991
0.99759	0.00011	0.00230	0.55988	0.34221	0.09791
0.99638	0.00023	0.00339	0.61620	0.28935	0.09445
0.99476	0.00046	0.00478	0.67420	0.23649	0.08932
0.99241	0.00090	0.00669	0.73424	0.18362	0.08213
0.98852	0.00187	0.00961	0.79702	0.13076	0.07221
0.98025	0.00465	0.01510	0.86406	0.07790	0.05803
0.94063	0.02504	0.03433	0.94063	0.02504	0.03433

TABLE 1 (continued)

 * INTERCOMP *
 * TERNARY EQUILIBRIUM PHASE DATA *
 * GENERATION AND ANALYSIS MODEL *
 * TEPDATA - RELEASE 1.0.0 *

PHASE DIAGRAM NUMBER 5 GENERATED AT SALINITY = 0.150E-01

 TYPE III PHASE ENVIRONMENT

INVARIANT POINT COMPOSITION

 C1 CONCENTRATION 0.03883
 C2 CONCENTRATION 0.85476
 C3 CONCENTRATION 0.10641

PLAIT POINT COMPOSITIONS

	RIGHT NODE	LEFT NODE
	-----	-----
C1 CONCENTRATION	0.00015	0.84619
C2 CONCENTRATION	0.99274	0.04274
C3 CONCENTRATION	0.00711	0.11107

RIGHT NODE TIE-LINE COMPOSITIONS

GLEIC PHASE COMPOSITION

MICELLAR PHASE COMPOSITION

	C1	C2	C3		C1	C2	C3
-----	0.00000	1.00000	0.00000	-----	0.03883	0.85476	0.10641
	0.00000	0.99997	0.00003		0.03453	0.86455	0.10092
	0.00000	0.99994	0.00006		0.03024	0.87478	0.09499
	0.00000	0.99990	0.00010		0.02594	0.88555	0.08852
	0.00000	0.99985	0.00015		0.02164	0.89699	0.08137
	0.00000	0.99978	0.00022		0.01734	0.90932	0.07334
	0.00000	0.99967	0.00033		0.01304	0.92288	0.06408
	0.00000	0.99950	0.00050		0.00875	0.93835	0.05291
	0.00000	0.99912	0.00088		0.00445	0.95744	0.03811
-----	0.00015	0.99274	0.00711	-----	0.00015	0.99274	0.00711

LEFT NODE TIE-LINE COMPOSITIONS

AQUEOUS PHASE COMPOSITION

MICELLAR PHASE COMPOSITION

	C1	C2	C3		C1	C2	C3
-----	1.00000	0.00000	0.00000	-----	0.03883	0.85476	0.10641
	0.99639	0.00004	0.00357		0.08584	0.76454	0.14962
	0.99259	0.00016	0.00726		0.14381	0.67431	0.18188
	0.98834	0.00038	0.01129		0.21091	0.58409	0.20500
	0.98333	0.00075	0.01591		0.28646	0.49386	0.21968
	0.97709	0.00139	0.02152		0.37050	0.40364	0.22586
	0.96866	0.00251	0.02883		0.46389	0.31341	0.22270
	0.95586	0.00476	0.03939		0.56872	0.22319	0.20809
	0.93168	0.01051	0.05781		0.69011	0.13296	0.17692
-----	0.84619	0.04274	0.11107	-----	0.84619	0.04274	0.11107

TABLE 1 (continued)

 * INTERCOMP *
 * TERNARY EQUILIBRIUM PHASE DATA *
 * GENERATION AND ANALYSIS MODEL *
 * TEPDATA - RELEASE 1.0.0 *

PHASE DIAGRAM NUMBER 6 GENERATED AT SALINITY = 0.168E-01

 TYPE II(+) PHASE ENVIRONMENT

INVARIANT POINT COMPOSITION

 C1 CONCENTRATION 0.00000
 C2 CONCENTRATION 1.00000
 C3 CONCENTRATION 0.00000

PLAIT POINT COMPOSITION

 C1 CONCENTRATION 0.81316
 C2 CONCENTRATION 0.05000
 C3 CONCENTRATION 0.13684

TIF-LINE COMPOSITIONS

 AQUEOUS PHASE COMPOSITION

C1	C2	C3
1.00000	0.00000	0.00000
0.99397	0.00008	0.00595
0.98819	0.00029	0.01152
0.98208	0.00066	0.01727
0.97514	0.00124	0.02362
0.96673	0.00217	0.03110
0.95566	0.00374	0.04060
0.93930	0.00673	0.05396
0.90955	0.01397	0.07649
0.81316	0.05000	0.13684

 MICELLAR PHASE COMPOSITION

C1	C2	C3
0.00000	1.00000	0.00000
0.01843	0.89444	0.08713
0.06156	0.78889	0.14955
0.12129	0.68333	0.19538
0.19464	0.57778	0.22758
0.28070	0.47222	0.24708
0.38001	0.36667	0.25333
0.49492	0.26111	0.24397
0.63171	0.15556	0.21274
0.81316	0.05000	0.13684

 * INTERCOMP *
 * TERNARY EQUILIBRIUM PHASE DATA *
 * GENERATION AND ANALYSIS MODEL *
 * TEPDATA - RELEASE 1.0.0 *

EL DORADO PHASE DATA (BNC=.30,.10,.30,PP=.95,.05)

THE FOLLOWING VALUES ARE SAVED ON A DISC FILE (UNIT NO. 10)
 FOR INPUT OF PHASE EQUILIBRIUM DATA TO INTERCOMP'S CFTE SIMULATOR

1	4	1						
0.420E-02	0.508E-02	0.777E-02	0.105E-01	0.150E-01	0.168E-01			
0.0000000	0.0698413	0.2833333	0.5007937	0.8547619	1.0000000			
0.0000000	0.1483635	0.1851264	0.1000137	0.1064072	0.0000000			
0.0000000	0.0200234	0.0666081	0.1309872	0.2100777	0.3031239	0.4111300	0.5376339	
0.6929107	0.9500000	0.9917057	0.9947982	0.9962791	0.9972313	0.9979379	0.9985135	
0.9990187	0.9994968	1.0000000						
0.0000000	0.0905664	0.1545716	0.2007822	0.2322816	0.2498251	0.2524089	0.2364947	
0.1918077	0.0453082	0.0081489	0.0051441	0.0036912	0.0027522	0.0020529	0.0014817	
0.0009792	0.0005026	0.0000000						
0.0698413	0.1206486	0.1804351	0.2484610	0.3246565	0.4095920	0.5047357	0.6133384	
0.7439286	0.9534921	0.9920861	0.9952046	0.9966772	0.9976061	0.9982786	0.9988085	
0.9992520	0.9996417	1.0000000						
0.1483635	0.1839140	0.2104854	0.2288174	0.2389797	0.2404020	0.2316162	0.2093713	
0.1651390	0.0419333	0.0077632	0.0047394	0.0032958	0.0023799	0.0017141	0.0011880	
0.0007466	0.0003580	0.0000000						
0.2833333	0.3366643	0.3930551	0.4526836	0.5158896	0.5832640	0.6558526	0.7357098	
0.8279703	0.9641667	0.9933893	0.9960985	0.9973590	0.9981392	0.9986917	0.9991156	
0.9994589	0.9997482	1.0000000						
0.1851264	0.1903577	0.1925291	0.1914628	0.1868190	0.1780069	0.1639805	0.1426855	
0.1089872	0.0313531	0.0064280	0.0038365	0.0026110	0.0018458	0.0013008	0.0008810	
0.0005398	0.0002515	0.0000000						
0.5007937	0.5458595	0.5918876	0.6389800	0.6872930	0.7370724	0.7887318	0.8430564	
0.9019395	0.9750397	0.9945861	0.9968807	0.9979263	0.9985606	0.9990012	0.9993330	
0.9995967	0.9998146	1.0000000						
0.1000137	0.0985495	0.0961232	0.0926325	0.0879213	0.0817436	0.0736859	0.0629631	
0.0476817	0.0181832	0.0049262	0.0029454	0.0019940	0.0014002	0.0009796	0.0006583	
0.0004001	0.0001848	0.0000000						
0.8547619	0.8645484	0.8747781	0.8855461	0.8969893	0.9093162	0.9228766	0.9383459	
0.9574404	0.9927381	0.9991152	0.9994995	0.9996720	0.9997755	0.9998463	0.9998987	
0.9999396	0.9999726	1.0000000						
0.1064072	0.1009186	0.0949869	0.0885168	0.0813716	0.0733426	0.0640802	0.0529088	
0.0381123	0.0071125	0.0008826	0.0004997	0.0003276	0.0002244	0.0001536	0.0001013	
0.0000604	0.0000274	0.0000000						
1.0000000	1.0000000	1.0000000	1.0000000	1.0000000	1.0000000	1.0000000	1.0000000	
1.0000000	1.0000000	1.0000000	1.0000000	1.0000000	1.0000000	1.0000000	1.0000000	
1.0000000	1.0000000	1.0000000						
0.0000000	0.0000000	0.0000000	0.0000000	0.0000000	0.0000000	0.0000000	0.0000000	
0.0000000	0.0000000	0.0000000	0.0000000	0.0000000	0.0000000	0.0000000	0.0000000	
0.0000000	0.0000000	0.0000000						
0.0000000	0.0200234	0.0666081	0.1309872	0.2100777	0.3031239	0.4111300	0.5376339	
0.6929107	0.9500000							
0.0000000	0.0055500	0.0063350	0.0073797	0.0088381	0.0110167	0.0146237	0.0217513	
0.0424849	1.0000000							

 * INTERCOMP *
 * TERNARY EQUILIBRIUM PHASE DATA *
 * GENERATION AND ANALYSIS MODEL *
 * TEPDATA - RELEASE 1.0.0 *

0.0698413	0.1206486	0.1804351	0.2484610	0.3246565	0.4095920	0.5047357	0.6133384
0.7439286	0.9534921						
0.0000000	0.0019463	0.0035471	0.0051917	0.0071725	0.0098995	0.0142296	0.0226362
0.0470099	1.0000000						
0.2833333	0.3366643	0.3930551	0.4526836	0.5158896	0.5832640	0.6558526	0.7357098
0.8279703	0.9641667						
0.0000000	0.0013211	0.0028039	0.0046013	0.0069629	0.0103691	0.0159227	0.0268881
0.0589790	1.0000000						
0.5007937	0.5458595	0.5918876	0.6389800	0.6872930	0.7370724	0.7887318	0.8430564
0.9019395	0.9750397						
0.0000000	0.0018748	0.0041623	0.0071065	0.0111413	0.0171287	0.0270613	0.0467792
0.1033150	1.0000000						
0.8547619	0.8645484	0.8747781	0.8855461	0.8969893	0.9093162	0.9228766	0.9383459
0.9574404	0.9927381						
0.0000000	0.0002716	0.0006360	0.0011439	0.0018882	0.0030596	0.0051130	0.0094449
0.0231566	1.0000000						
1.0000000	1.0000000	1.0000000	1.0000000	1.0000000	1.0000000	1.0000000	1.0000000
1.0000000	1.0000000						
0.0000000	0.0000000	0.0000000	0.0000000	0.0000000	0.0000000	0.0000000	0.0000000
0.0000000	1.0000000						
19							
1.0000000	1.0000000	1.0000000	1.0000000	1.0000000	1.0000000	1.0000000	1.0000000
1.0000000	1.0000000	1.0000000	1.0000000	1.0000000	1.0000000	1.0000000	1.0000000
1.0000000	1.0000000	1.0000000					
0.0000000	0.0000000	0.0000000	0.0000000	0.0000000	0.0000000	0.0000000	0.0000000
0.0000000	0.0000000	0.0000000	0.0000000	0.0000000	0.0000000	0.0000000	0.0000000
0.0000000	0.0000000	0.0000000					
0.7817952	0.7959513	0.8107124	0.8261973	0.8425721	0.8600833	0.8791247	0.9004035
0.9254702	0.9597505	0.9849940	0.9909873	0.9939691	0.9958273	0.9971256	0.9980982
0.9988620	0.9994826	1.0000000					
0.1483635	0.1415796	0.1341906	0.1260779	0.1170751	0.1069361	0.0952668	0.0813602
0.0636656	0.0367574	0.0144781	0.0088181	0.0059428	0.0041302	0.0028541	0.0018929
0.0011348	0.0005167	0.0000000					
0.5315403	0.5659176	0.6015584	0.6386451	0.6774362	0.7183163	0.7619010	0.8092930
0.8629961	0.9310471	0.9745535	0.9847180	0.9897400	0.9928689	0.9950624	0.9967154
0.9980236	0.9990963	1.0000000					
0.1851264	0.1806565	0.1749231	0.1677438	0.1588601	0.1478874	0.1342101	0.1167255
0.0930298	0.0547862	0.0230507	0.0143615	0.0098309	0.0069192	0.0048344	0.0032383
0.0019595	0.0009001	0.0000000					
0.3991927	0.4514762	0.5050150	0.5598799	0.6162009	0.6741970	0.7342416	0.7970240
0.8640646	0.9406312	0.9802496	0.9885249	0.9924079	0.9947579	0.9963781	0.9975887
0.9985447	0.9993314	1.0000000					
0.1000137	0.1005917	0.0999144	0.0979111	0.0944517	0.0893171	0.0821341	0.0722132
0.0580342	0.0343291	0.0151010	0.0096085	0.0066906	0.0047826	0.0033913	0.0023049
0.0014152	0.0006599	0.0000000					
0.0388309	0.0858390	0.1438087	0.2109140	0.2864567	0.3704978	0.4638857	0.5687247
0.6901136	0.8461907	0.9316801	0.9558555	0.9686584	0.9770886	0.9833339	0.9883354
0.9925866	0.9963949	1.0000000					
0.1064072	0.1496240	0.1818791	0.2049987	0.2196808	0.2258646	0.2227016	0.2080875
0.1769234	0.1110712	0.0578061	0.0393868	0.0288268	0.0215218	0.0159114	0.0112868
0.0072579	0.0035677	0.0000000					

TABLE 2 (continued)

 * INTERCOMP *
 * TERNARY EQUILIBRIUM PHASE DATA *
 * GENERATION AND ANALYSIS MODEL *
 * TEPDATA - RELEASE 1.0.0 *

0.0000000	0.0184275	0.0615576	0.1212891	0.1946381	0.2806967	0.3800076	0.4949230
0.6317052	0.8131578	0.9095487	0.9393044	0.9556573	0.9667252	0.9751400	0.9820753
0.9881894	0.9939691	1.0000000					
0.0000000	0.0871280	0.1495535	0.1953776	0.2275841	0.2470810	0.2533258	0.2439659
0.2127392	0.1368422	0.0764862	0.0539641	0.0405981	0.0311022	0.0236180	0.0172656
0.0115190	0.0059535	0.0000000					
10							
1.0000000	1.0000000	1.0000000	1.0000000	1.0000000	1.0000000	1.0000000	1.0000000
1.0000000	1.0000000						
0.0000000	0.0000000	0.0000000	0.0000000	0.0000000	0.0000000	0.0000000	0.0000000
0.0000000	1.0000000						
0.7817952	0.7959513	0.8107124	0.8261973	0.8425721	0.8600833	0.8791247	0.9004035
0.9254702	0.9597505						
0.0000000	0.0036496	0.0084563	0.0150135	0.0243787	0.0386233	0.0623807	0.1083832
0.2274089	1.0000000						
0.5315403	0.5659176	0.6015584	0.6386451	0.6774362	0.7183163	0.7619010	0.8092930
0.8628961	0.9310471						
0.0000000	0.0049825	0.0112020	0.0193052	0.0304316	0.0467872	0.0732498	0.1230368
0.2477772	1.0000000						
0.3991927	0.4514762	0.5050150	0.5598799	0.6162009	0.6741970	0.7342416	0.7970240
0.8640646	0.9406312						
0.0000000	0.0065601	0.0141641	0.0235408	0.0359046	0.0535458	0.0814592	0.1330576
0.2602088	1.0000000						
0.0388309	0.0858390	0.1438087	0.2109140	0.2864567	0.3704978	0.4638857	0.5687247
0.6901136	0.8461907						
0.0000000	0.0238441	0.0399050	0.0550579	0.0724297	0.0952863	0.1294413	0.1892802
0.3267296	1.0000000						
0.0000000	0.0184275	0.0615576	0.1212891	0.1946381	0.2806967	0.3800076	0.4949230
0.6317052	0.8131578						
0.0000000	0.0683305	0.0770228	0.0883705	0.1037770	0.1258786	0.1602603	0.2211954
0.3595304	1.0000000						
1							
5							
1.0000000							
0							
0							

TABLE 3

 * JNIFRCOMP *****
 * THREE_PHASE_RELATIVE_PERMEABILITY_MODEL *
 * HELPFRM - RELEASE 1.0.0 *

EL DORADO PROJECT - GURC SIMULATION STUDY
 HIGH NCAP KR(ADMPIE DATA FROM MP-124)

SATURATION TABLES WILL CONSIST OF 6 Y-ENTRIES WITH A SPACING OF .200
 WITH 5 ENTRIES BETWEEN ZERO AND SNWR WITH A SPACING OF .0550

THIS RUN WILL OUTPUT A DATA FILE ON UNIT 9

DATA:

RESIDUAL WETTING SATURATION - .2380
 RESIDUAL NON-WET SATURATION - .3300
 WETTING RELATIVE PERM AT SOR - 0.194
 NON-WET RELATIVE PERM AT SWR - 0.481
 WETTING CURVATURE EXPONENT - 2.568
 NON-WET CURVATURE EXPONENT - 1.941

CAPILLARY NUMBERS WILL BE CALCULATED INTERNALLY

OIL SATURATION X-ENTRIES WILL BE CALCULATED INTERNALLY

WATER SATURATION X-ENTRIES WILL BE CALCULATED INTERNALLY

CALCULATED CAPILLARY NUMBERS ARE

- 1 0.201E-04
- 2 0.299E-04
- 3 0.528E-03
- 4 0.934E-02
- 5 0.139E-01

CALCULATED PARAMETERS FROM DESATURATION CURVE

CAP NO.	SNWR	SWR	N	P
0.201E-04	0.3300	0.2380	1.9410	2.5680
0.299E-04	0.3087	0.2380	1.8802	2.5680
0.528E-03	0.1543	0.1267	1.4401	1.8347
0.934E-02	0.0000	0.0154	1.0000	1.1014
0.139E-01	0.0000	0.0000	1.0000	1.0000

TABLE 3 (continued)

CALCULATED OIL SATURATION X-ENTRY VALUES

1	0.0000
2	0.0550
3	0.1100
4	0.1543
5	0.1650
6	0.2000
7	0.2200
8	0.2750
9	0.3087
10	0.3300
11	0.4000
12	0.6000
13	0.7620
14	0.8000
15	0.8733
16	0.9846
17	1.0000

intercomp

CALCULATED OIL SATURATION Y-ENTRY VALUES

1	0.0000
2	0.0154
3	0.1267
4	0.2000
5	0.2380
6	0.4000
7	0.6000
8	0.6700
9	0.6913
10	0.8000
11	0.8457
12	1.0000

CALCULATED WATER SATURATION X-ENTRY VALUES

1	0.0000
2	0.0154
3	0.1267
4	0.2000
5	0.2380
6	0.4000
7	0.6000
8	0.6700
9	0.6913
10	0.8000
11	0.8457
12	1.0000

TABLE 3 (continued)

CALCULATED WATER SATURATION Y-ENTRY VALUES

1	0.0000
2	0.1543
3	0.2000
4	0.3087
5	0.3300
6	0.4000
7	0.6000
8	0.7620
9	0.8000
10	0.8733
11	0.9846
12	1.0000

CALCULATED MICELLAR SATURATION X-ENTRY VALUES

1	0.0000
2	0.0154
3	0.1267
4	0.1543
5	0.2000
6	0.2380
7	0.3087
8	0.3300
9	0.4000
10	0.6000
11	0.6700
12	0.6913
13	0.8000
14	0.8457
15	1.0000

CALCULATED MICELLAR SATURATION Y-ENTRY VALUES

1	0.0000
2	0.1543
3	0.2000
4	0.3087
5	0.3300
6	0.4000
7	0.6000
8	0.6700
9	0.6913
10	0.7620
11	0.8000
12	0.8457
13	0.8733
14	0.9846
15	1.0000

TABLE 3 (continued)

CALCULATED AQUEOUS RELATIVE PERMEABILITIES

CAPILLARY NUMBER = 0.201E-04

SO	SA	0.0000	0.0154	0.1267	0.2000	0.2300	0.4000	0.6000	0.6700	0.6914	0.8000	0.8457	1.0000
0.0000	0.0000	0.0000	0.0000	0.0000	0.0000	0.0150	0.1232	0.1940	0.1940	0.2462	0.5115	0.6231	1.0000
0.1543	0.0000	0.0000	0.0000	0.0000	0.0000	0.0423	0.1940	0.1940	0.1940	0.2462	0.5115	0.6231	0.6231
0.2000	0.0000	0.0000	0.0000	0.0000	0.0000	0.0634	0.1940	0.1940	0.1940	0.2462	0.5115	0.5115	0.5115
0.3086	0.0000	0.0000	0.0000	0.0000	0.0000	0.1940	0.1940	0.1940	0.1940	0.2462	0.2462	0.2462	0.2462
0.3300	0.0000	0.0000	0.0000	0.0000	0.0000	0.1940	0.1940	0.1940	0.1940	0.1940	0.1940	0.1940	0.1940
0.4000	0.0000	0.0000	0.0000	0.0000	0.0000	0.0771	0.1232	0.1232	0.1232	0.1232	0.1232	0.1232	0.1232
0.6000	0.0000	0.0000	0.0000	0.0000	0.0000	0.0156	0.0156	0.0156	0.0156	0.0156	0.0156	0.0156	0.0156
0.7620	0.0000	0.0000	0.0000	0.0000	0.0000	0.0000	0.0000	0.0000	0.0000	0.0000	0.0000	0.0000	0.0000
0.8000	0.0000	0.0000	0.0000	0.0000	0.0000	0.0000	0.0000	0.0000	0.0000	0.0000	0.0000	0.0000	0.0000
0.8733	0.0000	0.0000	0.0000	0.0000	0.0000	0.0000	0.0000	0.0000	0.0000	0.0000	0.0000	0.0000	0.0000
0.9846	0.0000	0.0000	0.0000	0.0000	0.0000	0.0000	0.0000	0.0000	0.0000	0.0000	0.0000	0.0000	0.0000
1.0000	0.0000	0.0000	0.0000	0.0000	0.0000	0.0000	0.0000	0.0000	0.0000	0.0000	0.0000	0.0000	0.0000

CAPILLARY NUMBER = 0.299E-04

SO	SA	0.0000	0.0154	0.1267	0.2000	0.2300	0.4000	0.6000	0.6700	0.6914	0.8000	0.8457	1.0000
0.0000	0.0000	0.0000	0.0000	0.0000	0.0000	0.0175	0.1381	0.2175	0.2175	0.2462	0.5115	0.6231	1.0000
0.1543	0.0000	0.0000	0.0000	0.0000	0.0000	0.0462	0.2462	0.2462	0.2462	0.2462	0.5115	0.6231	0.6231
0.2000	0.0000	0.0000	0.0000	0.0000	0.0000	0.0679	0.2462	0.2462	0.2462	0.2462	0.5115	0.5115	0.5115
0.3086	0.0000	0.0000	0.0000	0.0000	0.0000	0.2462	0.2462	0.2462	0.2462	0.2462	0.2462	0.2462	0.2462
0.3300	0.0000	0.0000	0.0000	0.0000	0.0000	0.1791	0.2125	0.2175	0.2175	0.2175	0.2175	0.2175	0.2175
0.4000	0.0000	0.0000	0.0000	0.0000	0.0000	0.0781	0.1381	0.1381	0.1381	0.1381	0.1381	0.1381	0.1381
0.6000	0.0000	0.0000	0.0000	0.0000	0.0000	0.0175	0.0175	0.0175	0.0175	0.0175	0.0175	0.0175	0.0175
0.7620	0.0000	0.0000	0.0000	0.0000	0.0000	0.0000	0.0000	0.0000	0.0000	0.0000	0.0000	0.0000	0.0000
0.8000	0.0000	0.0000	0.0000	0.0000	0.0000	0.0000	0.0000	0.0000	0.0000	0.0000	0.0000	0.0000	0.0000
0.8733	0.0000	0.0000	0.0000	0.0000	0.0000	0.0000	0.0000	0.0000	0.0000	0.0000	0.0000	0.0000	0.0000
0.9846	0.0000	0.0000	0.0000	0.0000	0.0000	0.0000	0.0000	0.0000	0.0000	0.0000	0.0000	0.0000	0.0000
1.0000	0.0000	0.0000	0.0000	0.0000	0.0000	0.0000	0.0000	0.0000	0.0000	0.0000	0.0000	0.0000	0.0000

TABLE 3 (continued)

CAPILLARY NUMBER = 0.529E-03	
SD	0.0000 0.0154 0.1267 0.2000 0.2300 0.4000 0.6000 0.6700 0.6914 0.8300 0.8457 1.0000
0.0000	0.0000 0.0000 0.0000 0.0000 0.0203 0.1056 0.2493 0.3726 0.4000 0.5524 0.6281 1.0000
0.1543	0.0000 0.0000 0.0000 0.0103 0.0308 0.1621 0.4474 0.5773 0.6200 0.6231 0.6231 0.6231
0.2000	0.0000 0.0000 0.0000 0.0102 0.0307 0.1616 0.4467 0.5373 0.5402 0.5524 0.5524 0.5524
0.3086	0.0000 0.0000 0.0000 0.0101 0.0305 0.1508 0.3713 0.3939 0.4000 0.4000 0.4000 0.4000
0.3300	0.0000 0.0000 0.0000 0.0101 0.0304 0.1506 0.3491 0.3726 0.3726 0.3726 0.3726 0.3726
0.4000	0.0000 0.0000 0.0000 0.0100 0.0303 0.1502 0.2493 0.2493 0.2493 0.2493 0.2493 0.2493
0.5000	0.0000 0.0000 0.0000 0.0139 0.0302 0.1056 0.1056 0.1056 0.1056 0.1056 0.1056 0.1056
0.7620	0.0000 0.0000 0.0000 0.0104 0.0000 0.0203 0.0000 0.0203 0.0000 0.0203 0.0000 0.0203
0.8000	0.0000 0.0000 0.0000 0.0094 0.0094 0.0094 0.0094 0.0094 0.0094 0.0094 0.0094 0.0094
0.8733	0.0000 0.0000 0.0000 0.0000 0.0000 0.0000 0.0000 0.0000 0.0000 0.0000 0.0000 0.0000
0.9846	0.0000 0.0000 0.0000 0.0000 0.0000 0.0000 0.0000 0.0000 0.0000 0.0000 0.0000 0.0000
1.0000	0.0000 0.0000 0.0000 0.0000 0.0000 0.0000 0.0000 0.0000 0.0000 0.0000 0.0000 0.0000
CAPILLARY NUMBER = 0.934E-02	
SD	0.0000 0.0154 0.1267 0.2000 0.2300 0.4000 0.6000 0.6700 0.6914 0.8300 0.8457 1.0000
0.0000	0.0000 0.0000 0.0000 0.0000 0.0000 0.0000 0.0000 0.0000 0.0000 0.0000 0.0000 0.0000
0.1543	0.0000 0.0000 0.0000 0.0000 0.0000 0.0000 0.0000 0.0000 0.0000 0.0000 0.0000 0.0000
0.2000	0.0000 0.0000 0.0000 0.0000 0.0000 0.0000 0.0000 0.0000 0.0000 0.0000 0.0000 0.0000
0.3086	0.0000 0.0000 0.0000 0.0000 0.0000 0.0000 0.0000 0.0000 0.0000 0.0000 0.0000 0.0000
0.3300	0.0000 0.0000 0.0000 0.0000 0.0000 0.0000 0.0000 0.0000 0.0000 0.0000 0.0000 0.0000
0.4000	0.0000 0.0000 0.0000 0.0000 0.0000 0.0000 0.0000 0.0000 0.0000 0.0000 0.0000 0.0000
0.5000	0.0000 0.0000 0.0000 0.0000 0.0000 0.0000 0.0000 0.0000 0.0000 0.0000 0.0000 0.0000
0.7620	0.0000 0.0000 0.0000 0.0000 0.0000 0.0000 0.0000 0.0000 0.0000 0.0000 0.0000 0.0000
0.8000	0.0000 0.0000 0.0000 0.0000 0.0000 0.0000 0.0000 0.0000 0.0000 0.0000 0.0000 0.0000
0.8733	0.0000 0.0000 0.0000 0.0000 0.0000 0.0000 0.0000 0.0000 0.0000 0.0000 0.0000 0.0000
0.9846	0.0000 0.0000 0.0000 0.0000 0.0000 0.0000 0.0000 0.0000 0.0000 0.0000 0.0000 0.0000
1.0000	0.0000 0.0000 0.0000 0.0000 0.0000 0.0000 0.0000 0.0000 0.0000 0.0000 0.0000 0.0000

TABLE 3 (continued)

CAPILLARY NUMBER = 0.139E-01											
50	54	0.0154	0.1267	0.2380	0.4000	0.6000	0.6700	0.6914	0.9000	0.8457	1.0000
0.0000	0.0000	0.0154	0.1267	0.2380	0.4000	0.6000	0.6700	0.6914	0.9000	0.8457	1.0000
0.1543	0.0000	0.0154	0.1267	0.2380	0.4000	0.6000	0.6700	0.6914	0.9000	0.8457	0.8457
0.2000	0.0000	0.0154	0.1267	0.2380	0.4000	0.6000	0.6700	0.6914	0.9000	0.8457	0.8000
0.3086	0.0000	0.0154	0.1267	0.2380	0.4000	0.6000	0.6700	0.6914	0.9000	0.8457	0.5014
0.3300	0.0000	0.0154	0.1267	0.2380	0.4000	0.6000	0.6700	0.6914	0.9000	0.8457	0.5700
0.4000	0.0000	0.0154	0.1267	0.2380	0.4000	0.6000	0.6700	0.6914	0.9000	0.8457	0.5000
0.6000	0.0000	0.0154	0.1267	0.2380	0.4000	0.6000	0.6700	0.6914	0.9000	0.8457	0.4000
0.7620	0.0000	0.0154	0.1267	0.2380	0.4000	0.6000	0.6700	0.6914	0.9000	0.8457	0.2380
0.8000	0.0000	0.0154	0.1267	0.2380	0.4000	0.6000	0.6700	0.6914	0.9000	0.8457	0.2000
0.8733	0.0000	0.0154	0.1267	0.2380	0.4000	0.6000	0.6700	0.6914	0.9000	0.8457	0.1267
0.9846	0.0000	0.0154	0.1267	0.2380	0.4000	0.6000	0.6700	0.6914	0.9000	0.8457	0.0154
1.0000	0.0000	0.0000	0.0000	0.0000	0.0000	0.0000	0.0000	0.0000	0.0000	0.0000	0.0000

TABLE 3 (continued)

CALCULATED OLFIE-RELATIVE PERMEABILITIES

CAPILLARY NUMBER = 0.201E+04

SA	SO	0.0550	0.1100	0.1543	0.1650	0.2000	0.2200	0.2750	0.3086	0.3300	0.4000	0.5000	0.7500	0.8000	0.873
0.0000	0.0000	0.0000	0.0000	0.0000	0.0000	0.0000	0.0000	0.0000	0.0000	0.0000	0.0140	0.1932	0.4813	0.5641	0.723
0.0154	0.0000	0.0000	0.0000	0.0000	0.0000	0.0000	0.0000	0.0000	0.0000	0.0000	0.0154	0.2109	0.4813	0.5641	0.723
0.1267	0.0000	0.0000	0.0000	0.0000	0.0000	0.0000	0.0000	0.0000	0.0000	0.0000	0.0339	0.4096	0.4813	0.5641	0.723
0.2000	0.0000	0.0000	0.0000	0.0000	0.0000	0.0000	0.0000	0.0000	0.0000	0.0000	0.0499	0.4813	0.4813	0.5641	0.550
0.2380	0.0000	0.0000	0.0000	0.0000	0.0000	0.0000	0.0000	0.0000	0.0000	0.0000	0.1155	0.4813	0.4813	0.4813	0.481
0.4000	0.0000	0.0000	0.0000	0.0000	0.0000	0.0000	0.0000	0.0000	0.0000	0.0000	0.0470	0.1032	0.1332	0.1032	0.133
0.6000	0.0000	0.0000	0.0000	0.0000	0.0000	0.0000	0.0000	0.0000	0.0000	0.0000	0.0140	0.0140	0.0140	0.0140	0.0140
0.6700	0.0000	0.0000	0.0000	0.0000	0.0000	0.0000	0.0000	0.0000	0.0000	0.0000	0.0000	0.0000	0.0000	0.0000	0.0000
0.6914	0.0000	0.0000	0.0000	0.0000	0.0000	0.0000	0.0000	0.0000	0.0000	0.0000	0.0000	0.0000	0.0000	0.0000	0.0000
0.8000	0.0000	0.0000	0.0000	0.0000	0.0000	0.0000	0.0000	0.0000	0.0000	0.0000	0.0000	0.0000	0.0000	0.0000	0.0000
0.8457	0.0000	0.0000	0.0000	0.0000	0.0000	0.0000	0.0000	0.0000	0.0000	0.0000	0.0000	0.0000	0.0000	0.0000	0.0000
1.0000	0.0000	0.0000	0.0000	0.0000	0.0000	0.0000	0.0000	0.0000	0.0000	0.0000	0.0000	0.0000	0.0000	0.0000	0.0000
SA	SO	0.0846	1.0000												
0.0000	0.9664	1.0000													
0.0154	0.9664	0.9664													
0.1267	0.7239	0.7239													
0.2000	0.5641	0.5641													
0.2380	0.4813	0.4813													
0.4000	0.1332	0.1332													
0.6000	0.0140	0.0140													
0.6700	0.0000	0.0000													
0.6914	0.0000	0.0000													
0.8000	0.0000	0.0000													
0.8457	0.0000	0.0000													
1.0000	0.0000	0.0000													

TABLE 3 (continued)

CAPILLARY NUMBER = 0.299E-04		0.1100	0.1543	0.1650	0.2000	0.2200	0.2750	0.3086	0.3300	0.4000	0.5000	0.7520	0.8000	0.8733		
SA	SD	0.0000	0.0550	0.1100	0.1543	0.1650	0.2000	0.2200	0.2750	0.3086	0.3300	0.4000	0.5000	0.7520	0.8000	0.8733
0.0000	0.0000	0.0000	0.0000	0.0000	0.0000	-0.0226	-0.0325	-0.0311	-0.0154	0.0000	0.0015	0.0237	0.2095	0.4813	0.5641	0.7239
0.0154	0.0000	0.0000	0.0000	-0.0235	-0.0337	-0.0322	-0.0160	0.0000	0.0017	0.0256	0.2264	0.4813	0.5641	0.7239	0.7239	0.7239
0.1267	0.0000	0.0000	0.0000	-0.0310	-0.0443	-0.0424	-0.0219	0.0000	0.0033	0.0505	0.4569	0.4813	0.5641	0.7239	0.7239	0.7239
0.2000	0.0000	0.0000	0.0000	-0.0313	-0.0447	-0.0423	-0.0212	0.0000	0.0061	0.0919	0.4813	0.4813	0.5641	0.7239	0.7239	0.7239
0.2380	0.0000	0.0000	0.0000	-0.0314	-0.0449	0.0000	0.0000	0.0000	0.0091	0.1356	0.4813	0.4813	0.5641	0.7239	0.7239	0.7239
0.4000	0.0000	0.0000	0.0000	0.0000	0.0000	0.0000	0.0000	0.0000	0.0094	0.0707	0.2095	0.2095	0.2095	0.2095	0.2095	0.2095
0.6000	0.0000	0.0000	0.0000	0.0000	0.0000	0.0000	0.0000	0.0000	0.0021	0.0237	0.0237	0.0237	0.0237	0.0237	0.0237	0.0237
0.6700	0.0000	0.0000	0.0000	0.0000	0.0000	0.0000	0.0000	0.0000	0.0015	0.0015	0.0015	0.0015	0.0015	0.0015	0.0015	0.0015
0.6914	0.0000	0.0000	0.0000	0.0000	0.0000	0.0000	0.0000	0.0000	0.0000	0.0000	0.0000	0.0000	0.0000	0.0000	0.0000	0.0000
0.8000	0.0000	0.0000	0.0000	0.0000	0.0000	0.0000	0.0000	0.0000	0.0000	0.0000	0.0000	0.0000	0.0000	0.0000	0.0000	0.0000
0.8457	0.0000	0.0000	0.0000	0.0000	0.0000	0.0000	0.0000	0.0000	0.0000	0.0000	0.0000	0.0000	0.0000	0.0000	0.0000	0.0000
1.0000	0.0000	0.0000	0.0000	0.0000	0.0000	0.0000	0.0000	0.0000	0.0000	0.0000	0.0000	0.0000	0.0000	0.0000	0.0000	0.0000
SA	SD	0.9846	1.0000													
0.0000	0.9664	1.0000														
0.0154	0.9664	0.9664														
0.1267	0.7239	0.7239														
0.2000	0.5641	0.5641														
0.2380	0.4813	0.4813														
0.4000	0.2095	0.2095														
0.6000	0.0237	0.0237														
0.6700	0.0015	0.0015														
0.6914	0.0000	0.0000														
0.8000	0.0000	0.0000														
0.8457	0.0000	0.0000														
1.0000	0.0000	0.0000														

interco

TABLE 3 (continued)

CAPILLARY NUMBER = 0.52RE-03																
SA	SD	0.0000	0.0550	0.1100	0.1543	0.1650	0.2000	0.2200	0.2750	0.3086	0.3300	0.4000	0.5000	0.7500	0.8000	0.9733
0.0000		0.0000	-0.0975	-0.0435	0.0000	0.0017	0.0137	0.0230	0.0554	0.0789	0.0751	0.1541	0.3635	0.5581	0.6200	0.7233
0.0154		0.0000	-0.0987	-0.0441	0.0000	0.0017	0.0142	0.0239	0.0573	0.0817	0.0780	0.1595	0.3759	0.5873	0.6400	0.7233
0.0267		0.0000	-0.0979	-0.0438	0.0000	0.0023	0.0186	0.0314	0.0752	0.1070	0.1282	0.2085	0.4807	0.7239	0.7239	0.7233
0.0280		0.0000	-0.0977	-0.0437	0.0000	0.0023	0.0188	0.0317	0.0752	0.1080	0.1301	0.2103	0.4834	0.6143	0.6200	0.6200
0.0400		0.0000	-0.0977	-0.0437	0.0000	0.0023	0.0189	0.0319	0.0762	0.1084	0.1306	0.2112	0.4958	0.5581	0.5681	0.5681
0.0500		0.0000	-0.0980	-0.0440	0.0000	0.0024	0.0191	0.0322	0.0771	0.1097	0.1321	0.2134	0.3635	0.3535	0.3535	0.3535
0.0700		0.0000	-0.0980	-0.0440	0.0000	0.0024	0.0192	0.0324	0.0772	0.1099	0.1321	0.2134	0.1541	0.1541	0.1541	0.1541
0.0914		0.0000	-0.0980	-0.0440	0.0000	0.0024	0.0192	0.0324	0.0772	0.1099	0.1321	0.2134	0.0951	0.0951	0.0951	0.0951
0.0900		0.0000	-0.0980	-0.0440	0.0000	0.0023	0.0173	0.0279	0.0593	0.0789	0.0789	0.0789	0.0789	0.0789	0.0789	0.0789
0.09457		0.0000	-0.0980	-0.0440	0.0000	0.0018	0.0137	0.0137	0.0137	0.0137	0.0137	0.0137	0.0137	0.0137	0.0137	0.0137
1.0000		0.0000	-0.0980	-0.0440	0.0000	0.0000	0.0000	0.0000	0.0000	0.0000	0.0000	0.0000	0.0000	0.0000	0.0000	0.0000
1.0000		0.0000	-0.0980	-0.0440	0.0000	0.0000	0.0000	0.0000	0.0000	0.0000	0.0000	0.0000	0.0000	0.0000	0.0000	0.0000
50	50	0.9846	1.0000													
0.0000		0.9664	1.0000													
0.0154		0.9664	0.9664													
0.0267		0.7230	0.7239													
0.0280		0.6200	0.6200													
0.0380		0.5681	0.5681													
0.0400		0.3635	0.3635													
0.0600		0.1541	0.1541													
0.0700		0.0951	0.0951													
0.0914		0.0789	0.0789													
0.0900		0.0137	0.0137													
0.09457		0.0000	0.0000													
1.0000		0.0000	0.0000													

TABLE 3 (continued)

CAPILLARY NUMBER = 0.934E-02																
SA	SD	0.0000	0.0550	0.1100	0.1543	0.1650	0.2000	0.2200	0.2750	0.3086	0.3300	0.4000	0.5000	0.7500	0.8000	0.8753
0.0000	0.0000	0.0540	0.1080	0.1515	0.1620	0.1663	0.2159	0.2191	0.2733	0.3074	0.3239	0.3926	0.5000	0.7479	0.7852	0.8572
0.0154	0.0000	0.0546	0.1094	0.1535	0.1643	0.1992	0.2191	0.2191	0.2733	0.3074	0.3239	0.3926	0.5000	0.7479	0.7852	0.8572
0.0167	0.0000	0.0542	0.1087	0.1526	0.1632	0.1980	0.2178	0.2178	0.2725	0.3059	0.3271	0.3967	0.5056	0.7568	0.7946	0.8572
0.2000	0.0000	0.0541	0.1085	0.1523	0.1629	0.1975	0.2174	0.2174	0.2719	0.3052	0.3265	0.3959	0.5045	0.7550	0.7952	0.8572
0.2380	0.0000	0.0541	0.1084	0.1522	0.1627	0.1974	0.2172	0.2172	0.2717	0.3050	0.3262	0.3956	0.5040	0.7470	0.7479	0.8572
0.4000	0.0000	0.0540	0.1082	0.1519	0.1624	0.1969	0.2167	0.2167	0.2710	0.3042	0.3253	0.3945	0.5039	0.7470	0.7479	0.8572
0.6000	0.0000	0.0540	0.1081	0.1517	0.1622	0.1966	0.2163	0.2163	0.2705	0.3036	0.3246	0.3925	0.5025	0.7470	0.7479	0.8572
0.6700	0.0000	0.0540	0.1080	0.1516	0.1621	0.1965	0.2162	0.2162	0.2703	0.3034	0.3239	0.3925	0.5025	0.7470	0.7479	0.8572
0.6914	0.0000	0.0540	0.1080	0.1516	0.1621	0.1965	0.2162	0.2162	0.2703	0.3029	0.3239	0.3925	0.5025	0.7470	0.7479	0.8572
0.8000	0.0000	0.0540	0.1080	0.1515	0.1620	0.1963	0.2163	0.2163	0.2703	0.3029	0.3239	0.3925	0.5025	0.7470	0.7479	0.8572
0.8457	0.0000	0.0540	0.1080	0.1515	0.1620	0.1963	0.2163	0.2163	0.2703	0.3029	0.3239	0.3925	0.5025	0.7470	0.7479	0.8572
1.0000	0.0000	0.0540	0.1080	0.1515	0.1620	0.1963	0.2163	0.2163	0.2703	0.3029	0.3239	0.3925	0.5025	0.7470	0.7479	0.8572
SA	SD	0.9846	1.0000													
0.0000	0.9664	1.0000														
0.0154	0.9664	0.9664														
0.0167	0.8572	0.8572														
0.2000	0.7852	0.7852														
0.2380	0.7479	0.7479														
0.4000	0.5889	0.5889														
0.6000	0.3926	0.3926														
0.6700	0.3239	0.3239														
0.6914	0.3029	0.3029														
0.8000	0.1963	0.1963														
0.8457	0.1515	0.1515														
1.0000	0.0000	0.0000														

intercor

TABLE 3 (continued)

CAPILLARY NUMBER = 0.130E-01																
SA	SD	0.0000	0.0550	0.1100	0.1543	0.1650	0.2000	0.2200	0.2750	0.3086	0.3300	0.4000	0.6000	0.7520	0.8000	0.8733
0.0000	0.0000	0.0550	0.1100	0.1543	0.1650	0.2000	0.2200	0.2750	0.3086	0.3300	0.4000	0.6000	0.7520	0.8000	0.8733	0.8733
0.0154	0.0000	0.0550	0.1100	0.1543	0.1650	0.2000	0.2200	0.2750	0.3086	0.3300	0.4000	0.6000	0.7520	0.8000	0.8733	0.8733
0.1267	0.0000	0.0550	0.1100	0.1543	0.1650	0.2000	0.2200	0.2750	0.3086	0.3300	0.4000	0.6000	0.7520	0.8000	0.8733	0.8733
0.2000	0.0000	0.0550	0.1100	0.1543	0.1650	0.2000	0.2200	0.2750	0.3086	0.3300	0.4000	0.6000	0.7520	0.8000	0.8733	0.8733
0.2380	0.0000	0.0550	0.1100	0.1543	0.1650	0.2000	0.2200	0.2750	0.3086	0.3300	0.4000	0.6000	0.7520	0.8000	0.8733	0.8733
0.4000	0.0000	0.0550	0.1100	0.1543	0.1650	0.2000	0.2200	0.2750	0.3086	0.3300	0.4000	0.6000	0.7520	0.8000	0.8733	0.8733
0.6000	0.0000	0.0550	0.1100	0.1543	0.1650	0.2000	0.2200	0.2750	0.3086	0.3300	0.4000	0.6000	0.7520	0.8000	0.8733	0.8733
0.6700	0.0000	0.0550	0.1100	0.1543	0.1650	0.2000	0.2200	0.2750	0.3086	0.3300	0.4000	0.6000	0.7520	0.8000	0.8733	0.8733
0.6914	0.0000	0.0550	0.1100	0.1543	0.1650	0.2000	0.2200	0.2750	0.3086	0.3300	0.4000	0.6000	0.7520	0.8000	0.8733	0.8733
0.8000	0.0000	0.0550	0.1100	0.1543	0.1650	0.2000	0.2200	0.2750	0.3086	0.3300	0.4000	0.6000	0.7520	0.8000	0.8733	0.8733
0.8457	0.0000	0.0550	0.1100	0.1543	0.1650	0.2000	0.2200	0.2750	0.3086	0.3300	0.4000	0.6000	0.7520	0.8000	0.8733	0.8733
1.0000	0.0000	0.0550	0.1100	0.1543	0.1650	0.2000	0.2200	0.2750	0.3086	0.3300	0.4000	0.6000	0.7520	0.8000	0.8733	0.8733
SA	SD	0.0846	1.0000													
0.0000	0.9846	1.0000														
0.0154	0.9846	0.9846														
0.1267	0.8733	0.8733														
0.2000	0.8000	0.8000														
0.2380	0.7620	0.7620														
0.4000	0.6000	0.6000														
0.6000	0.4000	0.4000														
0.6700	0.3300	0.3300														
0.6914	0.3086	0.3086														
0.8000	0.2000	0.2000														
0.8457	0.1543	0.1543														
1.0000	0.0000	0.0000														

TABLE 3 (continued)

CALCULATED MICELLAR RELATIVE PERMEABILITIES

CAPILLARY NUMBER = 0.201E-04

SA	SM	0.0154	0.1267	0.1543	0.2000	0.2380	0.3086	0.3300	0.4000	0.4700	0.5314	0.5800	0.6457	1.0000
0.0000	0.0000	0.0000	0.0000	0.0000	0.0000	0.0000	0.0019	0.0037	0.0156	0.1232	0.1740	0.2462	0.5115	0.6231
0.1543	0.0000	0.0000	0.0000	0.0000	0.0000	0.0000	0.0038	0.0107	0.0668	0.3321	0.3519	0.4013	0.6520	0.7574
0.2000	0.0000	0.0000	0.0000	0.0000	0.0000	0.0000	0.0048	0.0158	0.1145	0.3544	0.3208	0.3392	0.6856	0.6856
0.3086	0.0000	0.0000	0.0000	0.0000	0.0000	0.0000	0.0025	0.0195	0.1228	0.2773	0.3243	0.5149	0.5149	0.5149
0.3300	0.0000	0.0000	0.0000	0.0000	0.0000	0.0000	0.0017	0.0167	0.0960	0.2528	0.3023	0.3023	0.3023	0.3023
0.4000	0.0000	0.0000	0.0000	0.0000	0.0000	0.0000	0.0000	0.0043	0.0493	0.1932	0.1932	0.1932	0.1932	0.1932
0.6000	0.0000	0.0000	0.0000	0.0000	0.0000	0.0000	0.0000	0.0000	0.0000	0.0000	0.0000	0.0000	0.0000	0.0000
0.6700	0.0000	0.0000	0.0000	0.0000	0.0000	0.0000	0.0000	0.0000	0.0000	0.0000	0.0000	0.0000	0.0000	0.0000
0.6914	0.0000	0.0000	0.0000	0.0000	0.0000	0.0000	0.0000	0.0000	0.0000	0.0000	0.0000	0.0000	0.0000	0.0000
0.7620	0.0000	0.0000	0.0000	0.0000	0.0000	0.0000	0.0000	0.0000	0.0000	0.0000	0.0000	0.0000	0.0000	0.0000
0.8000	0.0000	0.0000	0.0000	0.0000	0.0000	0.0000	0.0000	0.0000	0.0000	0.0000	0.0000	0.0000	0.0000	0.0000
0.8457	0.0000	0.0000	0.0000	0.0000	0.0000	0.0000	0.0000	0.0000	0.0000	0.0000	0.0000	0.0000	0.0000	0.0000
0.9733	0.0000	0.0000	0.0000	0.0000	0.0000	0.0000	0.0000	0.0000	0.0000	0.0000	0.0000	0.0000	0.0000	0.0000
0.9846	0.0000	0.0000	0.0000	0.0000	0.0000	0.0000	0.0000	0.0000	0.0000	0.0000	0.0000	0.0000	0.0000	0.0000
1.0000	0.0000	0.0000	0.0000	0.0000	0.0000	0.0000	0.0000	0.0000	0.0000	0.0000	0.0000	0.0000	0.0000	0.0000

CAPILLARY NUMBER = 0.299E-04

SA	SM	0.0154	0.1267	0.1543	0.2000	0.2380	0.3086	0.3300	0.4000	0.4700	0.5314	0.5800	0.6457	1.0000
0.0000	0.0000	0.0000	0.0000	0.0000	0.0000	0.0000	0.0021	0.0041	0.0175	0.1391	0.2175	0.2462	0.5115	0.6231
0.1543	0.0000	0.0000	0.0000	0.0000	0.0000	0.0000	0.0052	0.0125	0.0664	0.3522	0.3755	0.3419	0.6544	0.7407
0.2000	0.0000	0.0000	0.0000	0.0000	0.0000	0.0000	0.0071	0.0196	0.1069	0.3473	0.4072	0.4151	0.6539	0.6839
0.3086	0.0000	0.0000	0.0000	0.0000	0.0000	0.0000	0.0074	0.0257	0.1465	0.2926	0.3356	0.3500	0.3500	0.3500
0.3300	0.0000	0.0000	0.0000	0.0000	0.0000	0.0000	0.0067	0.0250	0.1180	0.2684	0.3142	0.3142	0.3142	0.3142
0.4000	0.0000	0.0000	0.0000	0.0000	0.0000	0.0000	0.0037	0.0144	0.0664	0.2095	0.2095	0.2095	0.2095	0.2095
0.6000	0.0000	0.0000	0.0000	0.0000	0.0000	0.0000	0.0000	0.0024	0.0237	0.0237	0.0237	0.0237	0.0237	0.0237
0.6700	0.0000	0.0000	0.0000	0.0000	0.0000	0.0000	0.0000	0.0015	0.0015	0.0015	0.0015	0.0015	0.0015	0.0015
0.6914	0.0000	0.0000	0.0000	0.0000	0.0000	0.0000	0.0000	0.0000	0.0000	0.0000	0.0000	0.0000	0.0000	0.0000
0.7620	0.0000	0.0000	0.0000	0.0000	0.0000	0.0000	0.0000	0.0000	0.0000	0.0000	0.0000	0.0000	0.0000	0.0000
0.8000	0.0000	0.0000	0.0000	0.0000	0.0000	0.0000	0.0000	0.0000	0.0000	0.0000	0.0000	0.0000	0.0000	0.0000
0.8457	0.0000	0.0000	0.0000	0.0000	0.0000	0.0000	0.0000	0.0000	0.0000	0.0000	0.0000	0.0000	0.0000	0.0000
0.9733	0.0000	0.0000	0.0000	0.0000	0.0000	0.0000	0.0000	0.0000	0.0000	0.0000	0.0000	0.0000	0.0000	0.0000
0.9846	0.0000	0.0000	0.0000	0.0000	0.0000	0.0000	0.0000	0.0000	0.0000	0.0000	0.0000	0.0000	0.0000	0.0000
1.0000	0.0000	0.0000	0.0000	0.0000	0.0000	0.0000	0.0000	0.0000	0.0000	0.0000	0.0000	0.0000	0.0000	0.0000

TABLE 3 (continued)

CAPILLARY NUMBER = 0.528E-03															
SA	SM	0.0000	0.0154	0.1267	0.1513	0.2000	0.2340	0.3086	0.4000	0.5000	0.6000	0.7000	0.8000	0.9000	1.0000
0.0000	0.0000	0.0000	0.0000	0.0000	0.0015	0.0094	0.0203	0.0501	0.1056	0.2093	0.4025	0.5524	0.6231	0.6942	0.7653
0.1543	0.0000	0.0000	0.0019	0.0152	0.0336	0.0830	0.1015	0.1728	0.4509	0.5878	0.6206	0.6514	0.6842	0.7170	0.7500
0.2000	0.0000	0.0000	0.0017	0.0157	0.0350	0.0863	0.1055	0.1700	0.4722	0.5640	0.5719	0.6200	0.6200	0.6200	0.6200
0.3086	0.0000	0.0000	0.0013	0.0167	0.0380	0.0938	0.1144	0.1926	0.4834	0.4834	0.4755	0.4755	0.4755	0.4755	0.4755
0.3300	0.0000	0.0000	0.0013	0.0169	0.0386	0.0952	0.1160	0.1950	0.4986	0.4986	0.4845	0.4845	0.4845	0.4845	0.4845
0.4000	0.0000	0.0000	0.0010	0.0175	0.0403	0.0995	0.1211	0.2025	0.5135	0.5135	0.5035	0.5035	0.5035	0.5035	0.5035
0.4600	0.0000	0.0000	0.0003	0.0187	0.0444	0.0934	0.1080	0.1841	0.5291	0.5291	0.5191	0.5191	0.5191	0.5191	0.5191
0.6700	0.0000	0.0000	0.0002	0.0179	0.0390	0.0819	0.0951	0.0951	0.0951	0.0951	0.0951	0.0951	0.0951	0.0951	0.0951
0.6914	0.0000	0.0000	0.0001	0.0170	0.0373	0.0789	0.0789	0.0789	0.0789	0.0789	0.0789	0.0789	0.0789	0.0789	0.0789
0.7620	0.0000	0.0000	0.0000	0.0147	0.0327	0.0327	0.0327	0.0327	0.0327	0.0327	0.0327	0.0327	0.0327	0.0327	0.0327
0.8000	0.0000	0.0000	0.0000	0.0137	0.0137	0.0137	0.0137	0.0137	0.0137	0.0137	0.0137	0.0137	0.0137	0.0137	0.0137
0.8457	0.0000	0.0000	0.0000	0.0000	0.0000	0.0000	0.0000	0.0000	0.0000	0.0000	0.0000	0.0000	0.0000	0.0000	0.0000
0.8733	0.0000	0.0000	0.0000	0.0000	0.0000	0.0000	0.0000	0.0000	0.0000	0.0000	0.0000	0.0000	0.0000	0.0000	0.0000
0.9846	0.0000	0.0000	0.0000	0.0000	0.0000	0.0000	0.0000	0.0000	0.0000	0.0000	0.0000	0.0000	0.0000	0.0000	0.0000
1.0000	0.0000	0.0000	0.0000	0.0000	0.0000	0.0000	0.0000	0.0000	0.0000	0.0000	0.0000	0.0000	0.0000	0.0000	0.0000
CAPILLARY NUMBER = 0.934E-02															
SA	SM	0.0000	0.0154	0.1267	0.1543	0.2000	0.2380	0.3086	0.4000	0.5000	0.6000	0.7000	0.8000	0.9000	1.0000
0.0000	0.0000	0.0000	0.0000	0.0000	0.0000	0.0000	0.0000	0.0000	0.0000	0.0000	0.0000	0.0000	0.0000	0.0000	0.0000
0.1543	0.0000	0.0030	0.1014	0.1276	0.1543	0.1543	0.1543	0.1543	0.1543	0.1543	0.1543	0.1543	0.1543	0.1543	0.1543
0.2000	0.0000	0.0041	0.1039	0.1303	0.1747	0.1747	0.1747	0.1747	0.1747	0.1747	0.1747	0.1747	0.1747	0.1747	0.1747
0.3086	0.0000	0.0065	0.1093	0.1361	0.1899	0.1899	0.1899	0.1899	0.1899	0.1899	0.1899	0.1899	0.1899	0.1899	0.1899
0.3300	0.0000	0.0059	0.1103	0.1371	0.1920	0.1920	0.1920	0.1920	0.1920	0.1920	0.1920	0.1920	0.1920	0.1920	0.1920
0.4000	0.0000	0.0084	0.1133	0.1403	0.1853	0.1853	0.1853	0.1853	0.1853	0.1853	0.1853	0.1853	0.1853	0.1853	0.1853
0.4600	0.0000	0.0120	0.1201	0.1473	0.1926	0.1926	0.1926	0.1926	0.1926	0.1926	0.1926	0.1926	0.1926	0.1926	0.1926
0.6700	0.0000	0.0130	0.1217	0.1490	0.1943	0.1943	0.1943	0.1943	0.1943	0.1943	0.1943	0.1943	0.1943	0.1943	0.1943
0.6914	0.0000	0.0133	0.1221	0.1494	0.1948	0.1948	0.1948	0.1948	0.1948	0.1948	0.1948	0.1948	0.1948	0.1948	0.1948
0.7620	0.0000	0.0140	0.1233	0.1506	0.1959	0.1959	0.1959	0.1959	0.1959	0.1959	0.1959	0.1959	0.1959	0.1959	0.1959
0.8000	0.0000	0.0144	0.1238	0.1511	0.1963	0.1963	0.1963	0.1963	0.1963	0.1963	0.1963	0.1963	0.1963	0.1963	0.1963
0.8457	0.0000	0.0147	0.1242	0.1515	0.1963	0.1963	0.1963	0.1963	0.1963	0.1963	0.1963	0.1963	0.1963	0.1963	0.1963
0.8733	0.0000	0.0148	0.1244	0.1515	0.1963	0.1963	0.1963	0.1963	0.1963	0.1963	0.1963	0.1963	0.1963	0.1963	0.1963
0.9846	0.0000	0.0151	0.1244	0.1515	0.1963	0.1963	0.1963	0.1963	0.1963	0.1963	0.1963	0.1963	0.1963	0.1963	0.1963
1.0000	0.0000	0.0151	0.1244	0.1515	0.1963	0.1963	0.1963	0.1963	0.1963	0.1963	0.1963	0.1963	0.1963	0.1963	0.1963

TABLE 3 (continued)

CAPILLARY NUMBER = 0.139E-01	
SA	SM
0.0000	0.0000
0.1543	0.0154
0.2000	0.0154
0.3086	0.0154
0.3300	0.0154
0.4000	0.0154
0.6000	0.0154
0.6700	0.0154
0.6914	0.0154
0.7620	0.0154
0.8000	0.0154
0.8457	0.0154
0.8733	0.0154
0.9846	0.0154
1.0000	0.0154
	0.1267
	0.1543
	0.2000
	0.2340
	0.3086
	0.3300
	0.4000
	0.6000
	0.6700
	0.6914
	0.7620
	0.8000
	0.8457
	0.8733
	0.9846
	1.0000

TABLE 4
COREFLOOD 53⁽¹⁾ INPUT DATA

ϕ , fr.	0.274
k, md ⁽²⁾	565
S _{or} , pv	0.376
S _{wf} , pv	0.238
Preflush I, pv ⁽³⁾	0.40
Preflush II, pv ⁽⁴⁾	0.42
Surfactant slug, pv ⁽⁵⁾	0.112
Surfactant conc., meq/ml	0.085
NaCl, wt. %	0.7
Ca ⁺ + Mg ⁺⁺ , ppm	31
Polymer, ppm	900
Polymer drive, pv	0.48
NaCl, wt. %	1.0
Ca ⁺ + Mg ⁺⁺ , ppm	34
Polymer, ppm	1125

- (1) Reference 33
- (2) Average core plug permeability from well MP-106
- (3) 1.4% NaCl, 98.6 El Dorado Lake water (63 ppm NaCl, 35 ppm Ca⁺⁺ + Mg⁺⁺)
- (4) 2.9% NaCl, .102% CaCl₂, .097% MgCl₂, 96.9% El Dorado Lake water
- (5) Secondary butyl alcohol not accounted for in input data

TABLE 5
COREFLOOD SIMULATIONS*
SORPTION SENSITIVITY

<u>Sorption,</u> <u>ft³ surf./ft³pv</u>	<u>% Reversibility</u>	<u>Tertiary</u> <u>Oil Rec.</u>	<u>Surfactant Rec.,</u> <u>% of Injected</u>
.0036	0 (base case)	56.0	10.9
.0048	25	42.3	0.6
.0075	50	46.7	14.4
.0075	75	54.6	46.8
.0075	100	55.6	47.8
.01	100	21.2	0

* Coreflood 53 process variables with CSEL = 1.07 wt. % NaCl

TABLE 6
RESERVOIR PROPERTIES OF UPPER LAYER

TUBE NO.	GRID BLOCK NO.																			
	1	2	3	4	5	6	7	8	9	10	11	12	13	14	15	16	17	18	19	20
	NET THICKNESS, ft																			
1	8.0	7.7	7.5	7.3	7.1	6.8	6.6	6.3	6.3	6.3	6.5	6.5	6.7	7.0	7.2	7.4	7.7	7.9	8.1	8.7
2	8.0	7.9	7.7	7.6	7.3	7.0	6.7	6.5	6.2	6.2	6.2	6.2	6.5	6.7	7.0	7.2	7.4	7.9	8.1	8.7
3	8.2	7.9	8.1	8.0	7.8	7.3	7.0	6.7	6.5	6.2	6.0	6.2	6.2	6.5	7.0	7.2	7.4	7.9	8.1	8.7
4	8.2	7.9	7.8	7.8	7.8	7.5	7.3	7.0	6.7	6.5	6.2	6.2	6.5	6.7	7.0	7.2	7.4	7.9	8.4	8.7
5	8.2	7.9	7.9	7.7	7.6	7.3	7.3	7.0	6.8	6.5	6.5	6.5	6.7	7.0	7.2	7.5	7.7	7.9	8.4	8.7
	HORIZONTAL PERMEABILITY, md																			
1	425	400	400	400	400	400	375	350	325	325	300	300	275	275	250	250	250	250	225	225
2	425	425	425	375	350	325	300	275	250	250	250	225	225	225	225	225	225	225	225	225
3	425	375	325	275	250	250	225	225	200	200	175	175	175	200	200	200	200	200	200	225
4	400	350	325	275	250	225	200	200	175	175	150	150	150	175	175	175	175	200	200	225
5	400	375	350	325	300	250	225	175	150	125	125	125	125	150	150	150	175	175	200	225

TABLE 6 - (CONTINUED)
RESERVOIR PROPERTIES OF UPPER LAYER

TUBE NO.	GRID BLOCK NO.																			
	1	2	3	4	5	6	7	8	9	10	11	12	13	14	15	16	17	18	19	20
	VERTICAL PERMEABILITY, md																			
1	64.4	60.6	60.6	60.6	53.3	50.0	46.9	41.2	38.2	38.2	35.3	35.3	32.3	32.3	29.4	29.4	31.3	31.3	28.1	30.0
2	64.4	59.8	59.8	50.0	46.7	40.6	35.3	32.3	27.8	27.8	25.0	25.0	25.0	25.0	26.5	26.5	26.5	28.1	28.1	30.0
3	64.4	52.8	45.8	36.7	33.3	31.3	26.5	26.5	22.2	21.1	18.4	18.4	19.4	22.2	23.5	23.5	23.5	25.0	25.0	30.0
4	60.6	49.3	43.3	36.7	33.3	28.1	25.0	23.5	20.6	19.4	16.7	16.7	16.7	19.4	20.6	20.6	21.9	25.0	25.0	30.0
5	60.6	52.8	49.3	45.8	40.0	33.3	30.0	21.9	18.8	14.7	14.7	14.7	14.7	17.6	17.6	18.8	21.9	21.9	25.0	30.0
	FORMATION POROSITY, fraction																			
1	.26	.26	.26	.26	.255	.255	.255	.25	.25	.25	.25	.25	.25	.25	.25	.25	.25	.25	.25	.25
2	.26	.265	.26	.26	.255	.255	.25	.25	.245	.245	.245	.245	.245	.245	.245	.245	.245	.245	.245	.25
3	.265	.26	.26	.26	.255	.255	.25	.25	.245	.245	.245	.245	.245	.245	.245	.245	.245	.245	.245	.25
4	.265	.26	.255	.255	.255	.25	.245	.245	.245	.24	.24	.24	.24	.24	.24	.24	.24	.245	.245	.25
5	.265	.26	.255	.255	.25	.25	.245	.245	.24	.24	.235	.235	.235	.235	.24	.24	.24	.245	.245	.25

TABLE 7
RESERVOIR PROPERTIES OF LOWER LAYER

TUBE NO.	GRID BLOCK NO.										NET THICKNESS, ft	HORIZONTAL PERMEABILITY, md									
	1	2	3	4	5	6	7	8	9	10		11	12	13	14	15	16	17	18	19	20
1	6.8	7.0	7.3	7.5	8.2	8.1	7.8	7.6	7.6	7.4	7.4	7.2	7.2	7.2	7.4	7.3	7.3	7.1	7.2	7.3	
2	6.8	7.0	7.4	7.5	7.5	7.5	7.2	7.0	6.7	6.9	6.6	6.5	6.7	6.7	6.8	7.1	6.9	7.1	7.2	7.3	
3	6.8	7.0	6.8	6.8	7.0	6.9	6.7	6.6	6.4	6.2	6.2	6.2	6.4	6.6	6.8	6.9	6.9	7.1	7.2	7.3	
4	6.8	6.8	6.8	6.8	6.8	7.0	7.1	6.9	7.1	6.8	6.6	6.6	6.8	7.1	7.1	7.1	7.1	7.2	7.2	7.3	
5	6.8	6.8	7.2	7.2	7.2	7.4	7.6	7.6	7.6	7.8	7.5	7.5	7.5	7.5	7.5	7.4	7.4	7.2	7.4	7.3	
1	225	225	250	350	400	375	375	350	325	300	275	275	275	250	250	225	200	200	200	175	
2	225	250	275	275	275	275	250	225	200	200	175	175	175	175	175	175	175	175	175	175	
3	200	200	175	175	175	150	150	150	125	100	75	100	100	125	125	125	150	150	175	175	
4	175	175	150	125	125	125	100	100	100	100	100	100	100	100	125	125	150	150	150	175	
5	175	150	150	125	125	125	125	100	100	100	100	100	100	100	125	125	125	150	150	175	

TABLE 7 - (CONTINUED)
RESERVOIR PROPERTIES OF LOWER LAYER

TUBE NO.	GRID BLOCK NO.																			
	1	2	3	4	5	6	7	8	9	10	11	12	13	14	15	16	17	18	19	20
	VERTICAL PERMEABILITY, md																			
1	7.6	8.4	10.2	14.3	16.3	15.3	14.0	11.8	11.0	9.2	8.5	8.5	8.5	7.7	8.5	7.6	6.8	6.8	7.4	7.1
2	7.6	8.5	10.2	10.2	10.2	10.2	7.7	6.3	5.1	5.1	4.0	4.0	4.5	4.5	4.9	5.4	5.3	5.9	6.5	7.1
3	6.8	6.8	5.9	5.9	5.9	4.6	4.2	3.8	2.9	2.1	1.6	2.1	2.3	3.2	3.5	3.9	4.6	5.1	6.5	7.1
4	5.9	5.9	5.1	4.2	4.2	4.2	3.4	3.1	3.1	2.8	2.6	2.6	2.8	3.1	3.9	4.2	5.1	5.6	5.6	7.1
5	5.9	5.1	5.6	4.7	4.7	5.1	5.1	4.1	4.1	4.1	3.7	3.7	3.7	3.7	4.7	4.7	4.7	5.6	6.1	7.1
	FORMATION POROSITY, fraction																			
1	.22	.225	.23	.24	.24	.23	.225	.225	.22	.215	.21	.21	.21	.21	.21	.21	.21	.21	.21	.21
2	.22	.22	.225	.225	.225	.22	.215	.21	.205	.20	.195	.195	.195	.19	.20	.20	.205	.205	.21	.21
3	.215	.22	.22	.22	.215	.21	.205	.20	.19	.185	.18	.18	.185	.19	.195	.195	.20	.205	.21	.21
4	.215	.215	.215	.215	.21	.21	.21	.205	.20	.195	.19	.19	.195	.195	.20	.20	.205	.205	.21	.21
5	.215	.215	.215	.215	.215	.215	.215	.215	.21	.21	.205	.205	.205	.205	.205	.205	.205	.205	.21	.21

TABLE 8

RESERVOIR PROPERTIES OF SINGLE-LAYER MODEL

TUBE NO.	GRID BLOCK NO.																			
	1	2	3	4	5	6	7	8	9	10	11	12	13	14	15	16	17	18	19	20
	NET THICKNESS, ft																			
1	14.8	14.8	14.8	14.8	15.3	14.9	14.4	13.9	13.9	13.7	13.9	13.9	13.9	14.2	14.6	14.7	15.0	15.1	15.3	15.9
2	14.8	14.9	15.0	15.1	14.9	14.6	13.9	13.5	13.0	13.1	12.9	12.7	13.2	13.4	13.9	14.2	14.3	15.1	15.3	15.9
3	15.0	14.9	14.9	14.8	13.8	14.2	13.6	13.3	12.8	12.4	12.2	12.4	12.6	13.0	13.8	14.1	14.3	15.1	15.3	15.9
4	15.0	14.7	14.6	14.6	14.6	14.5	14.4	13.9	13.8	13.4	12.8	12.8	13.3	13.7	14.0	14.3	14.6	15.1	15.6	15.9
5	15.0	14.7	15.1	14.9	14.8	14.8	14.9	14.6	14.4	14.4	14.1	14.1	14.3	14.5	14.7	14.8	15.1	15.1	15.9	15.9
	HORIZONTAL PERMEABILITY, md																			
1	331	317	326	325	400	396	375	350	325	312	287	287	275	262	250	238	226	223	213	202
2	333	343	351	325	312	299	274	249	224	224	211	200	199	200	200	200	201	201	202	202
3	323	293	256	228	214	201	188	188	163	150	124	137	137	162	165	163	176	176	188	202
4	298	269	243	205	192	177	150	150	137	135	124	124	124	136	150	150	163	176	177	202
5	298	271	255	228	215	187	174	136	124	111	112	112	112	124	137	138	151	163	175	202
	POROSITY, fraction																			
1	.242	.243	.245	.25	.247	.241	.239	.236	.233	.231	.229	.229	.229	.226	.23	.233	.231	.231	.231	.232
2	.242	.244	.25	.242	.24	.237	.235	.229	.226	.221	.219	.219	.219	.217	.223	.223	.226	.232	.231	.232
3	.242	.241	.242	.24	.236	.233	.228	.225	.218	.215	.212	.212	.215	.217	.22	.223	.226	.229	.229	.232
4	.242	.239	.236	.236	.234	.231	.228	.225	.222	.215	.214	.214	.217	.217	.22	.225	.226	.226	.229	.232
5	.242	.239	.236	.236	.233	.232	.23	.227	.224	.22	.219	.219	.219	.219	.222	.223	.223	.226	.227	.232

TABLE 9
FLUID INJECTION DATA

	<u>North Lease</u>	<u>MP-118</u>	<u>Asymmetric Element</u>	<u>Symmetric Element*</u>	<u>Center Streamtube</u>
Pore Volume, bbl	910,500	—	47,000	28,700	5,560
Preflush I	(11/20/75)				
Avg. Rate, bpd	882	93	26	12	6
Cum. Inj., bbl	352,735	37,215	10,465	4,652	2,434
Preflush II	(12/21/76)				
Avg. Rate, bpd	1127	156	44	19	10
Cum. Inj., bbl	374,126	51,773	14,559	6,472	3,386
Micellar Slug	(11/17/77)				
Avg. Rate, bpd	273	38	14	5	3
Cum. Inj., bbl	99,479	13,969	4,981	1,746	914
Polymer Drive	(11/17/78)				
Avg. Rate, bpd	472**	59**	26***	9***	4***
Cum. Inj., bbl	—	—	—	—	—

* One-eighth of a five-spot

** Historical

*** Predicted

TABLE 10
DATA USED IN SIMULATION AT MP-131

Grid	Two-Layer Center Streamtube (20 x 1 x 2)
Permeability, Porosity, Net Thickness	Tables 6 and 7
Ternary Phase Equilibrium Data	Table 1
Micellar Slug Composition ⁽¹⁾	3rd Annual Report, p. I-12
Interfacial Tension Data	Figure 10
Cation Exchange Capacity	0.058 mg Ca ⁺⁺ /gm rock
Residual Oil to Waterflood	0.33
Irreducible Water Saturation	0.238
Relative Permeability (o/w)	Figures 13 and 14
Three-Phase Relative Permeability	Table 3
Surfactant Sorption	1.21 lb/bbl p.v.
Polymer Sorption	0.052 lb/bbl p.v.
Viscosity: Oil	5.2cp
Brine ⁽²⁾	1.07 cp
Micellar Slug ⁽³⁾	4.07 cp
Inaccessible Pore Volume to Polymer	0.1
Polymer Residual Resistance Factor	1.0
Longitudinal Dispersion (all phases)	4.0 ft
Transverse Dispersion (all phases)	0.005 ft.

(1) Alcohol was not accounted for as a slug component.

(2) Effect of shear rate and polymer concentration in aqueous phase is given in Figure 12.

(3) Effect of shear rate and polymer concentration on micellar phase viscosity is 3 cp greater than aqueous phase viscosity at same conditions for injection concentration of surfactant (Appendix E).

TABLE 11

RESULTS OF SENSITIVITY SIMULATIONS
IN CENTER STREAMTUBE (CST)
AND AREAL PATTERN PREDICTIONS

	No. Layers	CSEL, wt. % NaCl	Micellar Slug, pv	Polymer B. T., pv	Oil Recovery Poly. B. T. (1)	Oil Recovery at 1 pv (1)
Base Case, CST	1	.35	.164	.85	.383	.395
Two-Layer, CST	2	.35	.164	.85	.367	.390
Phase Behavior, CST	1	1.07	.164	.91	.495	.545
No Preflush, CST	1	.35	.164	.90	.335	.368
Slug Size, CST	1	.35	.082	.78	.154	.182
	1	.35	.328	.947	.696	.710
Residual Oil Sat., CST ⁽²⁾	1	.35	.164	.85	.303	.342
Asymmetric Element	1	.35	.106	.754	.211	.243
Symmetric Element ⁽³⁾	1	.35	.061	.646	.098	.134

(1) Fraction of residual oil

(2) $S_{or} = 0.23$, all other simulations $S_{or} = 0.33$

(3) One-eighth of a five-spot

FIGURE 1

.075 meq/ml SURFACTANT IN AQUEOUS PHASE
 50% OIL, 50% SURFACTANT SOLUTION (NO POLYMER)

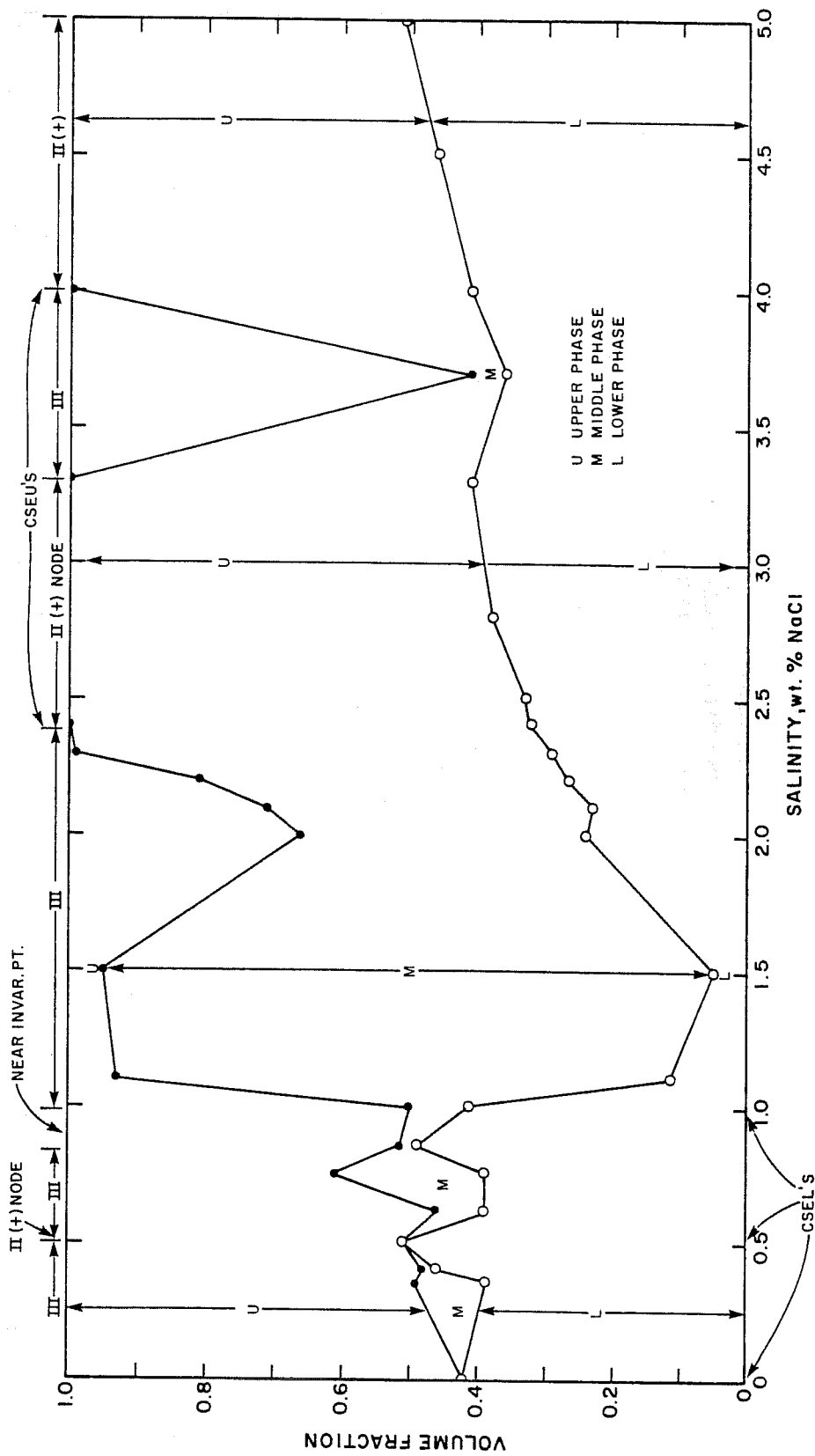


FIGURE 2
 .075 meq/ml SURFACTANT IN AQUEOUS PHASE
 900 PPM POLYMER
 50% OIL, 50% SURFACTANT POLYMER SOLUTION

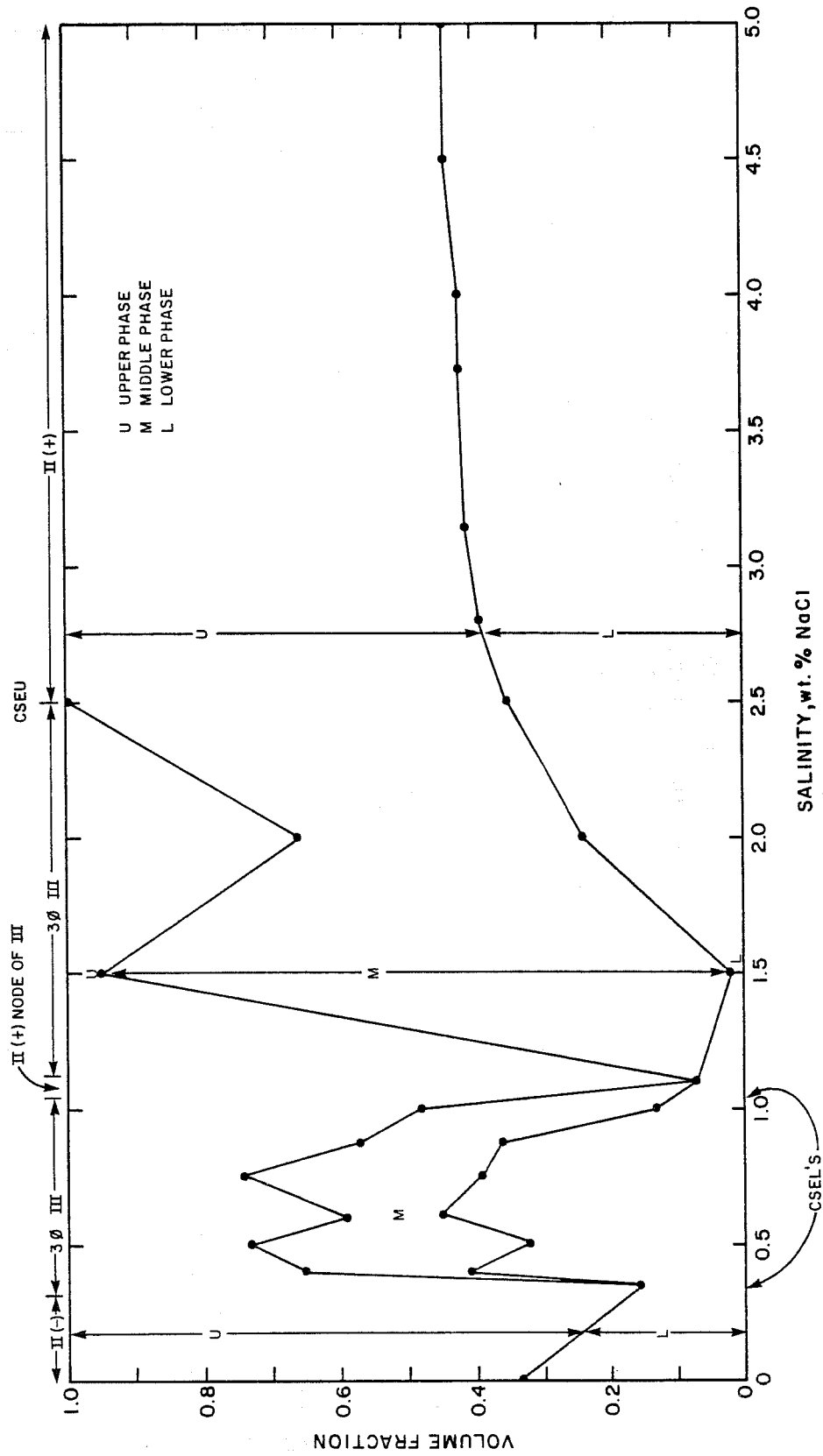


FIGURE 3
 .0375 meq/ml SURFACTANT IN AQUEOUS PHASE
 50% OIL, 50% SURFACTANT SOLUTION (NO POLYMER)

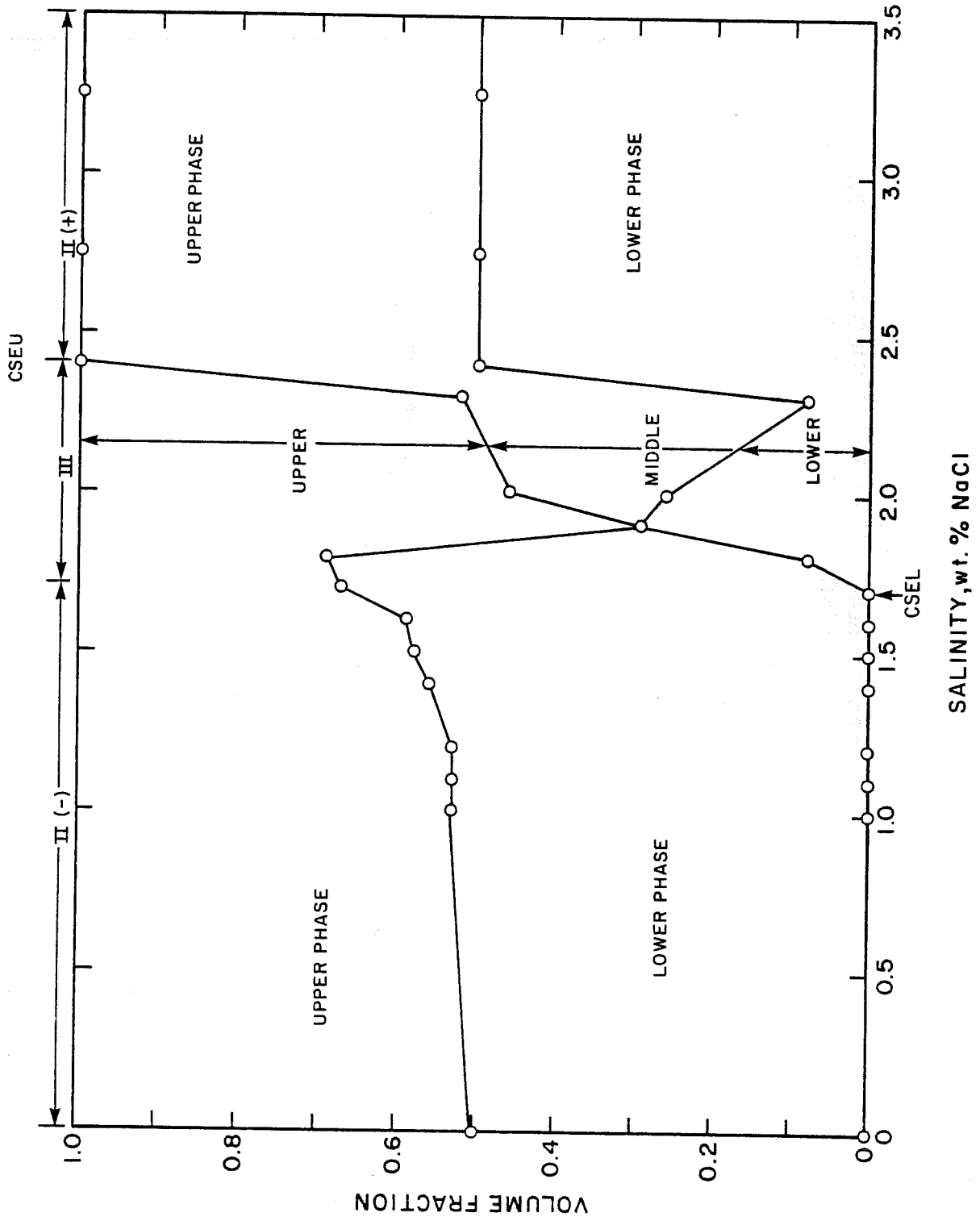


FIGURE 4
 .01875 meq/ml SURFACTANT IN AQUEOUS PHASE
 50% OIL, 50% SURFACTANT SOLUTION (NO POLYMER)

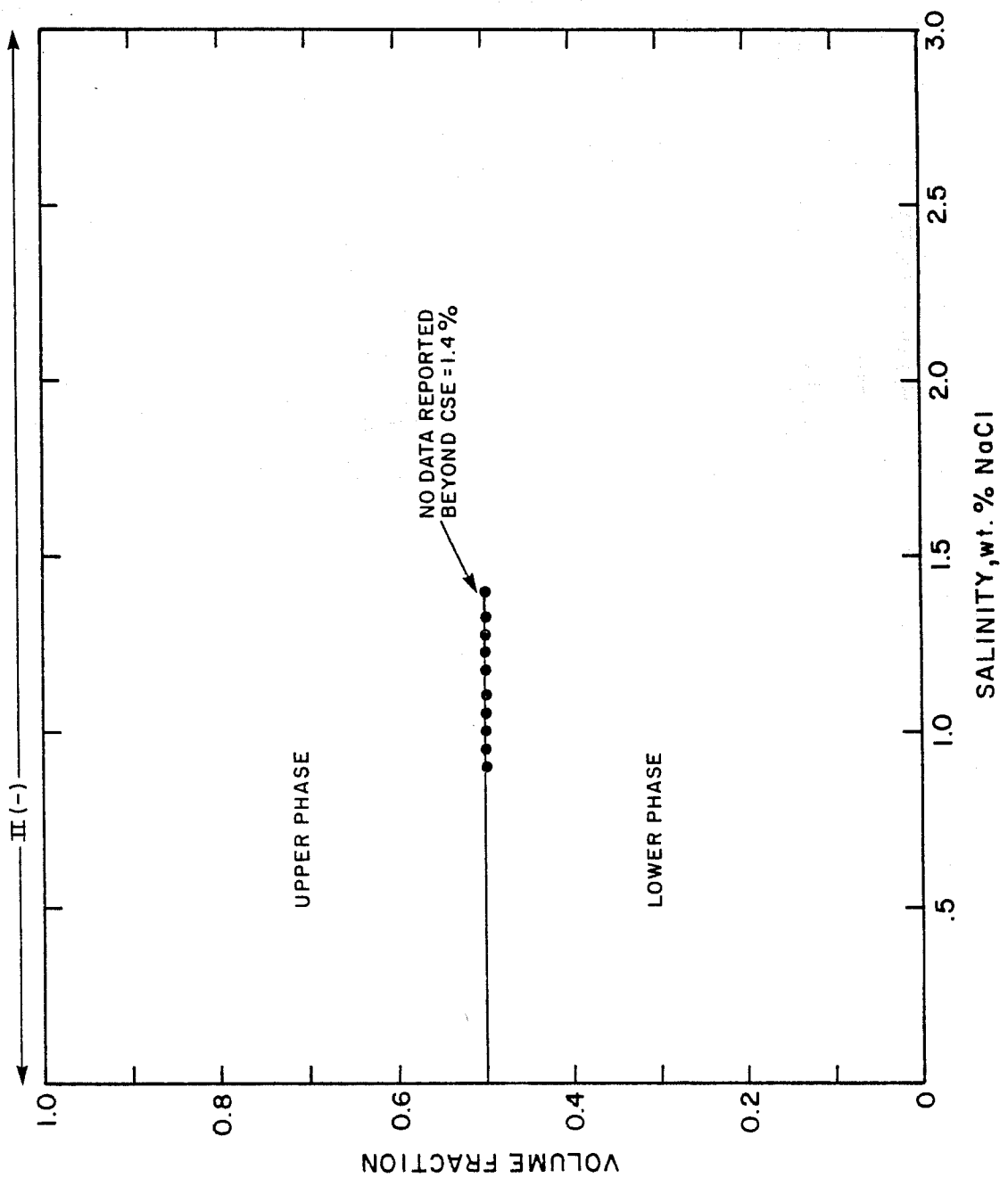
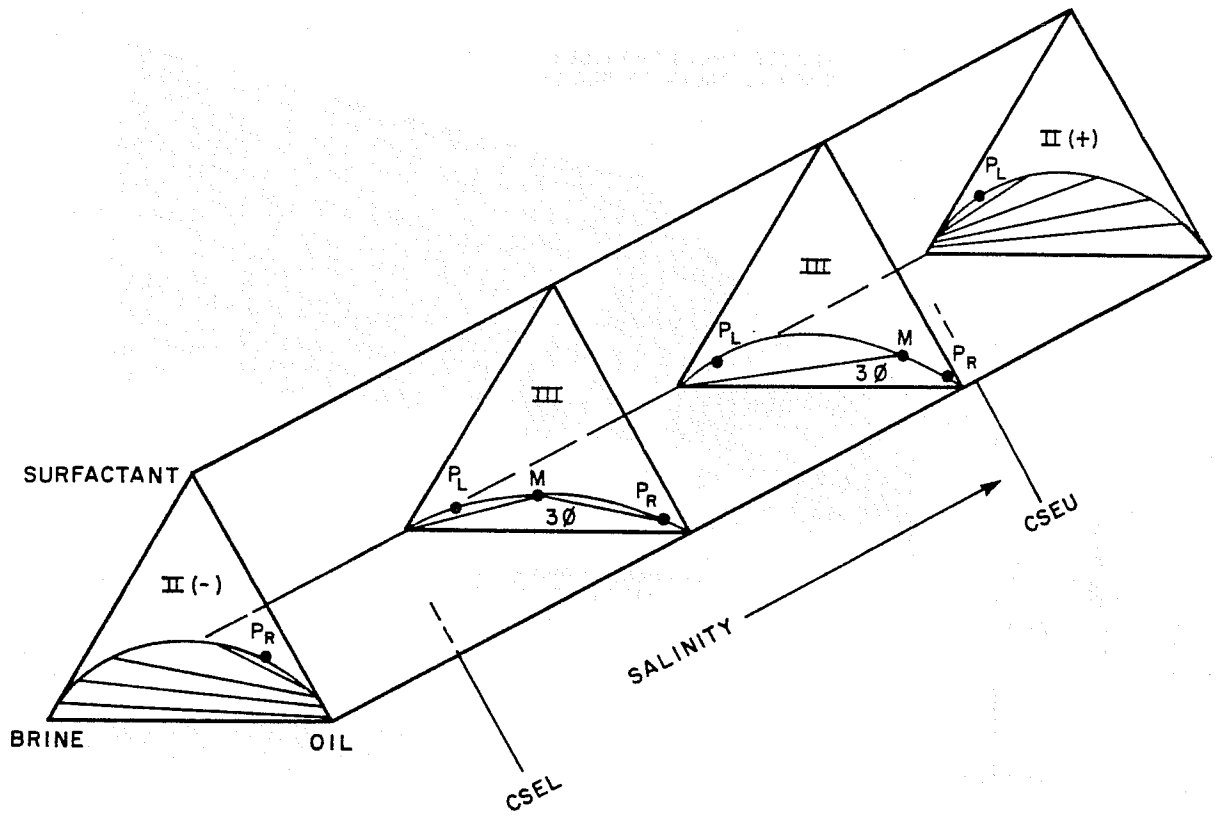


FIGURE 5
 QUALITATIVE PHASE BEHAVIOR



P_R : RIGHT PLAIT PT.
 P_L : LEFT PLAIT PT.
 M: INVARIANT PT.

FIGURE 6
 SALINITY REQUIREMENT DIAGRAMS
 CHESNEY (HWC) MICELLAR SLUG

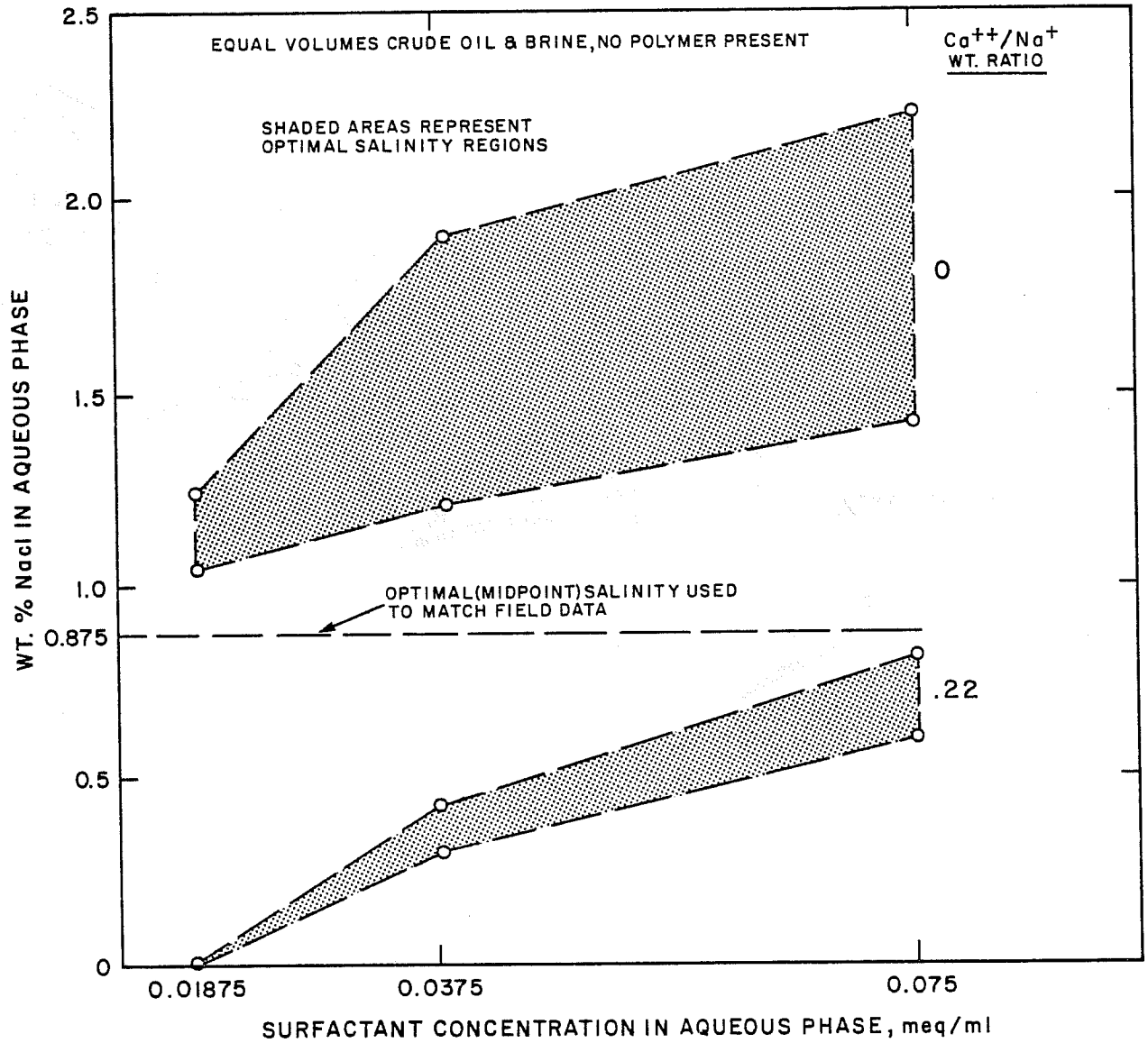


FIGURE 7
SURFACTANT SORPTION

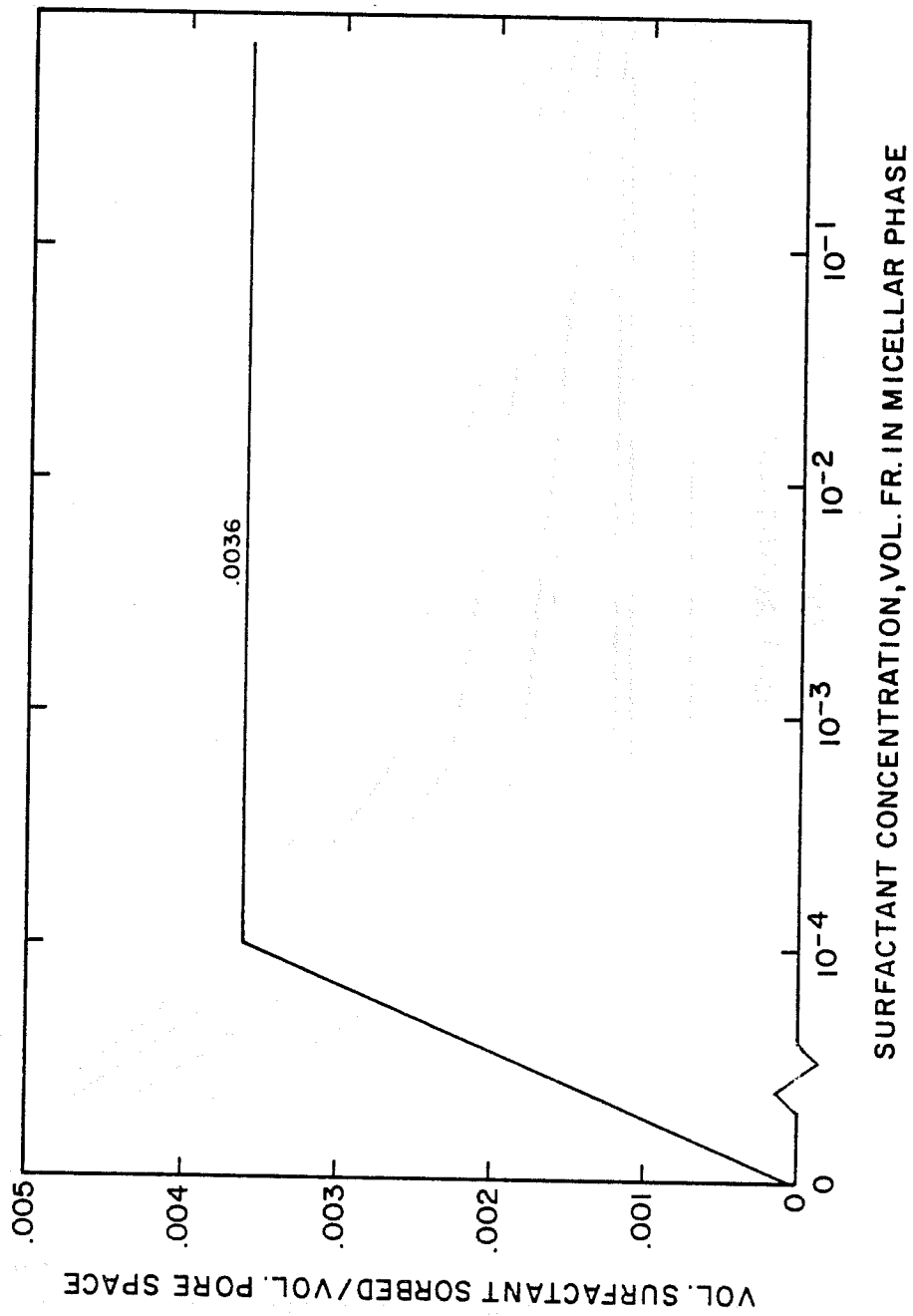


FIGURE 8
Na⁺ SORPTION

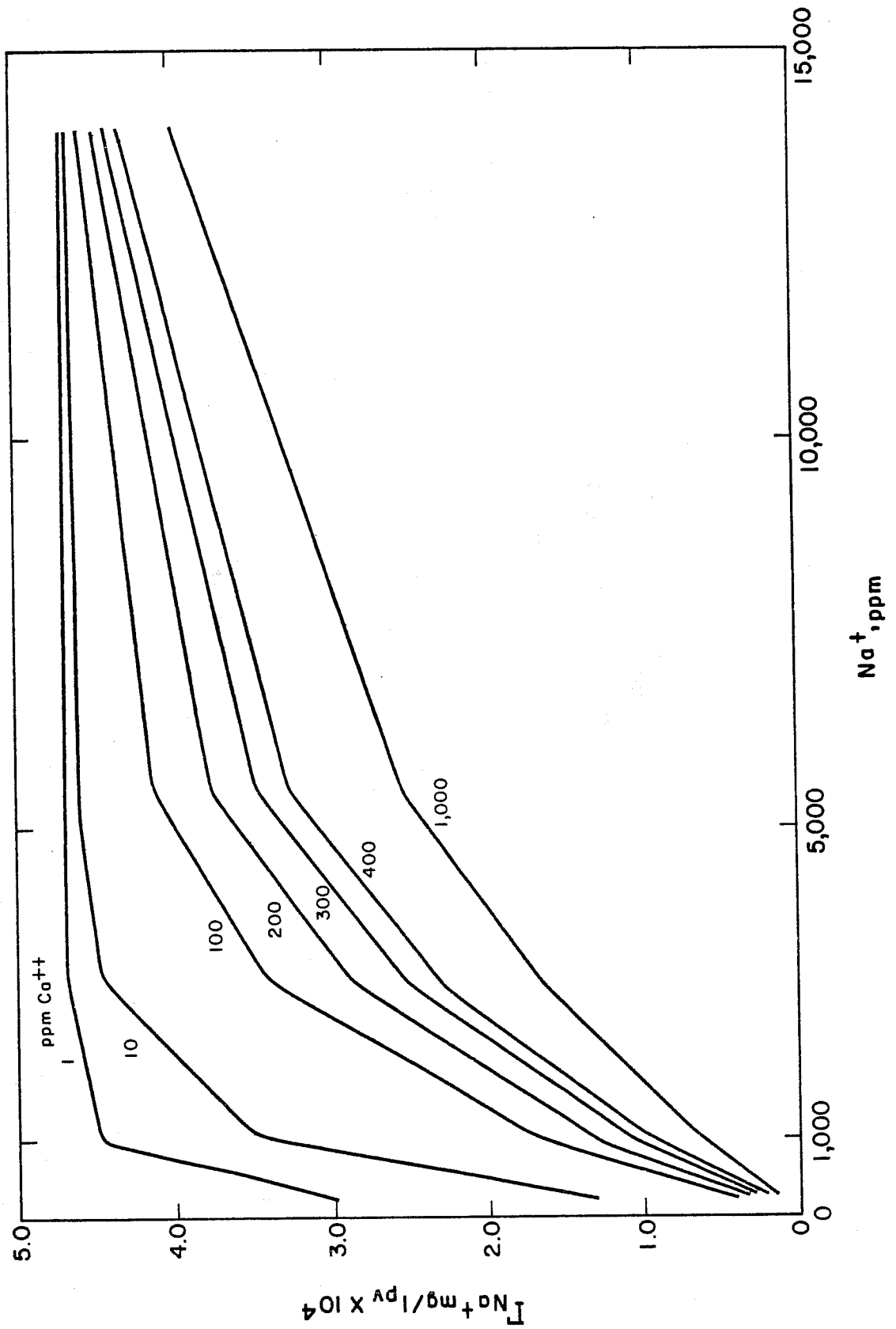


FIGURE 9
M⁺⁺ SORPTION

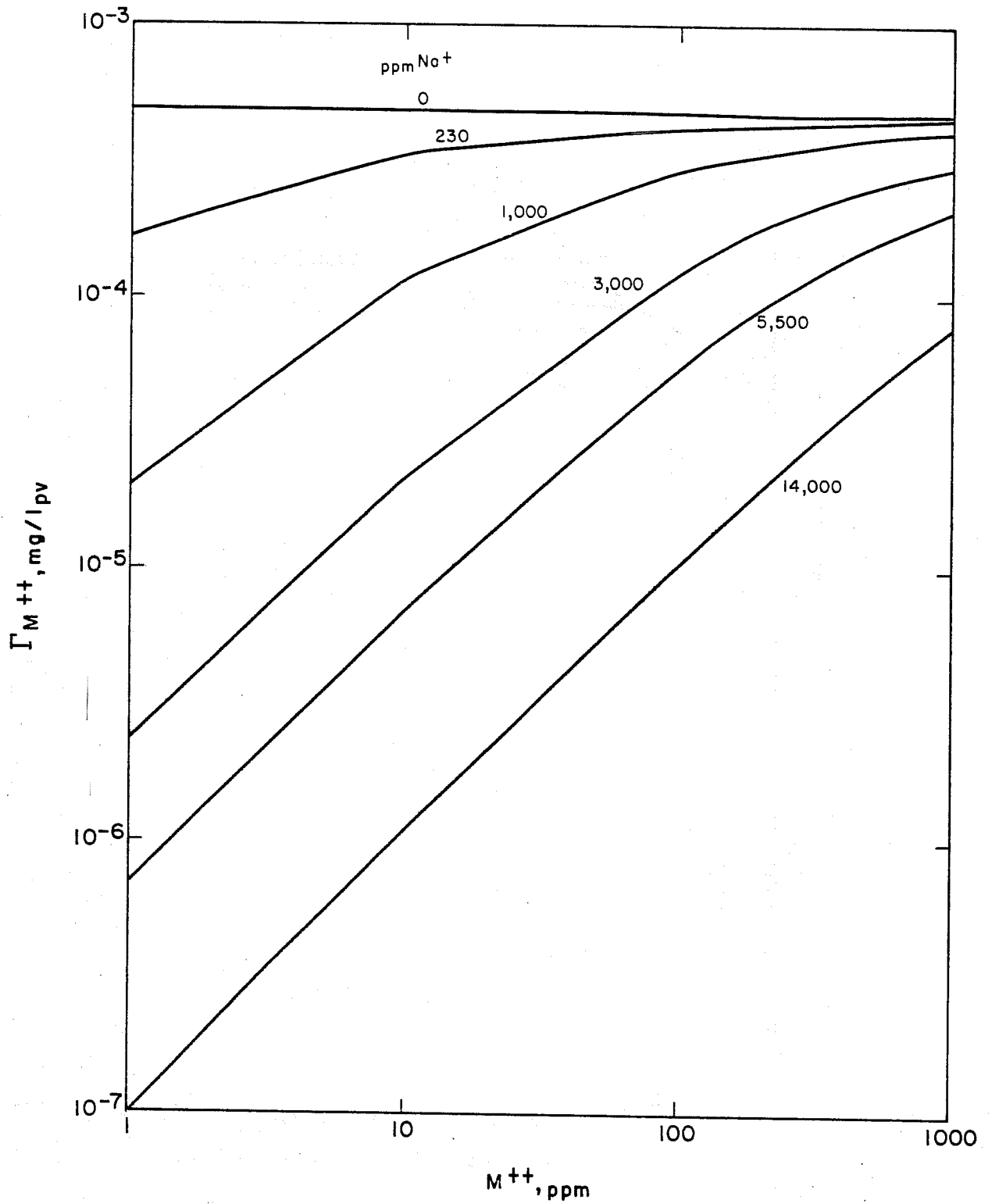


FIGURE 10

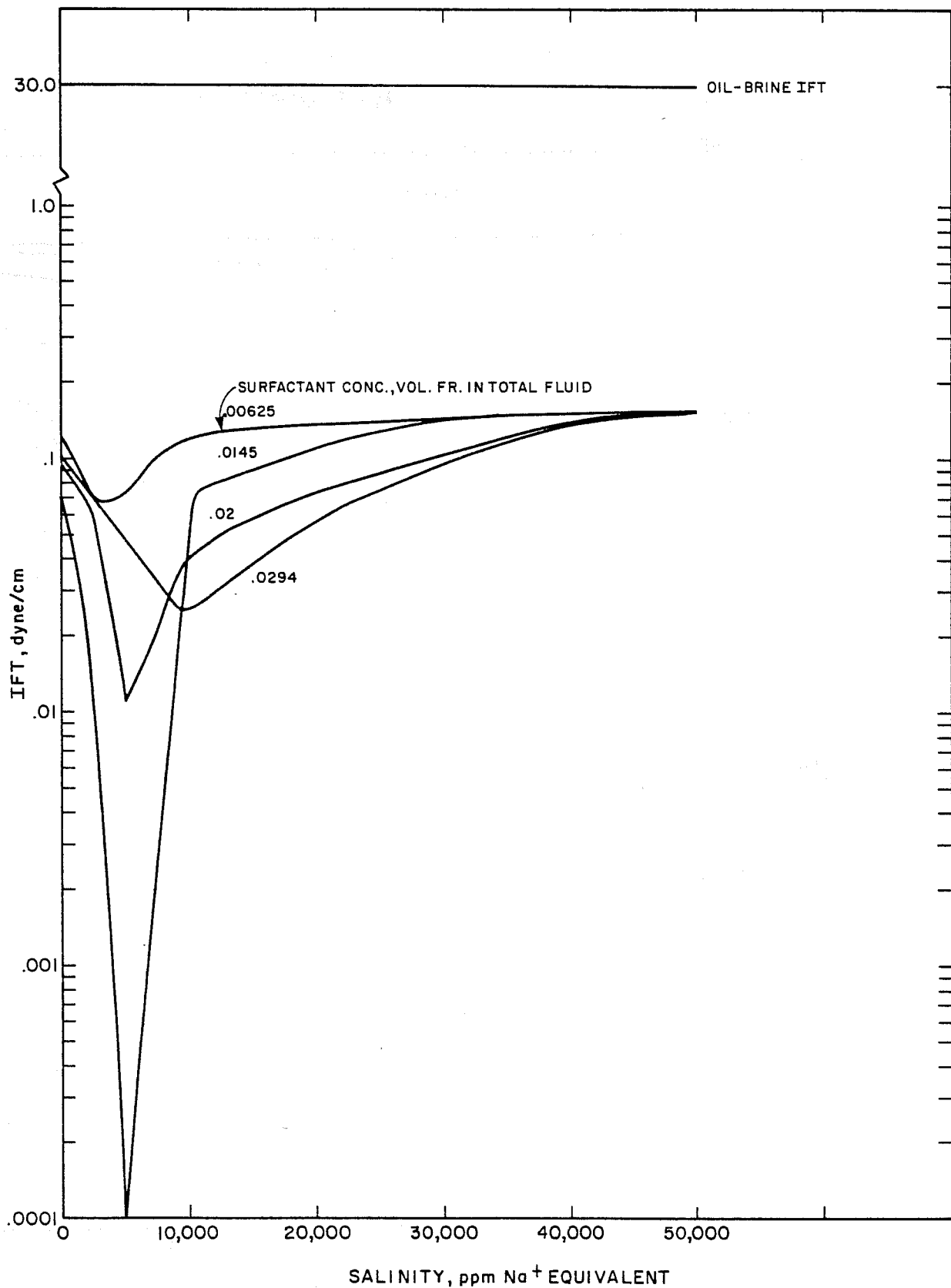
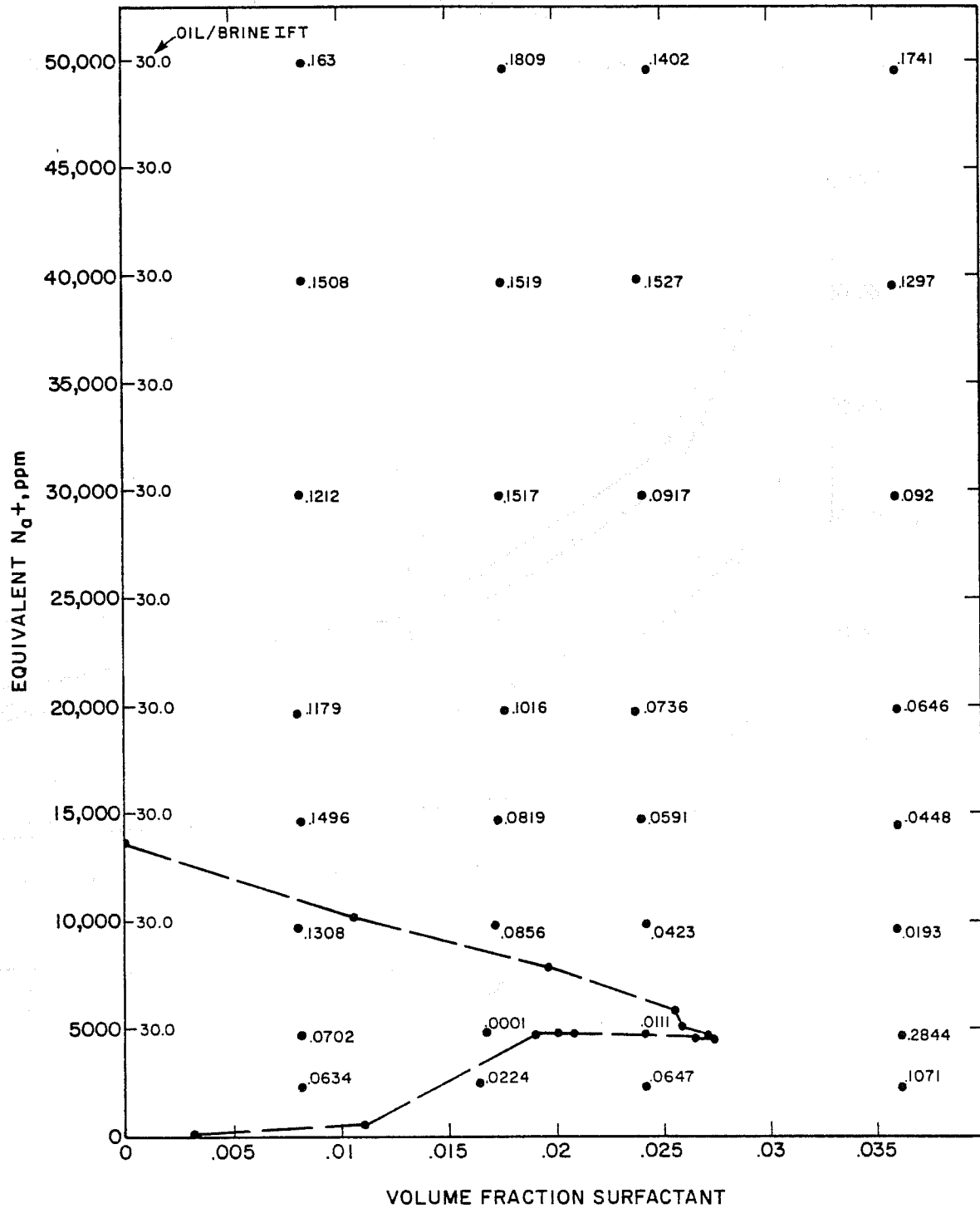


FIGURE 11
 PATH OF IFT IN GRID BLOCK 3
 CENTER STREAMTUBE



IFT REPRESENTED AS DYNE/CM

FIGURE 12
VISCOSITY FOR ABBOT BIOPOLYMER

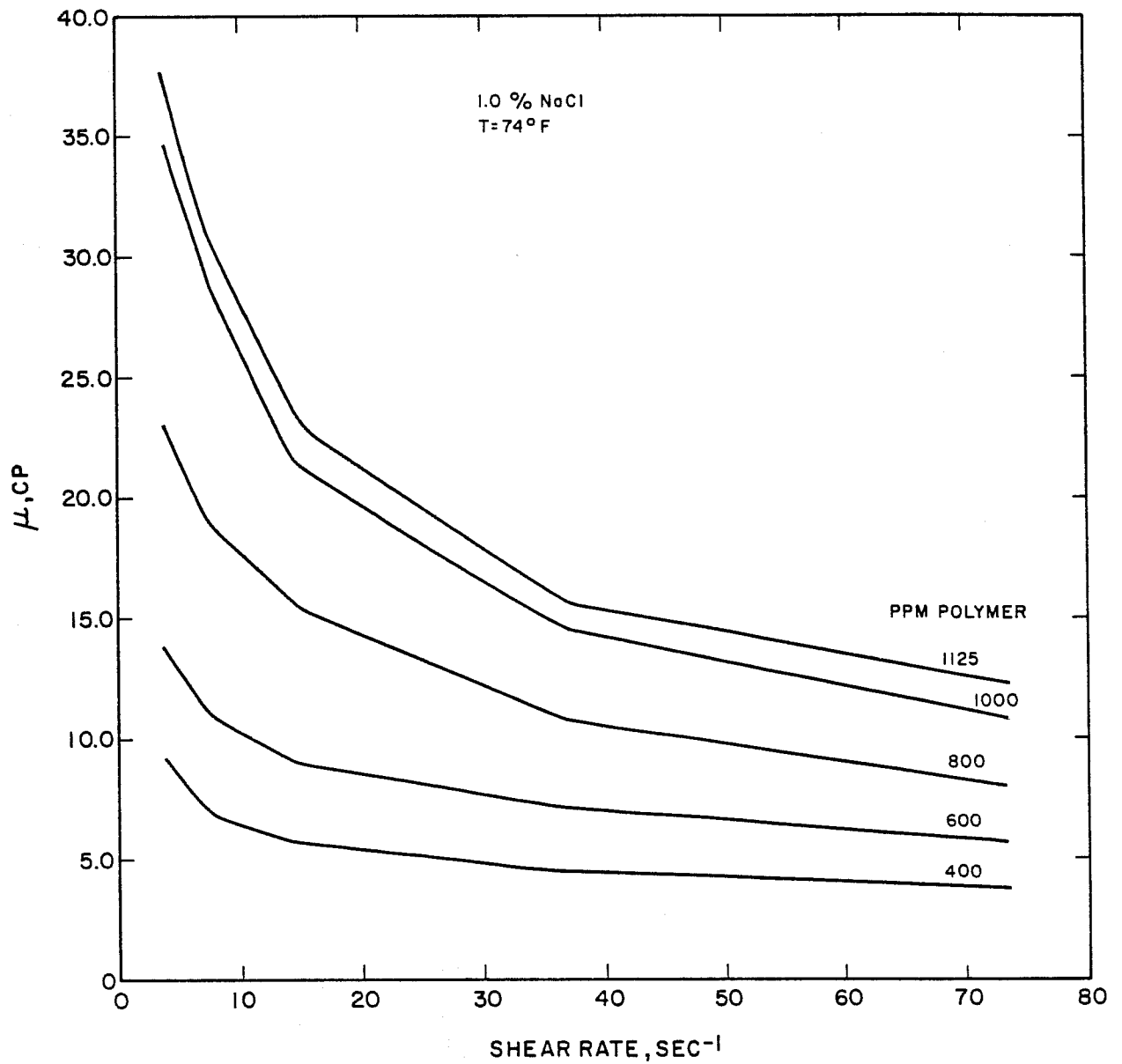


FIGURE 13
MP - 124 (OIL-DRAINAGE DATA)

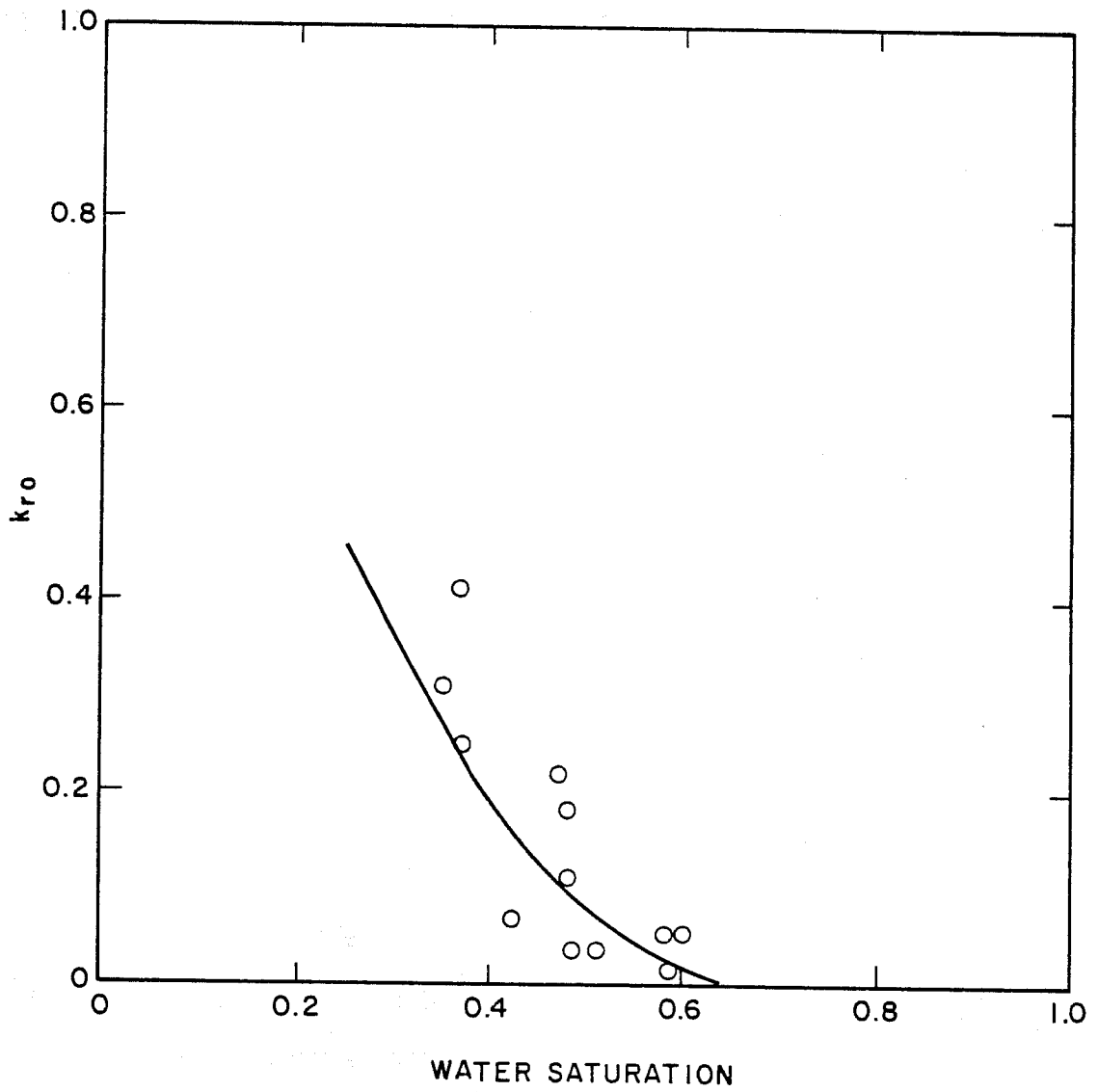


FIGURE 14
MP-124 (WATER DRAINAGE DATA)

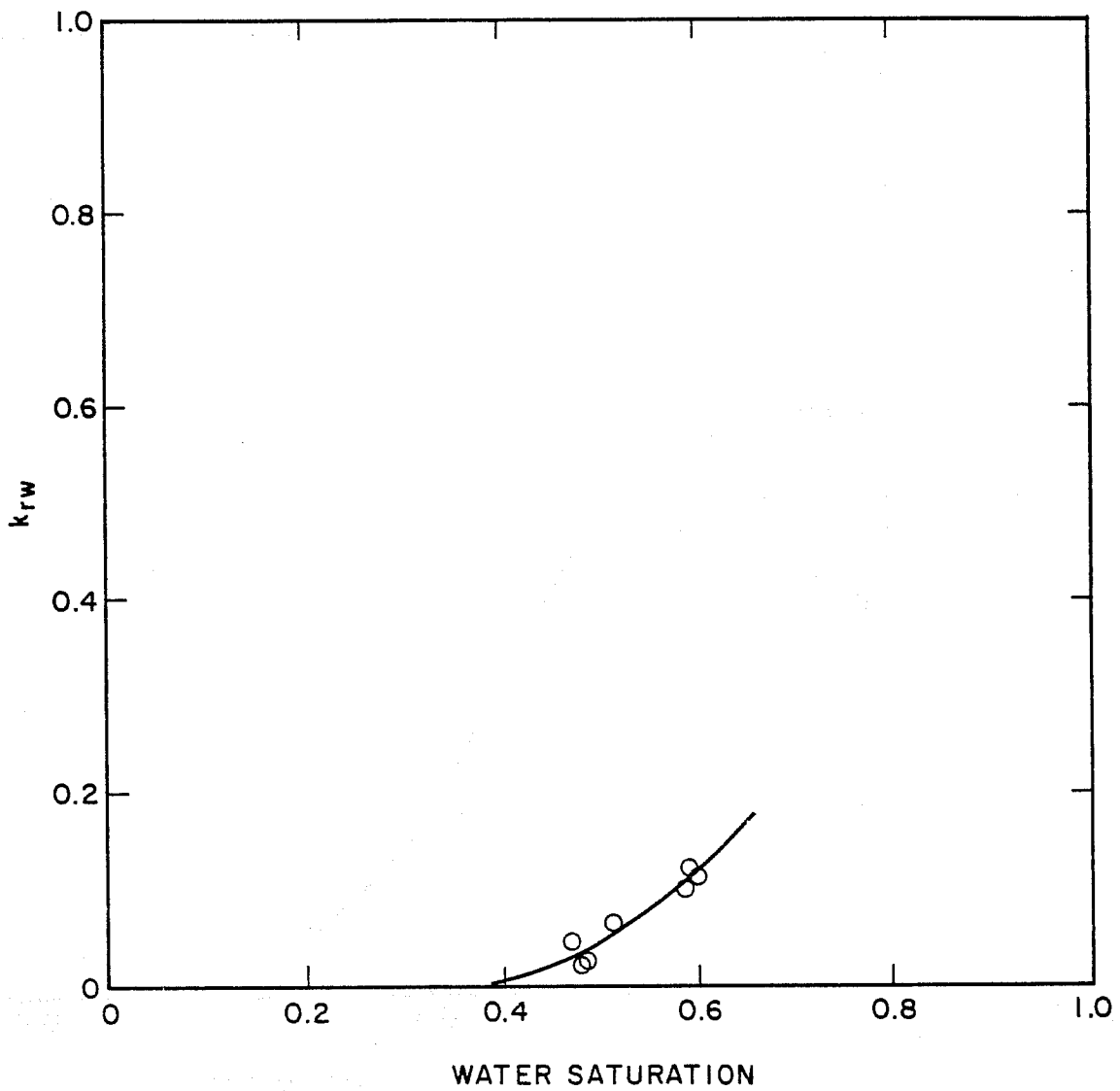


FIGURE 15
 CAPILLARY DESATURATION
 FOR ELDORADO (ADMIRE) AND BEREA SANDSTONE

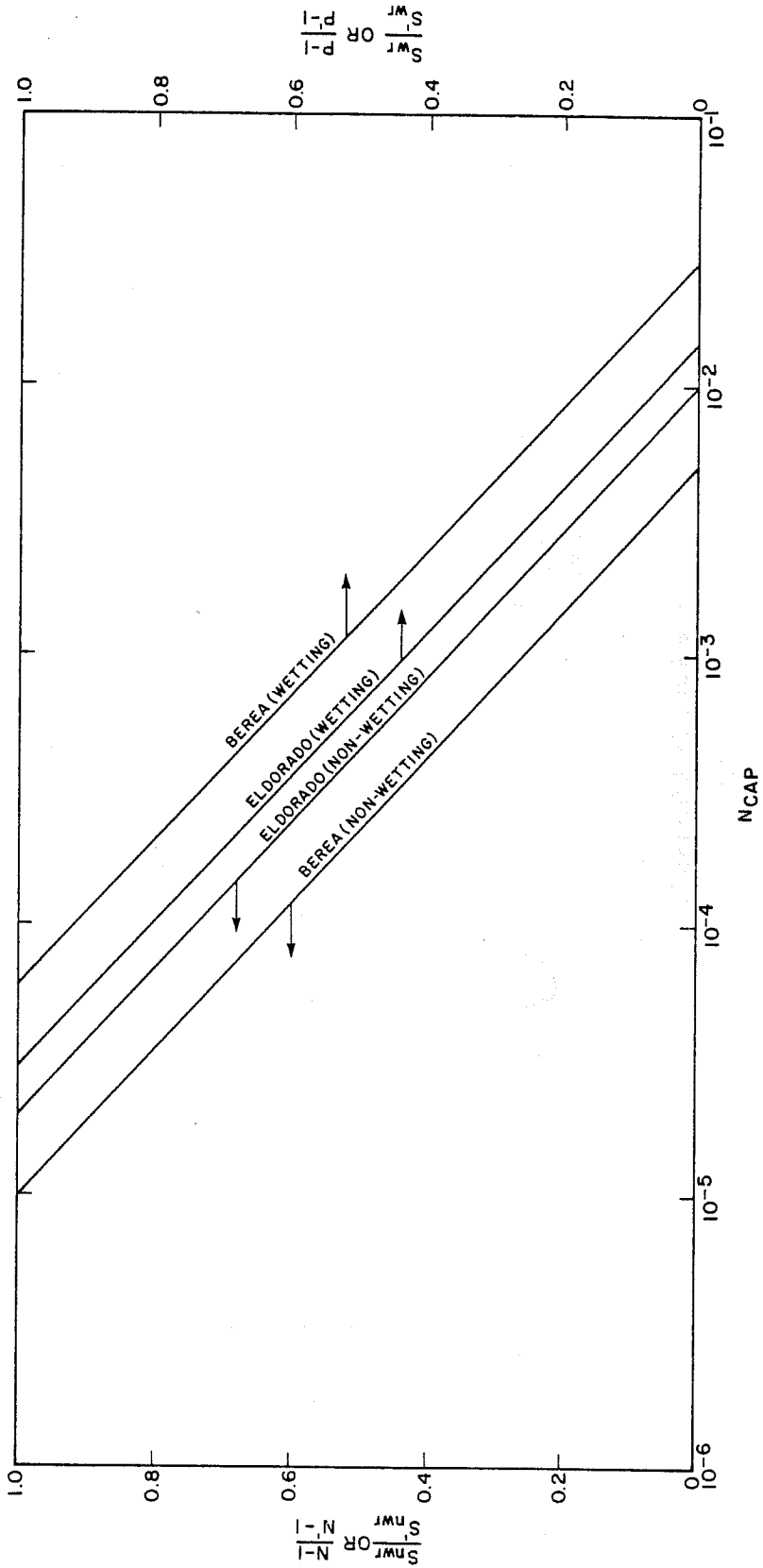


FIGURE 16
COREFLOOD 53 (SPE 8197)

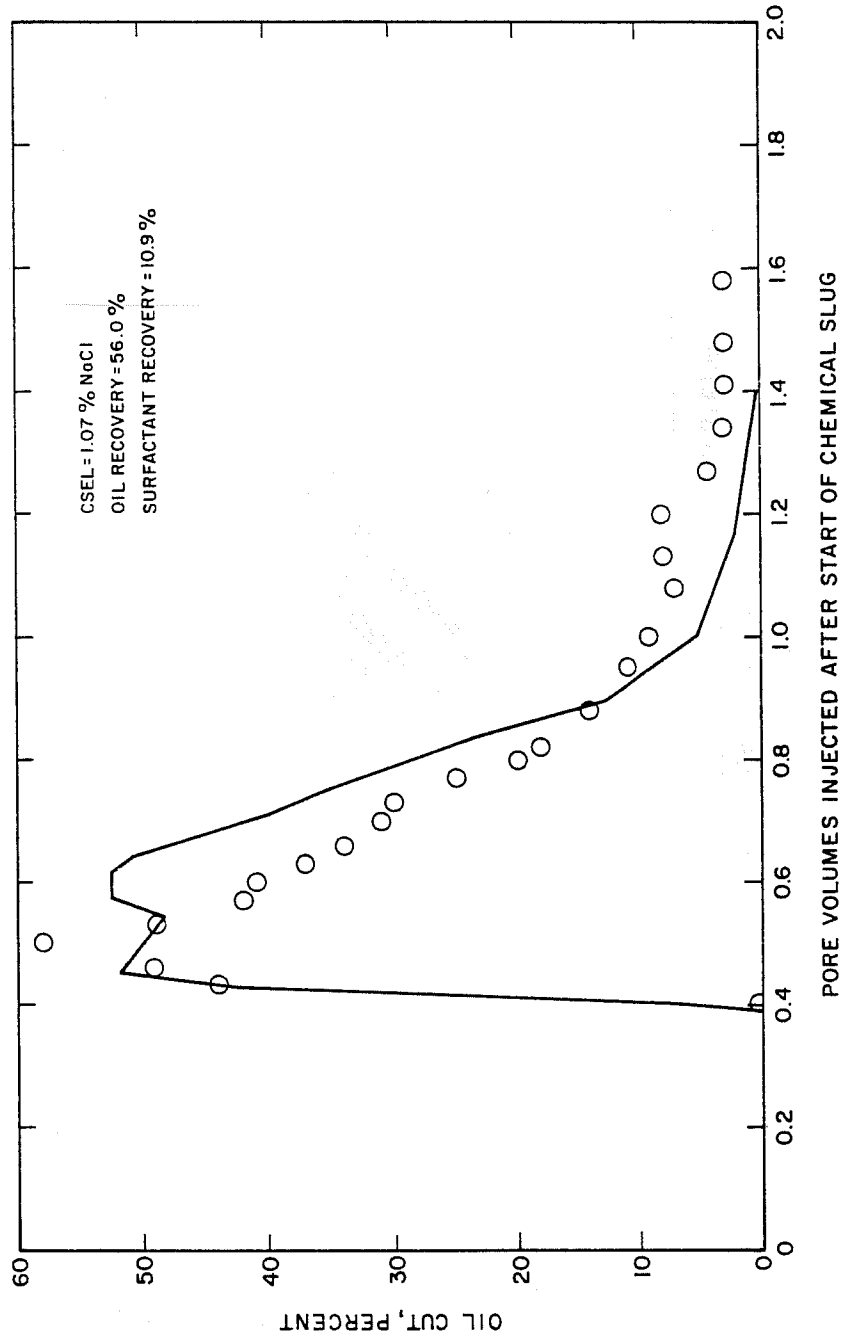
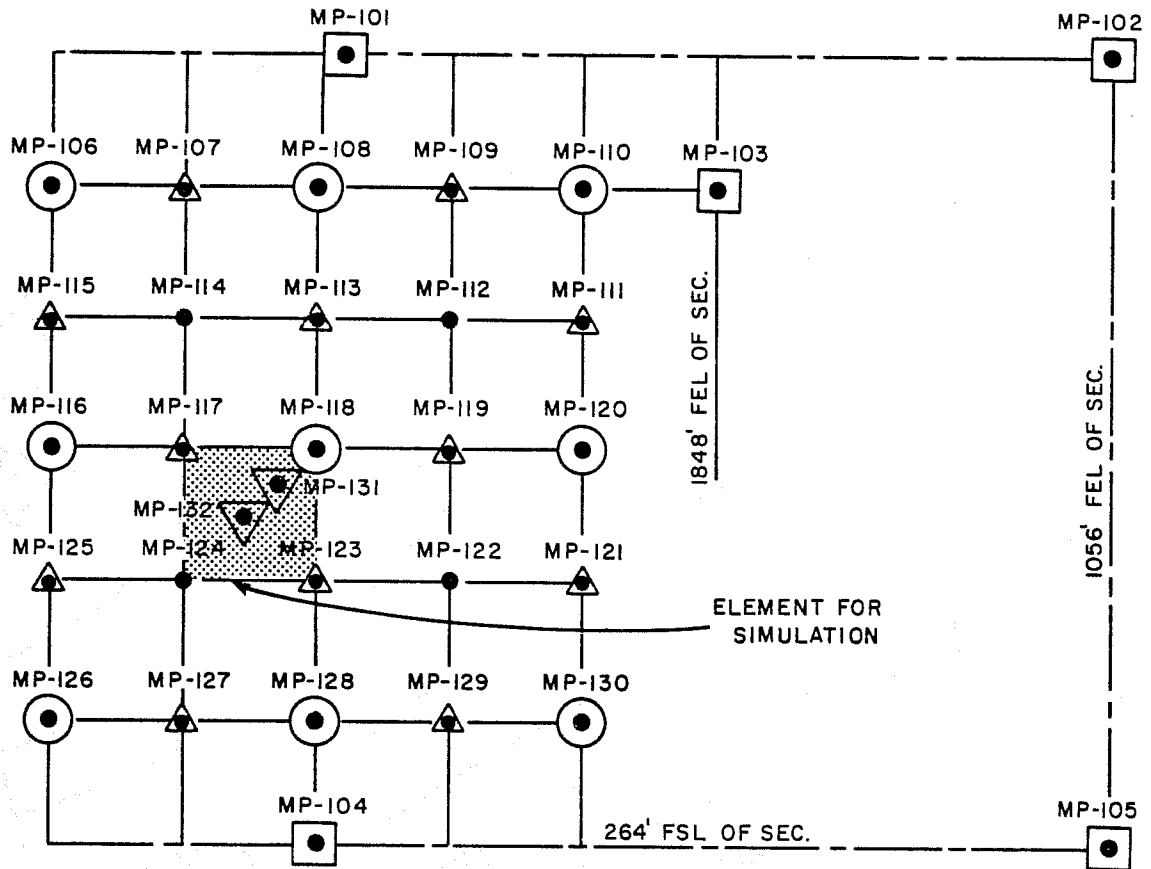


FIGURE 17



CHESNEY LSE.-SEC. 21



LEGEND

- PRODUCTION WELLS
- ⊙ INJECTION WELLS
- ▽ OBSERVATION WELLS
- ⊠ TEST WELLS
- △ MONITORING WELLS

FIGURE 18
GRID FOR EL DORADO MICELLAR-POLYMER SIMULATION

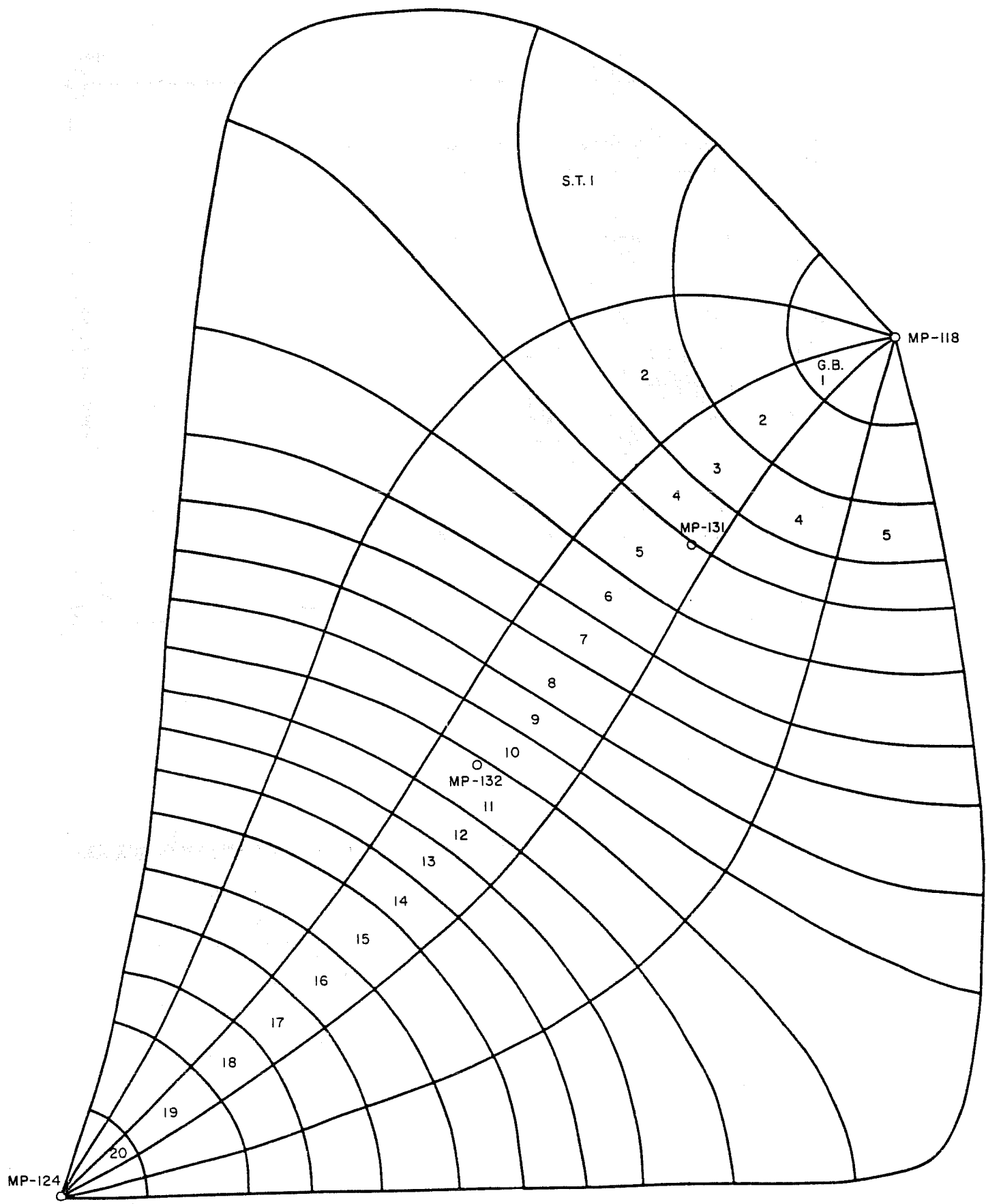
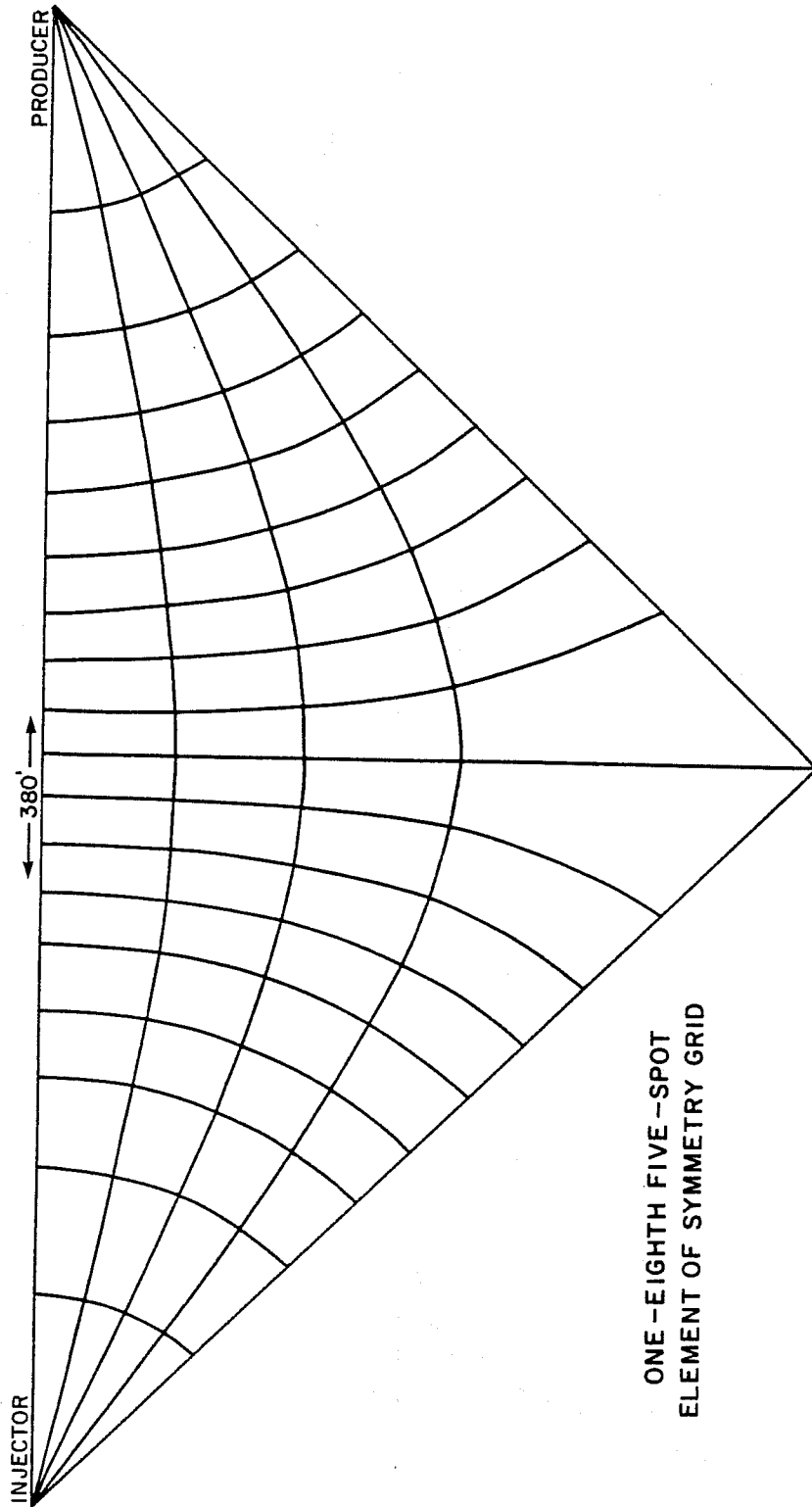


FIGURE 19



ONE - EIGHTH FIVE - SPOT
ELEMENT OF SYMMETRY GRID

FIGURE 20

FLUID SAMPLES AT MP-131

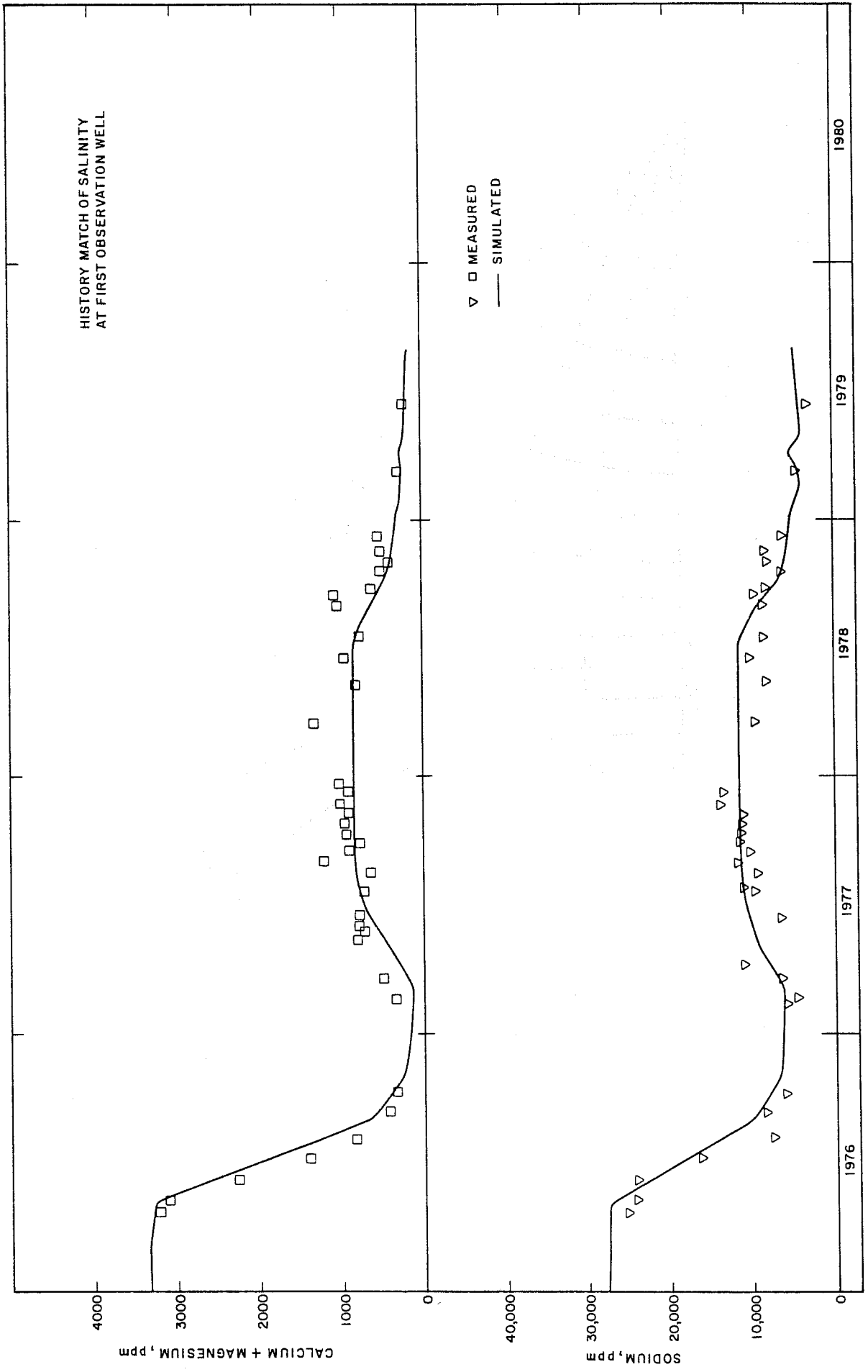


FIGURE 21
 FLUID SAMPLES AT MP-132

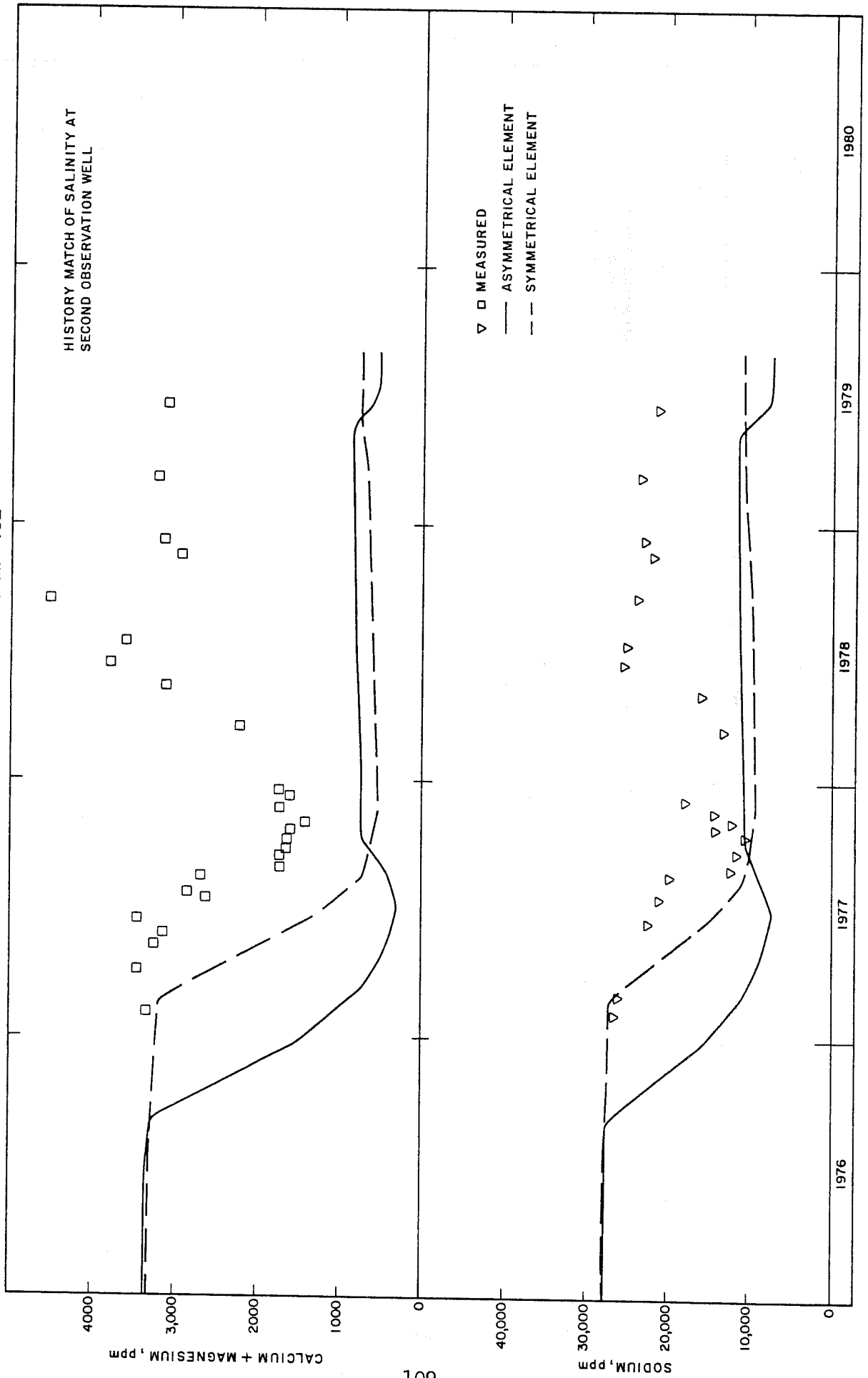


FIGURE 22

FLUID SAMPLES AT MP - 124

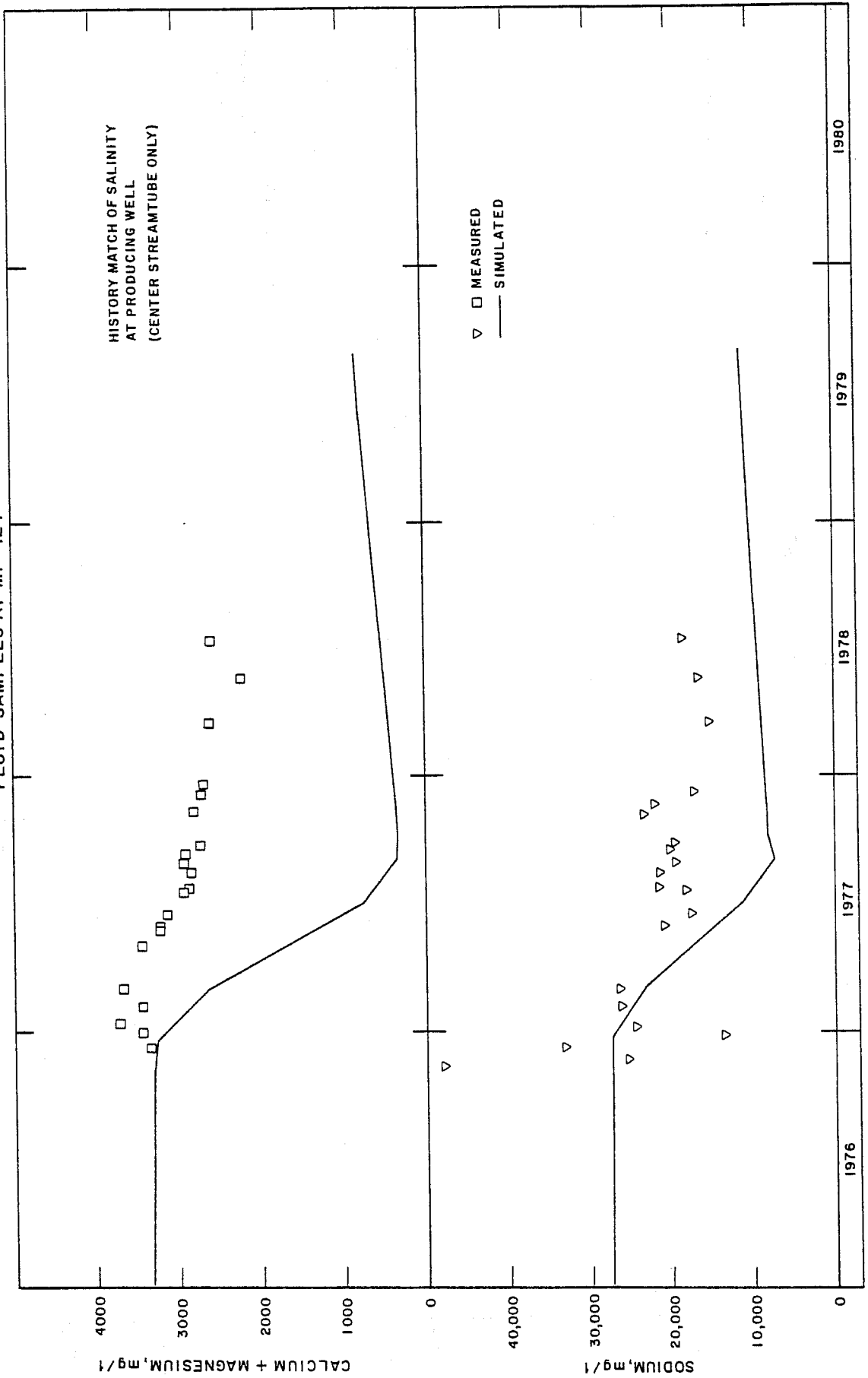


FIGURE 23
FLUID SAMPLES AT MP-124

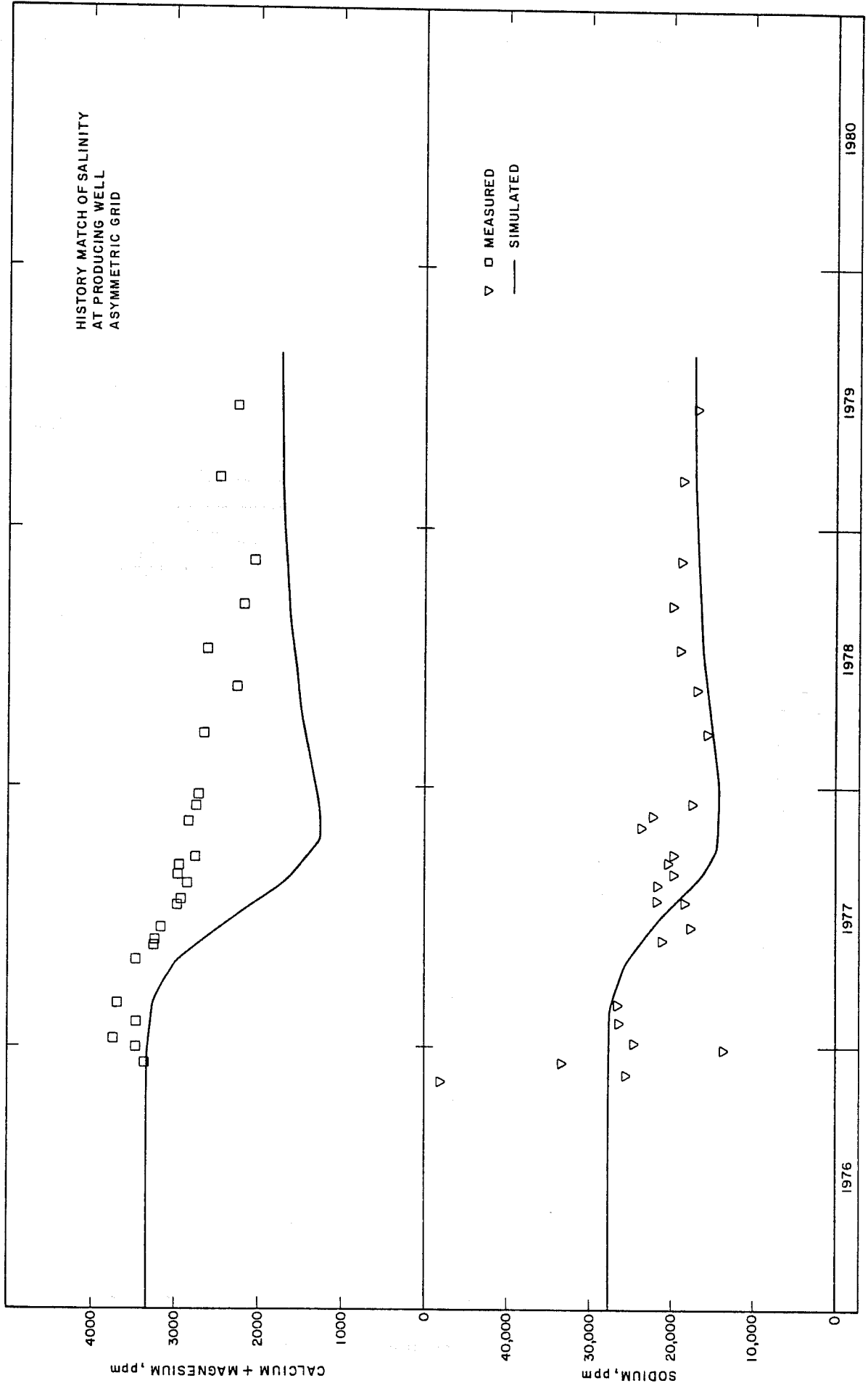


FIGURE 24

FLUID SAMPLES AT MP-131

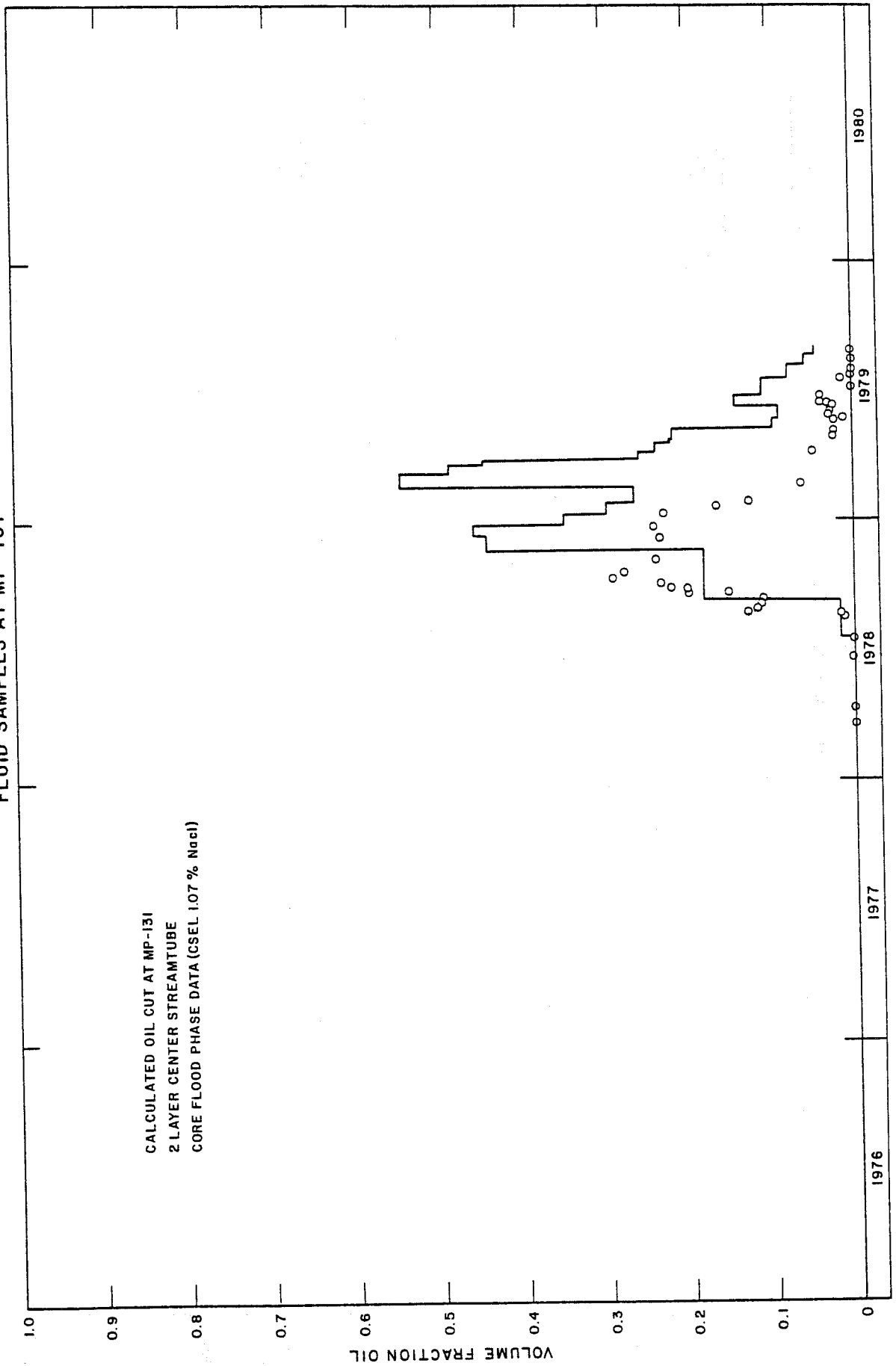


FIGURE 25

FLUID SAMPLES AT MP-131

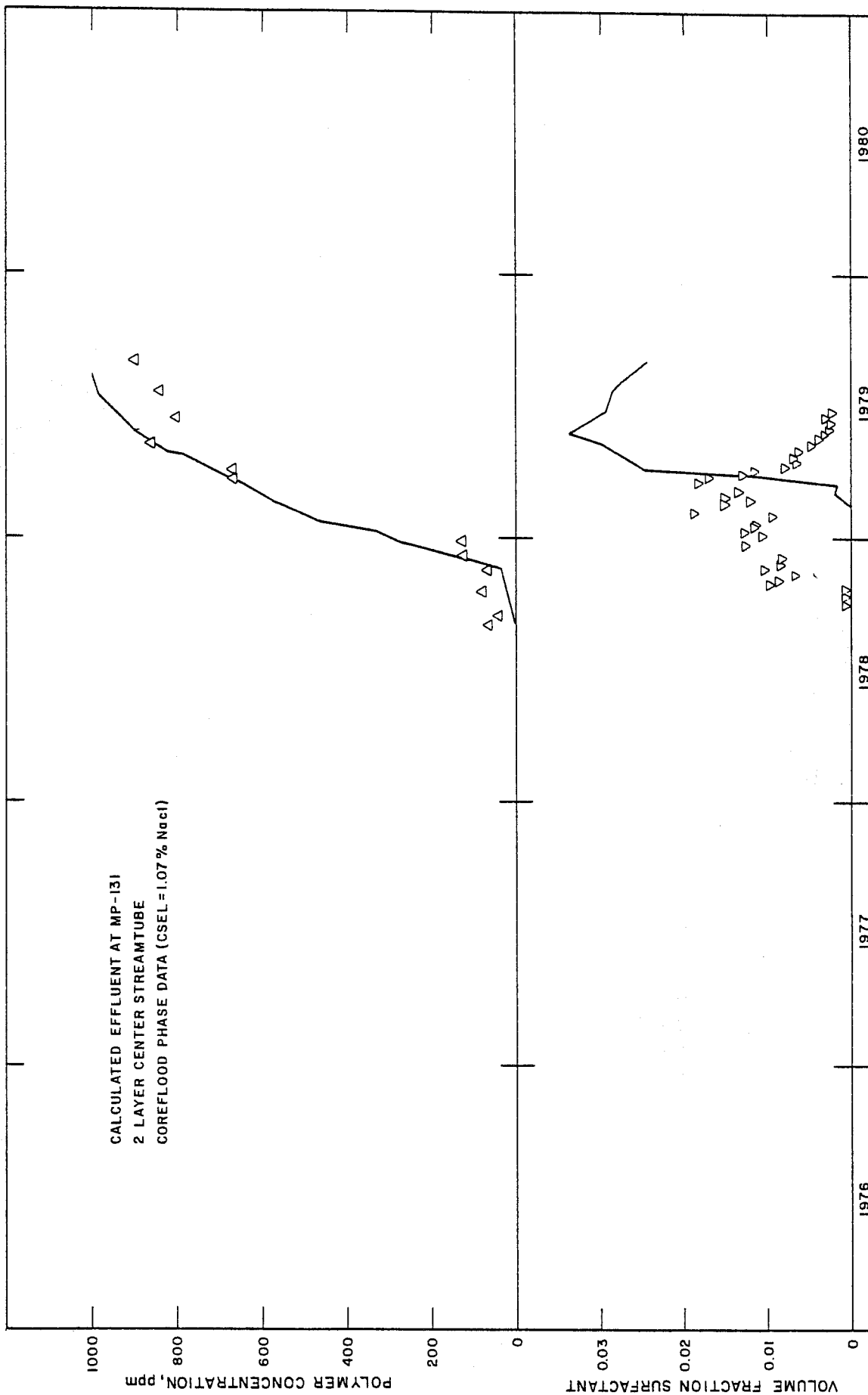


FIGURE 26

FLUID SAMPLES AT MP-131

CALCULATED OIL CUT AT MP-131
2 LAYER CENTER STREAMTUBE
HISTORY MATCH PHASE DATA (CSEL=0.35% NaCl)

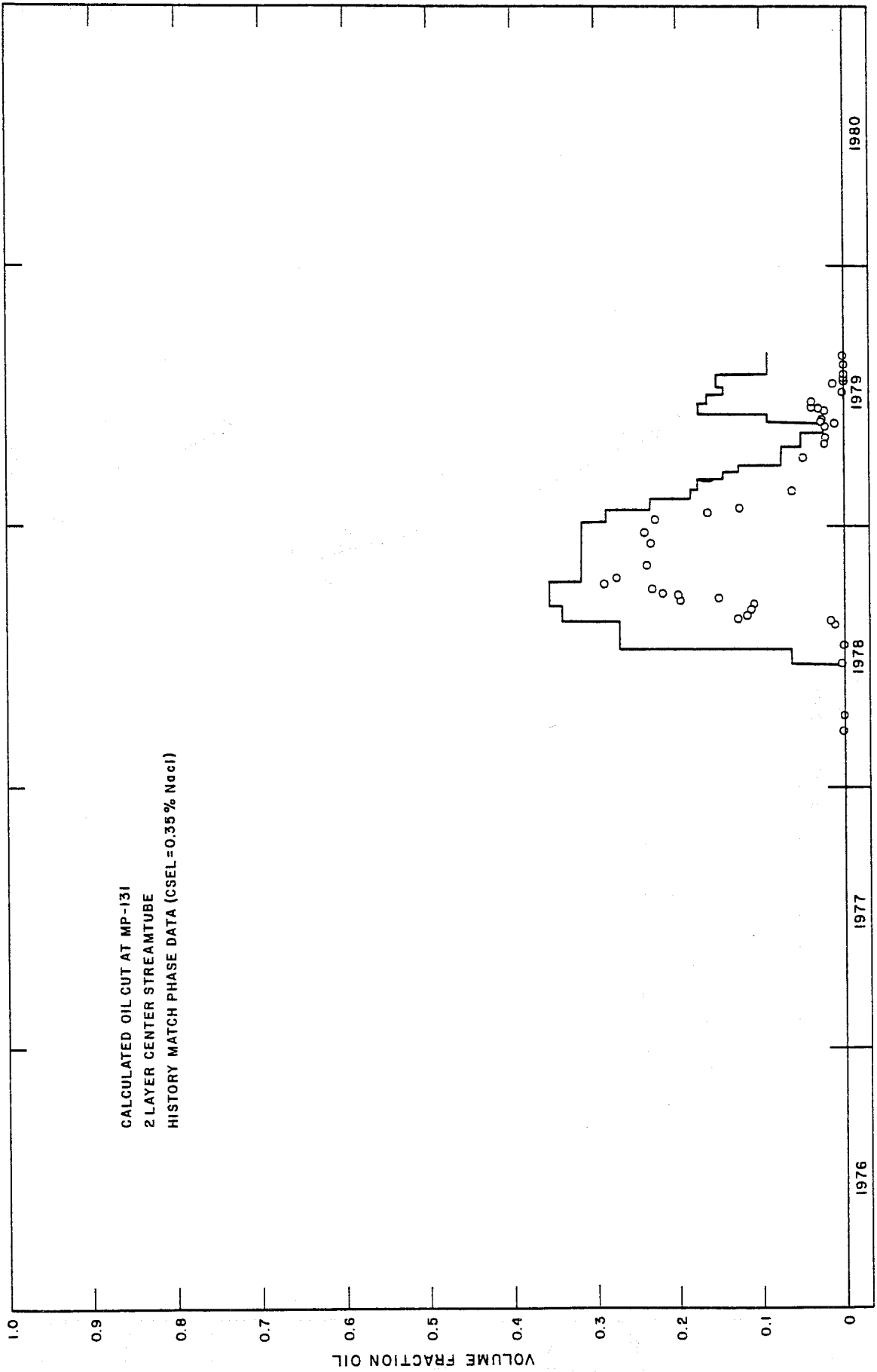


FIGURE 27

FLUID SAMPLES AT MP-131

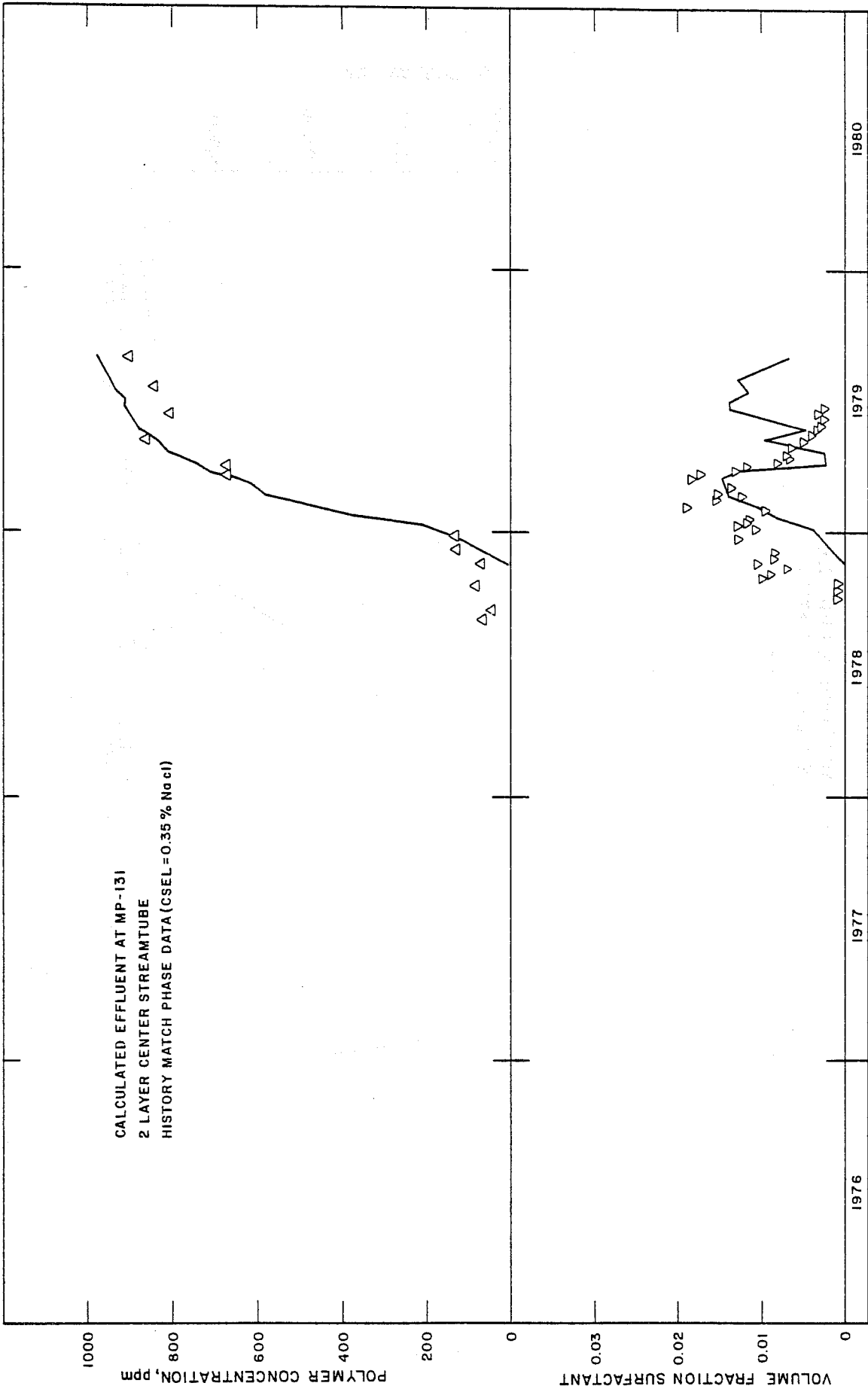


FIGURE 28
 PATH OF FLOOD IN GRID BLOCK 3
 CENTER STREAMTUBE

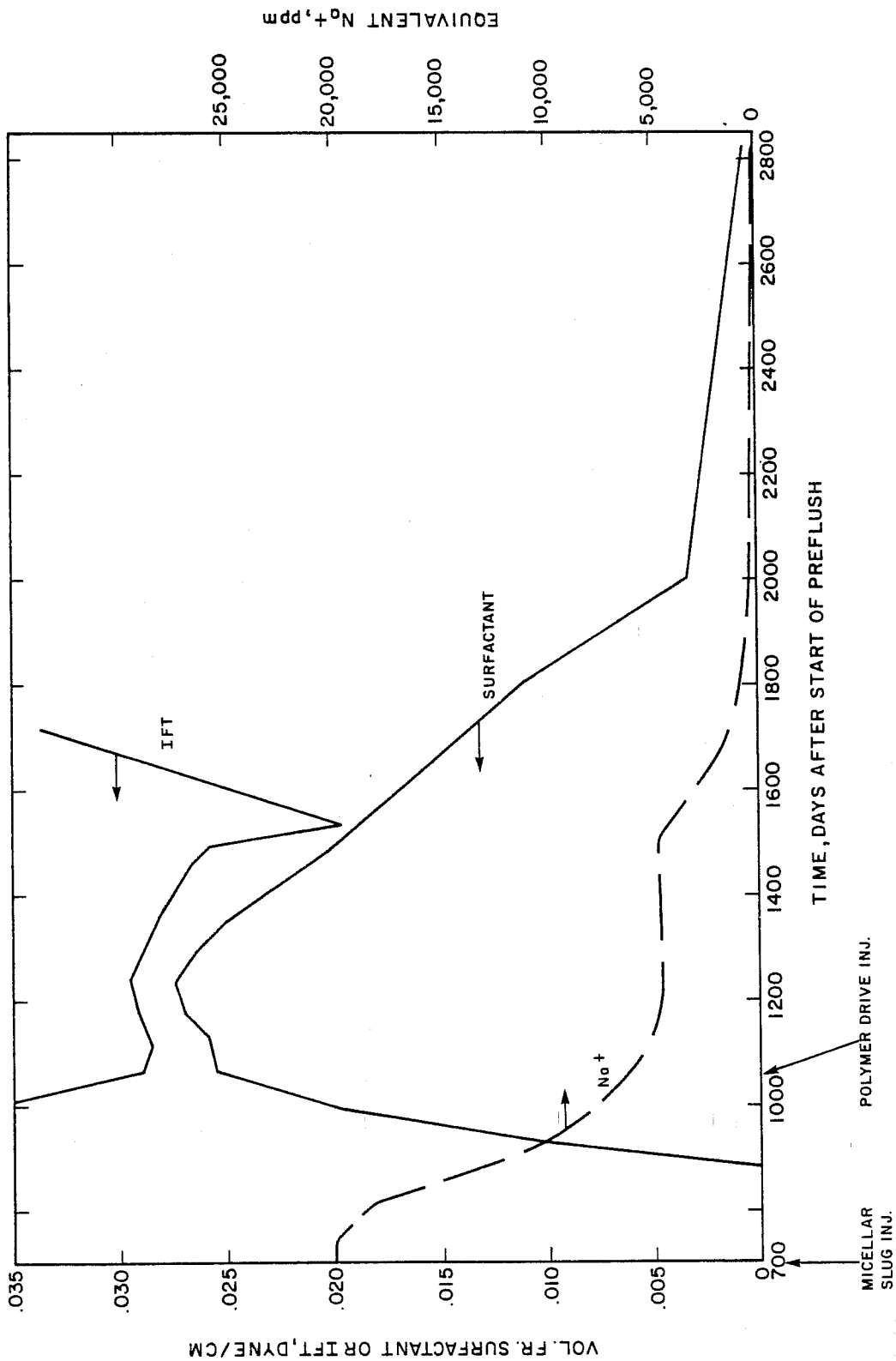


FIGURE 29
FLUID SAMPLES AT MP-131

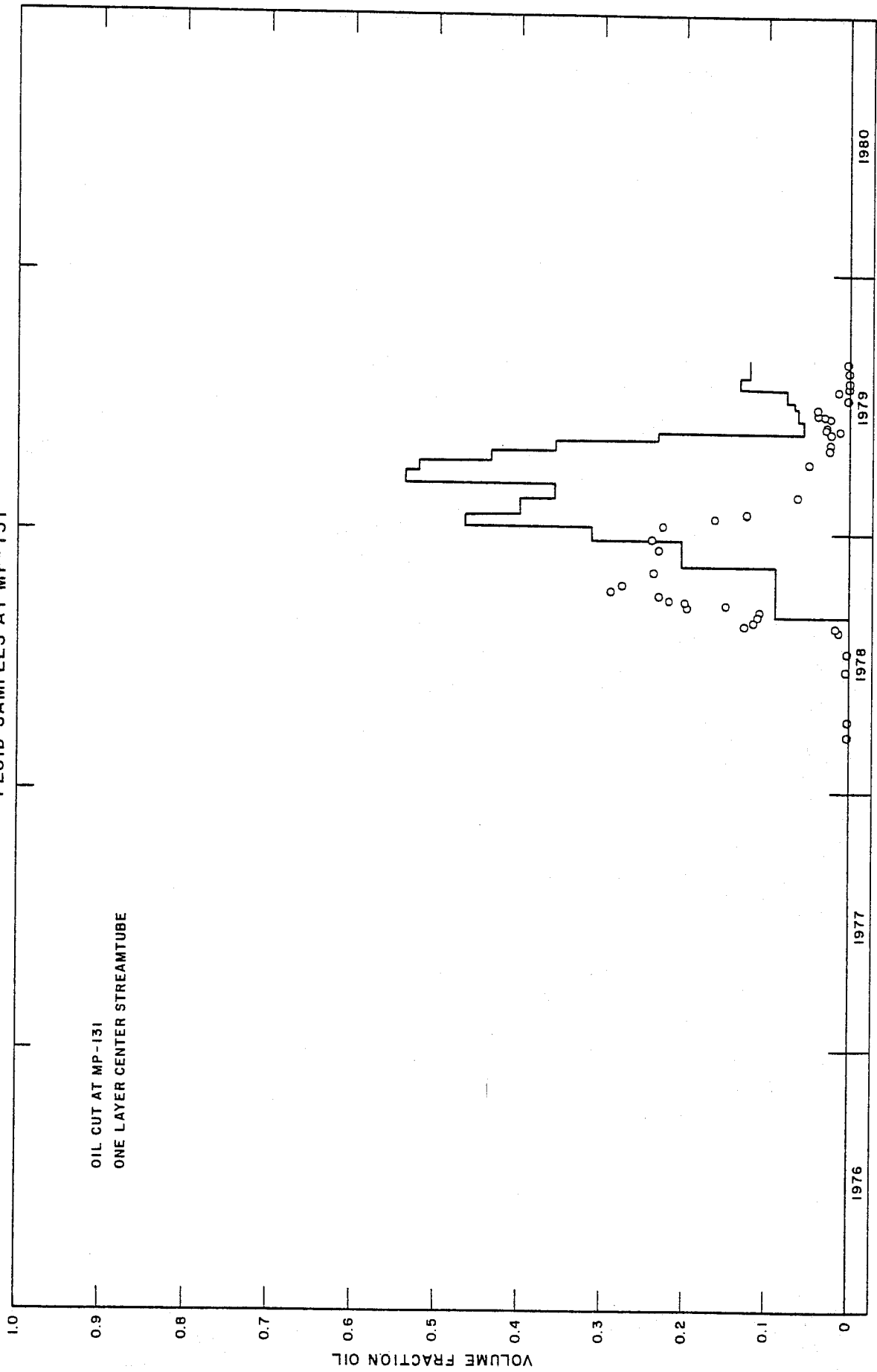


FIGURE 30
 FLUID SAMPLES AT MP-131

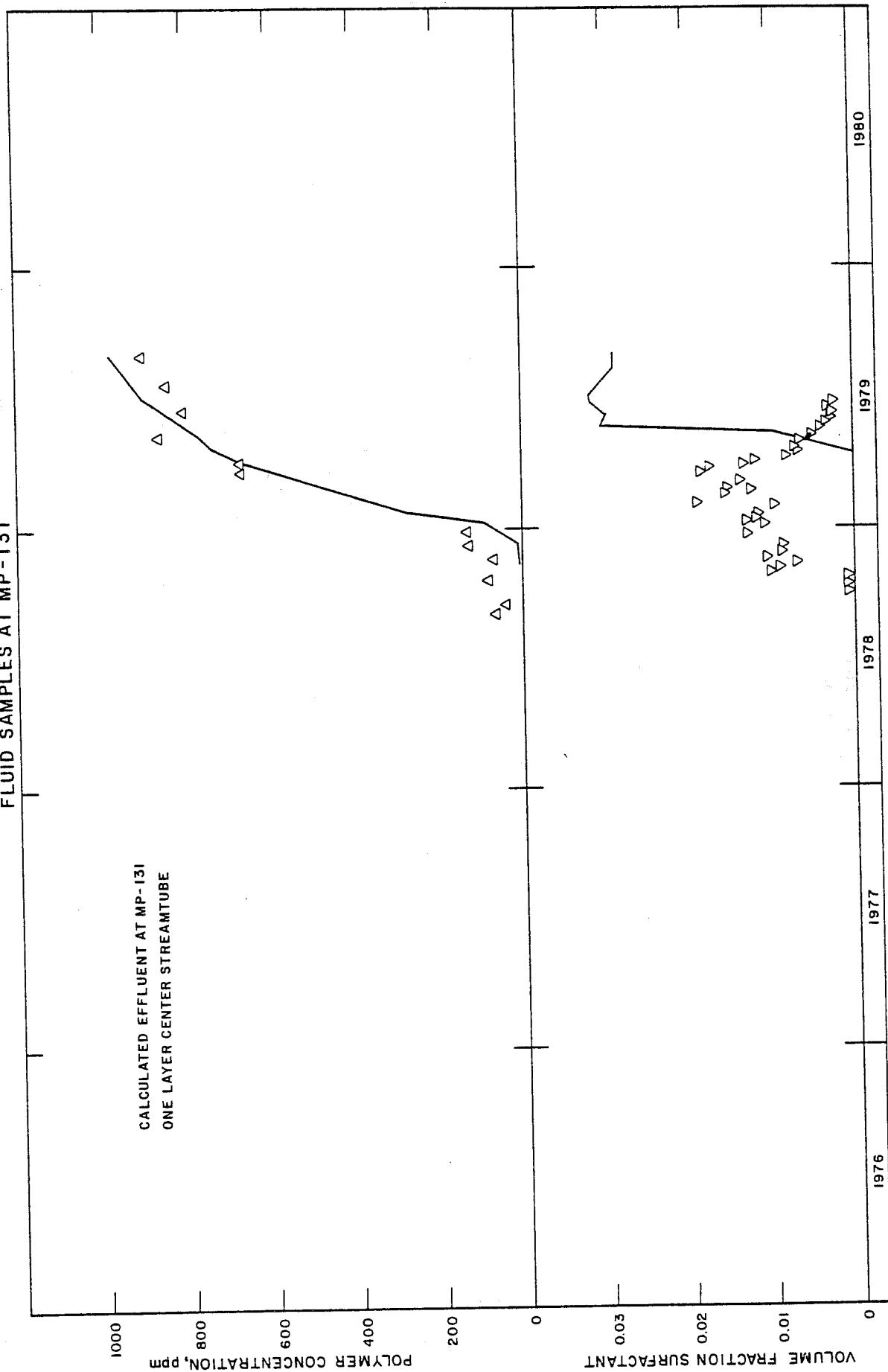


FIGURE 31
 INSTANTANEOUS PROFILES AT 19 % PV INJECTED AFTER PREFLUSH

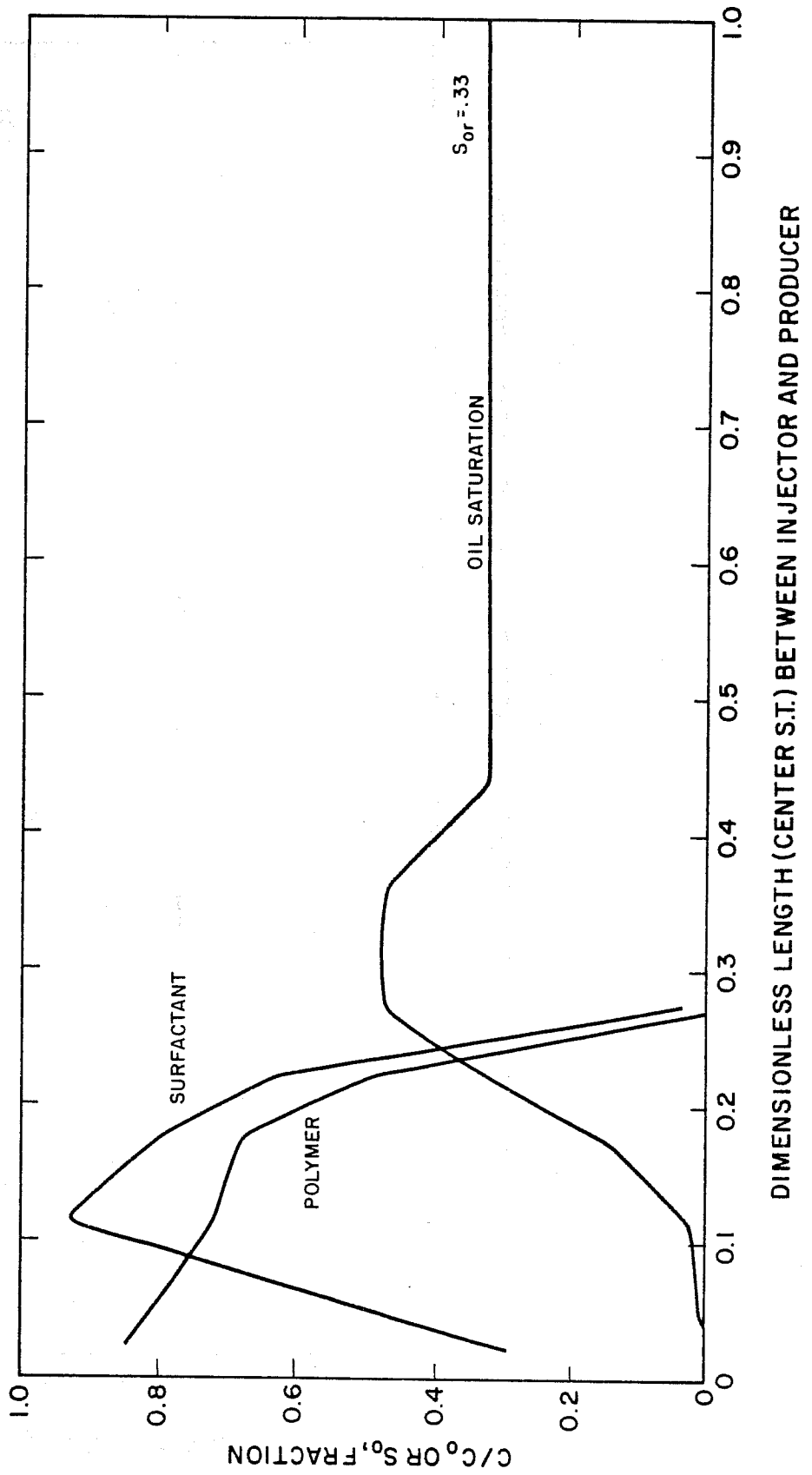


FIGURE 32
 INSTANTANEOUS PROFILES AT 36 % PV INJECTED AFTER PREFLUSH

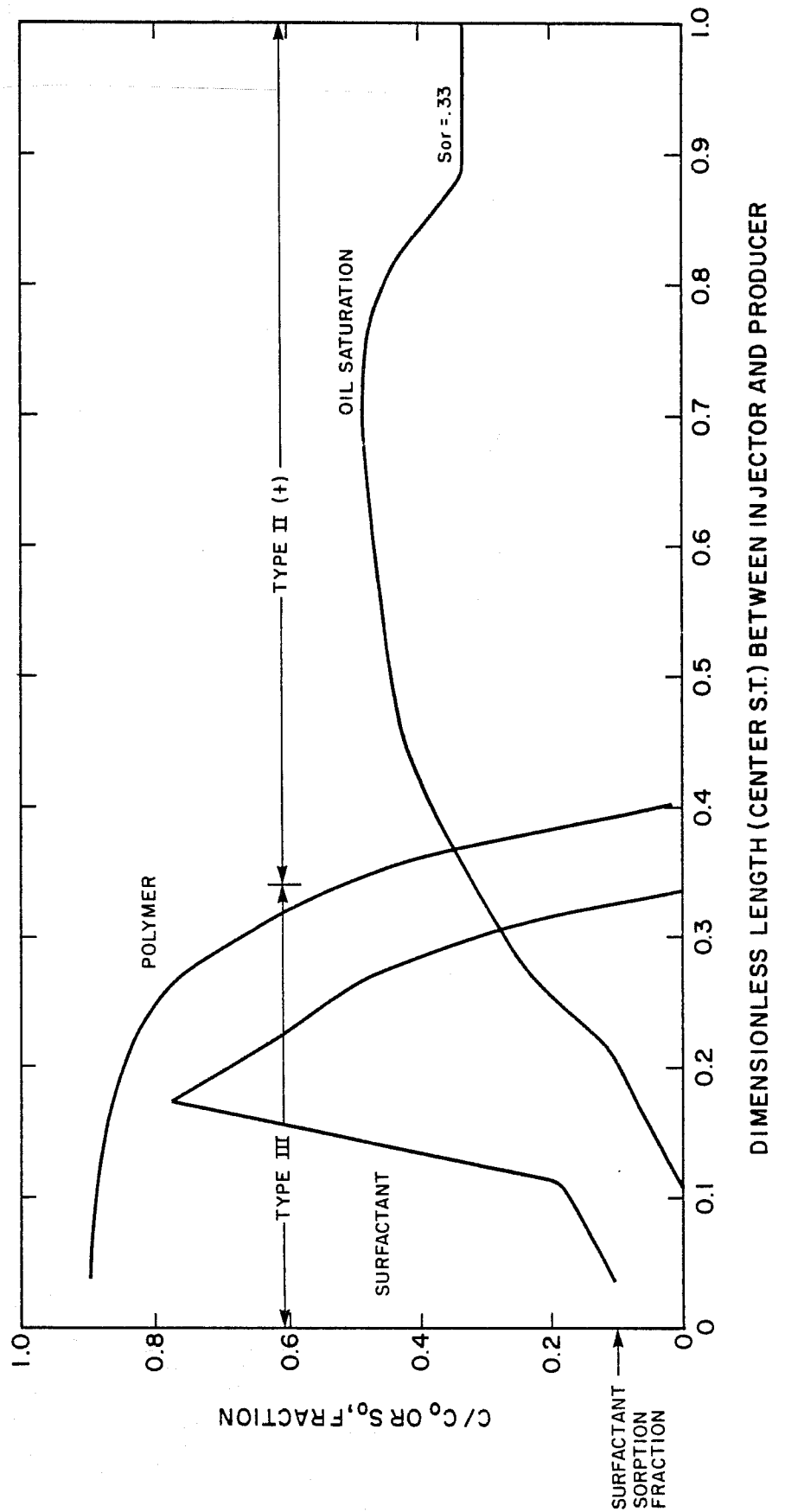


FIGURE 33
 INSTANTANEOUS PROFILES AT 79 % PV INJECTED AFTER PREFLUSH

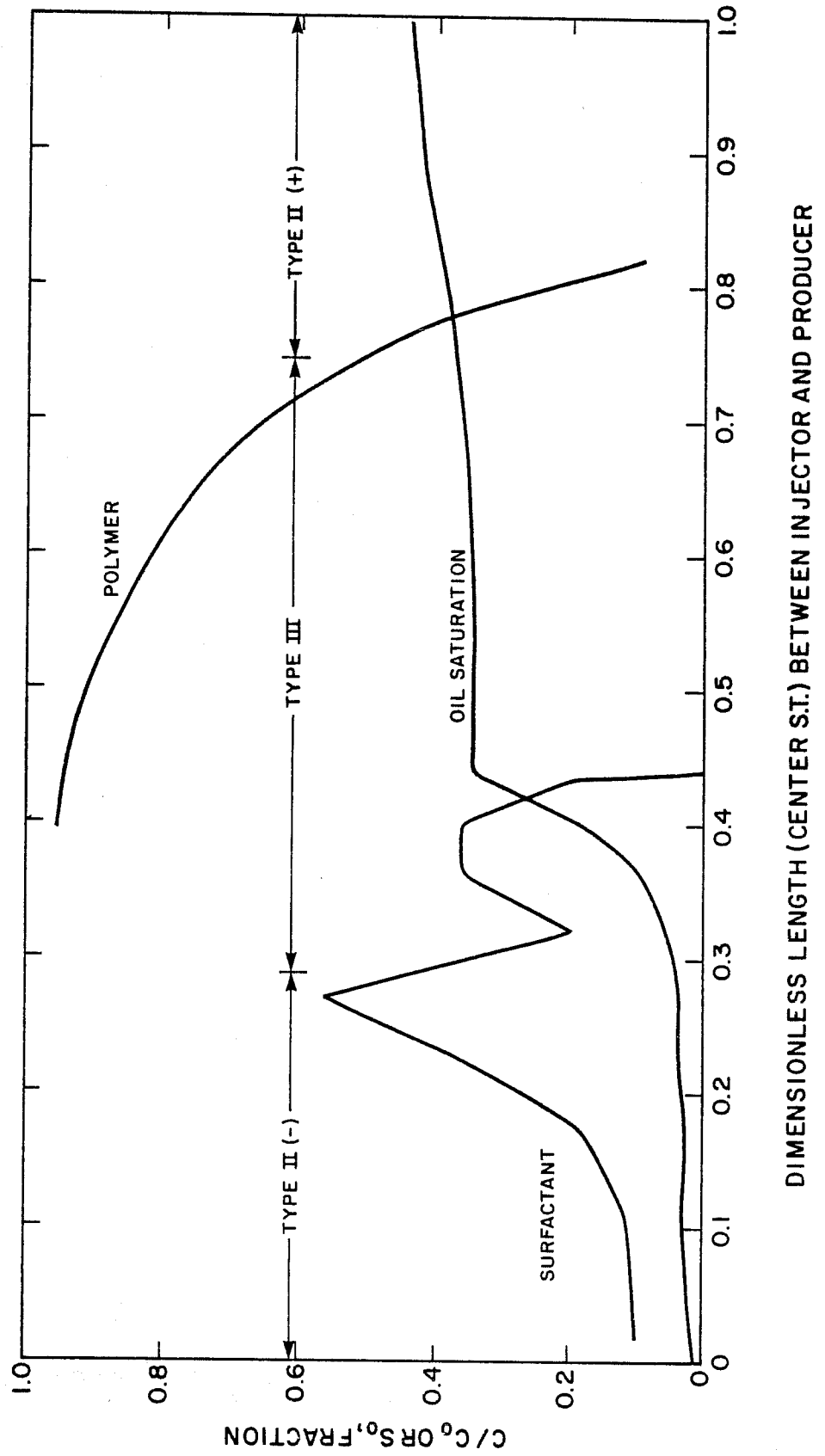


FIGURE 34
INSTANTANEOUS PROFILES AT 112 % PV INJECTED AFTER PREFLUSH

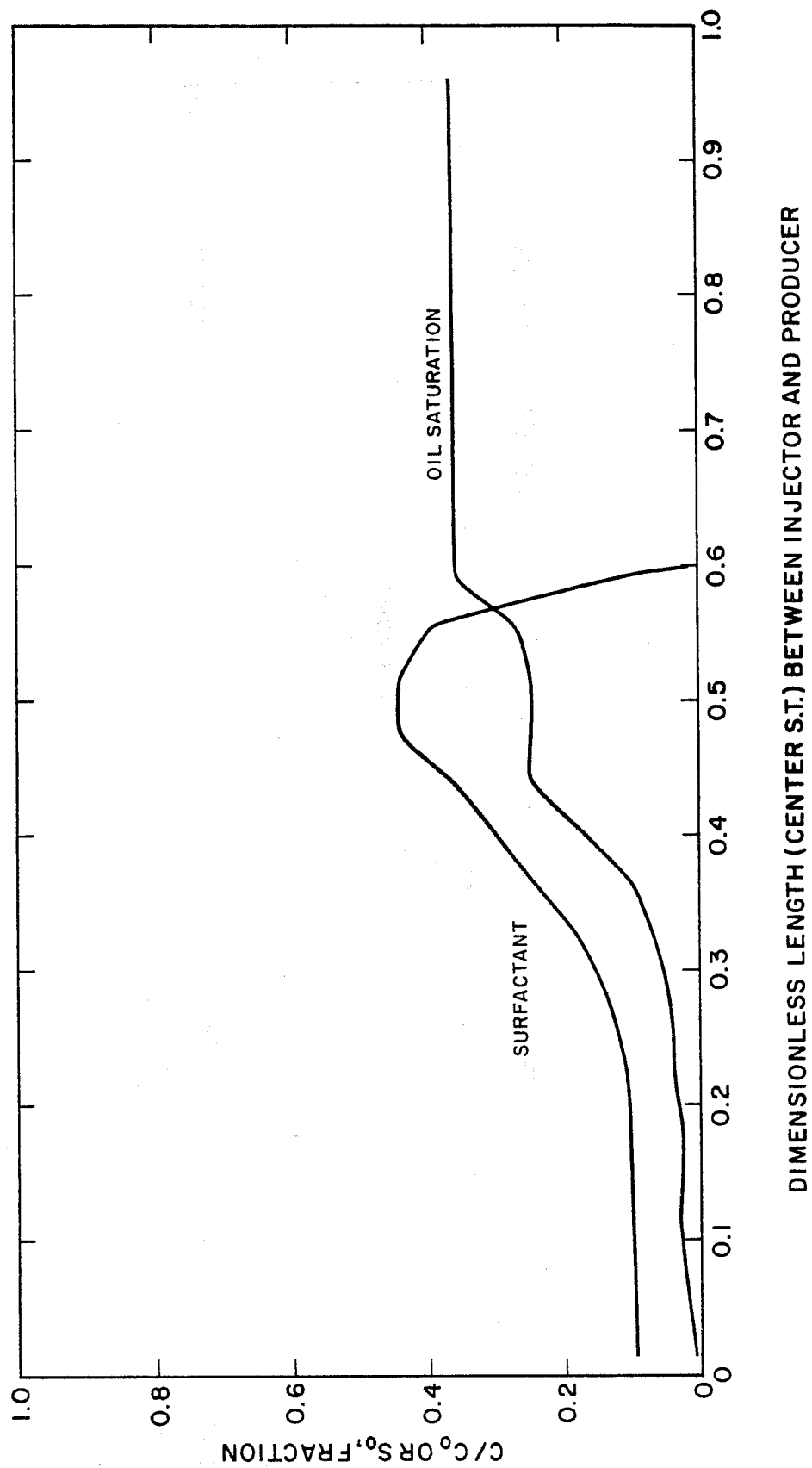


FIGURE 35
1 LAYER CENTER STREAMTUBE MODEL
BASE CASE RUN TO ULTIMATE RECOVERY

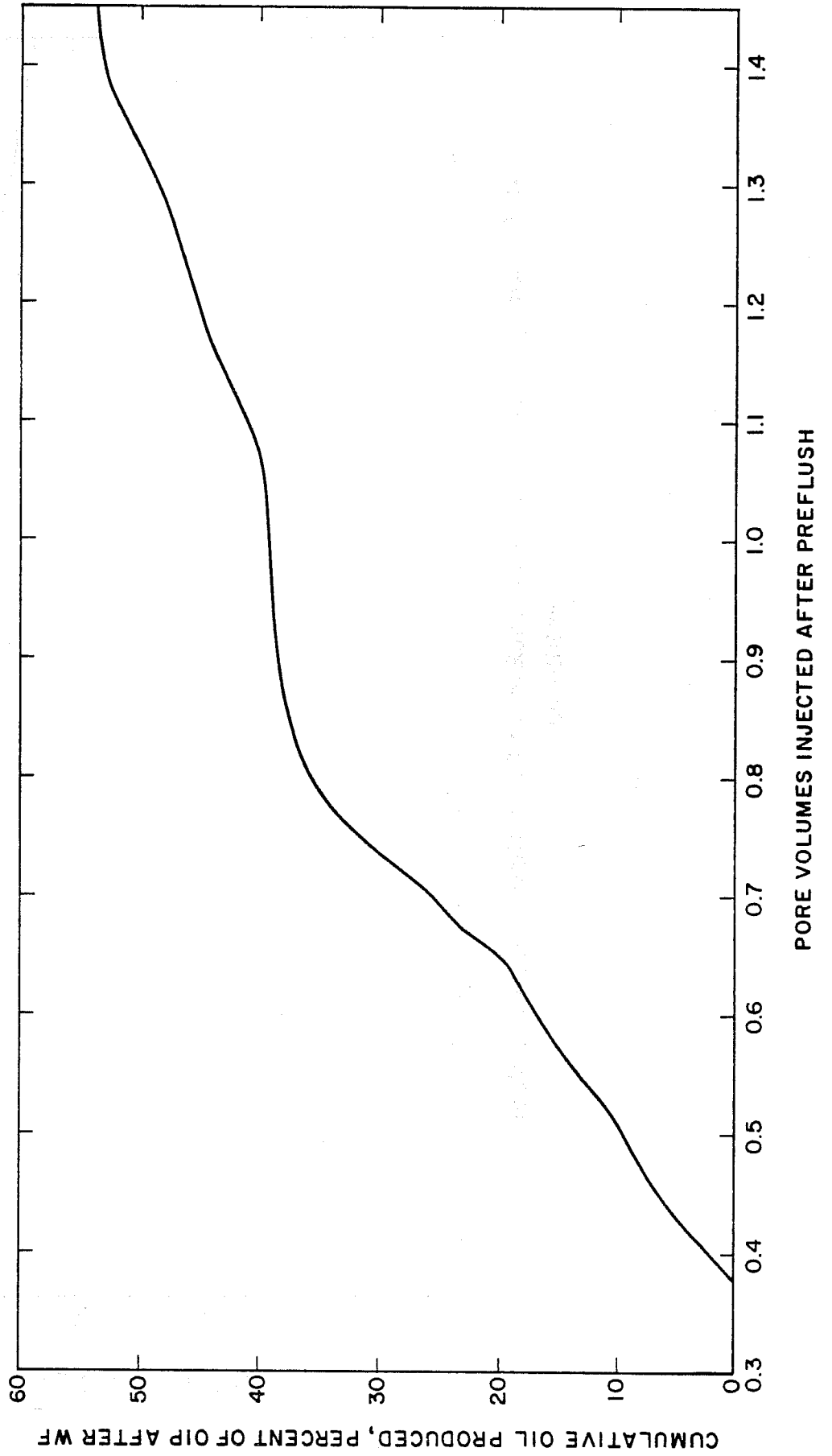


FIGURE 36
INSTANTANEOUS PROFILES AT 148% PV INJECTED AFTER PREFLUSH

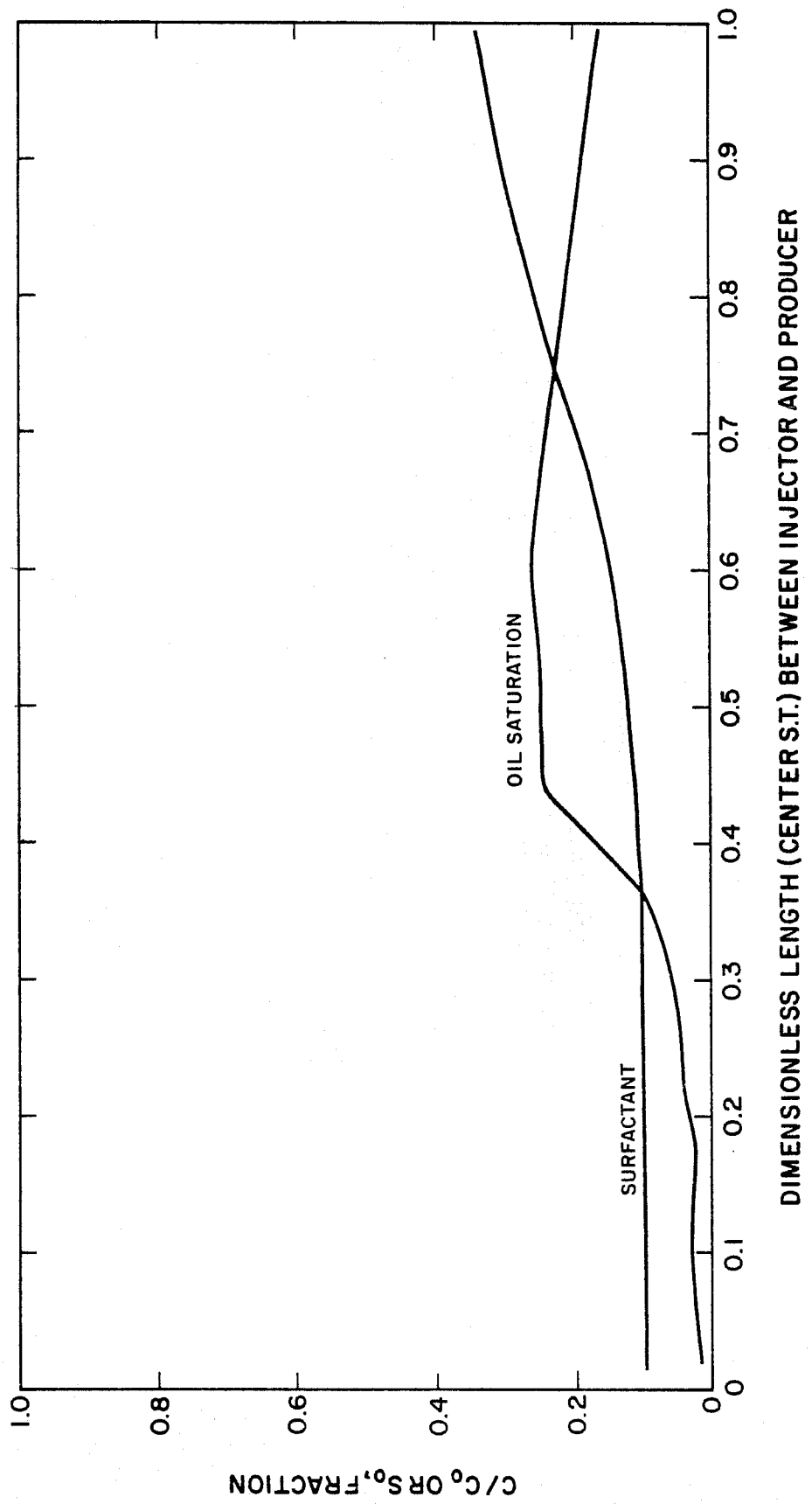


FIGURE 37
CENTER STREAMTUBE MODEL

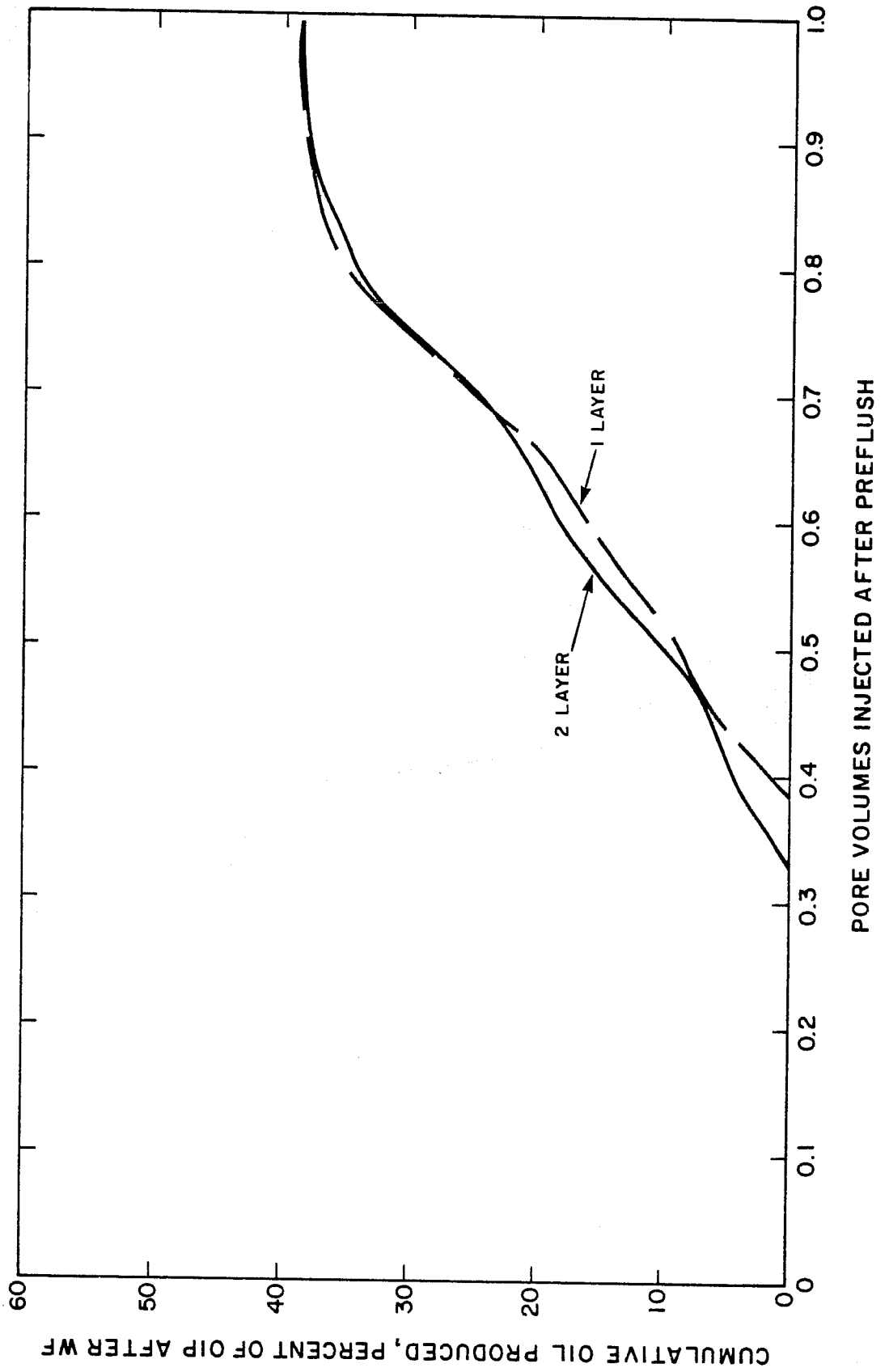


FIGURE 38
PREDICTED BEHAVIOR AT MP-132

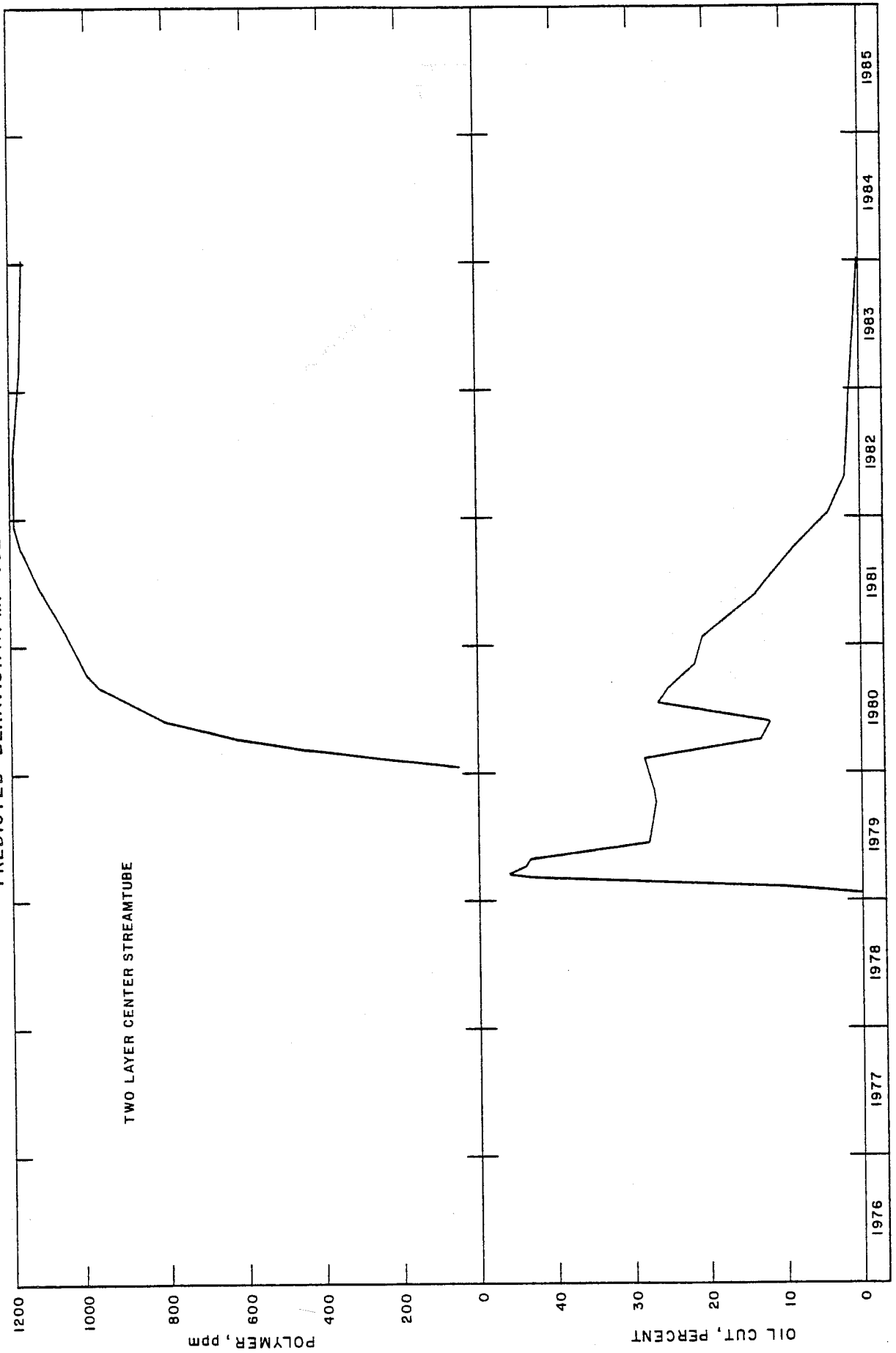


FIGURE 39

PREDICTED BEHAVIOR AT MP-124

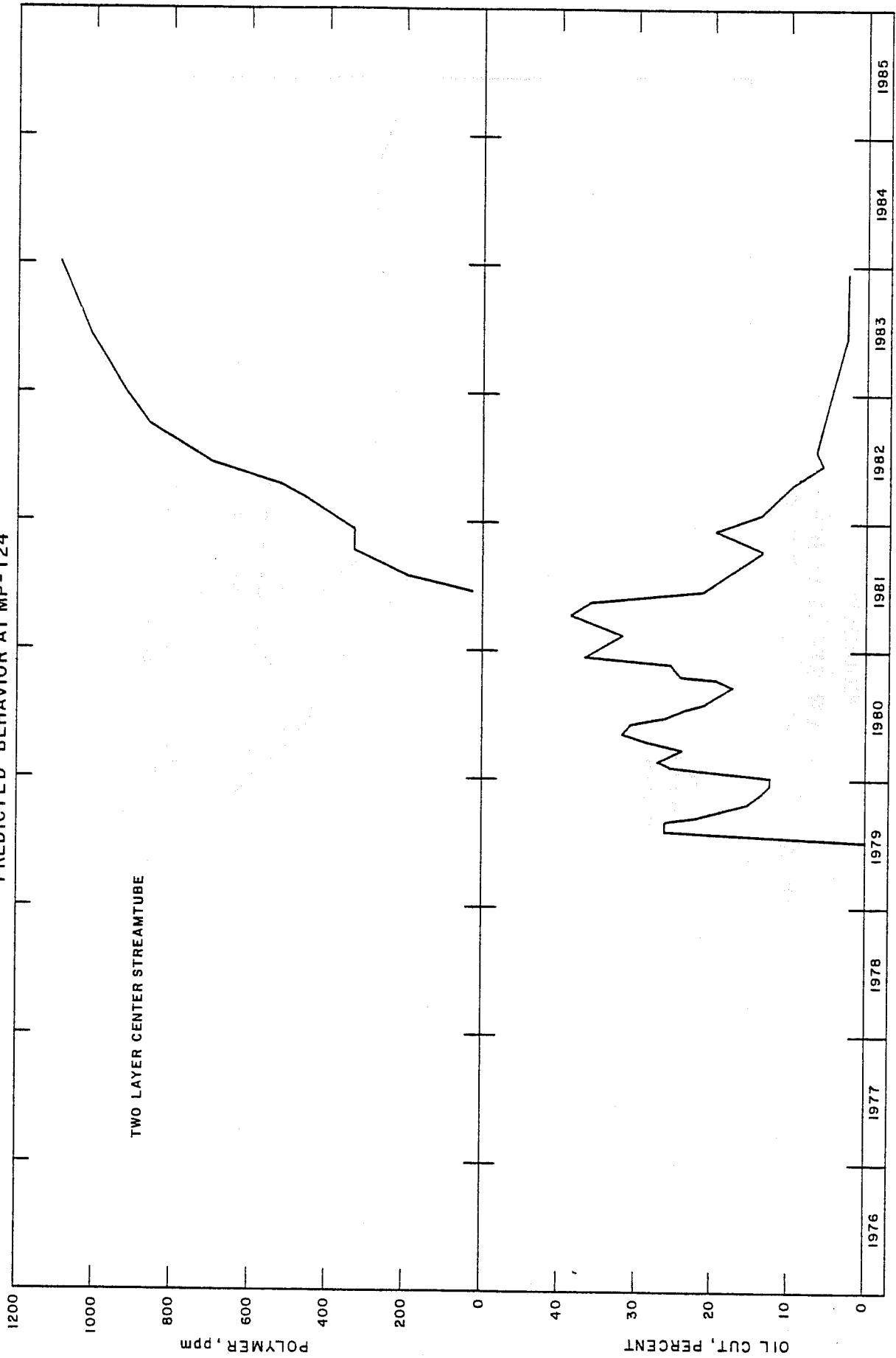


FIGURE 40
 CENTER STREAMTUBE
 100% P.V. INJECTED AFTER PRE-FLUSH

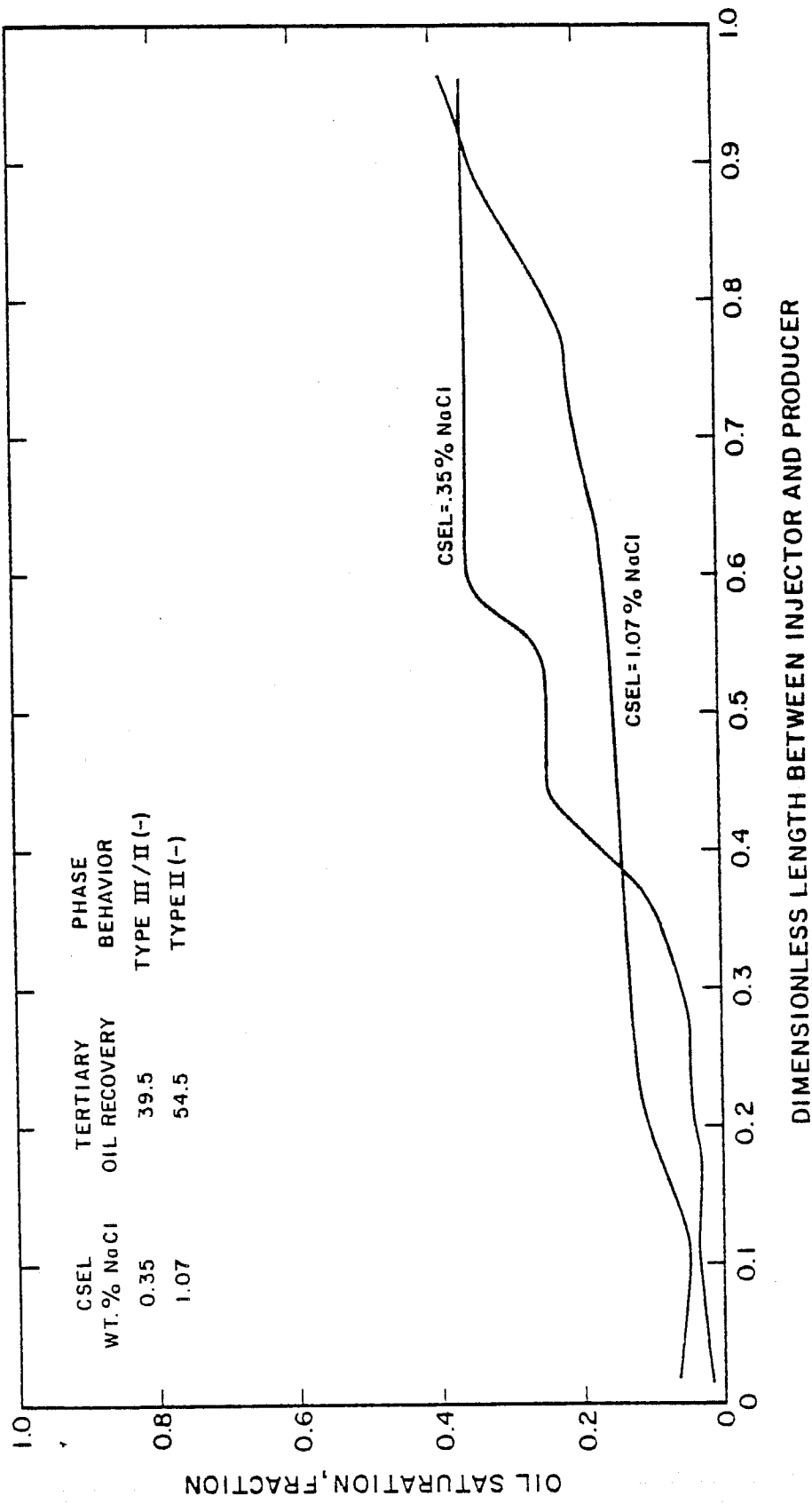


FIGURE 41
 SENSITIVITY TO PREFLUSH INJECTION
 CENTER STREAMTUBE MODEL

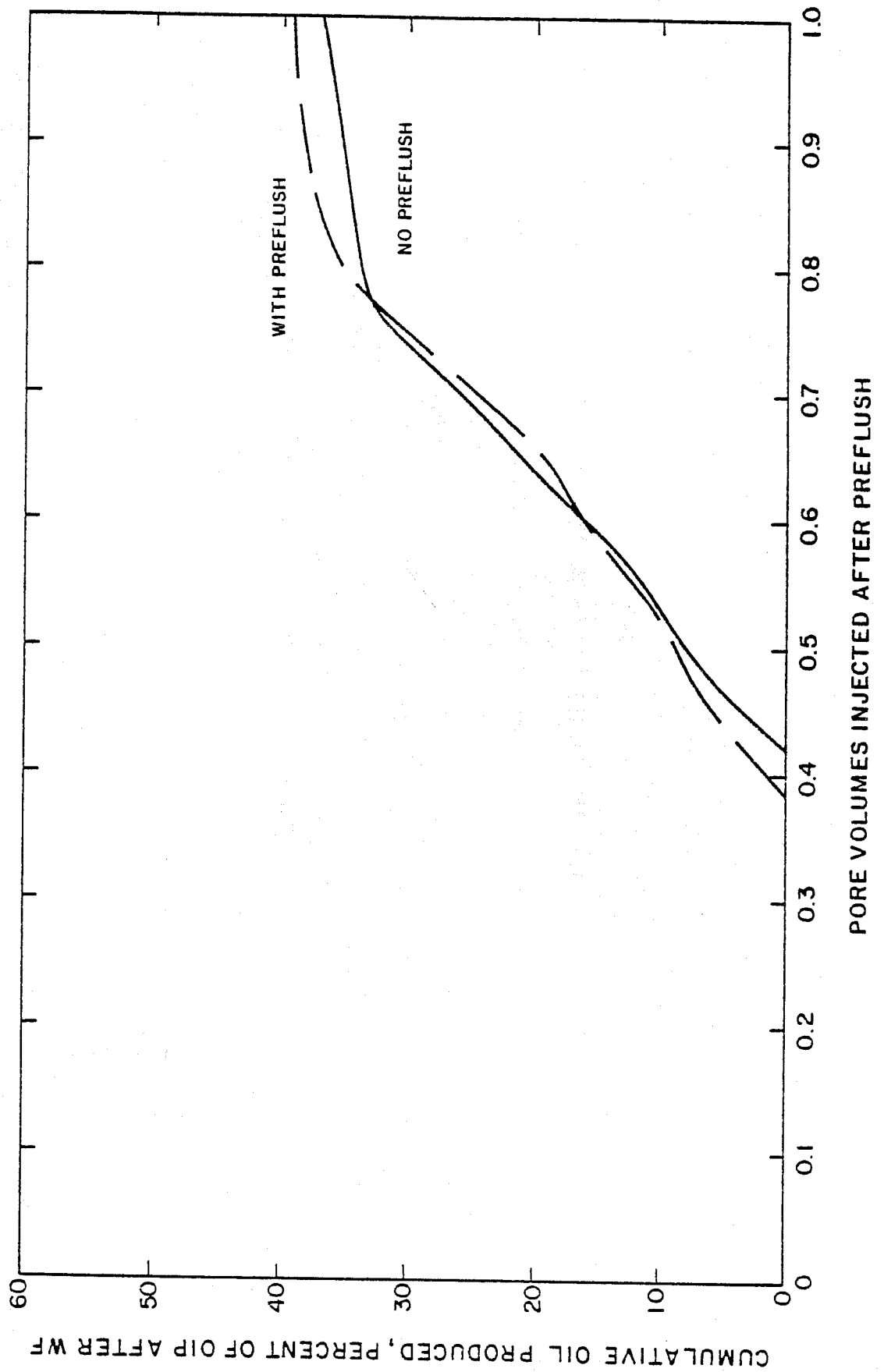


FIGURE 42
 INSTANTANEOUS PROFILES AT 77 % PV INJECTED (NO PREFLUSH)

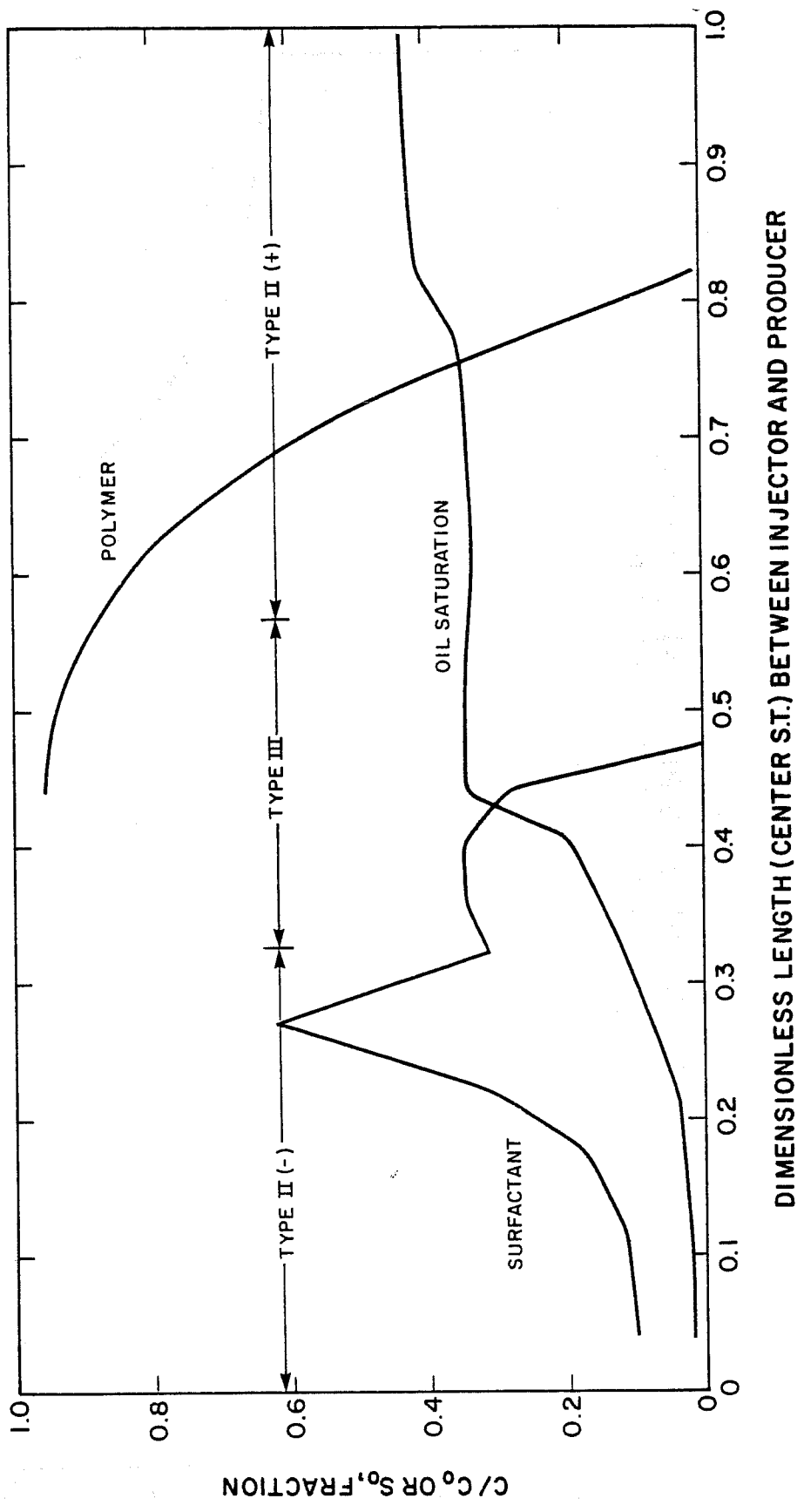


FIGURE 43

EFFECT OF MICELLAR SLUG SIZE
CENTER STREAMTUBE MODEL

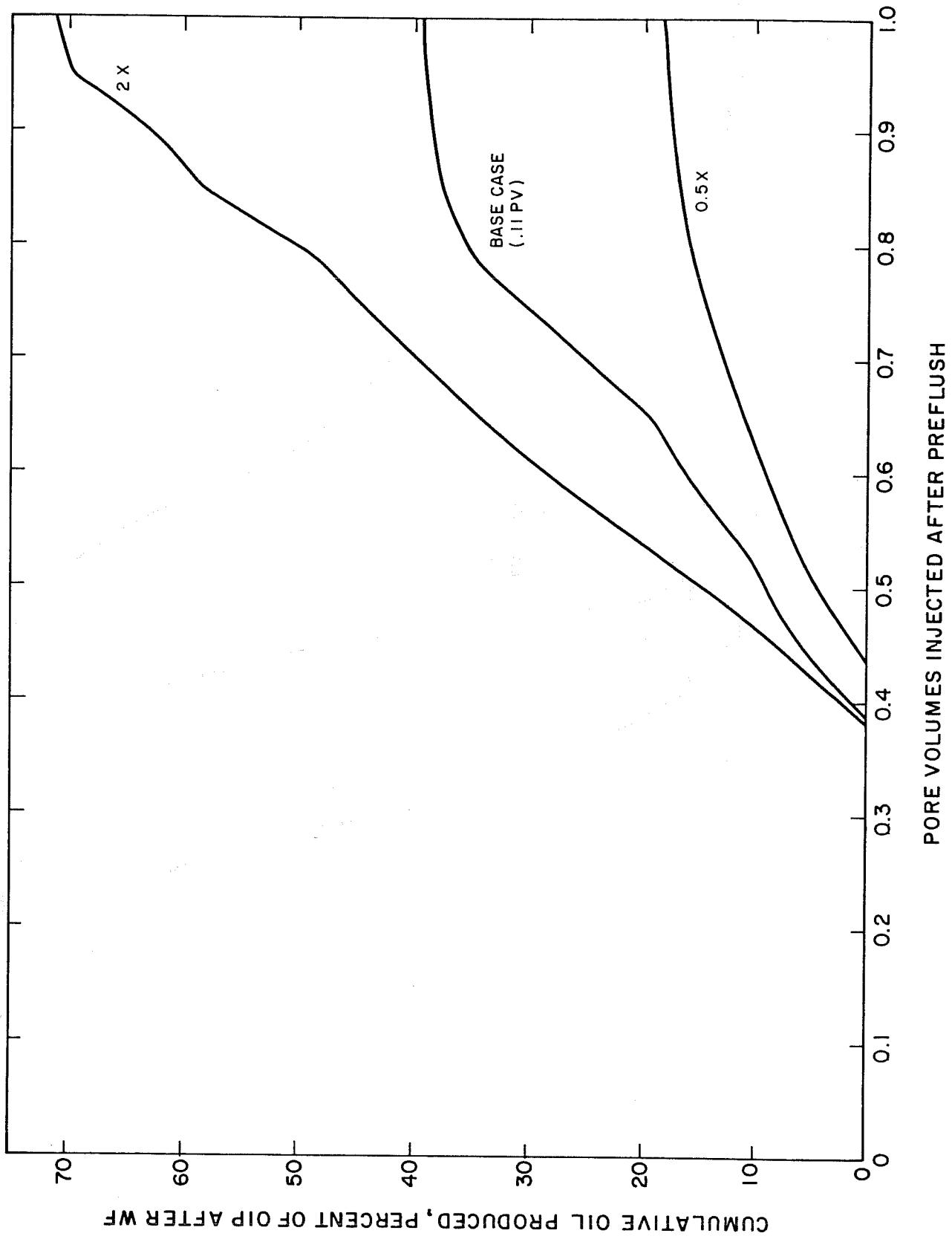


FIGURE 44

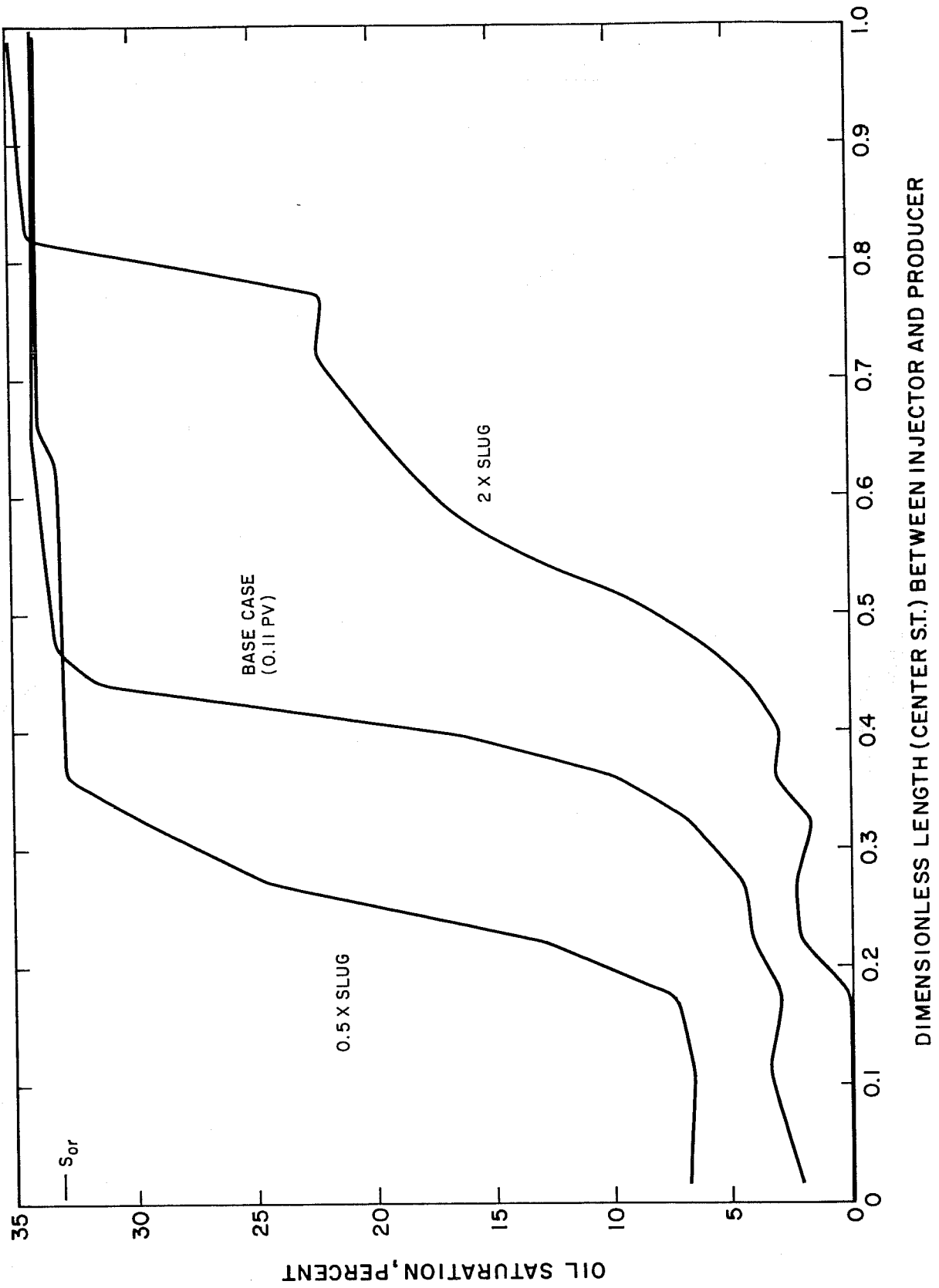


FIGURE 45

FLUID SAMPLES AT MP-131

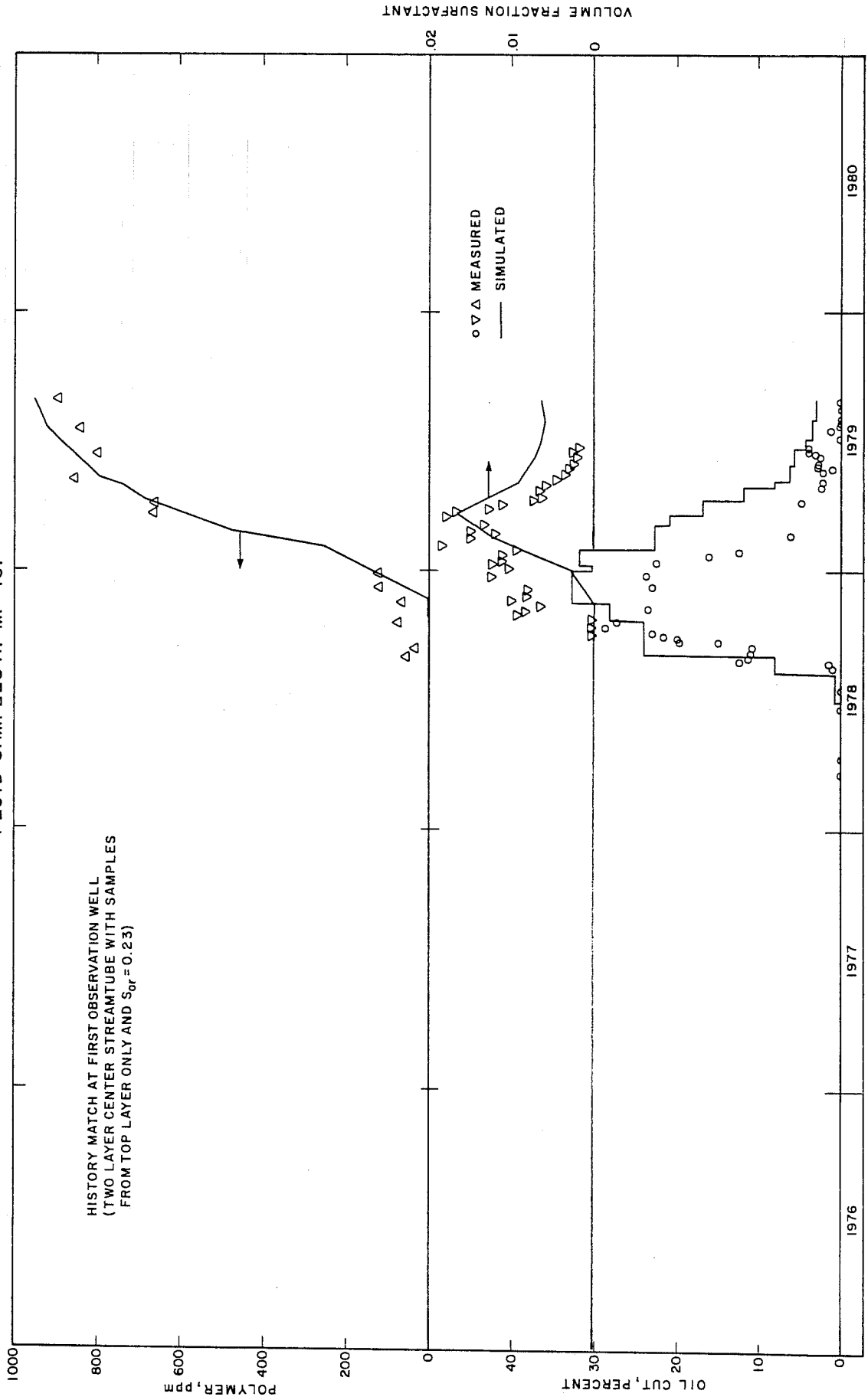


FIGURE 46

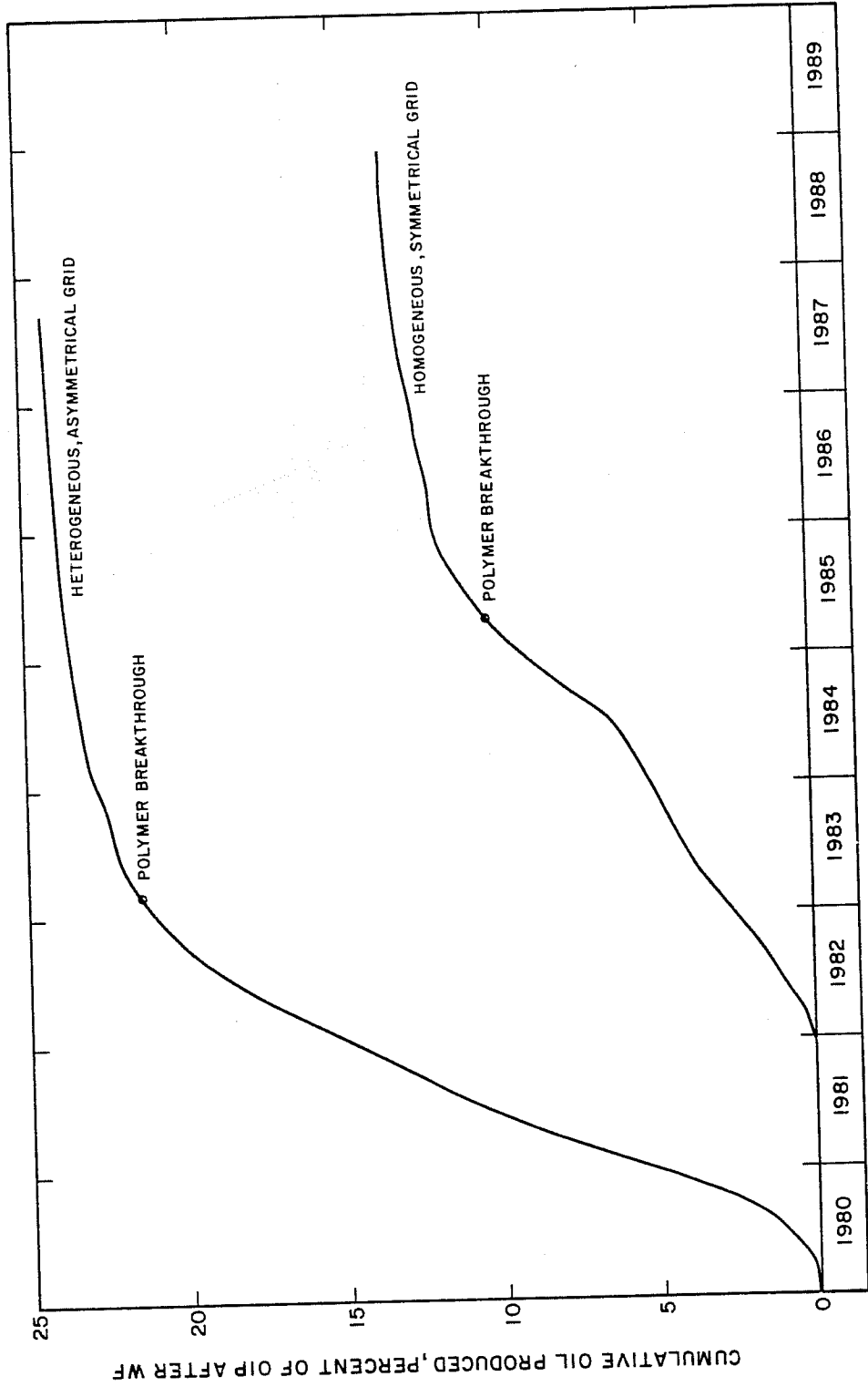


FIGURE 47
RESIDUAL OIL SATURATION AT 23%
PORE VOLUME INJECTED AFTER PREFLUSH
(AT END OF HISTORY, 8/31/79)

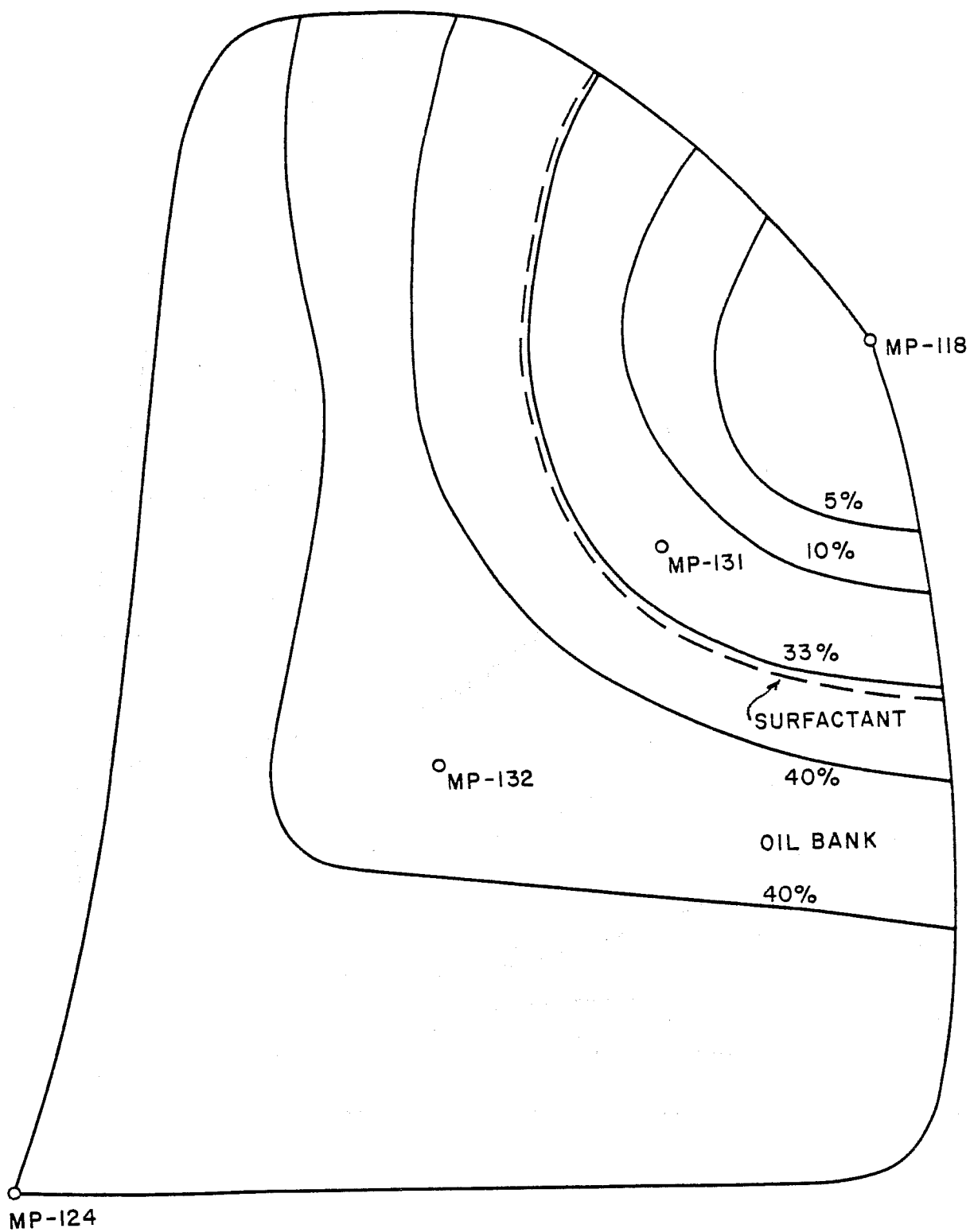


FIGURE 48
RESIDUAL OIL SATURATION AT 70%
PORE VOLUME INJECTED AFTER PREFLUSH
(AT POLYMER BREAKTHROUGH)

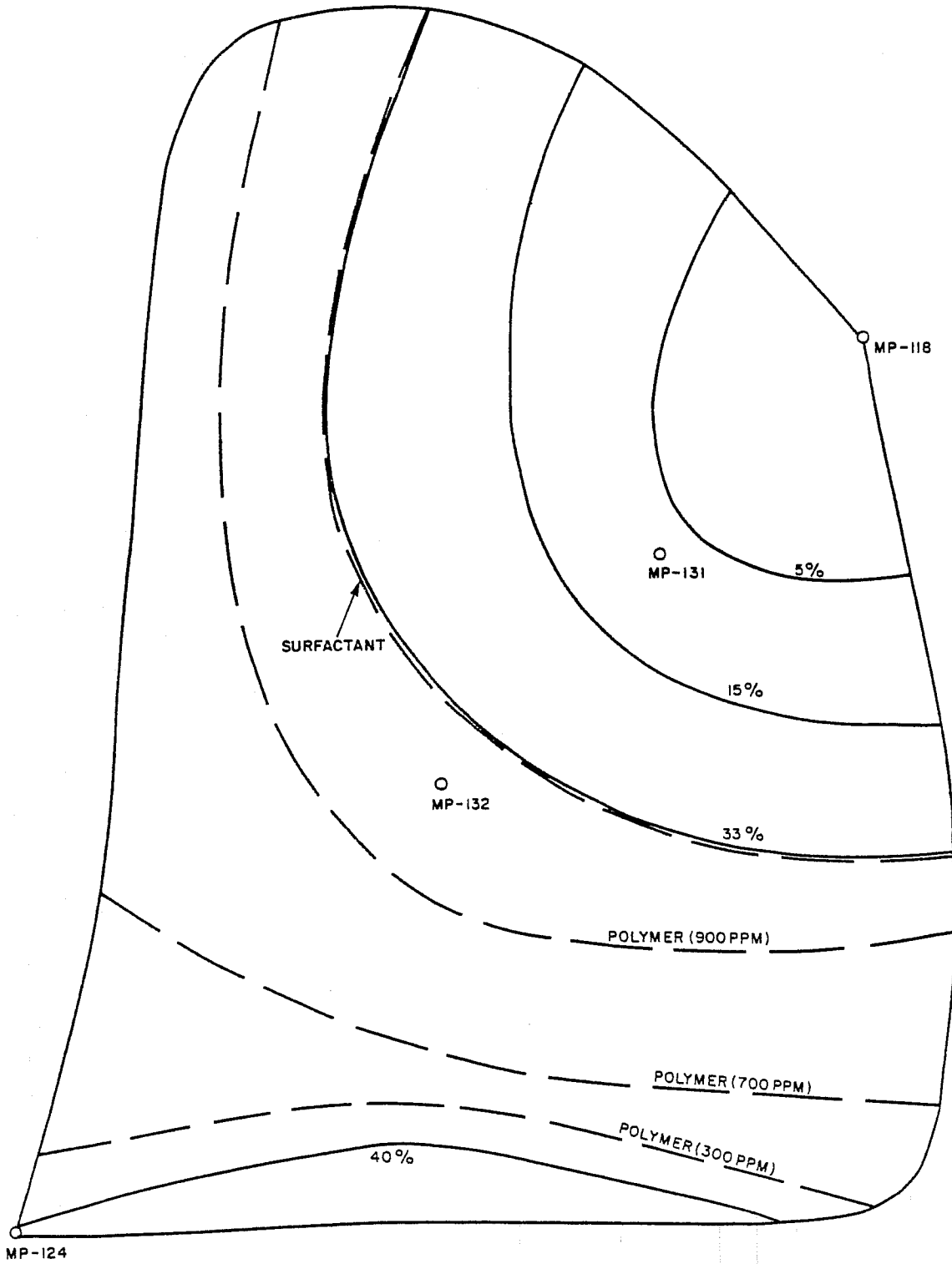


FIGURE 49

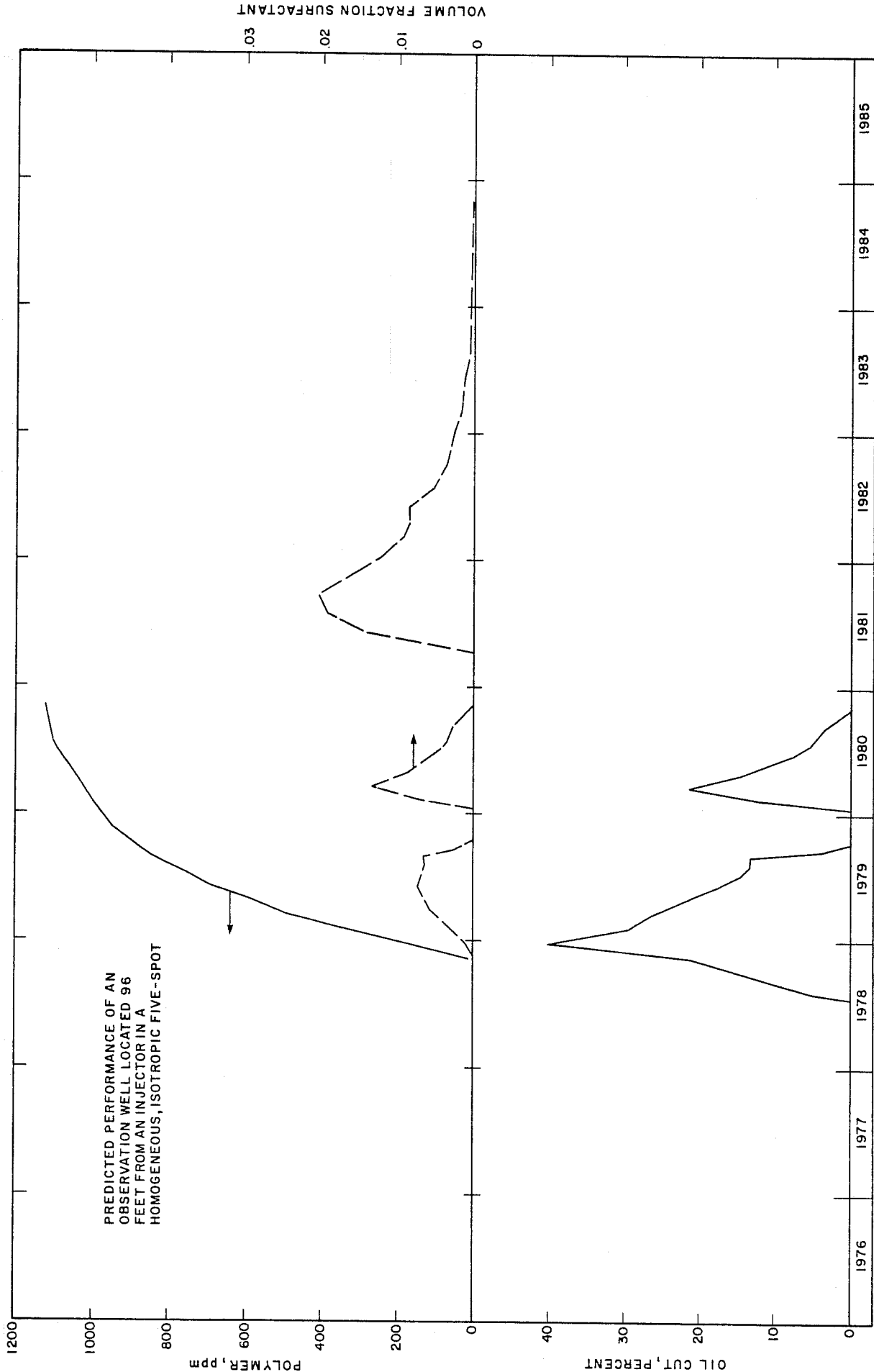


FIGURE 50

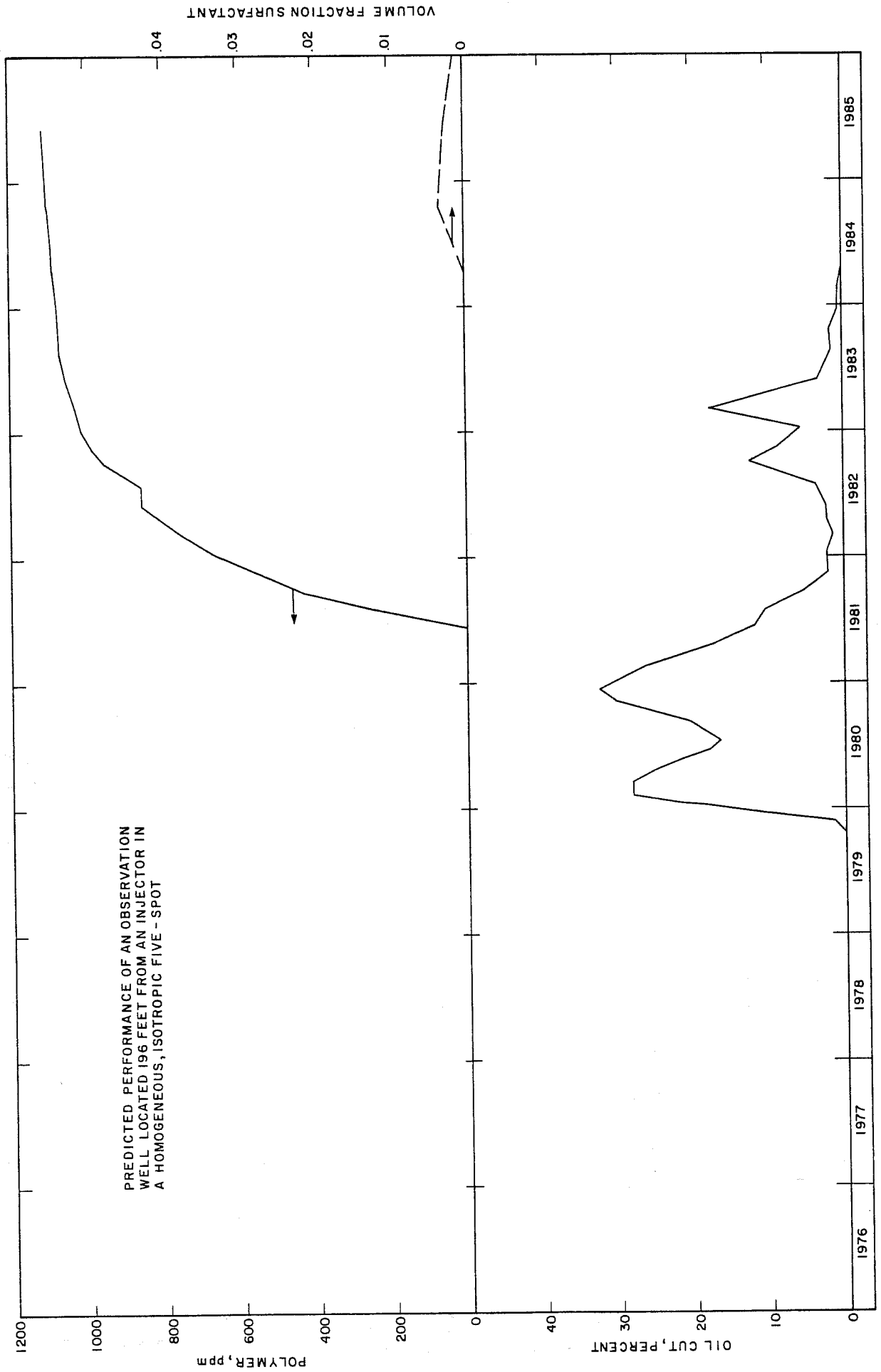


FIGURE 51

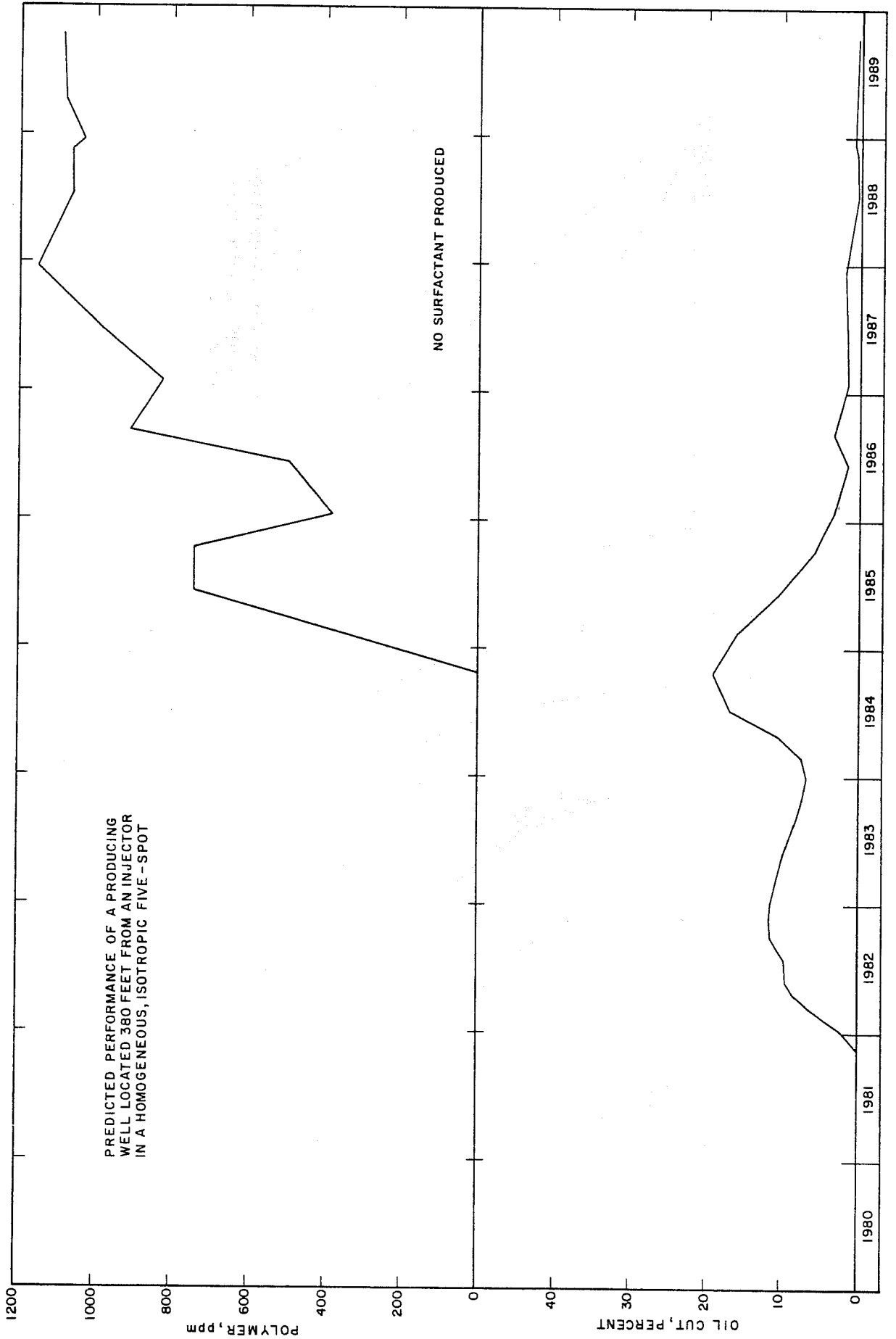


FIGURE 52

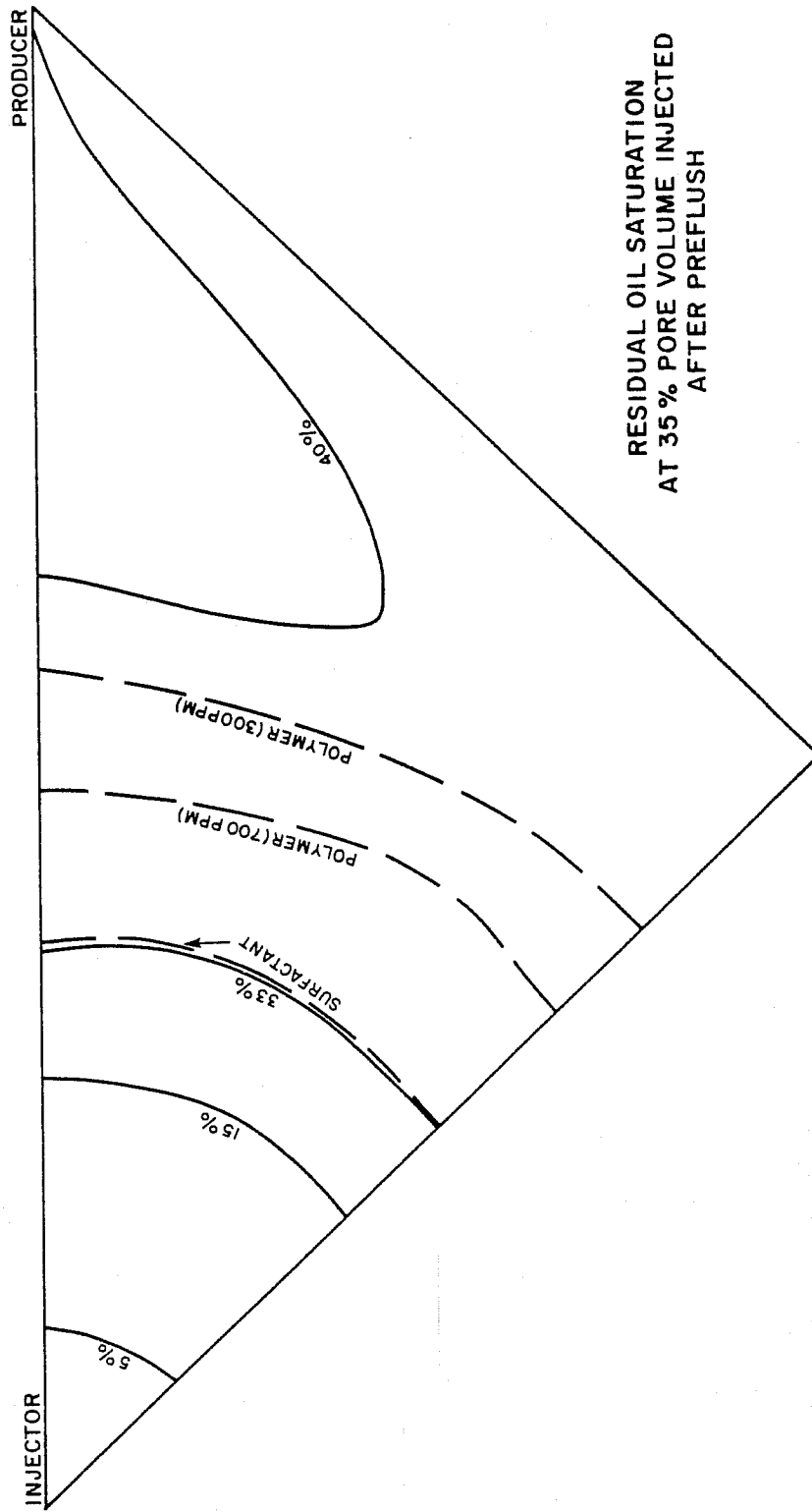
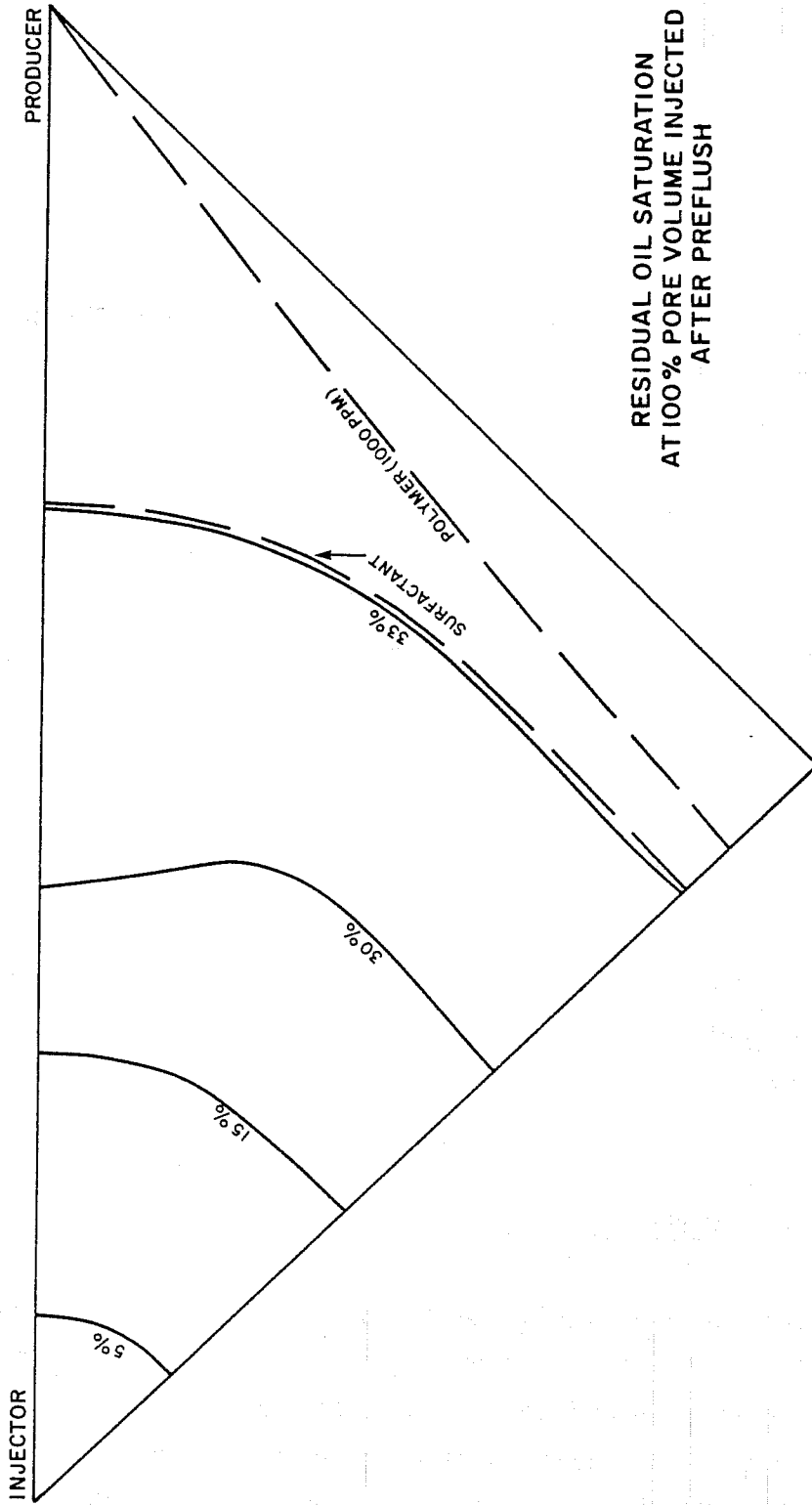


FIGURE 53



APPENDIX III

APPENDIX A CHEMICAL FLOOD MODEL DESCRIPTION

INTRODUCTION

INTERCOMP has developed a finite-difference-based numerical reservoir simulator for predicting micellar/polymer flood performance. The model solves for n components in three fluid phases. All components may partition among the phases satisfying either pseudoternary phase behavior or a general multicomponent, three-phase flash. Polymer characteristics such as inaccessible pore volume, resistance and residual resistance factors, and retention hystereses are included. Recovery mechanisms of swelling, solubilization, and interfacial effects are represented. Second-order spacial accuracy for the solution allows simulation of physical dispersion with a reasonable number of grid blocks.

Aside from the usual 3-D Cartesian geometry, the model allows for a general orthogonal coordinate system as well as a special conformal map used for five-spot symmetry elements.

The simulators to be described here are the product of the "Chemical Flooding Model Development" project undertaken by INTERCOMP for thirteen major oil companies and research organizations.

SIMULATOR CHARACTERISTICS

Chemical flooding is the name we use to denote those reservoir processes characterized by the injection of an agent which is primarily intended to reduce the interfacial tension between oil and water and, hence, allow the displacement and recovery of oil that is normally trapped by capillary forces as a waterflood residual. The process is known alternatively throughout the industry as miscible-type waterflooding, micellar flooding, micellar/polymer flooding, low tension waterflooding, surfactant flooding, and soluble oil flooding.

Although chemical flooding could be applied for secondary as well as tertiary oil recovery, the typical chemical flooding candidate is currently a watered-out oil zone; the in-situ water being a normal oil field brine, high in total dissolved solids and divalent cations. The chemical flooding process thus consists of: (1) a brine preflush, possibly with chemical additives, to condition the formation and provide a controlled fluid environment that will allow optimum activity of the following surfactant system; (2) a small slug of a surfactant fluid, generally consisting of a dilute concentration of petroleum sulfonates in brine and/or oil, with the possible additions of cosurfactants, polymers, and other chemicals to stabilize the system, enhance the surfactant activity, reduce adsorption losses, and control slug mobility; (3) a mobility control buffer consisting of a dilute solution of polymer in brine, used to protect against backside dilution or overrunning of the surfactant slug by drivewater and to enhance areal and vertical sweep efficiency; and (4) a waterdrive to sweep the displaced oil, water and injected fluids to the producers.

The process description varies somewhat according to the subtleties of a specific design; however, the above description appears to be the generally accepted characterization of the chemical flooding process.

Starting from this description, the simplest simulator would have to track four components - water, oil, polymer, and surfactant. However, since salinity and multivalent ions seem to have such strong effects on process features such as interfacial activity, phase behavior, sorption levels, and polymer viscosity, a simulator really needs to track six components before it has any real utility. Hence, INTERCOMP's first chemical flood simulator, CHEMFLD, was designed to track six components, usually water, oil, surfactant, polymer, Na^+ and Ca^{++} . Phase equilibria allowed the existence of a maximum of two phases for simplicity.

As the three-phase (aqueous, micellar, and oleic) description of the chemical flooding process gained wider acceptance, INTERCOMP's two-phase description became an obvious program limitation. Consequently, in addition to CHEMFLD we developed two three-phase models - CFTE and CFNC. In addition, we expanded the geometrical capability of these models to three dimensions and generalized the number of components tracked by the models from six to n .

The phase equilibria calculations in CFTE are based on the assumption of a ternary system, and the equilibrium data are input in the form of a series of ternary diagrams and tie lines. In CFNC, as in CHEMFLD, phase equilibrium is treated by means of partition coefficients, or K-values.

CFTE/CFNC

Capabilities

The number of conservation equations treated by CFTE/CFNC is not limited by program code but only by core storage capacity of the computer on which run. As a practical matter, however, we usually dimension the program for ten or less components. These components can partition themselves among three liquid phases - aqueous, oleic, and micellar. The version CFTE assumes that only three components - water, oil, and surfactant - enter into the phase equilibria. The remaining components are treated as trace elements and are assumed to proportion themselves between phases in the same fashion as the water. However, one of the trace components, polymer, may be allowed to partition entirely in the water-rich phase. The three-component phase equilibrium is specified by means of phase envelopes and tie lines, the shape of which may vary with salt concentration. The approach is similar to that employed by Pope and Nelson² except that phase envelopes and tie line data are input as tables rather than as parameters of fitted equations.

The version CFNC allows all components to participate in the phase equilibria. This phase equilibrium is specified by means of partition coefficients, or K-values, which themselves are functions of concentrations and are input as tables to the simulator.

The programs CFTE/CFNC can treat one-, two-, or three-dimensional problems using one of three coordinate options. These options are (1) standard Cartesian, (2) quarter five-spot isopotential streamline grid, and (3) generalized curvilinear orthogonal coordinates in the x-y plane. The third dimension with options (2) or (3) is the standard z-coordinate.

Irreversible sorption can be modeled by specifying a retention level below which the amount sorbed cannot decrease. Above this retention level sorption is treated reversibly. An additional feature is the residual resistance factor by which the relative permeability of a specified phase may be reduced based on the amount of sorbed material (usually polymer).

Conservation Equations and Assumptions

There are two key assumptions involved in the program formulation. First, there is no volume change upon mixing; that is, the volume occupied by a component is the same regardless of the phase in which it is distributed. Second, the fluids and rock are incompressible.

The conservation equation for component i can then be written

$$\phi \frac{\partial N_i}{\partial t} + \nabla \cdot \left(\sum_p \vec{u}_p C_{p_i} - \sum_p \phi S_p K_{p_i} \nabla C_{p_i} \right) = q_i \quad (1)$$

where N_i is the total volume fraction of species i ;

C_{p_i} is the volume fraction of species i in phase p ;

\vec{u}_p , S_p and K_p are superficial velocity, saturation and total diffusivity (both molecular and velocity dispersion) of phase p . Summing over all species and using the identities $\sum_i N_i = 1$, $\sum_i C_{p_i} = 1$ results in the overall continuity equation:

$$\nabla \cdot \left(\sum_p \vec{u}_p \right) = \sum_i q_i \quad (2)$$

We employ an IMPES solution procedure and solve Equation (2) implicitly for pressure with saturations and concentrations dated at the old time level. Equation (1) is then solved explicitly to obtain the new total concentration N_i in each grid block. An equilibrium calculation performed for each grid block yields phase concentrations C_{p_i} and saturations S_p . Because of the incompressibility assumption, the pressure solution need be obtained only once per time step and is decoupled from the flash calculation. It is in the flash calculation that CFTE and CFNC differ, as described in the previous section. The explicit treatment of phase saturations and concentrations imposes the usual stability limitations in that grid block throughput per time step must be maintained at about one-half grid block pore volume or less.

In IMPES-type simulators such as CFTE/CFNC, a simultaneous solution of a set of linear equations is performed only on the pressure equation. Because the pressure equation is decoupled from the individual species conservation equations, the time-consuming simultaneous solution of a linear equation need be performed only once per time step. The equilibrium flash calculations are then performed individually for each grid block.

SPECIAL FEATURES

Physical Dispersion

Dispersive flux is included for each component i with mass fraction W_{pi} as

$$\phi \sum_p S_p \rho_p K_{pi} \nabla w_{pi}$$

evaluated explicitly at time level n using central differences with respect to space. Phase saturations are included in the dispersional fluxes to reflect the cross-sectional area available for flow in each phase. We use a two-parameter model for the dispersion coefficient of each phase in each direction

$$K_{pi} = D_i/\tau + \alpha |\vec{u}_p|/\phi$$

where D_i/τ is molecular diffusion coefficient of species i over tortuosity and α is the dispersion parameter.

The anisotropic nature of the velocity dispersion tensor α cannot correctly be modeled with the standard 5- and 7-point finite-difference approximations unless the flow field is everywhere aligned with the coordinate axes. In many cases, however, the flow field does follow the coordinate axes quite closely. For example, in vertical cross sections the vertical flow component is often small compared to the horizontal component. We have, therefore, allowed the user to specify the values of α separately in the direction of each coordinate axis so that in those cases where the flow field is approximately aligned with the coordinates, the tensorial nature of velocity dispersion can be approximated.

Relative Permeability and Capillary Number

The relative permeability of each phase may be a function of up to three variables. These functions are input to the simulator as multi-dimensional tables. Thus, for a two-phase system, the relative permeability of each phase might be a function of its own saturation and the local capillary number, $N_{cp} = \frac{k|\nabla p|}{\sigma}$. An example is shown in Figure A-1. Note that negative values of input relative permeability may be used to facilitate the functional relationship between the capillary number and the residual oil saturation. If the value of the relative permeability determined as a function of capillary number and saturation is less than zero, the program sets the value equal to zero. For the three-phase systems, the relative permeability for the phase of intermediate wettability (say, the micellar phase) could be a function of both the aqueous and oleic phase saturations as well as the capillary number.

To facilitate the calculation of the local capillary number, the interfacial tension is input to the simulator as a function of composition, again in the form of a multidimensional table look-up. Thus, for each grid block each time step we (1) determine the interfacial tension σ by table look-up, given the phase compositions, (2) determine the local capillary number using the interfacial tension and a computed pressure gradient, $|\nabla p|$, and (3) determine the phase relative permeabilities by table look-up using the grid block saturations and the computed capillary number.

REFERENCES

1. Todd, M. R., P. M. O'Dell, and G. J. Hirasaki. "Methods for Increased Accuracy in Numerical Reservoir Simulators," Soc. Pet. Eng. J., Vol. 12, 515-530 (1972).
2. Pope, G. A., and G. A. Nelson. "A Chemical Flooding Compositional Simulator," SPE 6725, presented at the 52nd Annual Fall Meeting of the SPE of AIME, Denver, October 1977.

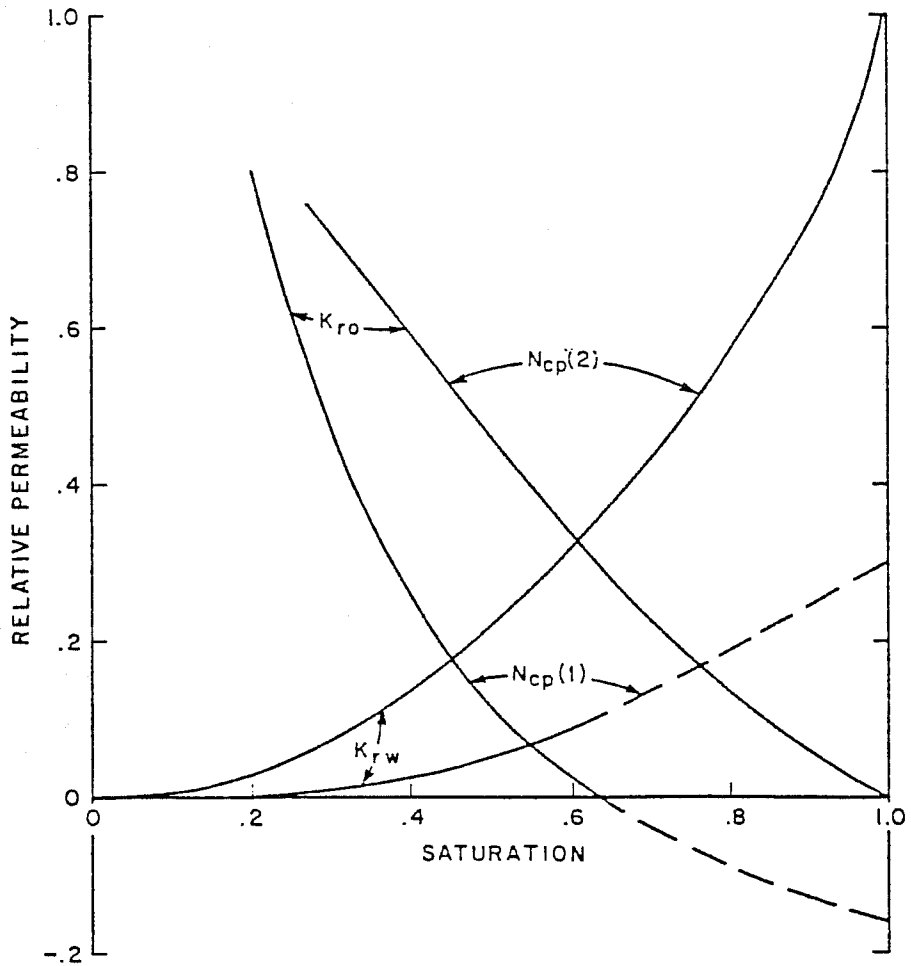


Fig. A-1- Relative permeability, functions of saturation and capillary number

APPENDIX B

DETAILS OF GRID CONSTRUCTION

This appendix discusses the use of non-Cartesian orthogonal grid systems, the generation of the grids used in this study, and the allocation of fluid within the asymmetrical grid used in the simulation of the Chesney lease process. Also discussed are the impact of fluid drift and rate imbalance upon the allocation of injected fluid. The influence of reservoir heterogeneity is not discussed here and a homogeneous, isotropic reservoir is assumed.

ORTHOGONAL GRID SYSTEMS

Finite Cartesian grid systems are often used in reservoir simulation. These systems consist of rectangular parallelepipeds of sufficient size and number to define the entire reservoir. These systems are not necessarily the most efficient grids for inter-well flow problems and can introduce significant orientation effects and numerical truncation errors.^{1,2} The use of curvilinear coordinates was proposed to increase the efficiency of a finite grid by allowing it to conform to reservoir geometry.³ These coordinate systems can be defined by a series of isopotential and isostreamlines generated for a given well geometry, even when fluid drift, rate imbalance, and reservoir heterogeneity influence the isopotential lines. For most reservoir problems, isopotential lines may change with time and a representative set must be chosen for use in defining the grid system. The set of isopotential lines chosen will define the maximum areal sweep during the simulation (since areas outside the grid cannot be swept) while crossflow between streamtubes may allow for reduced areal sweep. For most problems of inter-well flow, orthogonal curvilinear grids provide a more efficient means for defining a grid system, as no grid blocks are wasted and numerical truncation errors are reduced since flow paths are nearly parallel to grid boundaries and small grid spacings can be used efficiently in the direction of maximum pressure gradients.

EFFECT OF RATE IMBALANCE ON GRID CONSTRUCTION

A homogeneous, symmetrical, confined and rate-balanced five-spot pattern of injectors and producers will generate a streamline map as given in Figure B-1.⁴ This flow pattern can be used to generate the symmetric grid system presented in Figure 19 (main body of this report), and represents the ideal behavior in which one-fourth of the fluid injected into a well is produced by each of the four surrounding producers. The one-eighth element of symmetry is generated by bisecting the one-fourth element along a line between an injector and a producer.

For a homogeneous, symmetrical but unconfined, rate-imbalanced system as exists at El Dorado, the flow paths between wells tend to deviate from this idealized behavior. As shown in Figure B-2, fluid injected into the North lease is not uniformly distributed throughout the pattern even when fluid drift and heterogeneity are ignored. In the area of the observation wells, the pattern is not greatly distorted except that more than one-fourth of the fluid injected into MP-118 moves toward MP-124. This additional fluid may cause the area swept or the pore volume of slug effective between MP-118 and MP-124 to be greater than expected from a balanced, symmetrical pattern.

EFFECT OF FLUID DRIFT AT EL DORADO

A pressure gradient across the El Dorado pilot areas may result from any of several circumstances routinely encountered in oil field operations.⁵ Such a gradient has been reported in both the North and South leases, as the example given in Figure B-3. These gradients have been analyzed, and generally exist from west to east with a magnitude of 0.0304 psi/ft.⁶ The gradient varies with time, however, and values as high as 0.06 psi/ft have been reported.⁷ A 0.0304 psi/ft gradient could induce a fluid drift of almost 30 feet per year, and may adversely influence sweep efficiency in the pilot areas. This is illustrated in Figure B-4 for the Chesney lease pilot. This figure shows a marked reduction in the reservoir area swept between MP-118 and MP-124 along with less fluid moving through the area. Clearly, a pressure gradient can impact upon fluid flow in the pilot area.

The influence of a pressure gradient on the movement of a high-mobility preflush may be increased by the subsequent injection of low-mobility fluids. Considering a reservoir pressure drop of 100 psi between MP-118 and MP-124 (384 feet), an average linear pressure gradient of 0.26 psi/ft can be estimated. This gradient is significantly greater than the 0.06 psi/ft maximum gradient attributed to drift. When micellar fluid or polymer drive reaches MP-131, however, the pressure gradient between MP-118 and MP-131 is much greater than the gradient between MP-131 and MP-124 since the micellar fluid has about one-tenth the mobility of the preflush.⁸ This is graphically illustrated in Figure B-5, which is a linear simplification of the gradients for purposes of illustration. The low gradient of approximately 0.08 psi/ft ahead of the micellar bank corresponds to a much lower injection well rate at the same injection and production well pressure. This lower gradient is much more sensitive to fluid drift, as shown in Figure B-6. This figure was generated with the same drift (0.0304 psi/ft) as in Figure B-4, but at lower well rates and lower rate induced pressure gradients.

The influence of the injection of low-mobility fluids is actually greater than illustrated in Figure B-5 due to radial flow effects. Figure B-7 shows the pressure gradient calculated by Cities Service Company along a streamline between MP-118 and MP-124. In the region between the wells, the pressure gradient is much lower than the average gradient, while the regions near the wells have gradients much greater than average. Preflush movement in the inter-well region of the reservoir near MP-131 and MP-132 could be very sensitive to fluid drift during micellar fluid injection. This same analogy indicates that movement of micellar fluids will be relatively insensitive to fluid drift, however. In fact, once micellar fluids were injected into the El Dorado pilots, Cities Service Company's match of monitor well pressures were better when fluid drift was neglected.⁹

The impact of fluid drift on the movement of preflush fluid between MP-118 and MP-124 is illustrated in Figures B-8 and B-9. These figures were generated from two sets of streamline calculations provided by Cities Service Company. One set of calculations used no pressure gradient, and the second utilized a pressure gradient of 0.02 psi/ft. For streamline 31 traveling directly toward MP-124 from MP-118, in Figure B-8, the shift due to a pressure gradient of 0.02 psi/ft is not significant in arrival time or proximity to either MP-131 or MP-132, but the arrival at MP-124 is

noticeably late. The estimated path of the streamline with a gradient of 0.06 psi/ft, also shown in Figure B-8, shows a much greater shift, and the arrival of fluid at MP-132 could be significantly delayed. The displacement of streamline 16, traveling a longer path, is shown in Figure B-9. The same conclusions are reached for this streamline except that the influence of small gradients is much more significant. Such changes in pressure gradient and shifts in flow paths are one possible explanation for the apparently anomalous sampling of preflush and formation brine from MP-132.

ASYMMETRIC GRID

Incorporating all of the effects of fluid drift and rate imbalance into the definition of the grid system is an awkward task. The area swept by the preflush does not correspond exactly to the area swept by the micellar fluids,¹⁰ and the version of INTERCOMP's chemical flooding model used in this study (CFTE) does not allow for changing grid systems. Only one grid area could be utilized, and the area more closely corresponding to the area swept by micellar fluid was chosen. This grid area, as in Figure B-10, is not symmetrical and does not include the effects of fluid drift, reservoir heterogeneity, or fluctuating well rates. A more detailed description of the lobe between MP-118 and MP-124, Figure B-11, was used to define the grid system. The lobe contained 43 of the 100 streamlines originating at MP-118, which suggests that MP-124 receives 43% of the fluid injected into MP-118 when drift is ignored. This lobe was subdivided into five streamtubes as in Figure 2, with the upper and lower boundaries estimated between implied or present no-flow boundaries. This grid should approximate the area swept by micellar fluids.

Preflush fluids, because they have relatively high mobility, were assumed to be influenced by the 0.02 psi/ft drift defined as the field average.⁹ The flow paths of fluid under these circumstances are shown in Figure B-12. The preflush reaching MP-124 contacts less reservoir to the west and south of MP-118, and only 30 streamtubes connect the two wells. This implies that 30% of the preflush from MP-118 enters the area contacted by 43% of the injected micellar fluid from MP-118. An attempt was made to approximate this reduced volume of preflush in the allocation of preflush injected into the grid area, but the effects of fluctuating fluid drift and well rates and reservoir heterogeneity were excluded.

To allocate the preflush fluids between the five streamtubes defined for the grid system earlier, Figure B-12 was overlaid on Figure 18 (body of this report) to determine the number of streamlines within each streamtube. The streamline paths did not remain within single streamtubes at all times, and some judgment was used to allocate the number of streamlines within each streamtube. The final distribution of streamlines was based upon the location of streamlines within the grid at the isopotential grid line near MP-132. This distribution of streamlines was:

streamtube:	1	-	2 streamlines
	2	-	8 streamlines
	3	-	7 streamlines
	4	-	7 streamlines
	5	-	6 streamlines

The second step in allocating the preflush volumes in each streamtube was to calculate the fluid rate represented by each streamtube. This calculation was made using the radial form of Darcy's Law for each streamtube:

$$Q = 7.082 \left[\frac{kh(p_e - p_w)}{\mu \ln(r_e/r_w)} \right]$$

where:	Q	=	flow rate, bbl/d
	k	=	absolute permeability, darcies
	h	=	formation thickness, ft
	μ	=	viscosity, cp
	r_e	=	distance to point on streamline, ft
	r_w	=	wellbore radius, ft
	p_e	=	pressure at point on streamline, psi
	p_w	=	wellbore pressure, psi

The pressure drop at approximately 50 feet from MP-118 along each streamline was identified, and the flow rates along the streamlines were calculated. These calculations resulted in 28.12% of the preflush fluid injected into MP-118 entering the grid area with the following distribution:

streamtube:	1	-	1.79%
	2	-	7.26%
	3	-	6.54%
	4	-	6.69%
	5	-	5.84%

These allocation factors clearly have less preflush entering the upper streamtube due to fluid drift, while the distribution of fluid in the other streamtubes is relatively constant. The simulation of the preflush injection was run without crossflow between the streamtubes so that the streamtube receiving a small volume of preflush was not entirely swept.

For the injection of micellar fluids, the fraction of fluid entering the grid was increased from 28.1% to 36% of the injection into MP-118. This volume corresponds to 6.54% of the micellar slug entering the third streamtube with the rest of the fluid distributed according to formation transmissibility and fluid mobility. This allocation assumed that the volume fraction of micellar slug entering the center streamtube was the same as the volume fraction of preflush. During the injection of micellar slug and mobility buffer, crossflow was allowed between the streamtubes so that fluids could move across grid boundaries.

SIMULATING FLUID DRIFT

Although not attempted in this study, the CFTE model could have included approximations for fluid drift across the pilot area. The most direct method of incorporating fluid drift would have been to extend the grid to include sink and source wells located outside the pattern area, and establish the desired pressure gradient between these wells. This would require many additional grid blocks, however.

The same technique for establishing a pressure gradient within a grid system could be used without greatly expanding the grid by positioning a series of sink and source wells along opposite grid boundaries. The location of these wells must be chosen with great care so as not to completely disrupt the normal flow of fluid down the outer

streamtubes. Additional upper and lower streamtubes may be necessary. The interference of these wells with flow down the streamtubes cannot be completely eliminated in most cases, however.

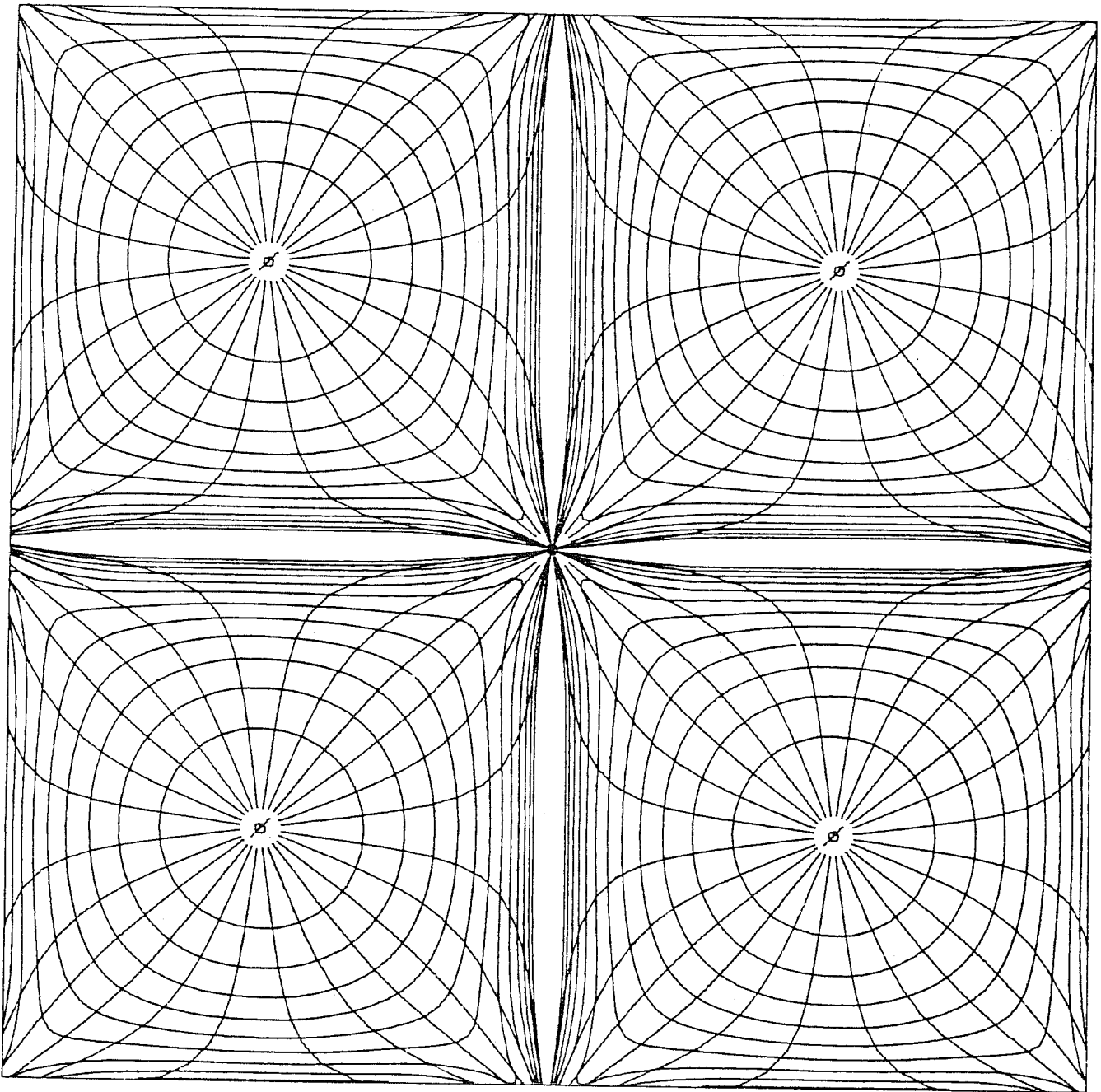
Another method of establishing a pressure gradient in the CFTE model would have been to modify the pressures calculated by the model to include fluid drift. This technique would require fluid losses and gains across boundaries, but could only be used after model modifications. Similarly, reservoir dip could have been used to impose an additional flow potential in the grid, but any differences in fluid densities would have interfered with calculated results. These techniques all potentially interfere with the model results and require a detailed knowledge of the direction, duration, and magnitude of the fluid drift over the life of the project.

REFERENCES

1. Yanosik, J. L., and T. A. McCracken. "A Nine-Point Finite Difference Reservoir Simulator for Realistic Prediction of Unfavorable Mobility Ratio Displacements," SPE 5734, presented at the Fourth Symposium on Numerical Simulation of Reservoir Performance, Los Angeles, February 19-20, 1976.
2. Todd, M. R., P. M. O'Dell, and G. J. Hirasaki. "Methods for Increased Accuracy in Numerical Reservoir Simulators," Society of Petroleum Engineers Journal, December 1972, pp. 515-530.
3. Hirasaki, G. J., and P. M. O'Dell. "Representation of Reservoir Geometry for Numerical Simulation," SPE 2807, presented at the Second Symposium on Numerical Simulation of Reservoir Performance, Dallas, February 5-6, 1970.
4. "El Dorado Micellar-Polymer Demonstration Project (First Annual Report)," BEREC/TPR-75/1, U. S. Energy Resources & Development Admin., October 1975.
5. "El Dorado Micellar-Polymer Demonstration Project (Fifth Annual Report)," DOE/ET/10370-53, U. S. Department of Energy, February 1980, p. I-11.
6. "El Dorado Micellar-Polymer Demonstration Project (Fourth Annual Report)," BETC-1800-40, U. S. Department of Energy, April 1979, p. I-23.
7. Fourth Annual Report, p. I-22.
8. Fourth Annual Report, p. I-27.
9. Fifth Annual Report, p. I-14.
10. Fifth Annual Report, p. I-15.

FIGURE B-1

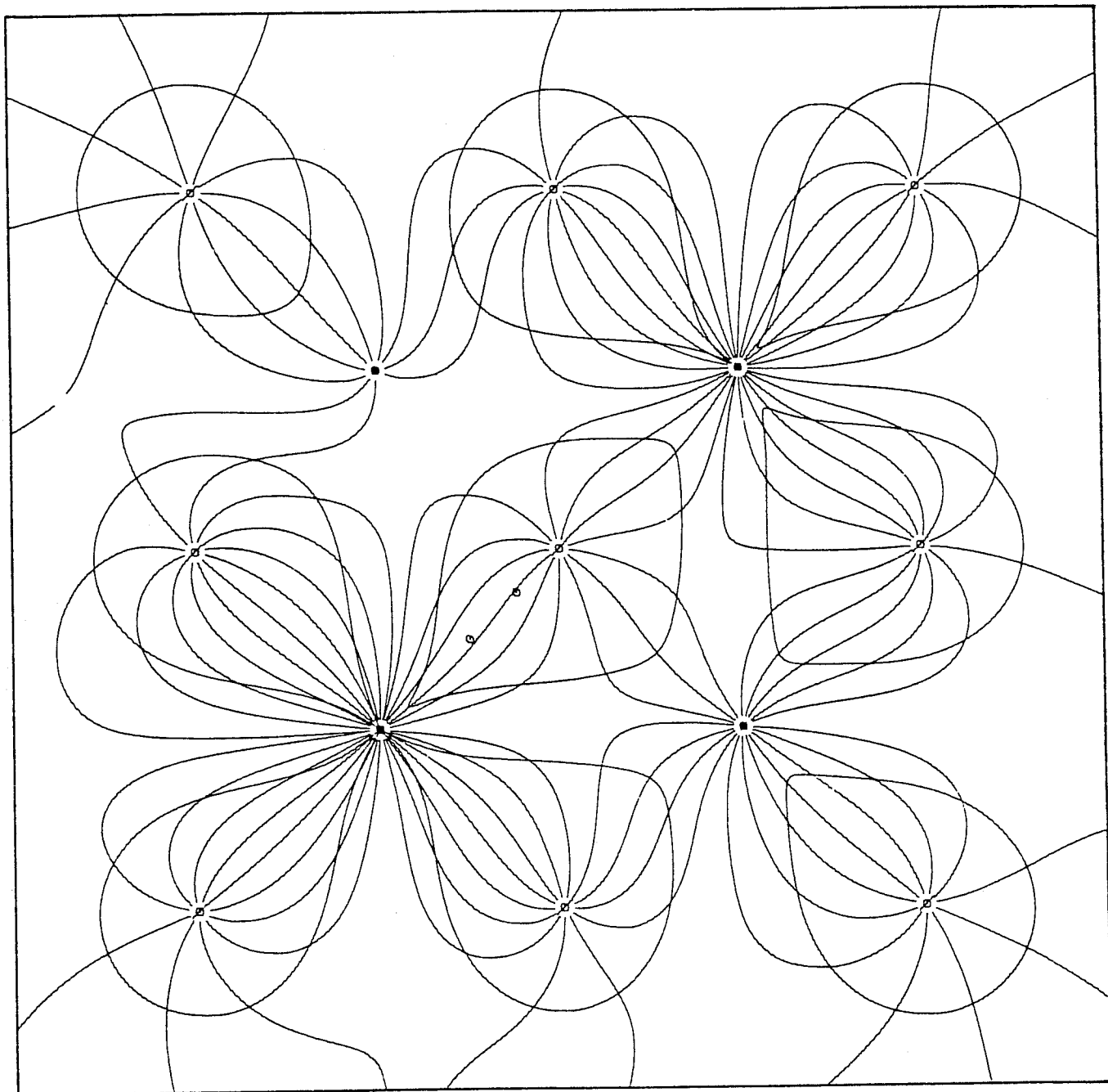
FLOOD FRONTS AND STREAMLINES FOR
RELATIVE RATE STUDY--CASE I



(From Ref. 4, p. 11-78)

FIGURE B-2
NORTH PATTERN PREFLOOD I FRONTS ON JUNE 30, 1978

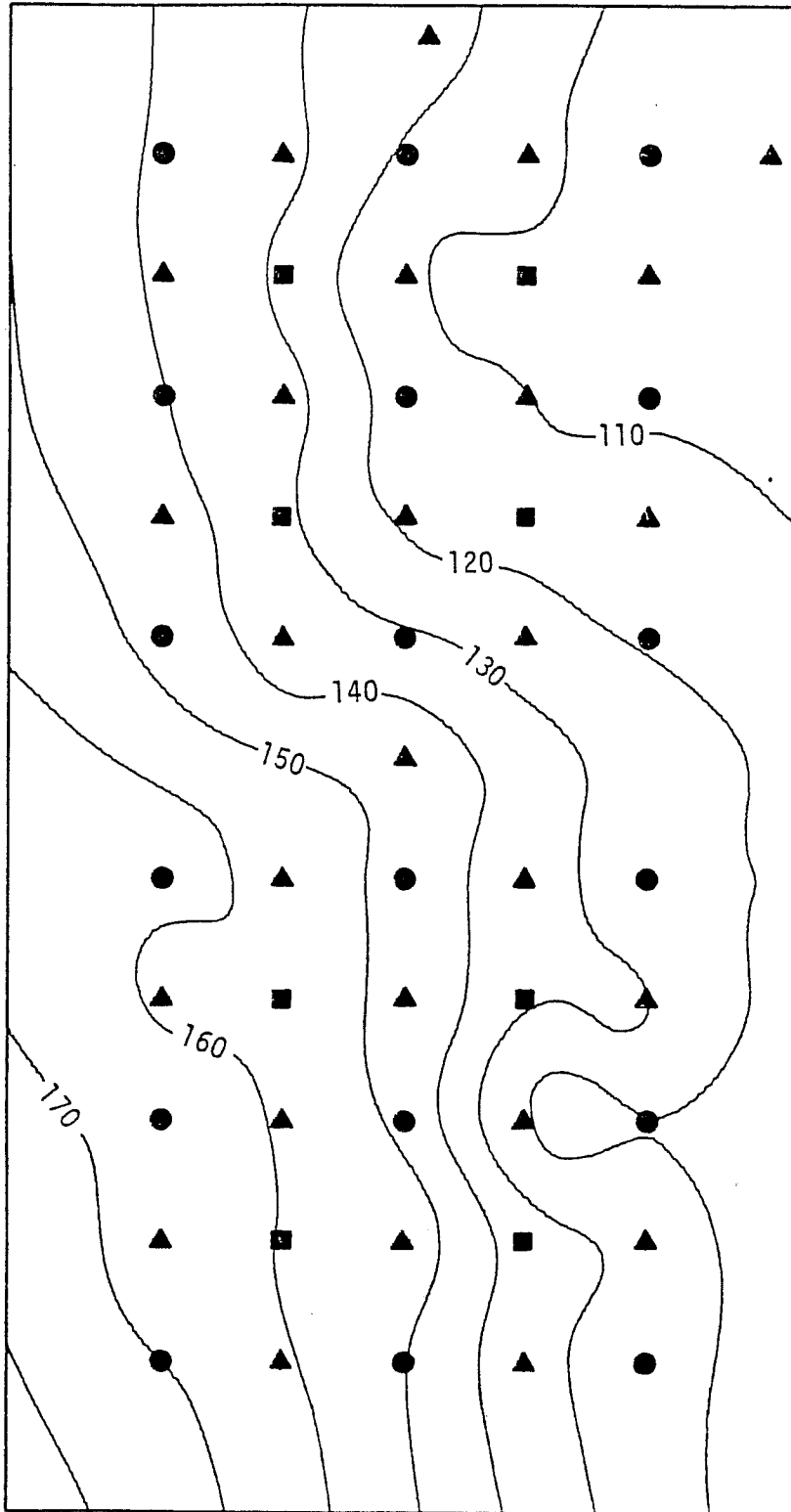
Computed with Average Well Rates for the Period from
November 18, 1975, to June 30, 1978



(From Ref. 6, p. II-114)

FIGURE B-3
OBSERVED MONITORING WELL PRESSURES

JUNE 28, 1978



Datum:
800 Feet Above
Mean Sea Level

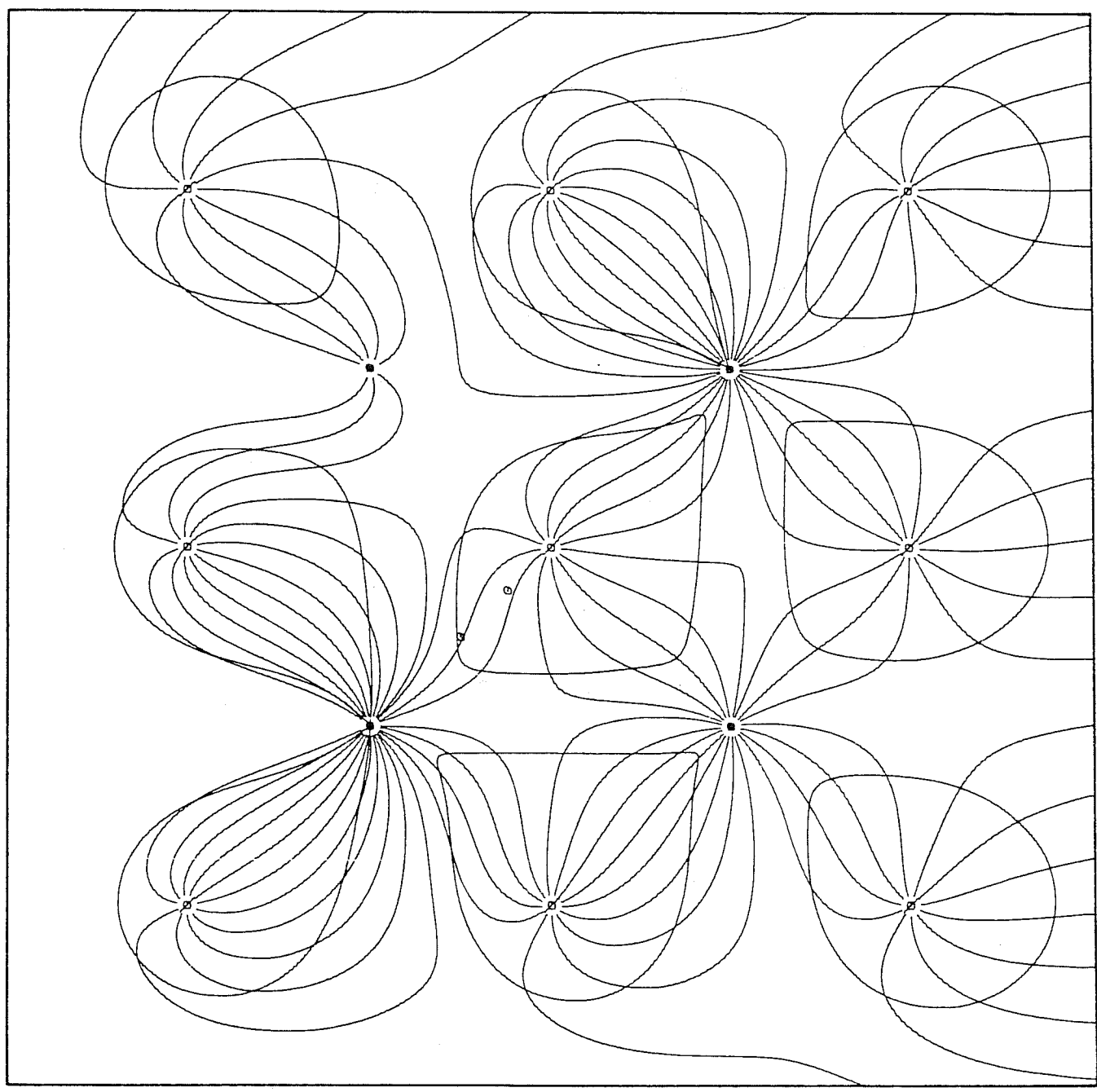
LEGEND

- Production Wells
- Injection Wells
- ▲ Monitoring Wells

(From Ref. 6, p. 11-77)

NORTH PATTERN PREFLOOD I FRONTS ON JUNE 30, 1978

Computed with 0.0304 psi/foot Gradient from 257 Degrees
and Average Well Rates for the Period from
November 18, 1975, to June 30, 1978



(From Ref. 6, p. II-127)

FIGURE B-5
 IDEALIZED CHANGES IN PRESSURE GRADIENTS BETWEEN MP-118 AND MP-124

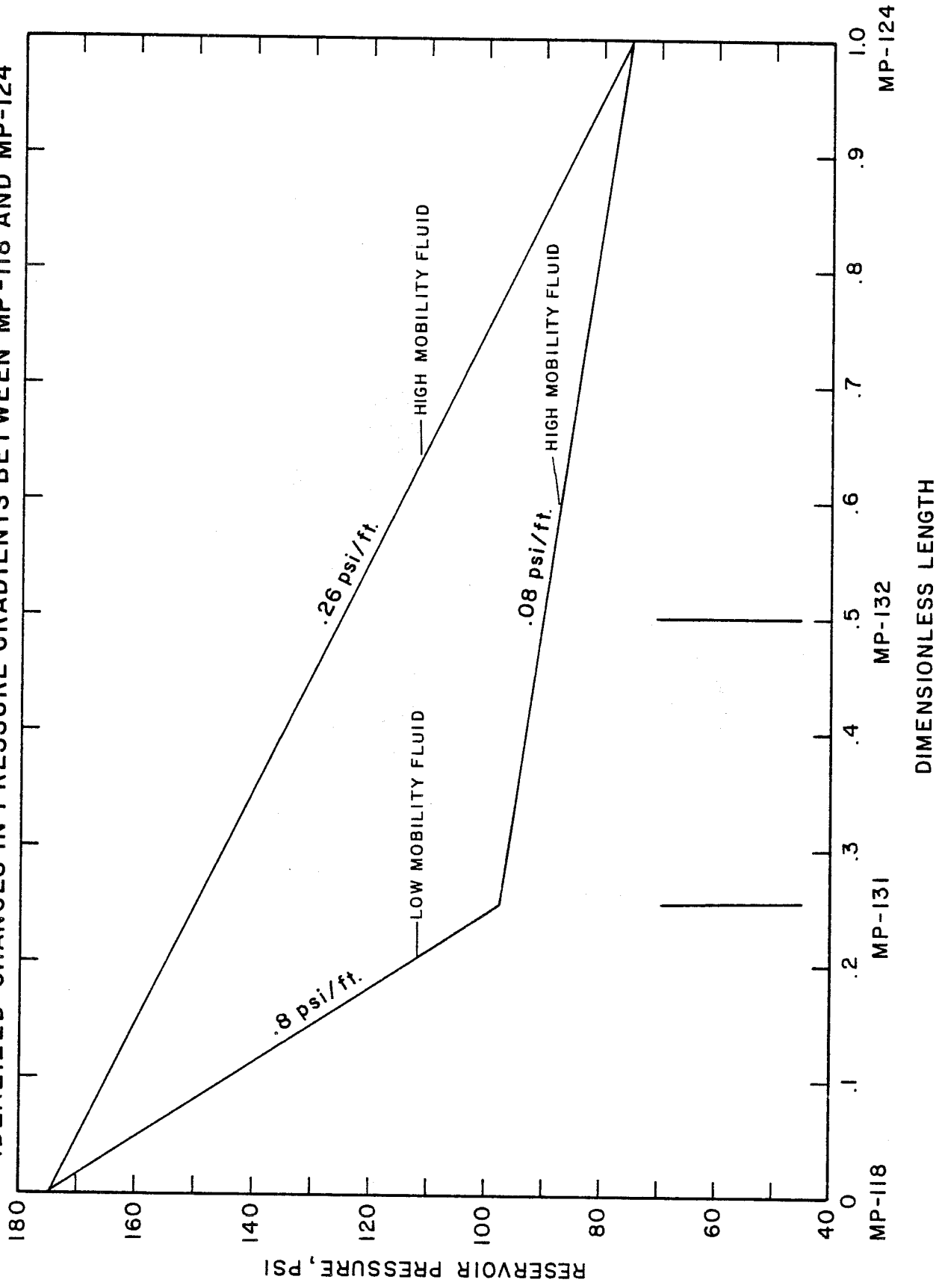
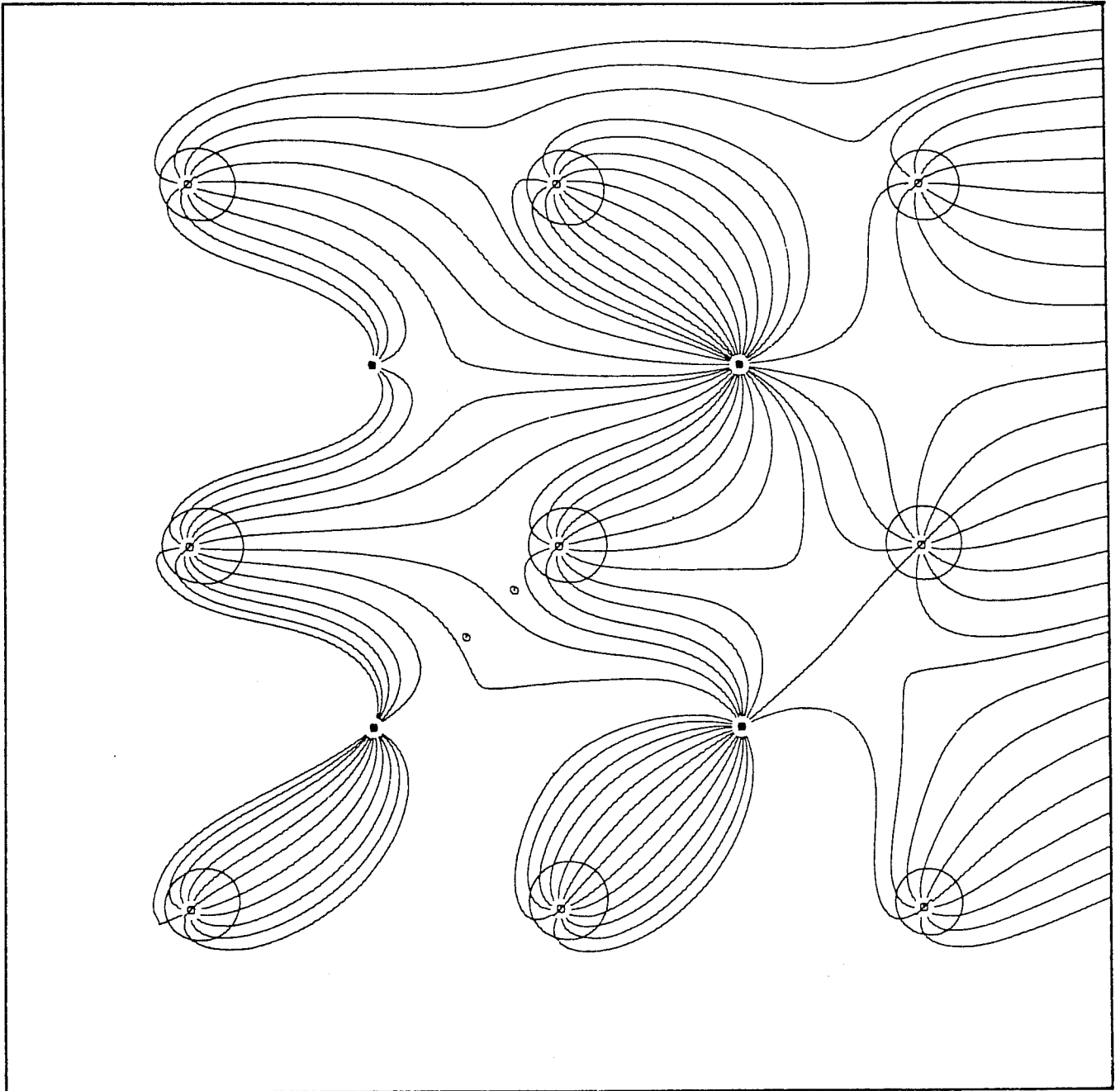


FIGURE B-6

NORTH PATTERN MICELLAR FLUID FRONTS ON JUNE 30, 1978

Computed with 0.0304 psi/foot Gradient from 257 Degrees
and Average Well Rates for the Period from
November 16, 1977, to June 30, 1978



(From Ref. 6, p. II-129)

FIGURE B-7
CALCULATED PRESSURE GRADIENT BETWEEN MP-118 AND MP-124

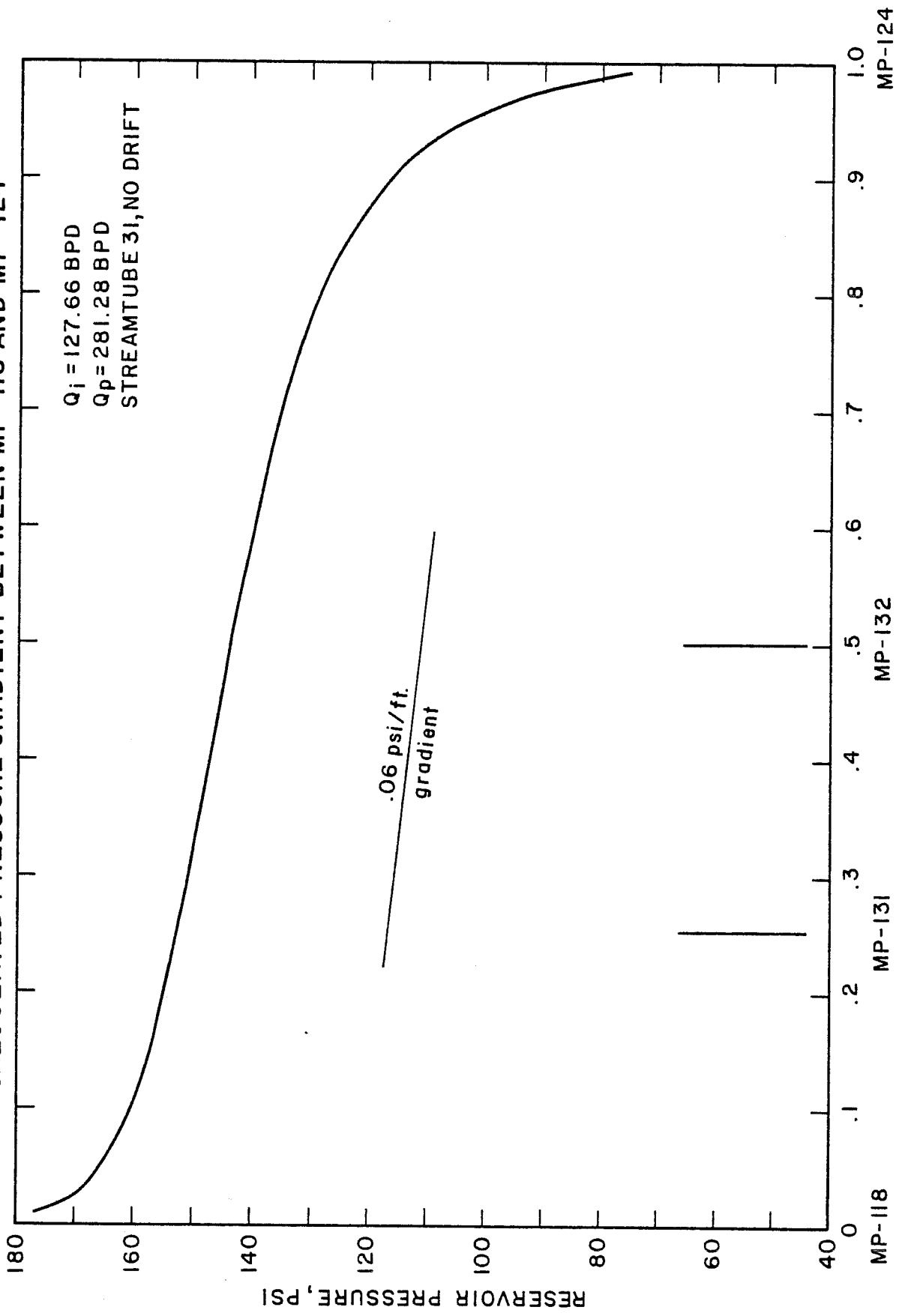


FIGURE B-8
EFFECT OF FLUID DRIFT ON STREAMTUBE 31

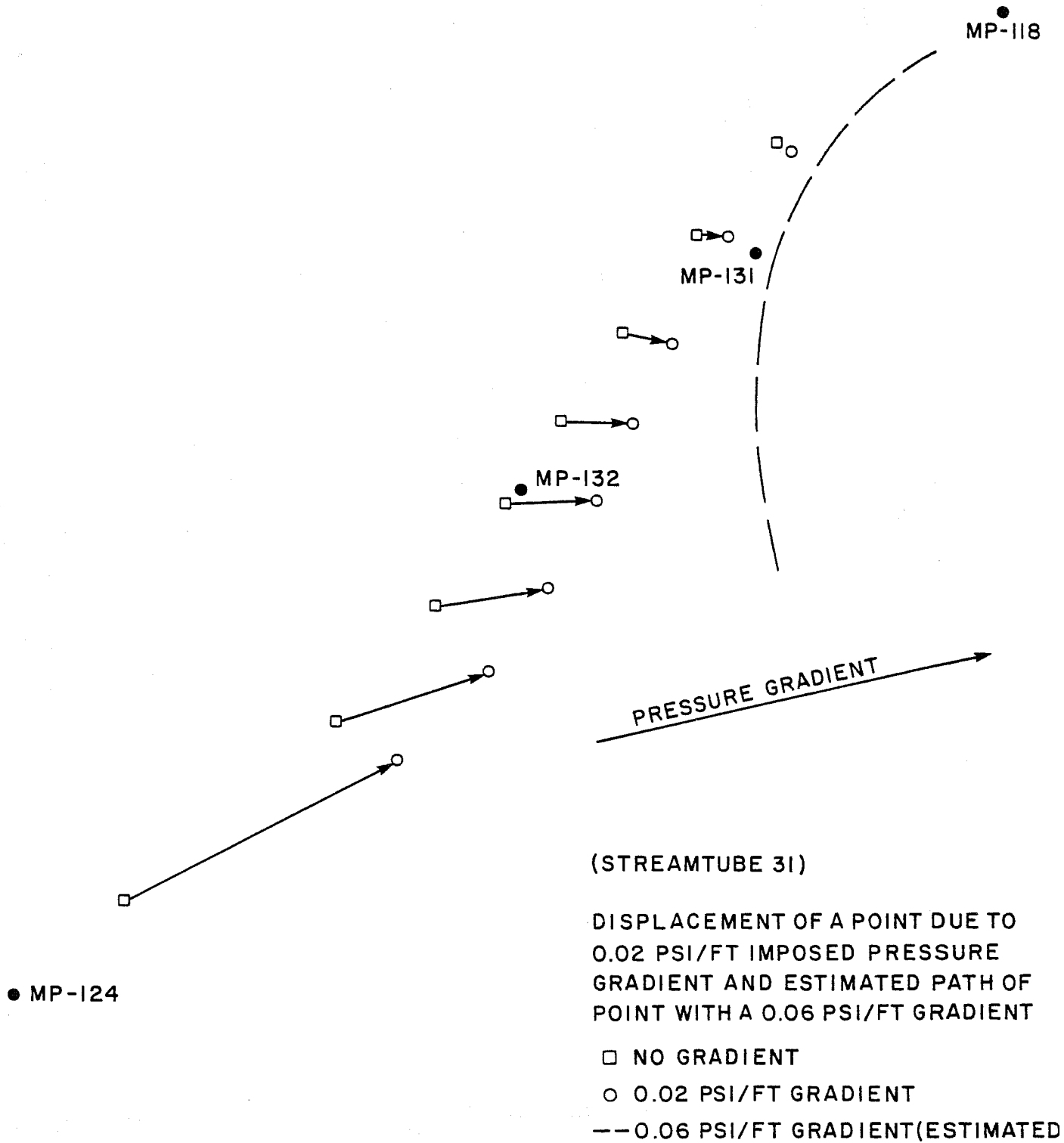
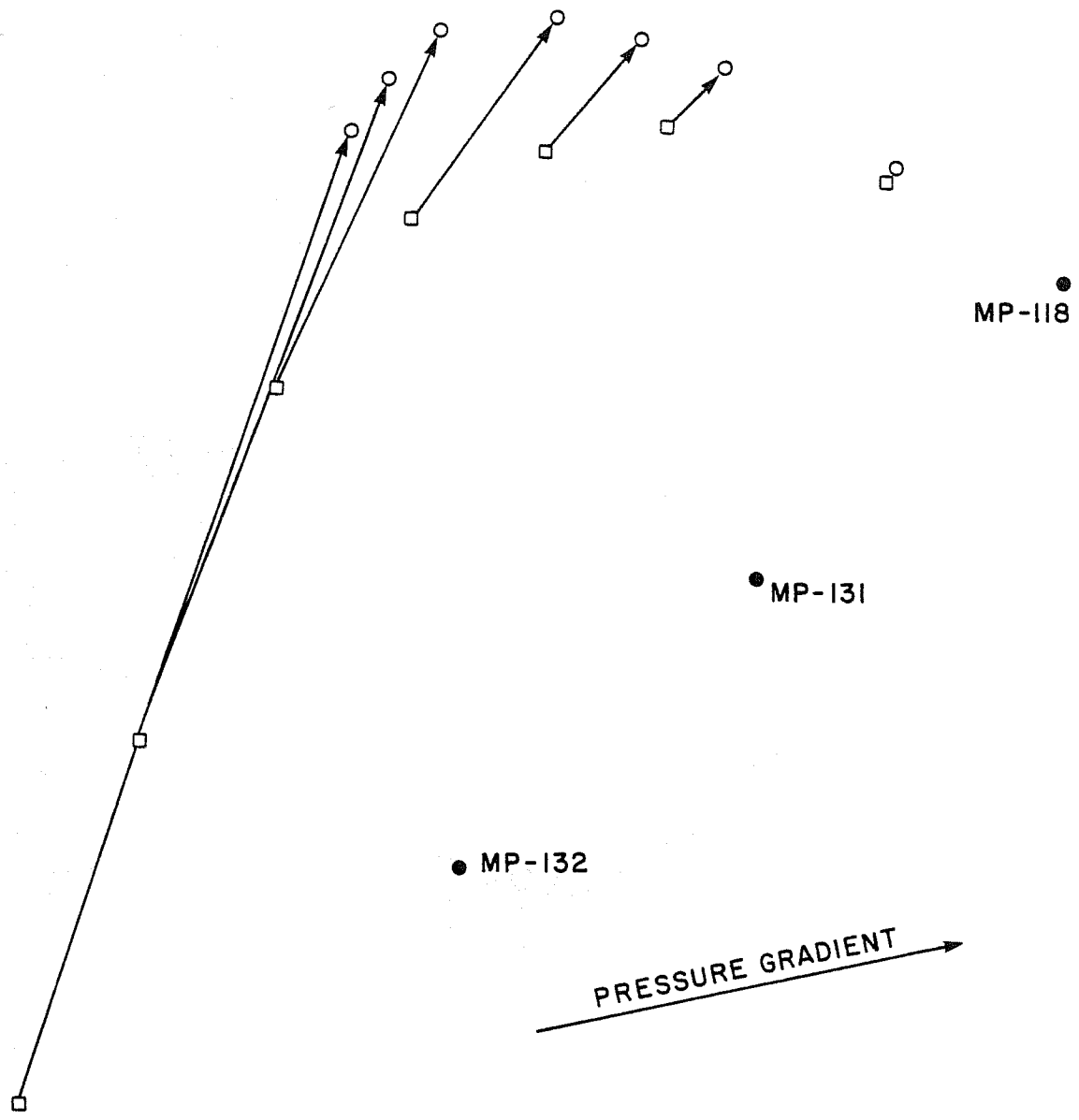


FIGURE B-9
EFFECT OF FLUID DRIFT ON STREAMTUBE 16



(STREAMTUBE 16)
DISPLACEMENT OF A POINT DUE TO
0.02 PSI/FT. IMPOSED PRESSURE
GRADIENT
□ NO GRADIENT
○ 0.02 PSI/FT GRADIENT

● MP-124

FIGURE B-10

CHESNEY LEASE PREFLOOD 2 FRONT ON 2/21/78. COMPUTED WITH
AVERAGE WELL RATES FOR THE PERIOD FROM 12/21/76 TO 2/20/78

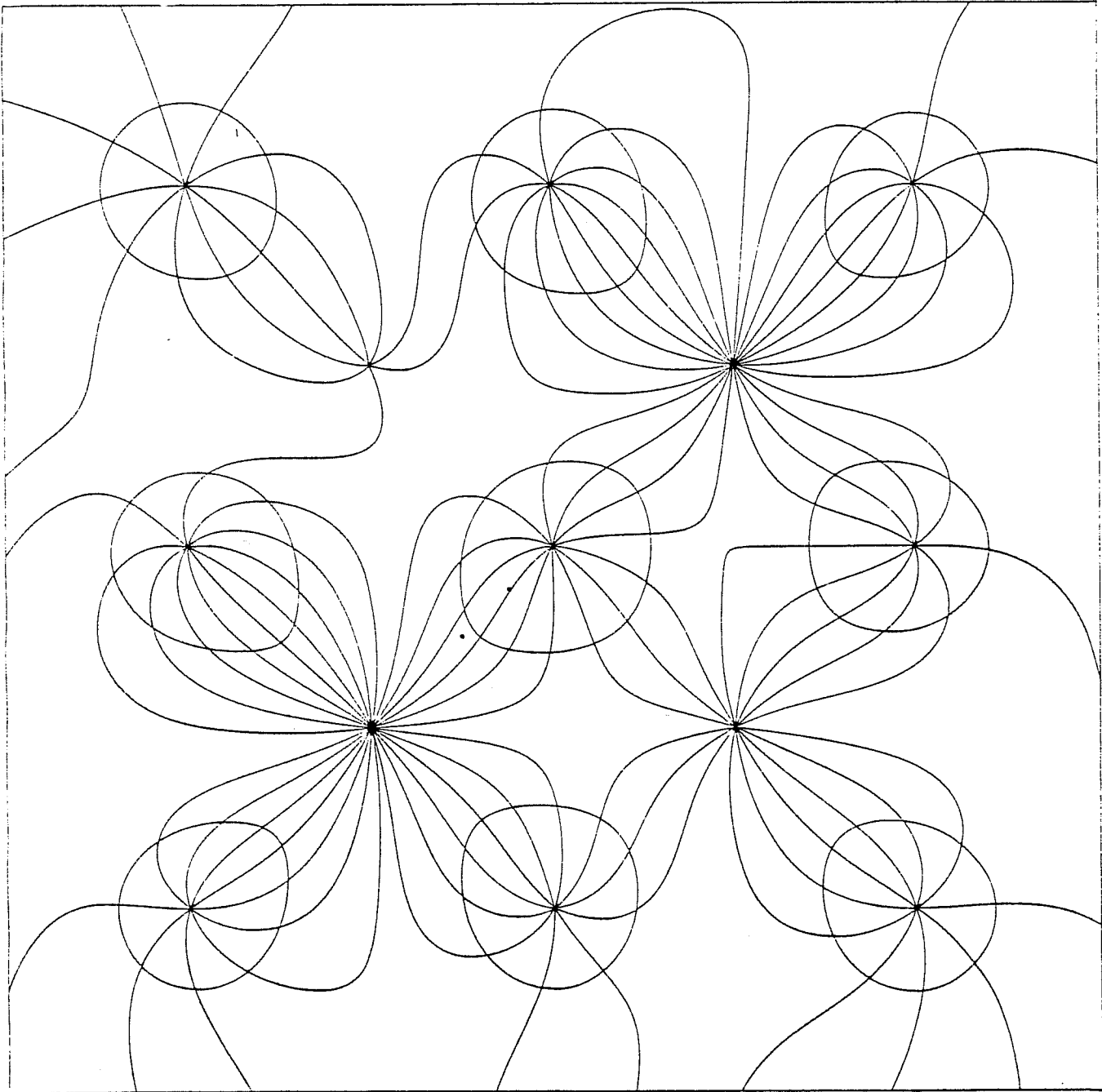


FIGURE B-11

MP-118 PREFLOOD 2 FRONT ON 2/21/78. COMPUTED WITH AVERAGE
WELL RATES FOR THE PERIOD FROM 12/21/76 TO 2/20/78

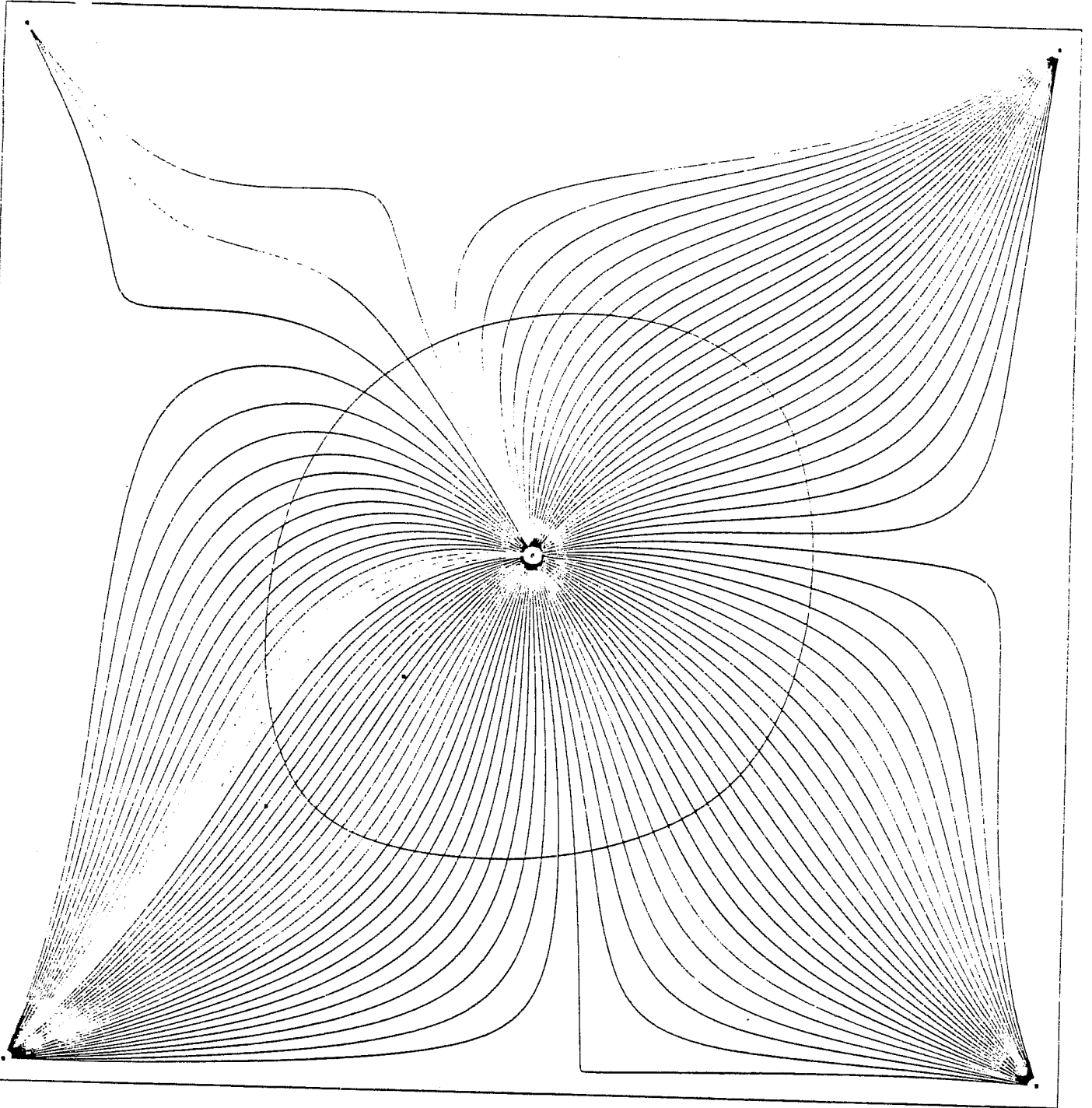
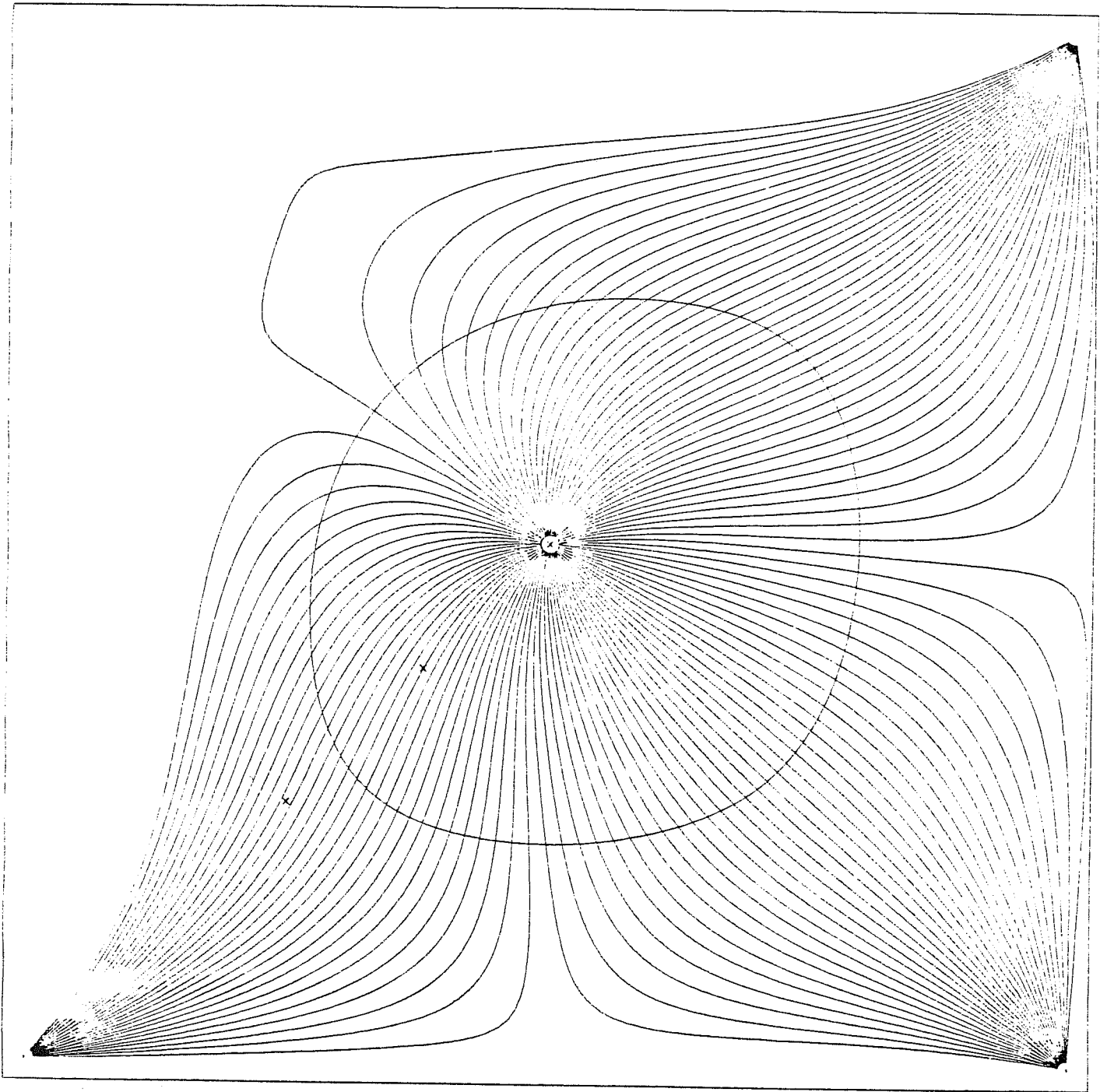


FIGURE B-12

MP-118 PREFLOOD 2 FRONT ON 2/21/78. COMPUTED WITH .02 PSI/FT
EXTERNALLY CAUSED PRESSURE GRADIENT AND AVERAGE WELL
RATES FOR THE PERIOD FROM 12/21/76 TO 2/20/78



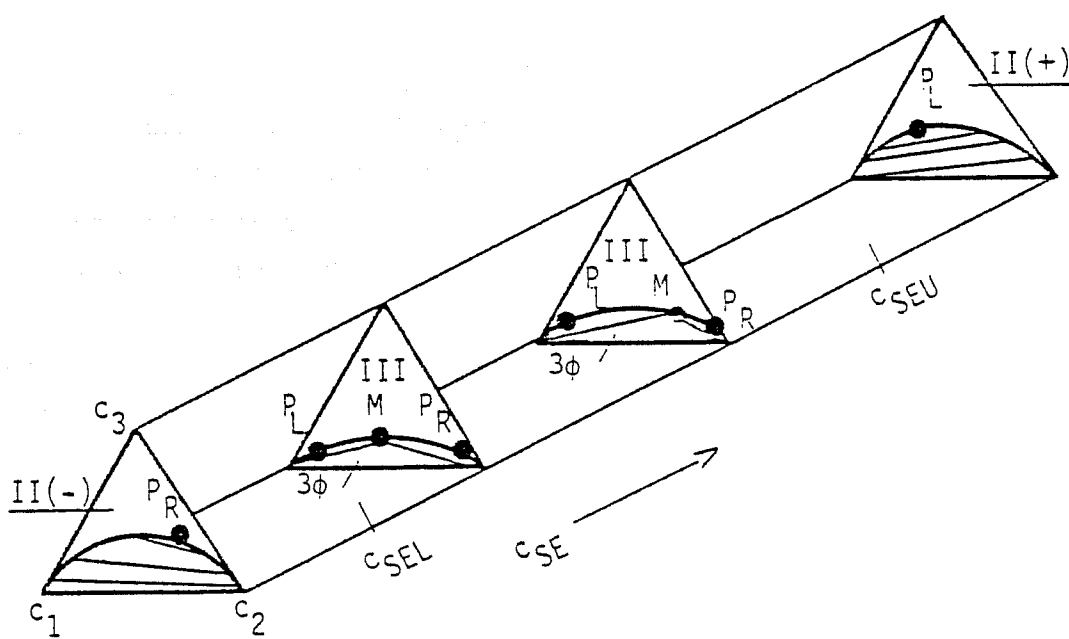
APPENDIX C
TERNARY PHASE EQUILIBRIA MODEL

1. INTRODUCTION

This appendix illustrates the calculation of idealized phase diagrams and the associated interfacial tension for a typical micellar fluid. The phase behavior is represented by ternary diagrams using the three pseudo components brine, oil, and chemical. These are calculated using the Hand approach as described in Section 2. All three phase types (II(-), II(+), III) and all associated features (plait points, invariant point) are shown as functions of salinity for a particular set of Hand parameters. The IFT is calculated for phase pairs using the Healy-Reed equations as described in Section 4.

2. CALCULATION OF PHASE DIAGRAMS

We can qualitatively depict the phase diagrams as shown below:

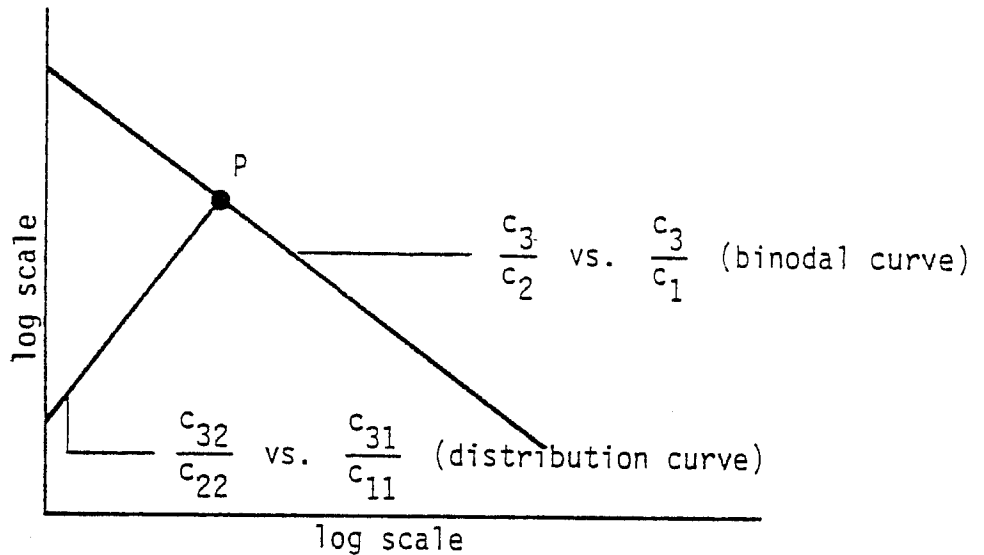


All features vary in a continuous way with an effective ionic strength ("salinity"), c_{SE} . This includes specifically the binodal curve, tie lines, plait points (left and right), and invariant point, M . We make the basic assumption that the binodal curve is the same function of c_{SE} for all three types of diagrams, so that all that distinguishes the Type III diagrams is the three phase triangle located by the point M , and the left and right node tie lines.

The basic idea is to model the diagrams with modified Hand equations, which in turn are based upon the observation that the phase boundary

(binodal curve) and distribution curve (tie lines) plot as straight lines on log plots as below.

HAND PLOT



In general, the curves vary with c_{SE} . This is discussed below. The approach and notation is similar to that in Ben Wang's thesis and SPE 6725 and SPE 7079. However, we have simplified and unified the calculations and at the same time improved the description, especially with regard to plait points, and have made the parameter determination more physical, so that they can be readily determined from experimental data.

For either Type II (-) to Type II (+) we have only two phases

below the binodal curve. The two basic equations are

$$\frac{c_{3j}}{c_{2j}} = A \left(\frac{c_{3j}}{c_{1j}} \right)^B \quad (1)$$

$$j = 1, 2$$

$$\frac{c_{32}}{c_{22}} = E \left(\frac{c_{31}}{c_{11}} \right)^F \quad (2)$$

These are equations for the binodal curve and distribution curve respectively. The parameters A, B, E, and F must be estimated as a function of c_{SE} as discussed below. We also know that

$$c_{11} + c_{21} + c_{31} = 1 \quad (3)$$

$$c_{12} + c_{22} + c_{32} = 1 \quad (4)$$

Equation (1) applies to either phase 1 or phase 2 i.e. either to the left or right of the plait point. Thus, we have five equations in six unknowns (the c_{ij} , $i = 1, 2, 3$, $j = 1, 2$). So we have one degree of freedom, as expected. We can take any one concentration such as c_{21} , and give it values between 0 and 1 and sweep out the phase diagram. We do this explicitly later, but for now we take a ratio defined below as our one degree of freedom.

$$\text{Let } R_{ij}^k = c_{ik}/c_{jk} \quad (5)$$

Let R_{31}^I be taken as independent. The following set of equations then yield the c_{ij} without iteration:

$$R_{32}^1 = A \left(R_{31}^1 \right)^B \quad (6)$$

$$c_{11} = \frac{R_{32}^1}{R_{31}^1 + R_{31}^1 R_{32}^1 + R_{32}^1} \quad (7)$$

$$c_{21} = 1 - (R_{31}^1 + 1)c_{11} \quad (8)$$

$$c_{31} = 1 - c_{11} - c_{21} \quad (9)$$

$$R_{32} = E \left(R_{31}^1 \right)^F \quad (10)$$

$$c_{12} = \frac{R_{32}^2}{R_{31}^2 + R_{31}^2 R_{32}^2 + R_{32}^2} \quad (11)$$

$$c_{22} = 1 - (R_{31}^2 + 1)c_{12} \quad (12)$$

$$c_{32} = 1 - c_{12} - c_{22} \quad (13)$$

R_{31}^1 varies between zero and infinity.

2.1 Parameter Estimation

The basic input is the set of three parameters c_{3MAX0} , c_{3MAX1} , and c_{3MAX2} . These are physically the maximum in the binodal curve (the "height" of the two phase region) at $c_{SE} = 0, 1,$ and $2,$ respectively. These are values easily visualized and obtained from even limited phase data and do not vary widely from case to case, so reasonable values can be assumed in the absence of any data (caution: some data are needed to support the assumption that the system fits the qualitative trends depicted, so having some data is highly desirable). The values do not

matter, however, because the extent of the single phase region directly affects the degree of miscibility. Thus, once again, some data are highly desirable.

We now use this interpolation scheme for A:

$$A_0 = \left[\frac{2 c_{3\text{MAX}0}}{1 - c_{3\text{MAX}0}} \right]^2 \quad (14)$$

$$A_1 = \left[\frac{2 c_{3\text{MAX}1}}{1 - c_{3\text{MAX}1}} \right]^2 \quad (15)$$

$$A_2 = \left[\frac{2 c_{3\text{MAX}2}}{1 - c_{3\text{MAX}2}} \right]^2 \quad (16)$$

$$A = A_0 + (A_1 - A_0)c_{\text{SE}} \quad c_{\text{SE}} \leq 1 \quad (17)$$

$$A = A_1 + (A_2 - A_1)(c_{\text{SE}} - 1) \quad c_{\text{SE}} \geq 1 \quad (18)$$

Recall that c_{SE} is in optimal salinity units (effective salinity divided by optimal effective salinity).

We assume B and F are constants. The most flexible scheme allows B and F to be arbitrary. However, many times the binodal curve is known but the tie lines are not. Thus we can get B, but not F, from the data available. In such cases, we will take $F = -1/B$ by analogy with those cases where we do have data, since this relationship tends to hold approximately. Furthermore, many times we do not have enough data to even estimate B properly. In such cases we take $B = -1$. This gives a symmetrical binodal curve. The deviation of most actual curves from this symmetry is probably not significant. The type of phase diagram

(II (-), III, II (+)) and the extent of the single phase region are the most important factors. It seems unlikely that the detailed shape of the curve is significant. Also, recall that since we are dealing with pseudo-ternary diagrams, the curves themselves shift around depending on the exact overall composition (especially with respect to alcohol), so it makes no sense at all to try to describe them in great detail with high precision, even when we have the large amount of data required to do so, which is hardly ever.

Let us return to parameter estimation. We still need E. We estimate E from the location of the plait point. This is done once again because it is a method easy to visualize and apply and has a direct physical meaning. Since equations (1) and (2) must apply at the plait point, P, we have

$$\frac{c_{3p}}{c_{2p}} = E \left(\frac{c_{3p}}{c_{1p}} \right)^F \quad (19)$$

$$\frac{c_{3p}}{c_{2p}} = A \left(\frac{c_{3p}}{c_{1p}} \right)^B \quad (20)$$

$$c_{1p} + c_{2p} + c_{3p} = 1 \quad (21)$$

Given A, B, and F from above, these equations can be used to calculate E as a function c_{2p} . For the special case of $B = -1$ and $F = +1$, we can calculate all the phase concentrations (c_{ij}) explicitly.

From equation (1) we can solve for c_{31} ($j = 1$)

$$c_{31} = \frac{1}{2} \left[-Ac_{21} + \sqrt{(Ac_{21})^2 + 4Ac_{21}(1-c_{21})} \right] \quad (22)$$

and

$$c_{11} = 1 - c_{21} - c_{31} \quad (23)$$

From equation (19) we calculate

$$E = c_{1p} / c_{2p} \quad (24)$$

where

$$c_{3p} = \frac{1}{2} \left[-Ac_{2p} + \sqrt{(Ac_{2p})^2 + 4Ac_{2p}(1-c_{2p})} \right] \quad (24a)$$

and

$$c_{1p} = 1 - c_{2p} - c_{3p} \quad (24b)$$

Note that c_{2p} is an input parameter.

From equation (2) we have

$$c_{32} = h c_{22} \quad (25)$$

where

$$h \equiv Ec_{31} / c_{11} \text{ is known} \quad (26)$$

Substituting this into equation (1) with $j = 2$ and solving for c_{22}

$$c_{22} = \frac{A}{h^2 + Ah + A} \quad (27)$$

Then

$$c_{32} = h c_{22} \quad (28)$$

and
$$c_{12} = 1 - c_{22} - c_{32} \quad (29)$$

We now know all c_{ij} .

The only difference between Type II (-) and II (+) is that for II (-) we input c_{2PR} and for II (+) c_{2PL} . The limits on II (-) are $0 \leq c_{SE} \leq c_{SEL}$ and on II (+) $c_{SEU} \leq c_{SE} \leq 2$.

In summary, for II (-), we increment c_{SE} up to c_{SEL} and for each c_{SE} we increment c_{21} from 0 to c_{2PR} . The input parameters are c_{3MAX0} , c_{3MAX1} , and c_{2PR}^* . The c_{ij} are calculated from equations (22) through (29). For II (+) we increment c_{SE} from c_{SEU} to 2.0, and for each c_{SE} we increment c_{21} from 0 to c_{2PL}^* . The c_{ij} are calculated from the same equations as before.

2.2 Type III

For Type III, we must calculate the left node and the right node separately. First we calculate the invariant point (M) as a function of c_{SE} from

$$c_{2M} = \frac{c_{SE} - c_{SEL}}{c_{SEU} - c_{SEL}} \quad (30)$$

$$c_{3M} = \frac{1}{2} \left(-Ac_{2M} + \sqrt{(Ac_{2M})^2 + 4Ac_{2M}(1-c_{2M})} \right) \quad (31)$$

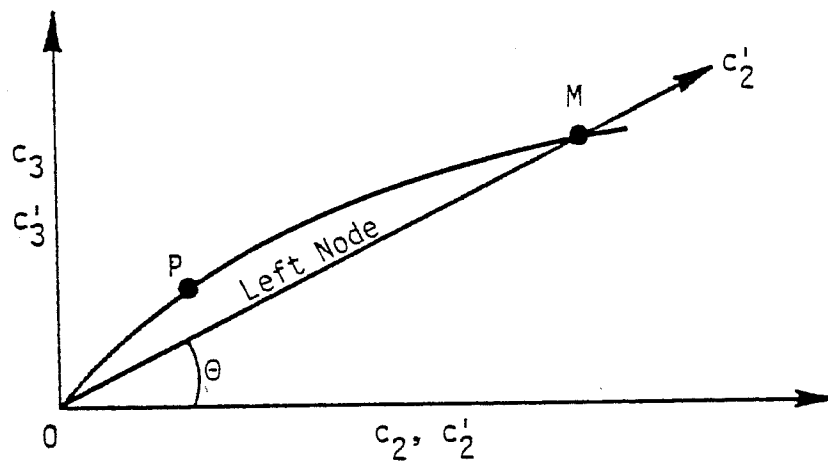
$$c_{1M} = 1 - c_{2M} - c_{3M} \quad (32)$$

2.2.1. Left node

The plait point must vary between zero and the II (+) value c_{2PL}^* . By interpolation

$$c_{2PL} = c_{2PL}^* + \frac{c_{2PL}^*}{c_{SEU} - c_{SEL}} (c_{SE} - c_{SEU}) \quad (33)$$

We now do a coordinate rotation as shown below



This enables us to apply the Hand equation in the new coordinate system as

$$\frac{c'_{32}}{c'_{22}} = E \left(\frac{c'_{31}}{c'_{11}} \right) \quad (34)$$

where

$$c'_{2j} = c_{2j} \sec \theta \quad (35)$$

$$c'_{3j} = c_{3j} - c_{2j} \tan \theta \quad (36)$$

$$c'_{1j} = 1 - c'_{2j} - c'_{3j} \quad (37)$$

let

$$\beta = \sec \theta = \sqrt{c_{2M}^2 + c_{3M}^2} / c_{2M} \quad (38)$$

$$\alpha = \tan \theta = c_{3M} / c_{2M} \quad (39)$$

Again taking $F = 1$, we can calculate E explicitly from

$$E = c'_{1p} / c'_{2p} = \frac{1 - (\beta - \alpha)c_{2p} - c_{3p}}{\beta c_{2p}} \quad (40)$$

where

$$c_{2p} = c_{2p1}$$

and c_{1p} and c_{3p} are given by equation (24a) and (24b) as before.

We can now calculate c_{31} and c_{11} as before and solve equation (34) for c_{22}

$$c_{22} = \frac{A}{h'^2 + Ah' + A} \quad (41)$$

where

$$h' = \frac{\beta E c'_{31}}{c'_{11}} + \alpha \quad (42)$$

and then

$$c_{32} = h' c_{22} \quad (43)$$

$$c_{12} = 1 - c_{22} - c_{32} \quad (44)$$

We now know all c_{ij} for the left node. We increment c_{21} from zero to c_{2PL} for each c_{SE} as before.

2.2.2. Right node

The process is almost the same as for the left node except we calculate c_{2PR} from

$$c_{2PR} = c_{2PR}^* + \frac{1 - c_{2PR}^*}{c_{SEU} - c_{SEL}} (c_{SE} - c_{SEL}) \quad (45)$$

We first calculate c_{32} from

$$c_{32} = \frac{1}{2} \left[-Ac_{12} + \sqrt{(Ac_{12})^2 + 4Ac_{12}(1-c_{12})} \right] \quad (46)$$

and

$$c_{22} = 1 - c_{12} - c_{32} \quad (47)$$

Note that c_{12} is now incremented rather than c_{21} (this is simply more convenient).

Let

$$h' \equiv \frac{\beta c_{32}}{E c_{11}} + \alpha \quad (48)$$

Then

$$c_{11} = \frac{A}{h^{-2} + Ah' + A} \quad (49)$$

$$c_{31} = h' c_{11} \quad (50)$$

$$c_{21} = 1 - c_{11} - c_{31} \quad (51)$$

where

$$\alpha = c_{3M} / c_{1M} \quad (52)$$

$$\beta = \sqrt{c_{3M}^2 + c_{1M}^2} / c_{1M} \quad (53)$$

$$c'_{1j} = \beta c_{1j} \quad (54)$$

$$c'_{3j} = c_{3j} - \alpha c_{1j} \quad (55)$$

$$c'_{2j} = 1 - c'_{1j} - c'_{3j} \quad (56)$$

$$E = c'_{1p} / c'_{2p} \quad (57)$$

and c'_{1p} and c'_{2p} are calculated using equations (54) to (56) and (24 a) and (24 b). We now know all c_{ij} for the right node.

3. SUMMARY OF CALCULATION PROCEDURE

I. Given: c_{3MAX1} , c_{3MAX0} , c_{3MAX2} = height of binodal curve when
 $c_{SE} = 1, 0, \text{ and } 2$

c_{SEL} , c_{SEU} = minimum and maximum effective salinities
for Type III

c_{2PR}^* , c_{2PL}^* = oil coordinate of plait point in
Type II(-) and Type II(+) regions

Seven input parameters

II. For $c_{SE} < c_{SEL}$ - Type II(-)

1. Calculate parameter A from (17)
2. Calculate c_{3PR}^* and c_{1PR}^* from (24a) and (24b) using c_{2PR}^*
3. Calculate E from (24) and c_{1PR}^* and c_{2PR}^* .
4. Pick c_{21} , calculate c_{31} and c_{21} from (22) and (23).
5. Calculate h from (26)
6. Calculate c_{22} , c_{32} , c_{12} from (27) - (29)

III. For $c_{SE} > c_{SEU}$ - Type II(+)

1. Calculate parameter A from (18)
2. Calculate c_{3PL}^* and c_{1PL}^* from (24a) and (24b) using c_{2PL}^*
3. Calculate E from (24) and c_{1PL}^* and c_{3PL}^* .
4. Pick c_{21} , calculate c_{31} and c_{11} from (22) and (23)
5. Calculate h from (26)
6. Calculate c_{22} , c_{32} , c_{12} from (27) - (29)

IV. For $c_{SEL} < c_{SE} < c_{SEU}$ - Type III

1. Calculate c_{2M} from (30)
2. Calculate A from (17) or (18)
3. Calculate c_{3M} and c_{1M} from (31) and (32)
4. Left node - Type II(+)
 - a. Calculate θ , γ , and β from (38) and (39)
 - b. Calculate c_{2PL} from (33)
 - c. Calculate c_{3PL} and c_{1PL} from (24a) and (24b) using c_{2PL}
 - d. Calculate E from (40)
 - e. Pick c_{21} , calculate c_{31} and c_{11} from (22) and (23)
 - f. Calculate h' from (42)
 - g. Calculate c_{32} , c_{12} , and c_{22} from (41) - (44)

5. Right node - Type II(-)

- a. Calculate α and β from (52) and (53)
- b. Calculate c_{2PR} from (45)
- c. Calculate c_{3PR} and c_{1PR} from (24a) and (24b) using c_{2PR}
- d. Calculate E from (40)
- e. Pick c_{12} , calculate c_{32} and c_{12} from (22) and (23)
- f. Calculate h' from (48)
- g. Calculate c_{31} , c_{11} , c_{21} from (49) - (51)

4. INTERFACIAL TENSION CALCULATIONS

We use the Healy and Reed type equations. For Type II(-) and the left node

$$\log \gamma_{WM} = G_{12} + \frac{G_{11}}{G_{13}(c_{12} / c_{32}) + 1} \quad (58)$$

For II(+) and the right node

$$\log \gamma_{MO} = G_{22} + \frac{G_{21}}{G_{23}(c_{21} / c_{31}) + 1} \quad (59)$$

For the three phase region, the IFT does not vary (at fixed c_{SE}). The values are given by equation (58) with $c_{21} = c_{2M}$ and $c_{31} = c_{3M}$. This scheme should give consistent IFT's as a function of composition and salinity (c_{SE}). The input parameters are the six G_{ij} (or just three G_{ij} 's assuming symmetry).

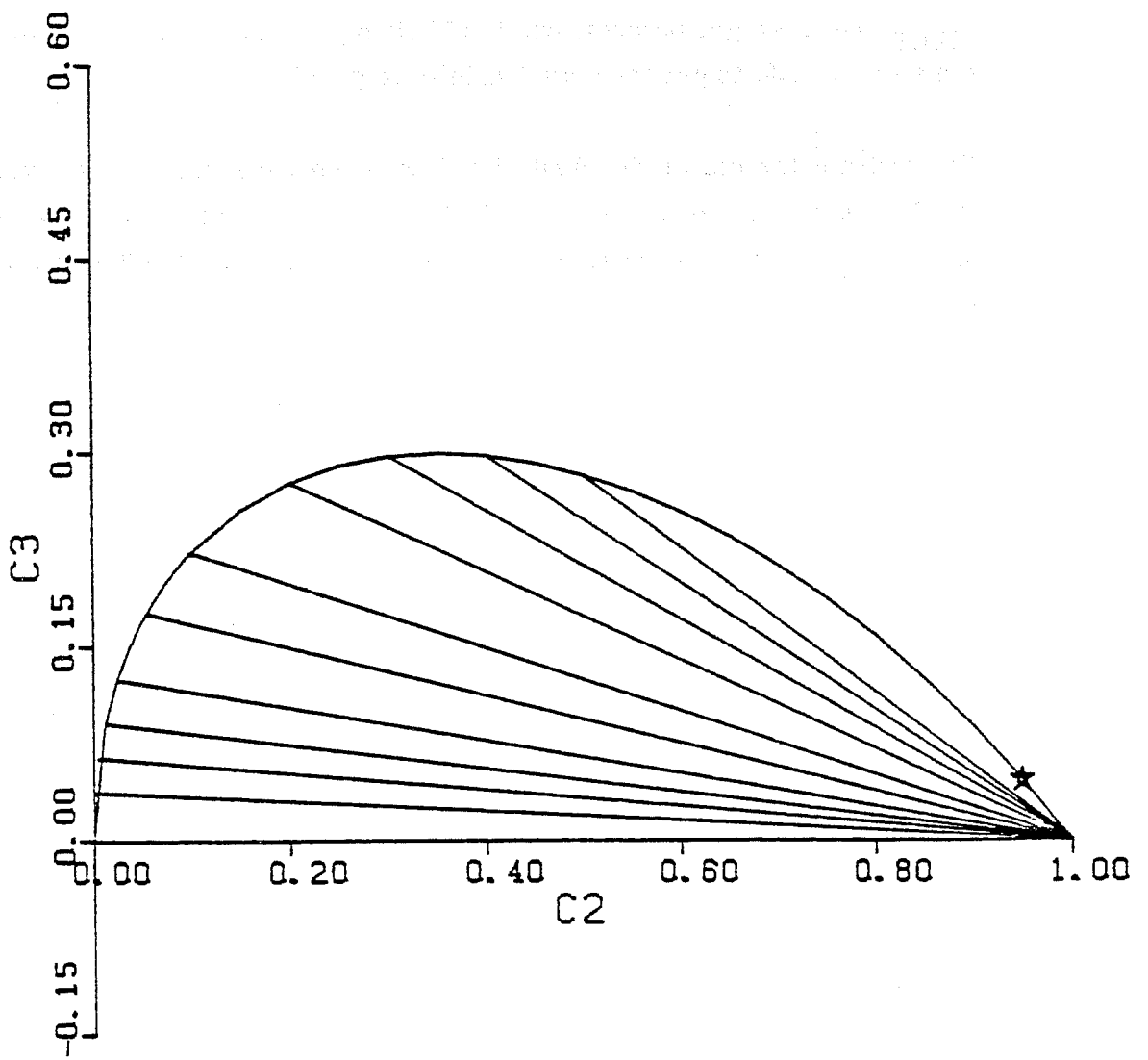
5. RESULTS

The results for types II(-), II(+), III) and corresponding IFT's are shown on pp. C-18 through C-35. Phase diagrams are on right rectangular coordinates with c_{3j} plotted versus c_{2j} (c_{1j} is by difference and is not shown on this type plot). To the left of the plait point (c_{2PR} , c_{3PR}), $j = 1$, and to the right, $j = 2$, for these II(-) diagrams.

The Type II(-) diagrams are swept out from $c_{SE} = 0$ to $c_{SEL} = 0.8$ in these examples. Type III goes from $c_{SE} = 0.8$ to $c_{SE} = 1.2$, and Type II(+) from $c_{SE} = 1.2$ to 2.0 (an arbitrary cut-off). Optimal salinity is $c_{SE} = c_{SEOP} = 1$. The units are arbitrary, or "optimal salinity units" if you wish. Given the actual c_{SEOP} , say 2 weight percent, one would simply multiply the printed c_{SE} by this same factor, 2.0, to get the actual salinity to go with each diagram.

To illustrate the use of the Healy-Reed equations, IFT results are presented on pp. C-34 and C-35 for one total surfactant concentration (0.03) and a particular set of G_{ij} 's. IFT is presented as both explicit and implicit (through the solubilization ratio) functions of salinity.

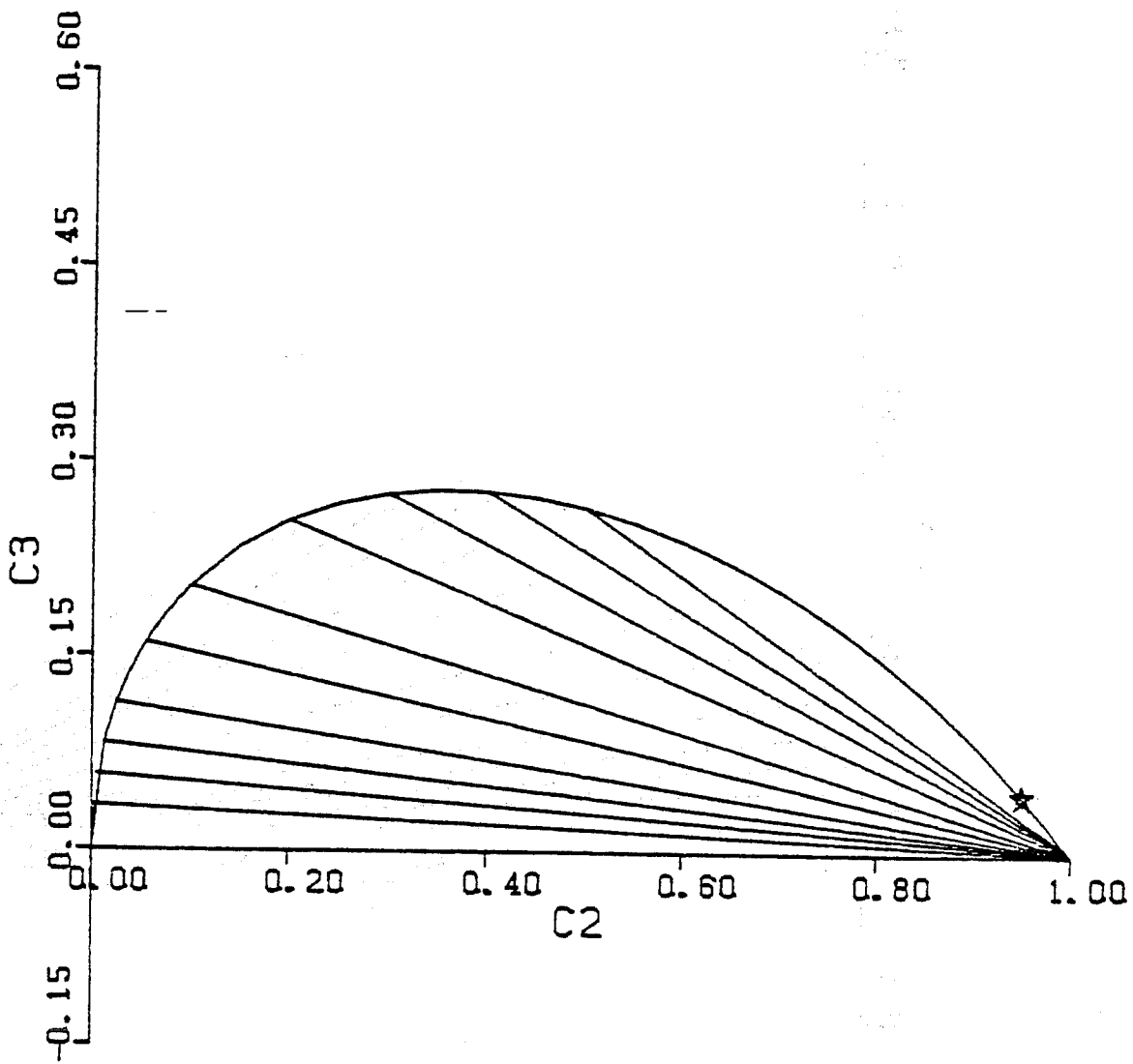
CSE=0.00
C3MAX0=.3 C3MAX1=.1 C3MAX2=.3
C2PR=.95 C2PL=.05



C3MAX0=.3
C2PR=.95

CSE=.20
C3MAX1=.1

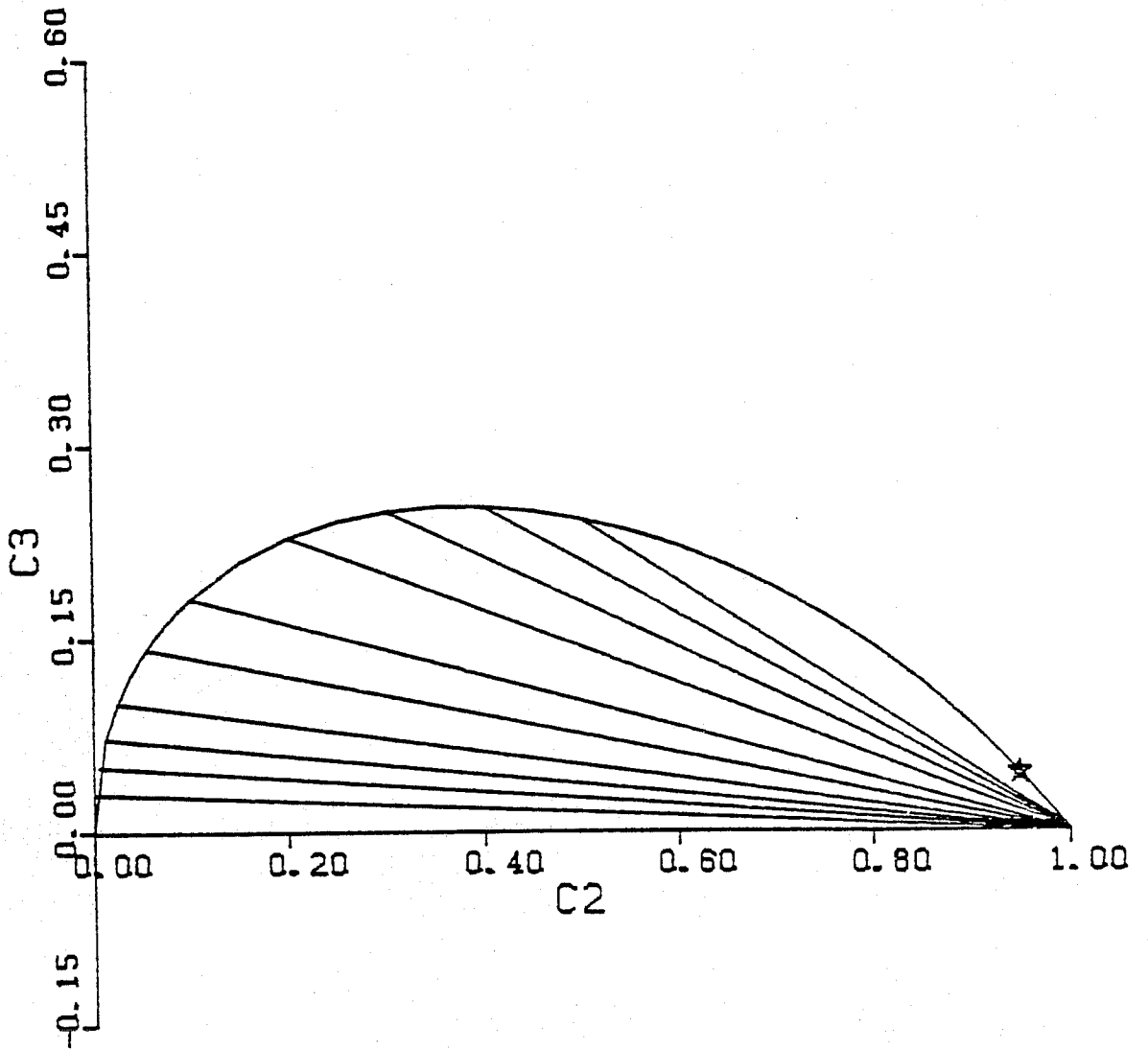
C3MAX2=.3
C2PL=.05



C3MAX0=.3
C2PR=.95

CSE=.40
C3MAX1=.1

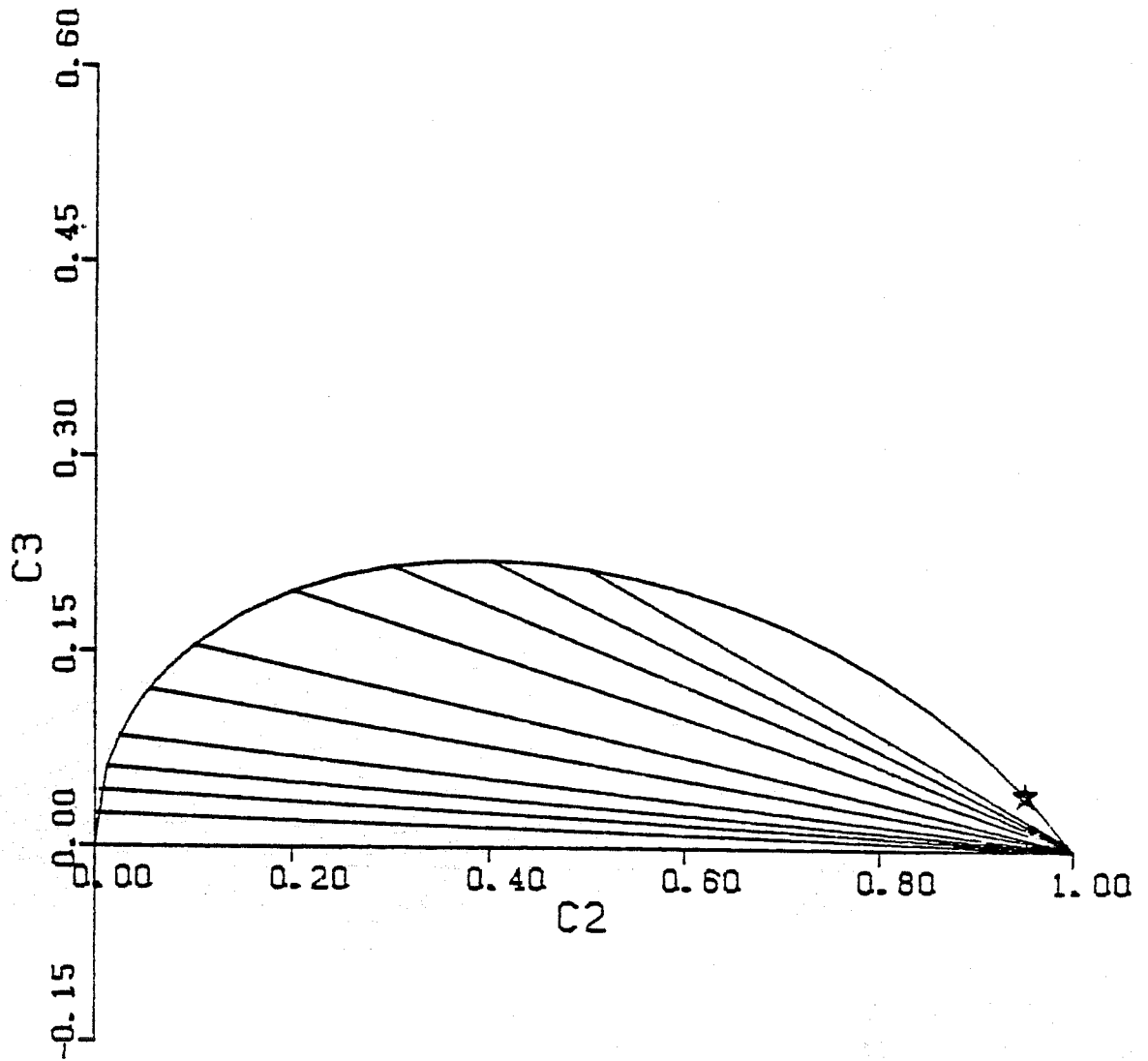
C3MAX2=.3
C2PL=.05



C3MAX0=.3
C2PR=.95

CSE=.60
C3MAX1=.1

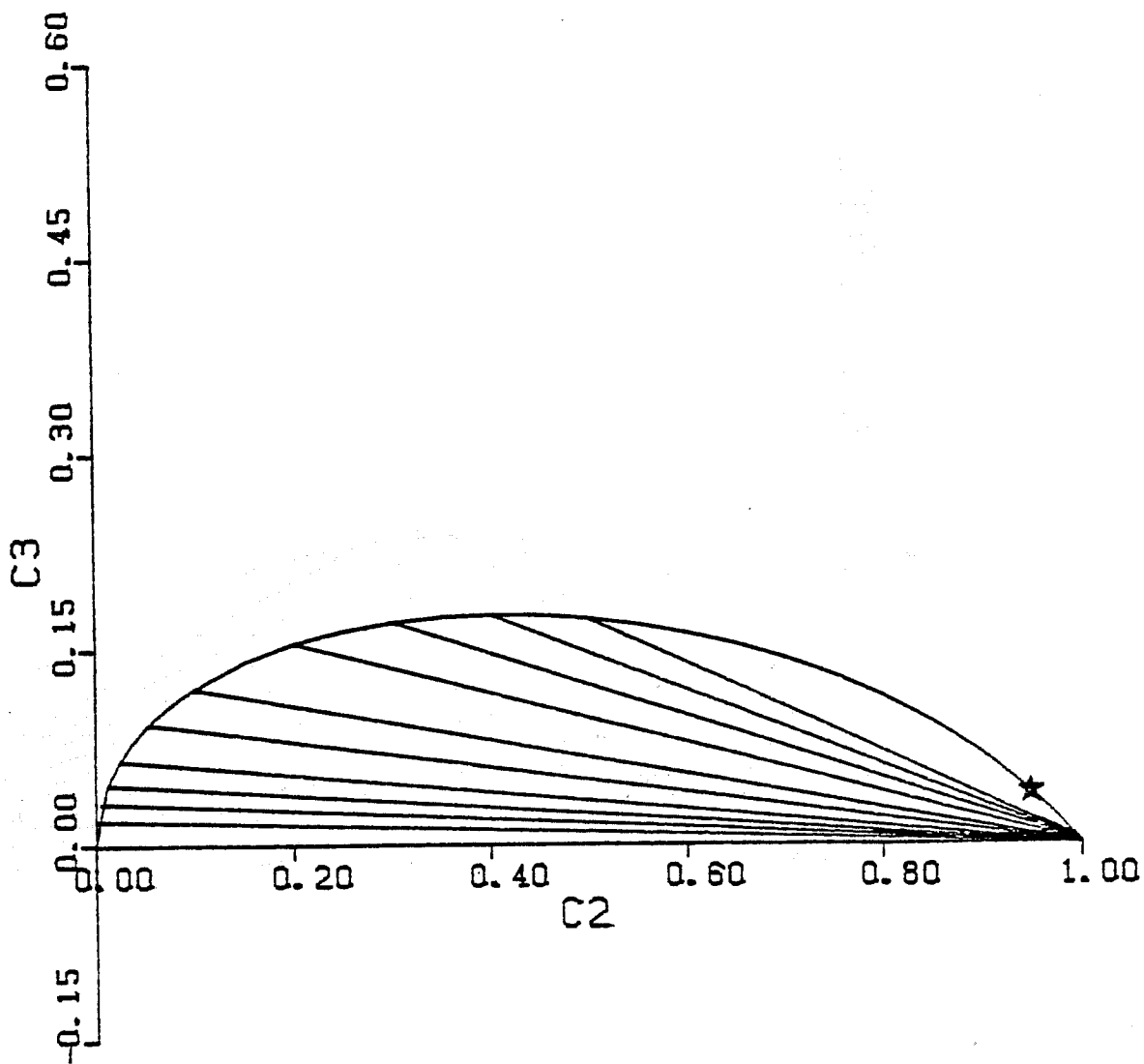
C3MAX2=.3
C2PL=.05



C3MAX0=.3
C2PR=.95

CSE=.80
C3MAX1=.1

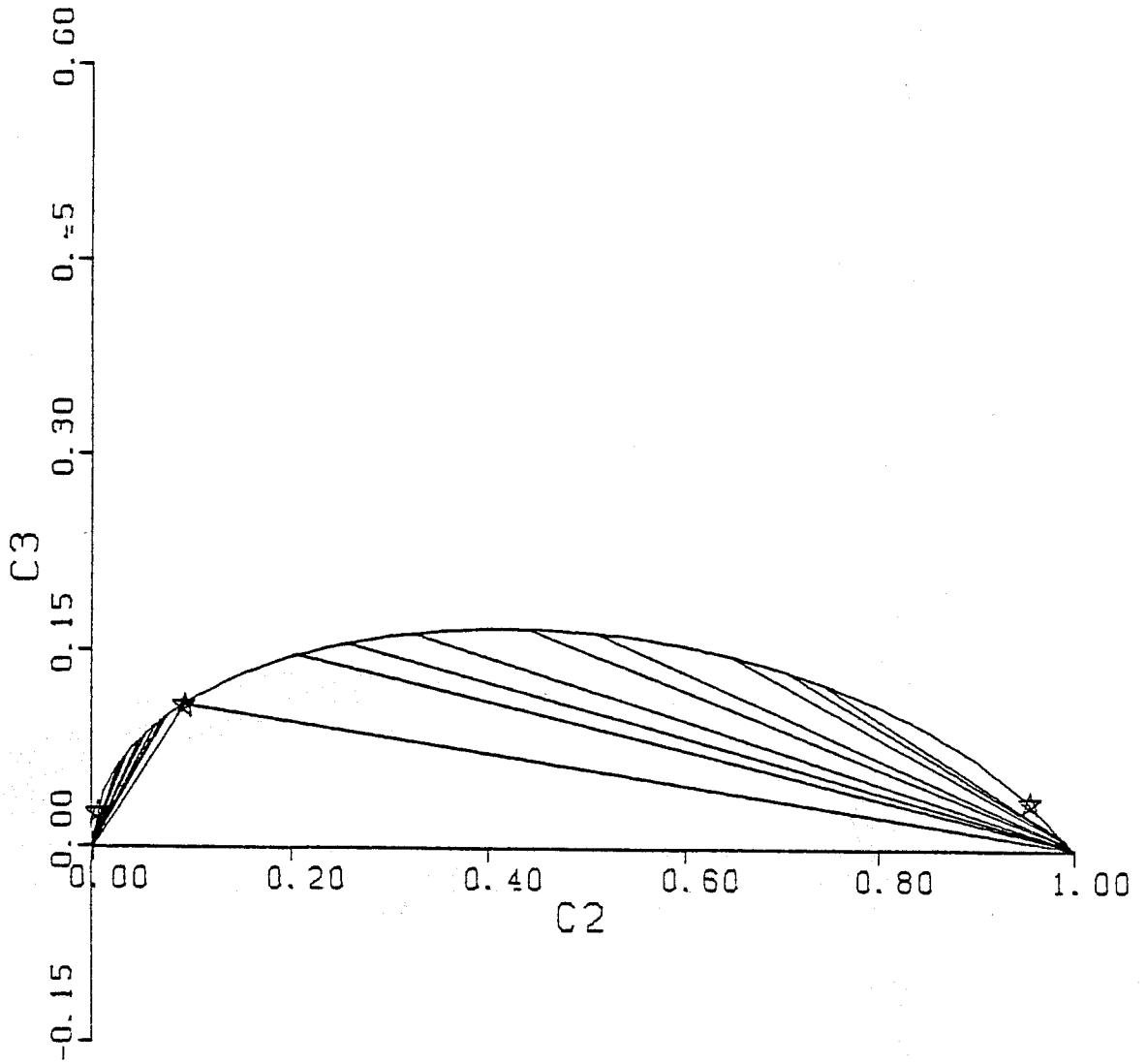
C3MAX2=.3
C2PL=.05



C3MAX0=.3
C2PR=.95

TYPE III
C3MAX1=.1
CSE=.84

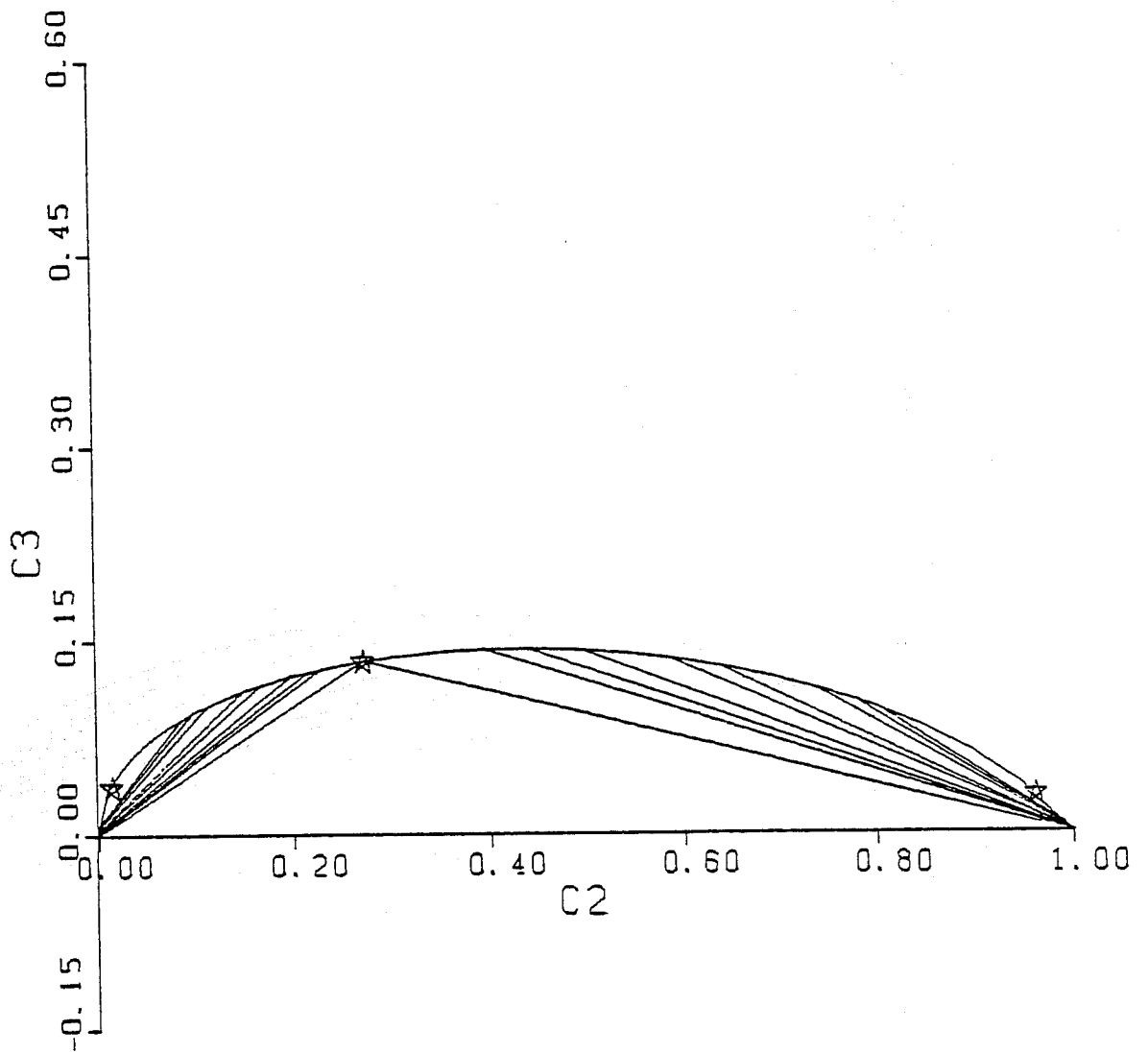
C3MAX2=.3
C2PL=.05



C3MAX0=.3
C2PR=.95

TYPE III
C3MAX1=.1
CSE=.91

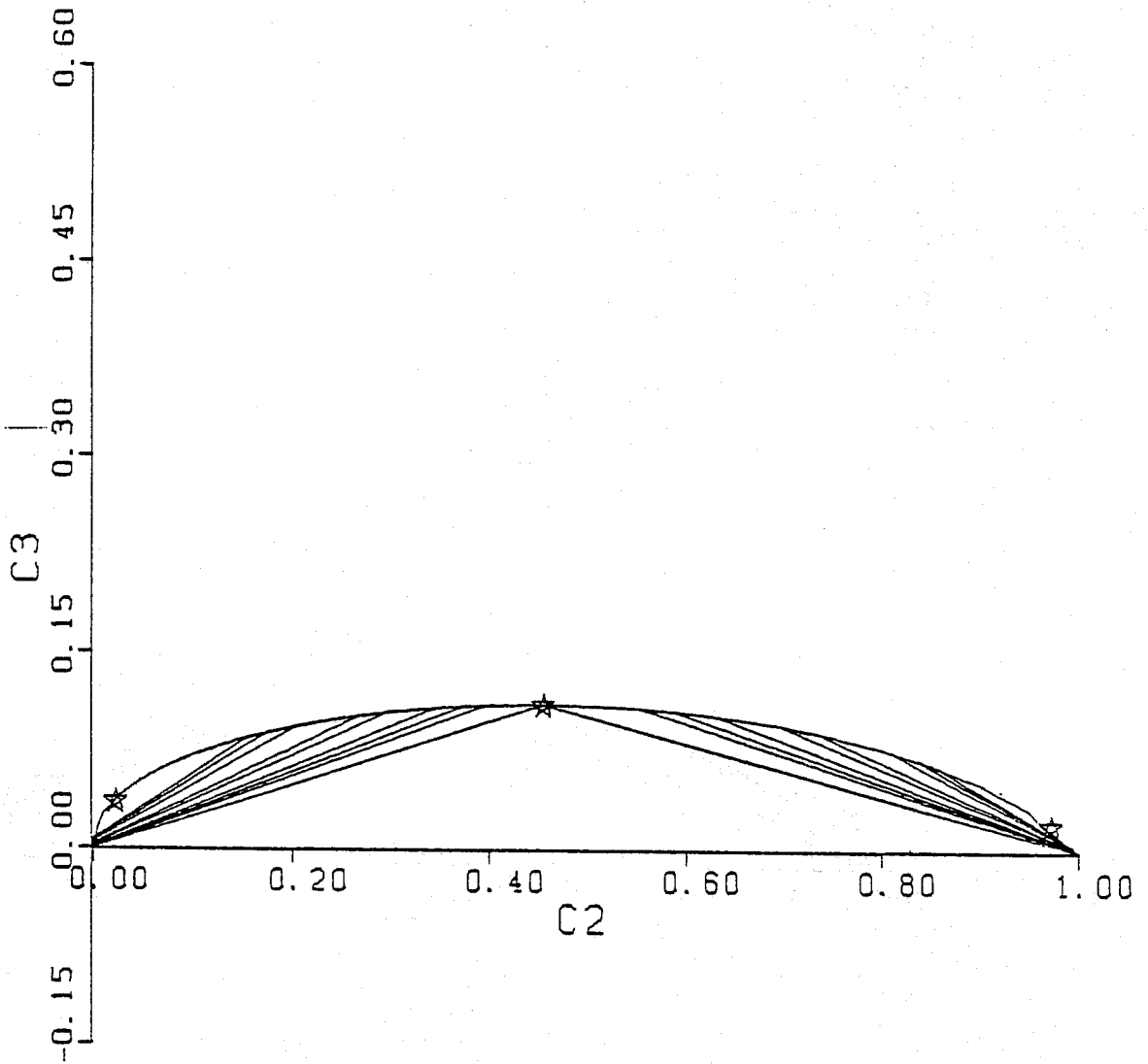
C3MAX2=.3
C2PL=.05



C3MAX0=.3
C2PR=.95

TYPE III
C3MAX1=.1
CSE=.98

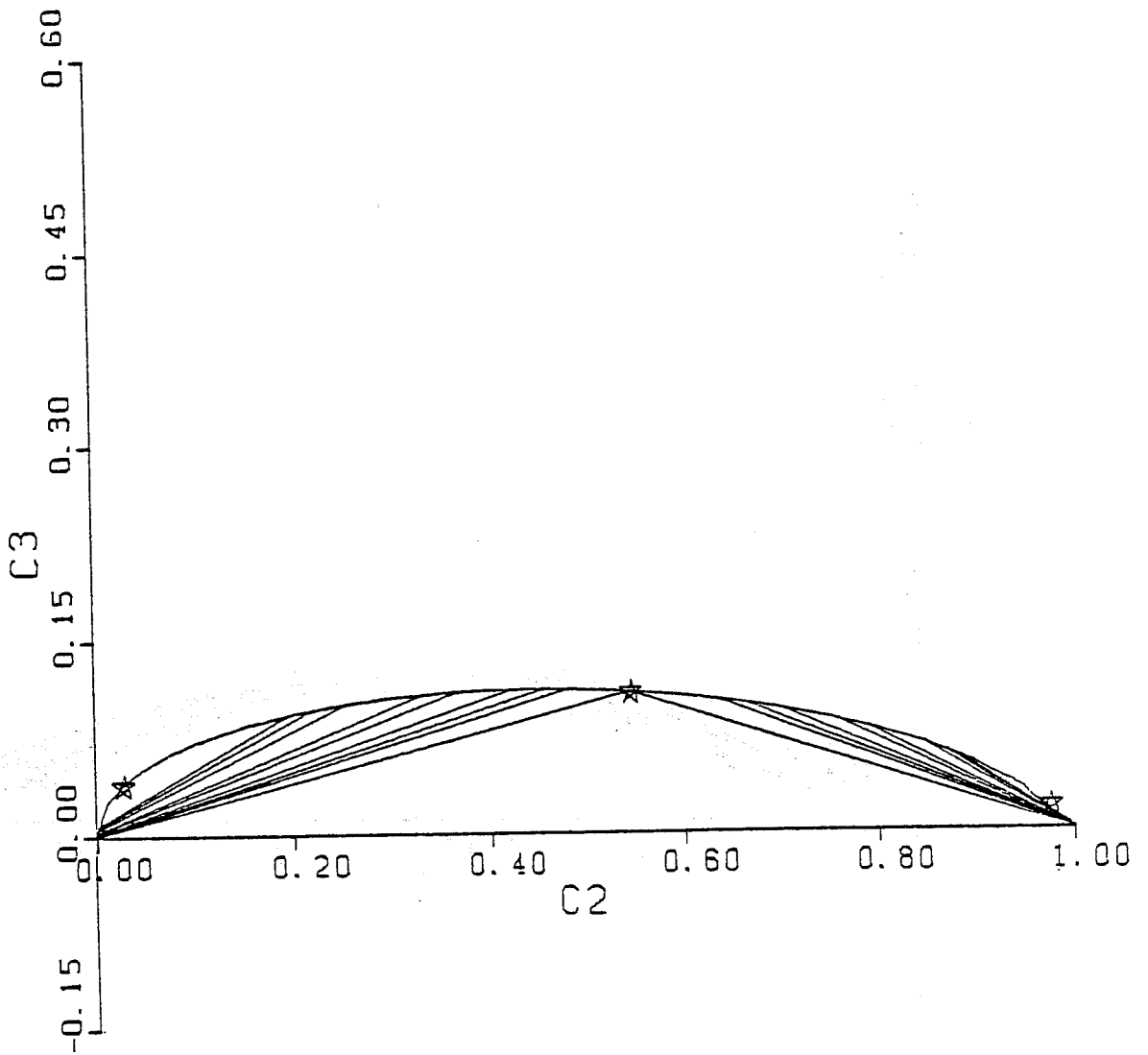
C3MAX2=.3
C2PL=.05



C3MAX0=.3
C2PR=.95

TYPE III
C3MAX1=.1
CSE=1.02

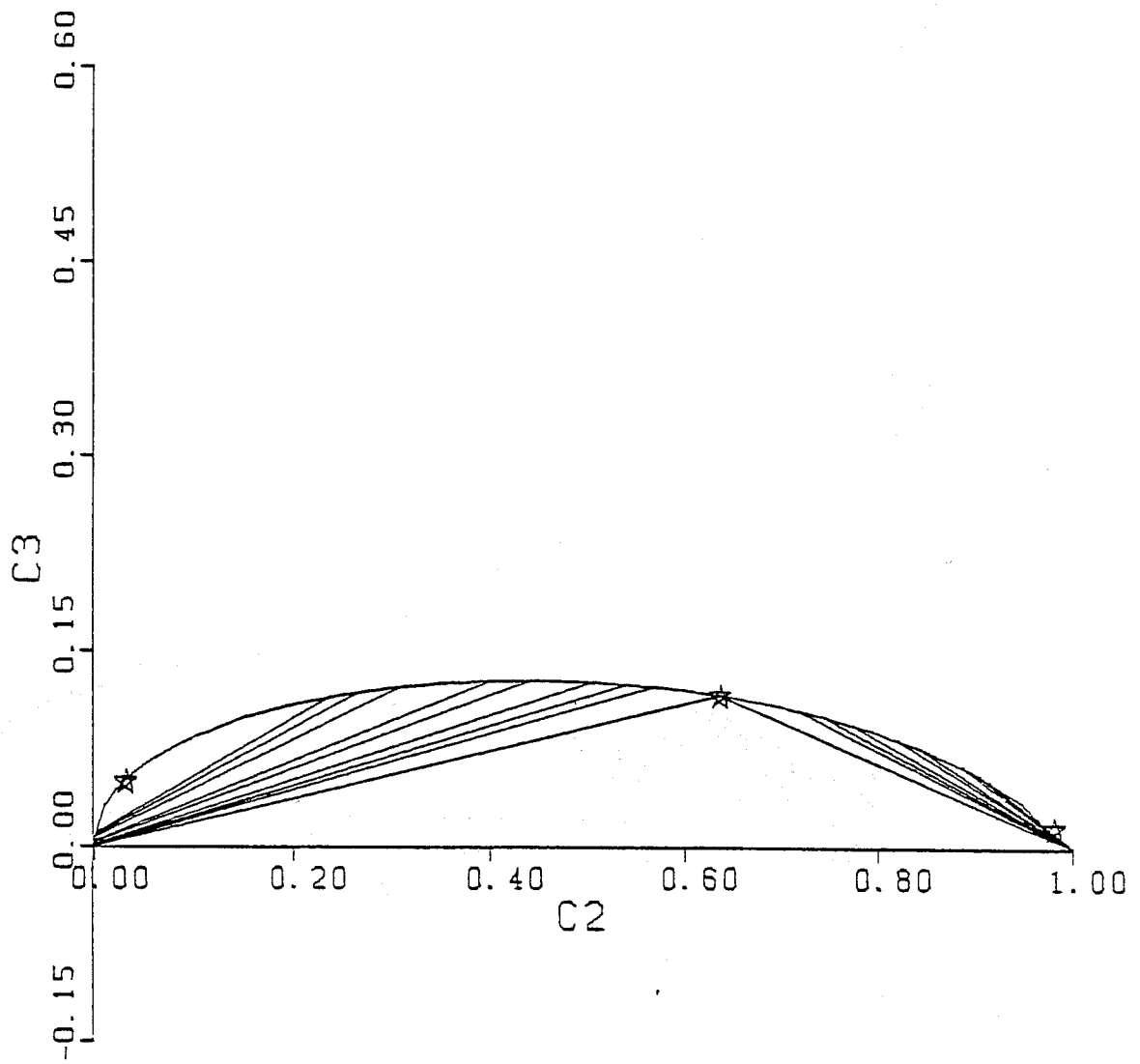
C3MAX2=.3
C2PL=.05



C3MAX0=.3
C2PR=.95

TYPE III
C3MAX1=.1
CSE=1.05

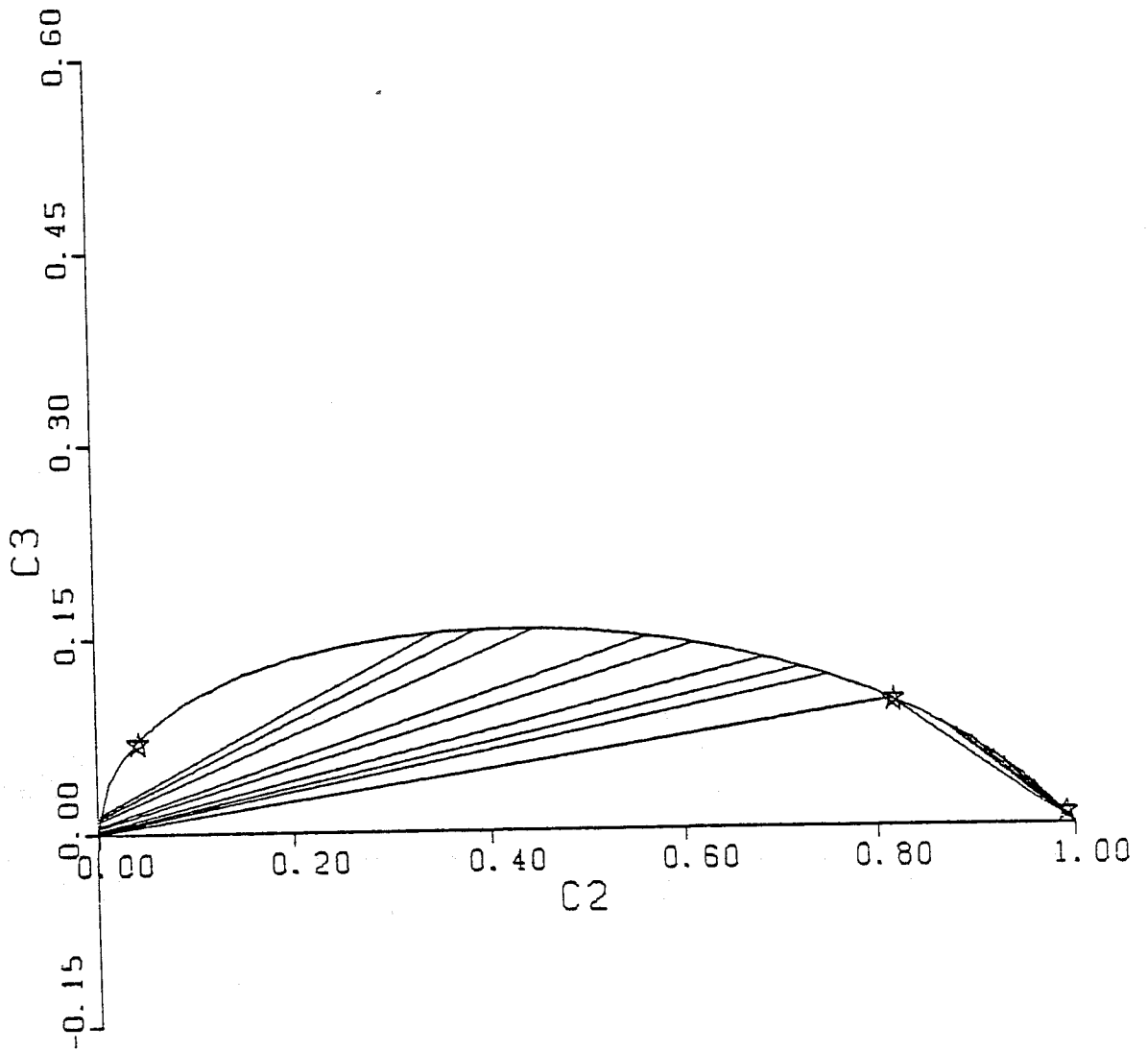
C3MAX2=.3
C2PL=.05



C3MAX0=.3
C2PR=.95

TYPE III
C3MAX1=.1
CSE=1.13

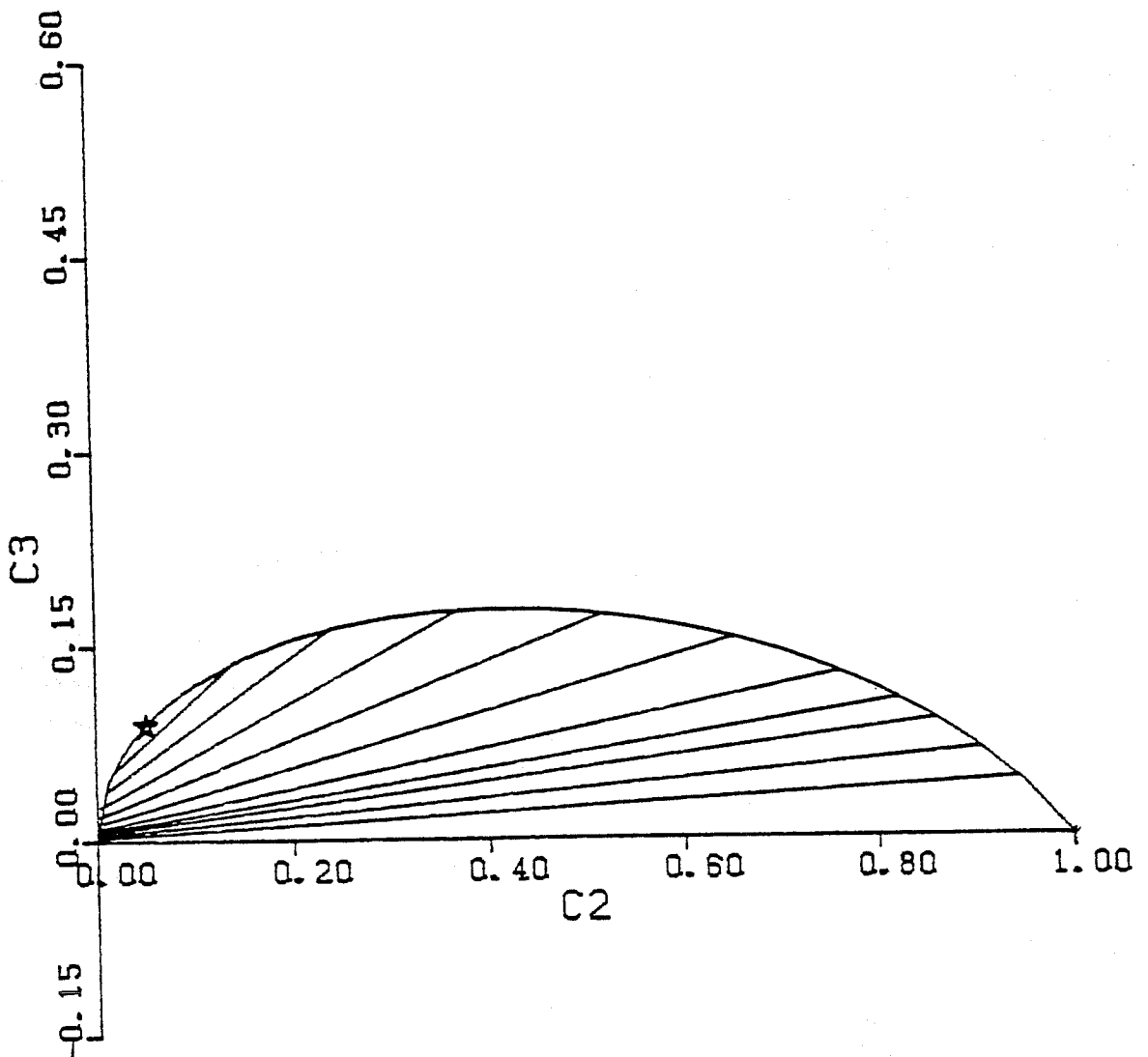
C3MAX2=.3
C2PL=.05



C3MAX0=.3
C2PR=.95

CSE=1.20
C3MAX1=.1

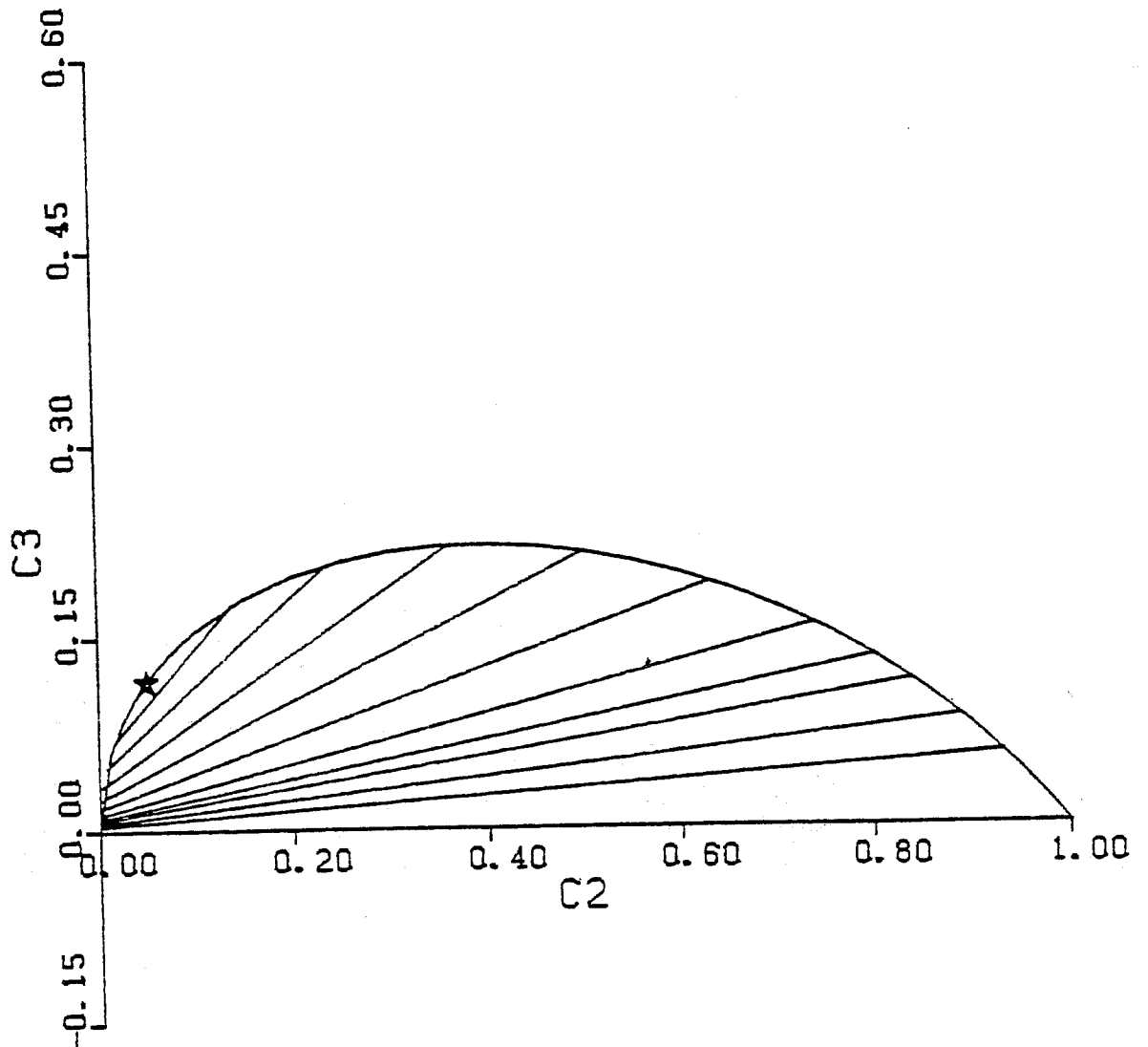
C3MAX2=.3
C2PL=.05



C3MAX0=.3
C2PR=.95

CSE=1.40
C3MAX1=.1

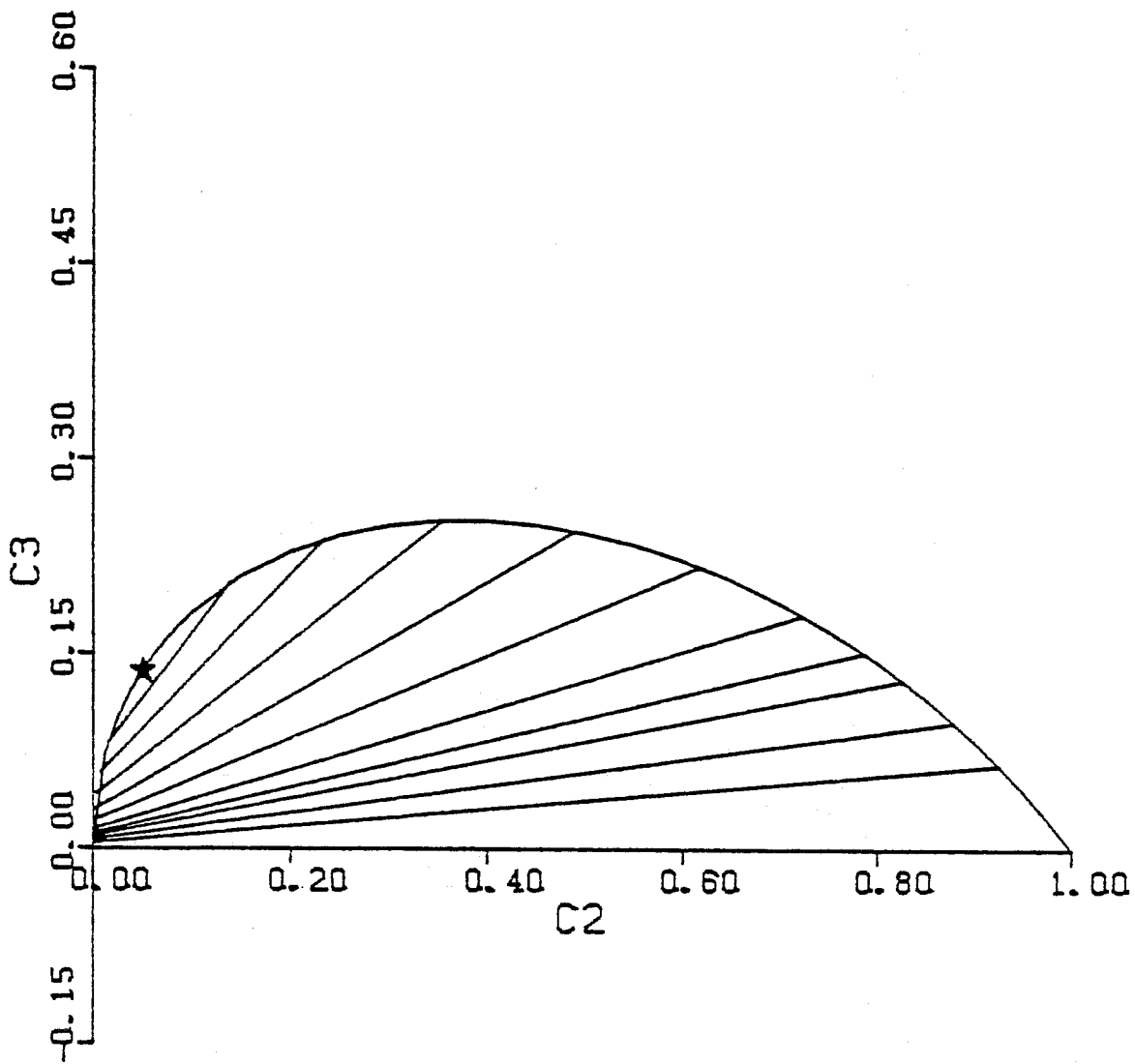
C3MAX2=.3
C2PL=.05



C3MAX0=.3
C2PR=.95

CSE=1.60
C3MAX1=.1

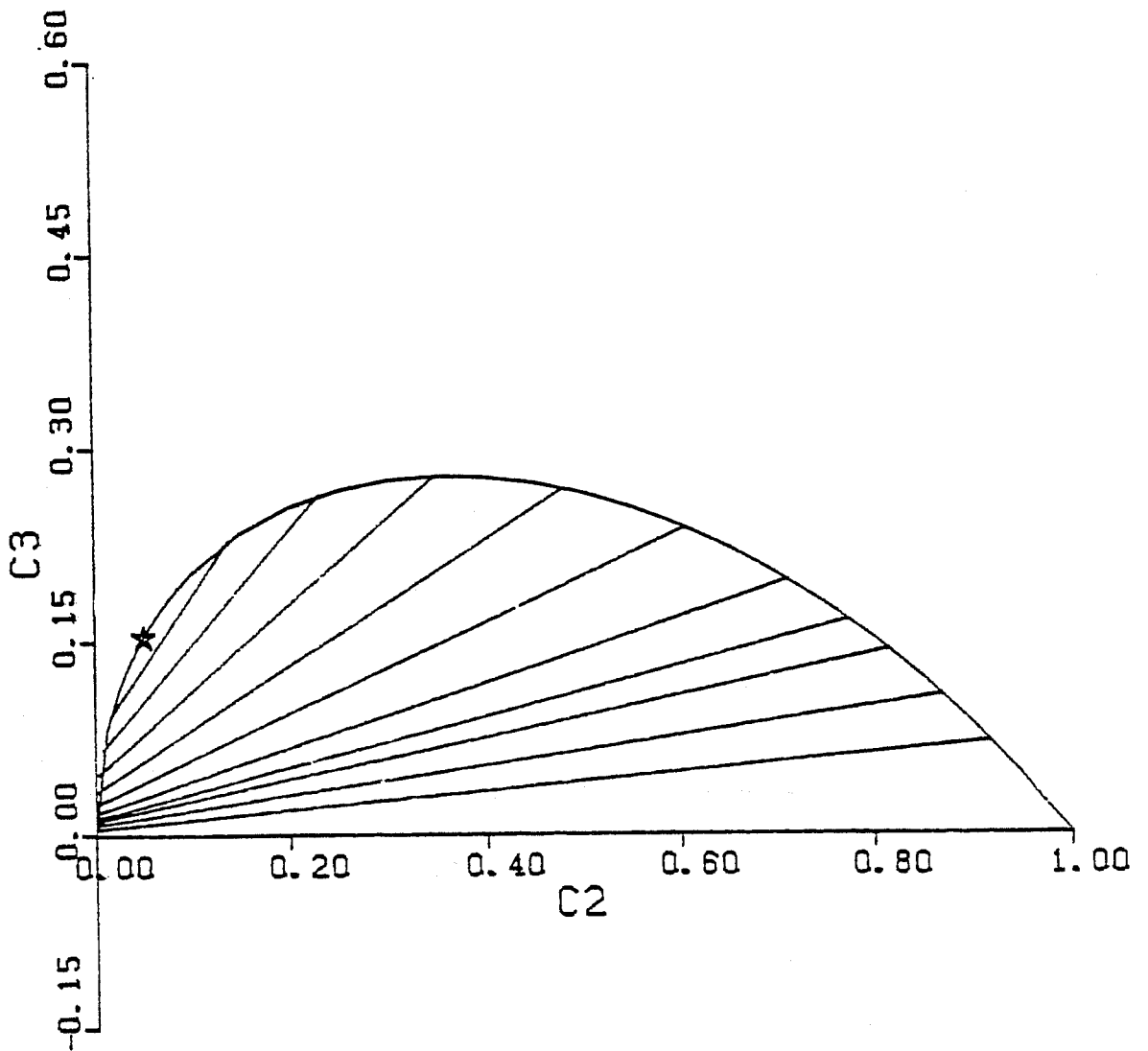
C3MAX2=.3
C2PL=.05



C3MAX0=.3
C2PR=.95

CSE=1.80
C3MAX1=.1

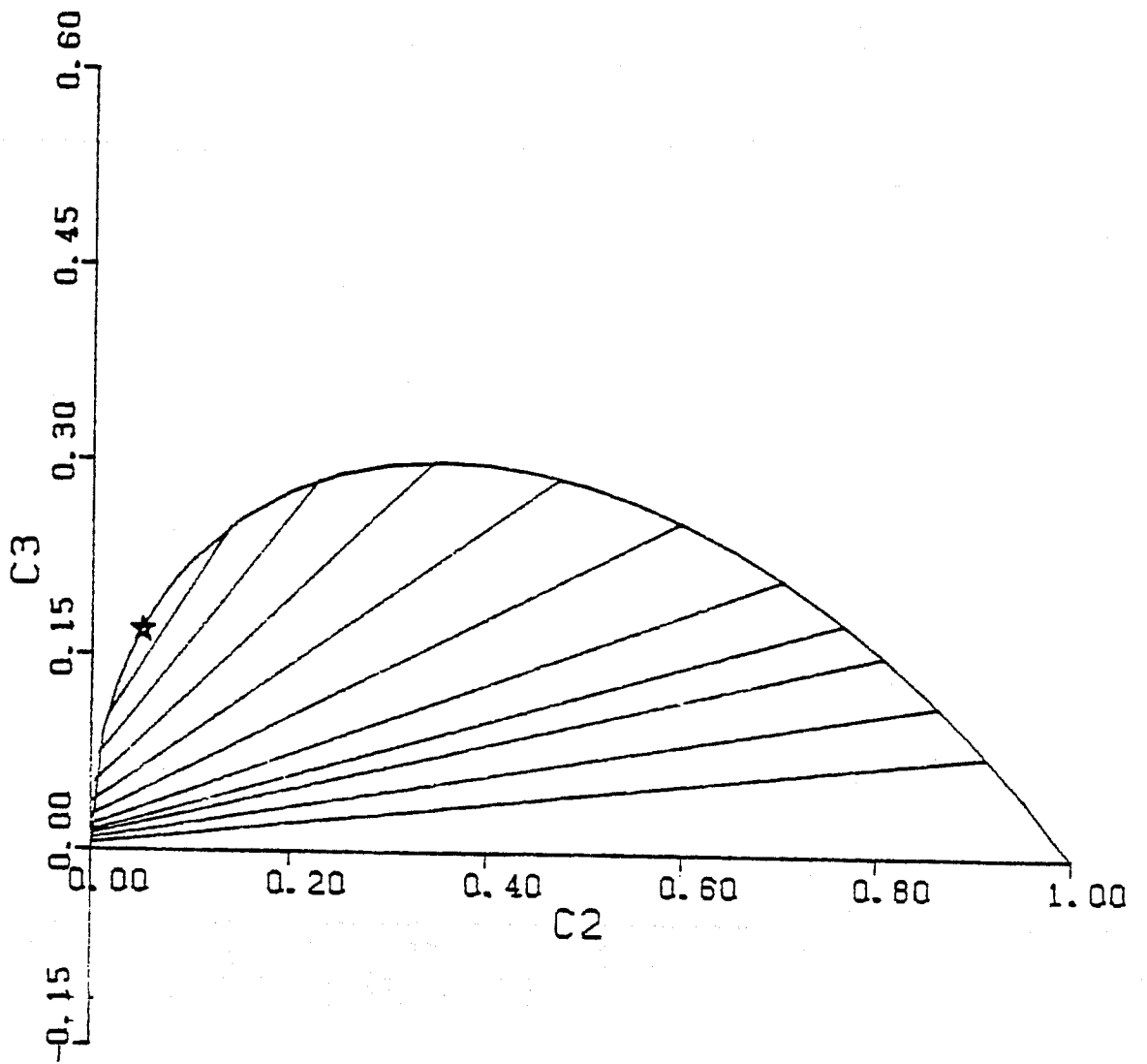
C3MAX2=.3
C2PL=.05



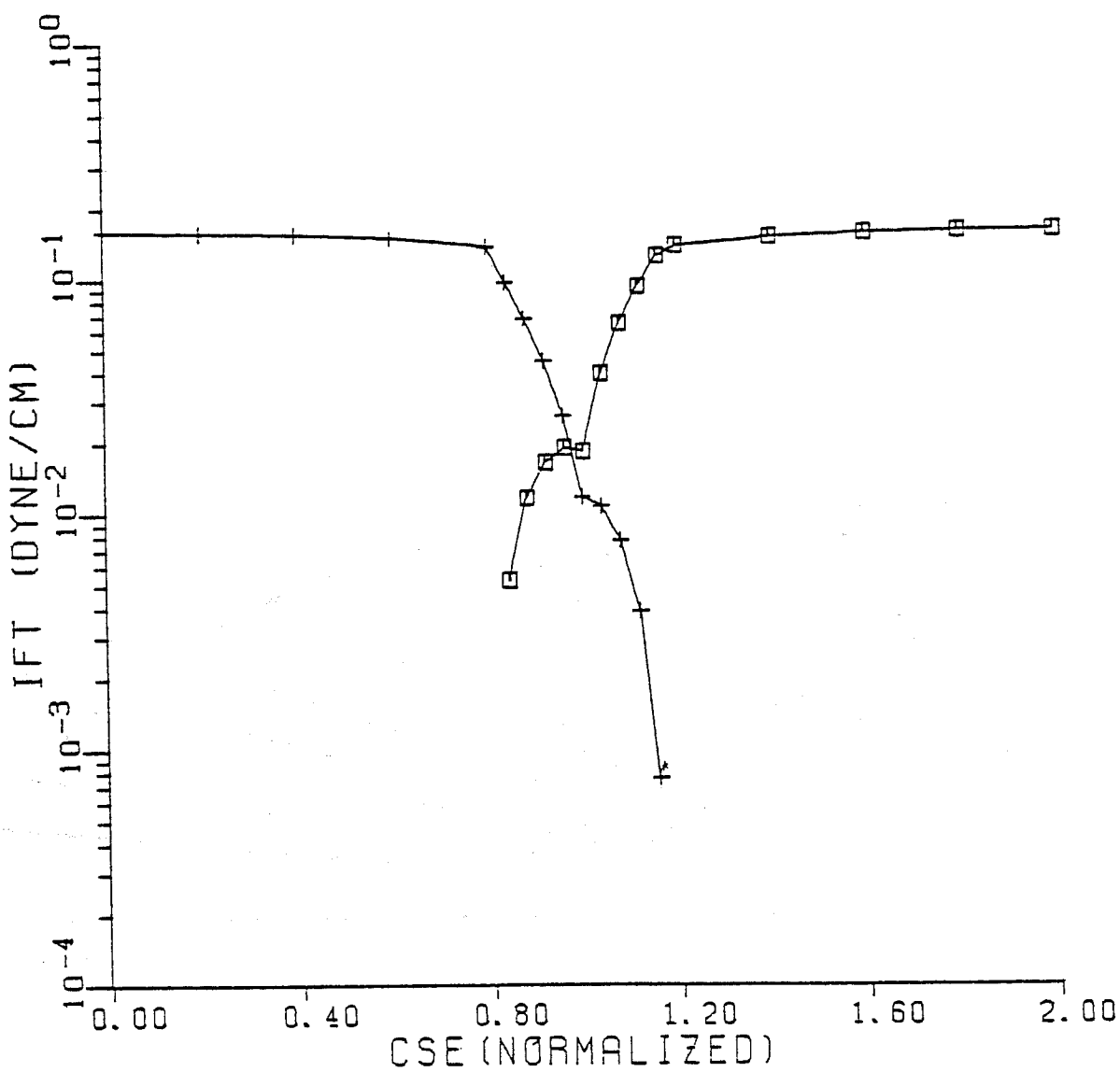
C3MAX0=.3
C2PR=.95

CSE=2.00
C3MAX1=.1

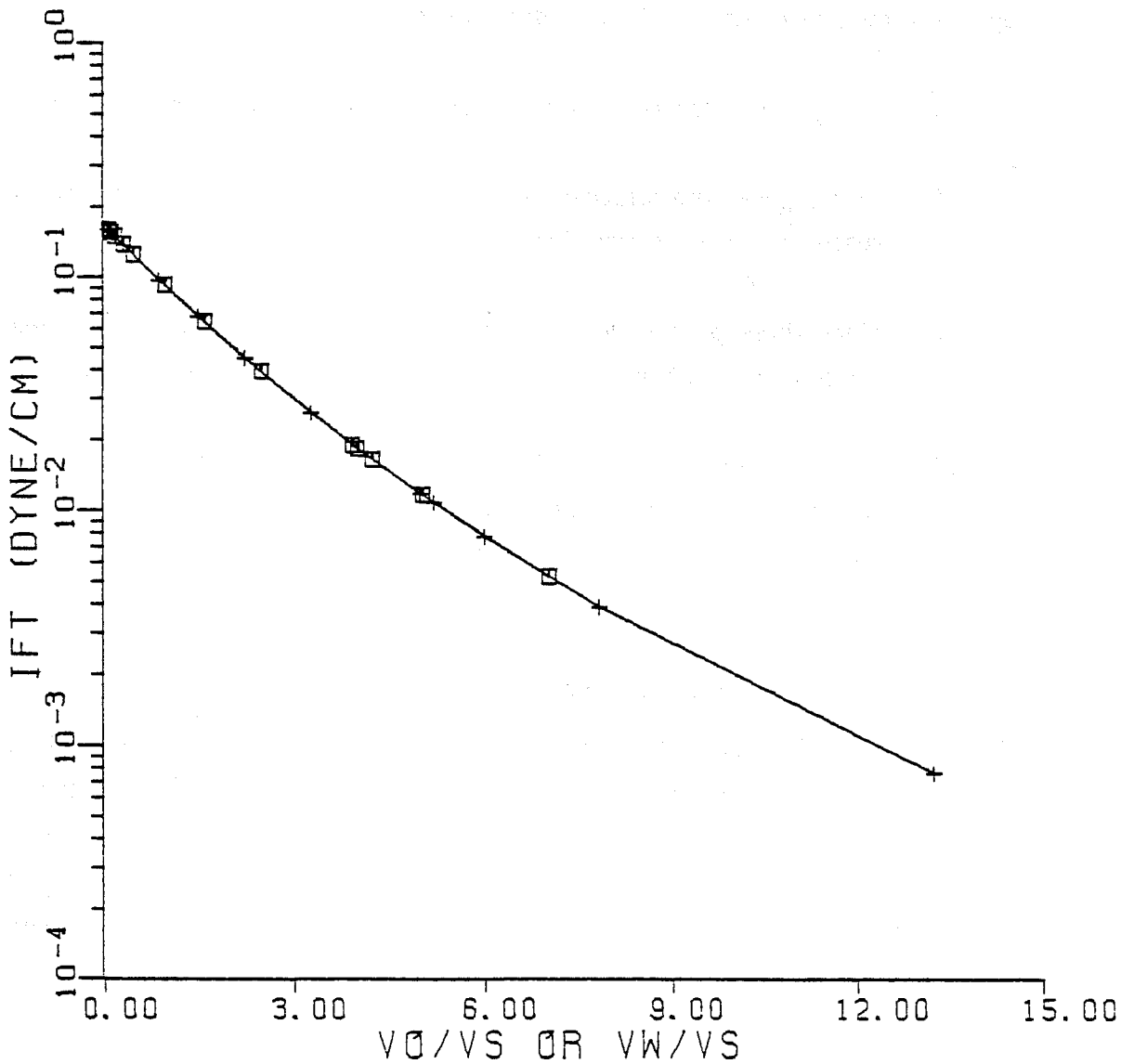
C3MAX2=.3
C2PL=.05



C1=.485 C2=.485 C3=.030
 G11= 6.2850 G12= -7.058 G13= .0450
 G21= 6.2850 G22= -7.058 G23= .0450
 C3MAX0=.30 C3MAX1=.10 C3MAX2=.30
 C2PR=.95 C2PL=.05 CSEL= .80 CSEU=1.20



C1=.485 C2=.485 C3=.030
 G11= 6.2850 G12=-7.058 G13= .0450
 G21= 6.2850 G22=-7.058 G23= .0450
 C3MAX0=.30 C3MAX1=.10 C3MAX2=.30
 C2PR=.95 C2PL=.05 CSEL=.80 CSEU=1.20



APPENDIX D
DESCRIPTION OF HIGH-CAPILLARY-NUMBER
RELATIVE PERMEABILITY MODEL

Experimental studies on low-interfacial-tension (IFT), high-capillary-number (N_{cap}) relative permeabilities (k_r 's) are quite sparse;¹⁻⁴ consequently, the philosophy in developing a relative permeability model is to ensure that the relative permeabilities approach the proper limits. Specifically, we require:

1. As $N_{cap} \rightarrow 0$, the relative permeabilities approach their water-oil values.
2. As $N_{cap} \rightarrow \infty$, the relative permeabilities approach miscibility (equal to their respective phase saturations).
3. When three phases flow, the intermediate wetting phase must become the wetting phase when the original wetting phase is absent (and vice versa).

We illustrate the relative permeability model using the "second drainage" (oil saturation increasing from S_{or}) steady-state water-oil relative permeabilities from the Bell Creek Unit A micellar-polymer flood.⁵

Two-Phase Relative Permeabilities

Two-phase relative permeabilities apply in the absence of surfactant, in the type II(-) or II(+) phase environments, or in either of the two-phase lobes of the type III phase environment.⁶ We presume that one phase preferentially wets the rock surfaces, and that, therefore, the phases can be identified as wetting (subscript w) or nonwetting (subscript nw). The functional form of the two-phase relative permeabilities is assumed to be

$$k_{rnw} = k_{rnw}^o \left[\frac{1 - S_w - S_{nwr}}{1 - S_{nwr} - S_{wr}} \right]^n \quad (1)$$

$$k_{rw} = k_{rw}^o \left[\frac{S_w - S_{wr}}{1 - S_{nwr} - S_{wr}} \right]^p \quad (2)$$

where:

S_{nwr}, S_{wr} = residual phase saturations

k_{rnw}^o, k_{rw}^o = end-point relative permeabilities (relative permeability value at other phase's residual saturation)

n, p = "curvatures" in reduced saturation space

S_w = wetting phase saturation

For Bell Creek the wetting phase is the water phase, the nonwetting the oil. In the type II(+) phase environments, k_{rw} is, therefore, the aqueous phase relative permeability and k_{rnw} is the microemulsion phase relative permeability. In the type II(-) environments, the microemulsion phase wets and the oleic phase is nonwetting.

At waterflood conditions (low N_{cap}), Figures D-1 and D-2 show the fit of Equations (1) and (2) to the Bell Creek data. The relative permeabilities indicate a large water curvature $p' = 7.5$, with $(k_{rw}^o)' < (k_{rnw}^o)'$, both of which indicate a water wetting character. Note that the primes designate a water-oil (no surfactant) quantity.

In accordance with item 2 (above), as N_{cap} increases the parameters in Equations (1) and (2) must approach the following limits:

$$\lim_{N_{cap} \rightarrow \infty} (p \text{ or } n) = \lim_{N_{cap} \rightarrow \infty} (k_{rw}^o \text{ or } k_{rnw}^o) = 1 \quad (3a)$$

$$\lim_{N_{cap} \rightarrow \infty} (S_{wr} \text{ or } S_{nwr}) = 0 \quad (3b)$$

N_{cap} can become very large in the vicinity of the plait points of the type II(-) or II(+) regions.

Based on experimental data,^{7,8} we let the end-point relative permeabilities change linearly with the other phase's residual saturation.

$$k_{rnw}^o = (k_{rnw}^o)' + \left[\frac{S_{wr}' - S_{wr}}{S_{wr}'} \right] \left[1 - (k_{rnw}^o)' \right] \quad (4a)$$

$$k_{rw}^o = (k_{rw}^o)' + \left[\frac{S_{nwr}' - S_{nwr}}{S_{nwr}'} \right] \left[1 - (k_{rw}^o)' \right] \quad (4b)$$

Equations (4) thus satisfy the limits (3) and item 1 (above).

The S_{wr} (or S_{nwr}) relationship to N_{cap} comes from published correlations,⁹ the idealization of which is shown in Figure D-3. We also let the curvatures, n and p , follow the same normalized curves. The latter feature is not as well grounded in experimental evidence as are the residual phase saturations or Equations (4). Some evidence exists that the curvatures change more slowly than the residual phase saturations,^{1,2} and other evidence indicates that they change at about the same rate.⁴ None of the evidence published to date is entirely convincing, however; hence, we use the curves of Figure D-3 on the curvatures knowing they approach the correct limits at the large and small N_{cap} extrema.

The procedure to calculate relative permeabilities at a given N_{cap} for two-phase relative permeabilities is:

1. Determine the water-oil values in Equations (1) and (2), p' , n' , or S_{wr}' , S_{nwr}' , $(k_{rw}^o)'$, and $(k_{rnw}^o)'$ (Figures D-1 and D-2).
2. Estimate p , n , S_{wr} , and S_{nwr} at the given N_{cap} from Figure D-3.
3. Calculate k_{rw}^o and k_{rnw}^o from S_{wr} and S_{nwr} , and Equations (4).
4. Calculate k_{rw} and k_{rnw} for various S_w from Equations (1) and (2).

The results of this procedure for Bell Creek are shown in Figures D-4 and D-5.

Three-Phase Relative Permeabilities

Over certain ranges of electrolyte and surfactant concentration, the surfactant-brine-oil system will form three phases according to the conventional type III formalism. The extent of the three-phase region in the pseudo-ternary diagram varies with a number of things,⁹ but at constant electrolyte the three-phase region of the pseudo-ternary may be viewed on a "sub-ternary" (ST) diagram as shown in Figure D-6. The ST diagram is not, in general, an equilateral triangle, but may be viewed so without loss of generality, particularly when dealing with phase saturations. We use subscripts a, o and m to denote aqueous, oleic, and microemulsion phases. For fixed electrolyte, N_{cap} is constant within the ST diagram; the same cannot be said in the two-phase lobes on either side of the ST diagram where N_{cap} must approach infinity at the respective plait points. Within these lobes, the relative permeabilities are calculated as above, where N_{cap} in the type II(+) lobe is calculated from the microemulsion-water IFT, and that in the type II(-) lobe from the microemulsion-oil IFT. In the three-phase region, N_{cap} is calculated from the maximum of the two IFT's. The aqueous phase relative permeabilities in the ST region must be continuous with the wetting phase relative permeabilities in the type II(+) lobe and the oleic phase relative permeabilities continuous with the nonwetting phase relative permeabilities in the type II(-) lobe.

Following item 3 above, the microemulsion phase relative permeabilities must be continuous with the nonwetting relative permeabilities in the type II(+) lobe and with the wetting phase relative permeabilities in the type II(-) lobe. Hence, there will be a need to interpolate microemulsion properties between the wetting and nonwetting limits based on where the overall composition falls in the ST diagram. The simplest interpolating function that satisfies the requirements that $g = 0$ when $S_o = 0$ and $g = 1$ when $S_a = 0$ is

$$g(S_o, S_a) = \frac{S_o(1 - S_a)}{S_o + S_a} \quad (5)$$

The microemulsion residual saturation follows from this as

$$S_{mr} = S_{nwr} + g \cdot (S_{wr} - S_{nwr}) \quad (6)$$

This equation plots in Figure D-6 as the nearly straight line near the base of the ST region.

The existence of a trapped microemulsion phase has been verified experimentally as an important surfactant loss mechanism.¹⁰ The existence of three trapped phases also distinguished the current model from that proposed by Stone¹¹ for oil-water-gas relative permeabilities. Note that S_{nwr} on the OM axis and S_{mr} on the AM axis are not, in general, equal because their respective IFT's are different.

With this as introduction, it follows that the relative permeabilities for the aqueous, oleic, and microemulsion phases in the ST region are

$$k_{ro} = k_{rnw}^o \left[\frac{S_o - S_{or}}{1 - S_{ar} - S_{or} - S_{mr}^*} \right]^n \quad (7)$$

$$k_{ra} = k_{rw}^o \left[\frac{S_a - S_{ar}}{1 - S_{ar} - S_{or} - S_{mr}^*} \right]^p \quad (8)$$

$$k_{rm} = k_{rm}^o \left[\frac{1 - S_o - S_a - S_{mr}^*}{1 - S_{ar} - S_{or} - S_{mr}^*} \right]^r \quad (9)$$

$$S_{ar} = \min(S_{wr}, S_a) \quad (10a)$$

$$S_{or} = \min(S_{nwr}, S_o) \quad (10b)$$

$$S_{mr}^* = \min(S_{mr}, 1 - S_o - S_a) \quad (10c)$$

where S_{wr} , S_{nwr} , p , n , k_{rw}^o , and k_{rnw}^o are from the appropriate two-phase relative permeabilities in the adjoining lobes based on the maximum IFT in each. The

requirements of Equation (10) are necessary to make the three-phase relative permeabilities approach the two-phase limits smoothly. Note that, for example, it would be meaningless to speak of a trapped aqueous phase saturation in the type II(-) lobe.

The microemulsion relative permeability end-points and curvature follow in a similar manner to Equation (6)

$$k_{rm}^o = k_{rnw}^o + g \cdot (k_{rw}^o - k_{rnw}^o) \quad (11)$$

$$r = n + g \cdot (p - n) \quad (12)$$

Note again that Equations (11) and (12) allow the microemulsion to be wetting or nonwetting at the appropriate two-phase boundaries.

The procedure for calculating three-phase relative permeabilities is:

1. Calculate the two-phase quantities S_{wr} , S_{nwr} , k_{rw}^o , k_{rnw}^o , p , and n as described above at the minimum N_{cap} that applies at the boundary between the two- and three-phase regions. This minimum N_{cap} is calculated with the greater of the two IFT's, water-microemulsion or microemulsion-oil.
2. The three-phase relative permeabilities as a function of both S_o and S_a follow from Equations (5)-(12).

Lines of constant k_{ro} , k_{ra} , and k_{rm} are plotted on Figures D-7 - D-9 for Bell Creek data. Note that, as desired, the microemulsion takes on wetting or nonwetting character in the respective two-phase lobe.

Description of Desaturation Curves

The desaturation of oil and water as a function of capillary number is one of the most important relationships used in this relative permeability model. The capillary desaturation curve for Berea (Figure D-3) shows that the residual oil saturation is reduced by low IFT (high N_{cap}) much sooner than is the residual water saturation. This behavior is a characteristic of "water-wet" rock. In "oil-wet" rock, this behavior is reversed, and much lower IFT's (higher N_{cap} 's) are required to mobilize oil. The desaturation curves, therefore, must reflect the wettability of the reservoir rock.

The critical nonwetting capillary number is defined as the capillary number when the residual to the nonwetting phase begins to decrease ($S_{nwr}/S_{nwr}' \neq 1.0$). The range of this number has been identified⁹ as $N_{cap} = 10^{-5}$ for water-wetting reservoirs and $N_{cap} = 10^{-4}$ for oil-wetting reservoirs.

One technique for calculating reservoir wettability is to ratio the end-points of the relative permeability curves. This defines the parameter R from the maximum relative permeabilities to oil and water when one or the other phase is at a residual waterflood condition (high IFT, low N_{cap}). This wettability parameter is defined as:

$$R = k_{rw}^o / k_{rnw}^o \quad (13)$$

For purposes of interpolation, the wetting parameter R is defined as 0.1 at $N_{cap} = 10^{-5}$ for water-wet rock, and as 10.0 at $N_{cap} = 10^{-4}$ for oil-wet rock. With a given set of relative permeability end-points, a degree of wettability can then be calculated. The distance that a desaturation curve will be shifted can be estimated as:

$$I = 1/2 (\log R + 1) \quad (14)$$

The nonwetting critical capillary number for a specified value of R will be:

$$\log (N_{cap})_{crit. nw} = \log (10^{-5}) + 1/2 (\log R + 1) \quad (15)$$

or

$$\log (N_{\text{cap}})_{\text{crit. nw}} = 1/2 \log R - 9/2 \quad (16)$$

This relationship gives a critical nonwetting desaturation number ranging from 10^{-5} at $R = 0.1$ to 10^{-4} at $R = 10.0$. The wetting desaturation curve shift is calculated in the same manner except that the shift is in the opposite direction of the nonwetting curve, and the original value of the critical wetting capillary number at $R = 0.1$ is 6×10^{-5} (Berea). Once the critical capillary numbers have been estimated, lines parallel to those in Figure D-3 can be drawn to complete the description of the desaturation curves.

REFERENCES

1. Leverett, M. C. "Flow of Oil-Water Mixtures Through Unconsolidated Sands," Transactions, AIME, 1938, Vol. 132, pp. 149-171.
2. Lefebvre, E. J. "Factors Affecting Liquid-Liquid Relative Permeabilities of a Consolidated Porous Medium," Soc. Pet. Eng. J., February 1973, pp. 39-47.
3. Talash, A. W. "Experimental and Calculated Relative Permeability Data for Systems Containing Tension Additives," SPE 5810, presented at the Improved Recovery Symposium of SPE of AIME, Tulsa, Oklahoma, March 22-24, 1976.
4. Bardon, C., and D. Longeron. "Influence of Very Low Interfacial Tension on Relative Permeability," SPE 7609, presented at the SPE 53rd Annual Meeting, Houston, Texas, October 1-4, 1978.
5. "Pilot Demonstration - Enhanced Oil Recovery by Micellar-Polymer Water-flooding: Bell Creek Field," Monthly Technical Progress Report, February 1979.

6. Nelson, R. C., and G. A. Pope. "Phase Relationships in Chemical Flooding," Soc. Pet. Eng. J., October 1978, pp. 325-338.
7. Abrams, A. "The Influence of Fluid Viscosity, Interfacial Tension, and Flow Velocity on Residual Oil Saturation Left by Waterflood," Soc. Pet. Eng. J., October 1975, pp. 435-447.
8. Stegemeier, G. L. "Mechanisms of Entrapment and Mobilization of Oil in Porous Media," Improved Oil Recovery by Surfactant and Polymer Flooding (ed. D. O. Shah and R. S. Schechter), Academic Press, New York, 1977.
9. Gupta, S. P., and S. P. Trushenski. "Micellar Flooding - Compositional Effects on Oil Displacement," Soc. Pet. Eng. J., April 1979, pp. 116-128.
10. Glover, C. J., M. C. Puerto, J. M. Maerker, and E. L. Sandvik. "Surfactant Phase Behavior and Retention in Porous Media," Soc. Pet. Eng. J., June 1979, pp. 183- 193.
11. Stone, H. L. "Probability Model for Estimated Three-Phase Relative Permeability," J. Pet. Tech., February 1979, pp. 214-218.

FIGURE D-1
FIT OF OIL RELATIVE PERMEABILITY DATA

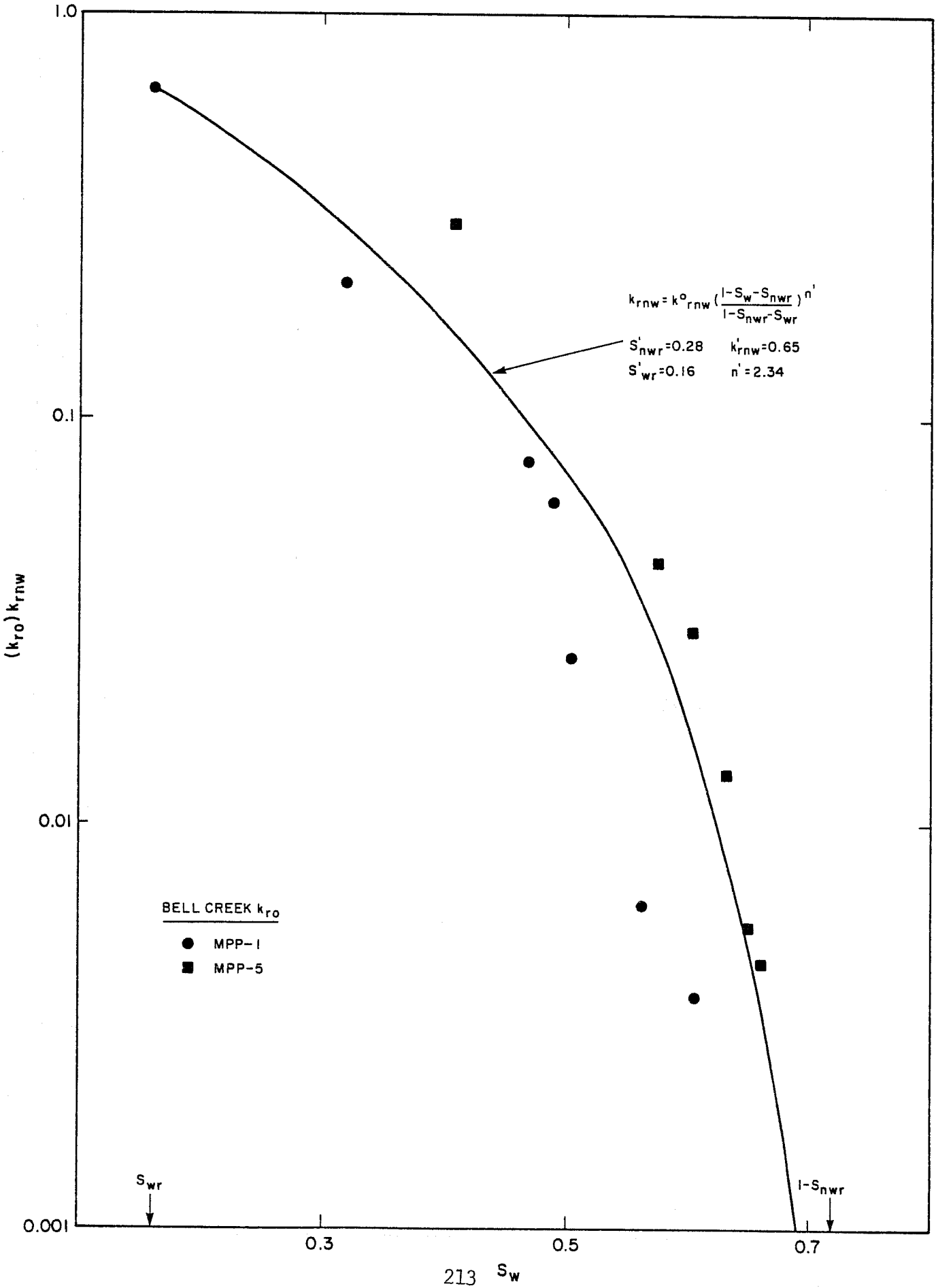


FIGURE D-3
 DESATURATION CURVES FOR BEREA SANDSTONE (WATER WET)

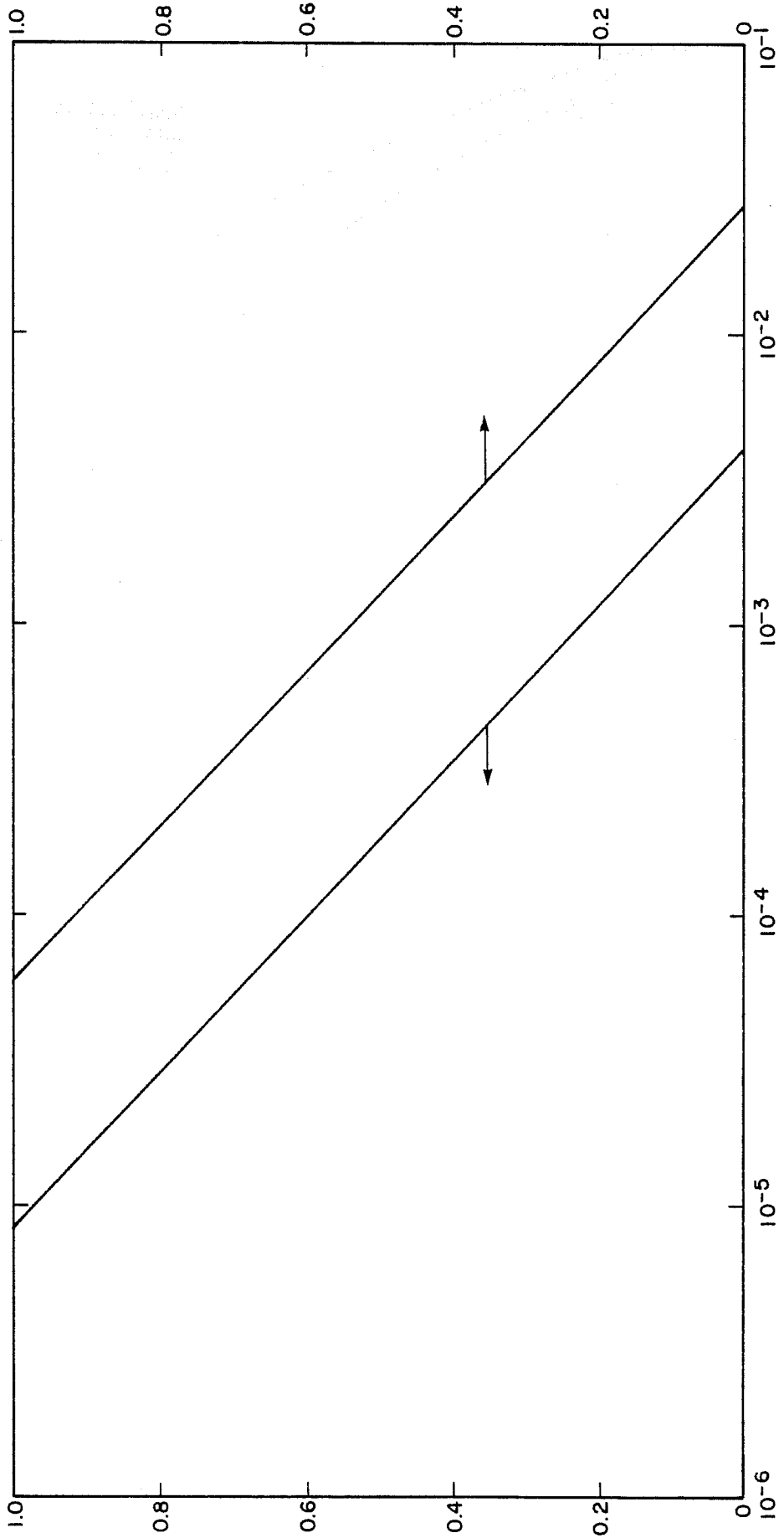


FIGURE D-4
CHANGE IN NON-WETTING k_r WITH N_{CAP}

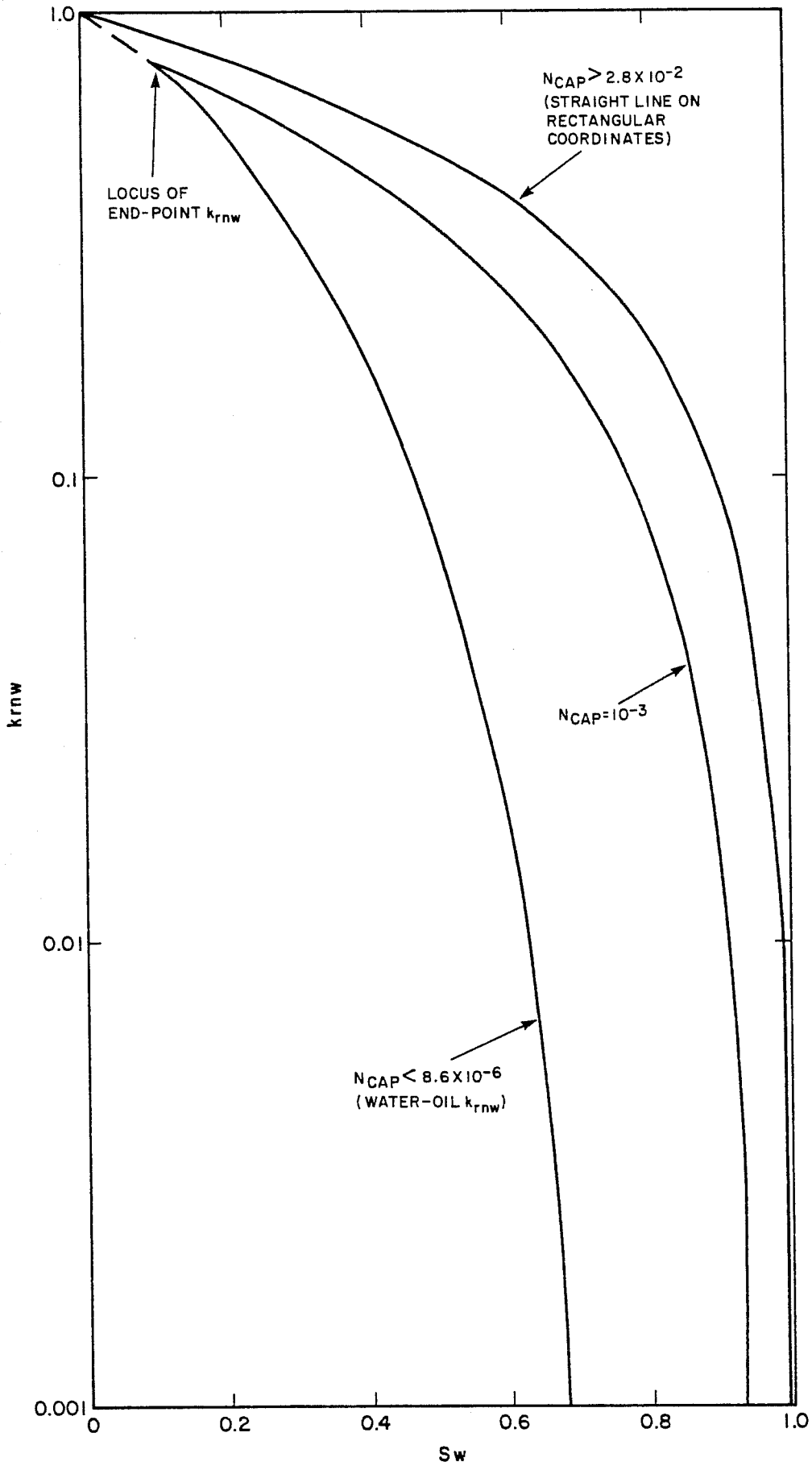


FIGURE D-5
CHANGE IN WETTING PHASE k_r WITH N_{CAP}

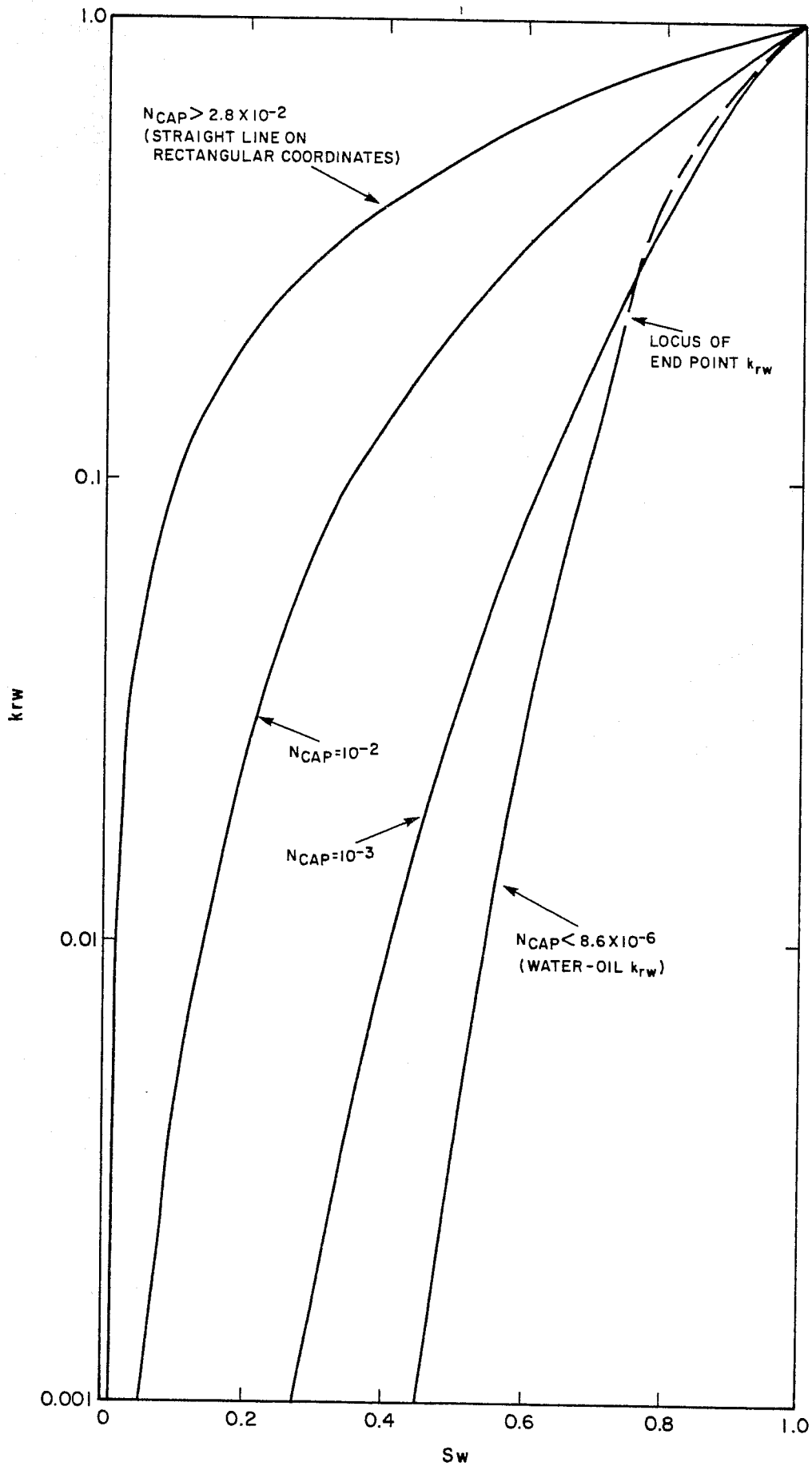


FIGURE D-6
 PHASE TRAPPING IN A THREE PHASE DIAGRAM

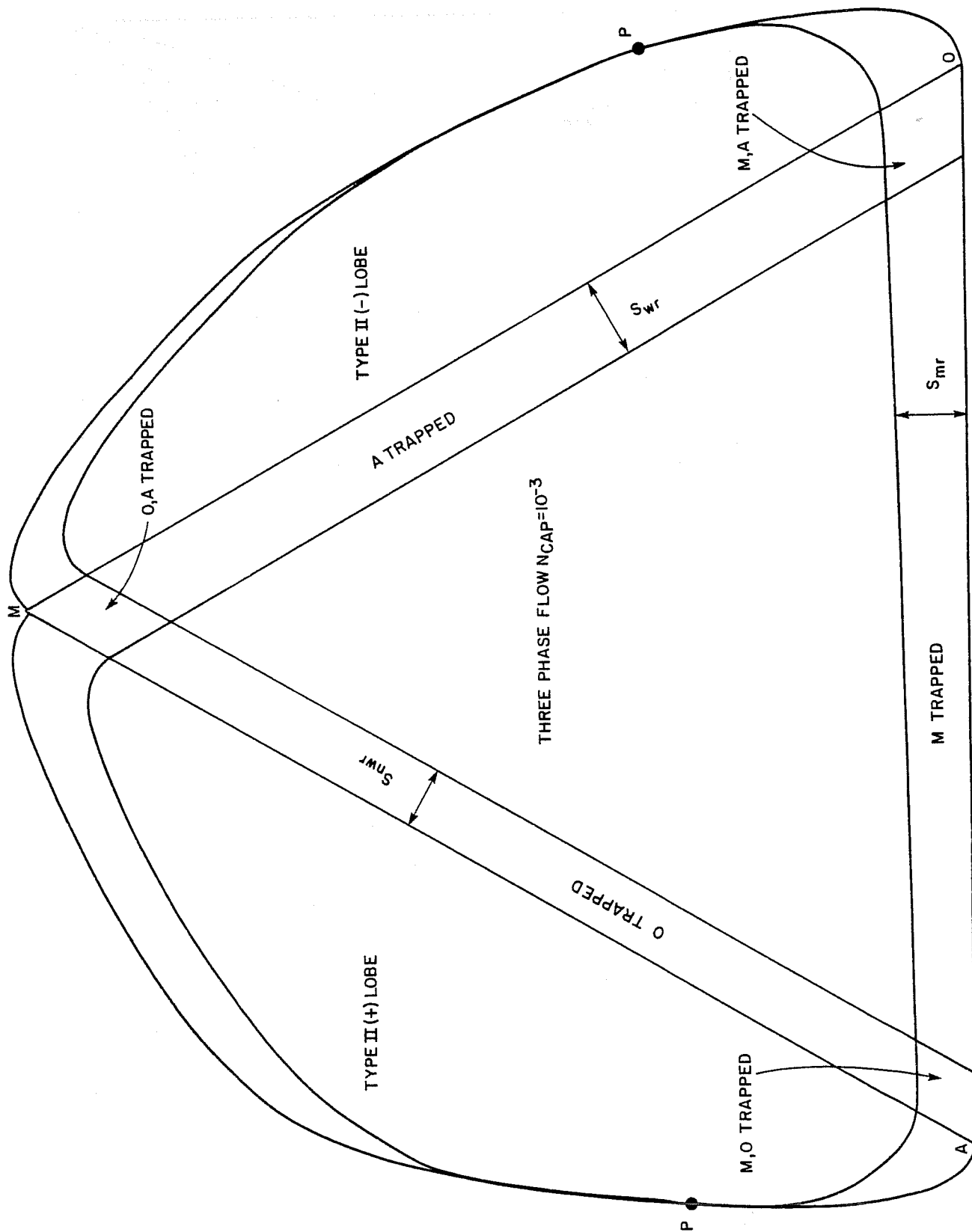
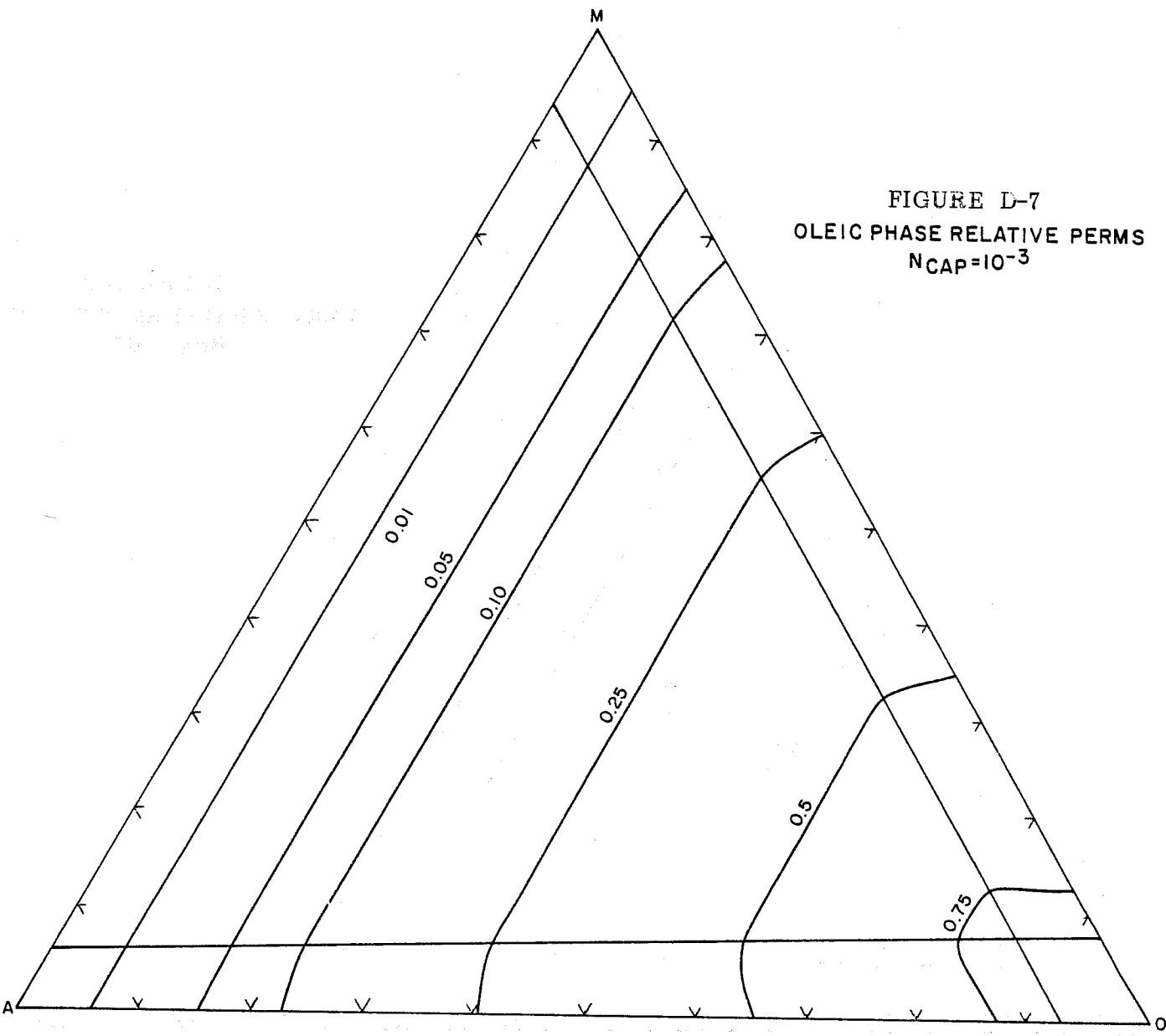


FIGURE D-7
OLEIC PHASE RELATIVE PERMS
NCAP=10⁻³



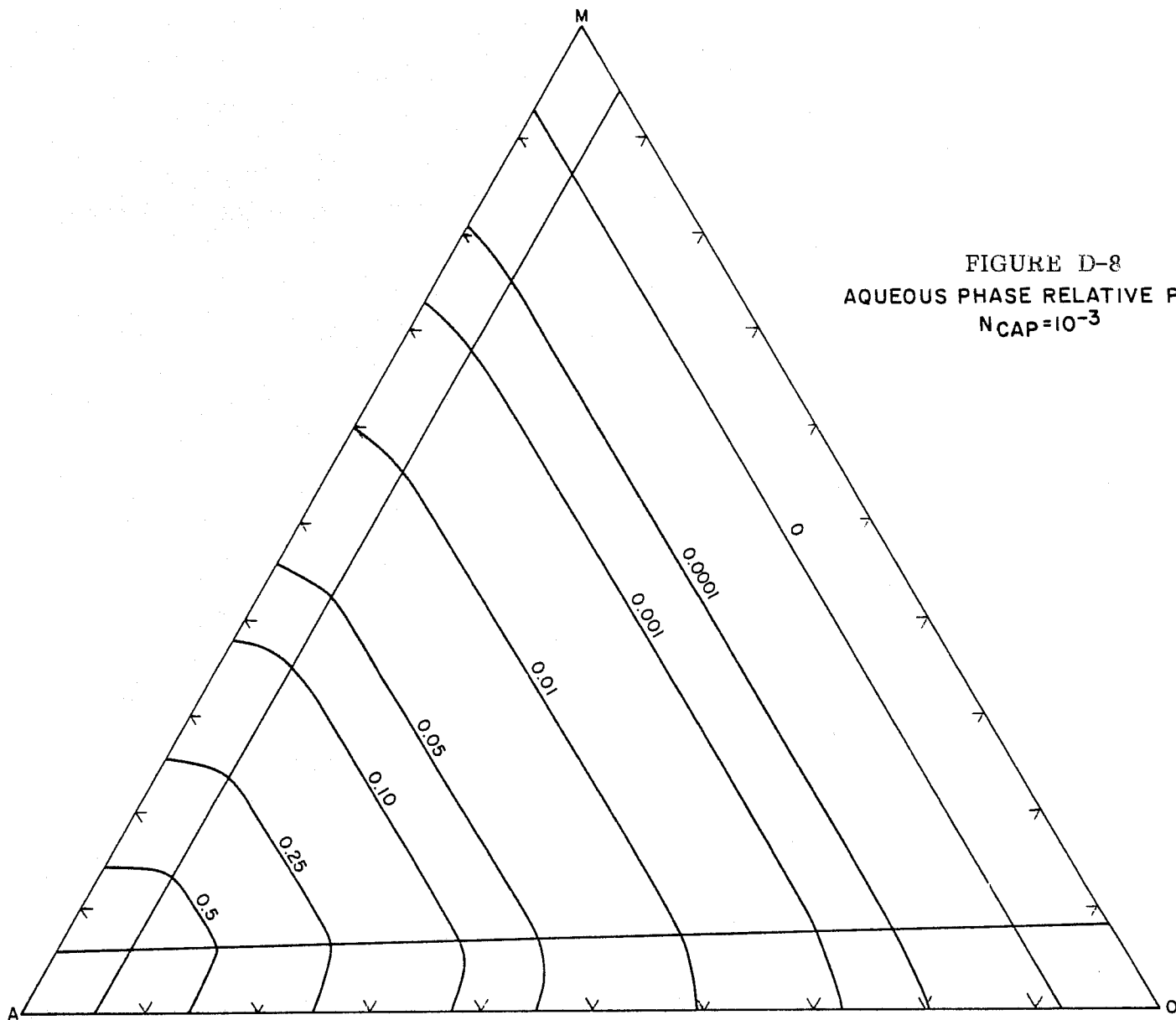


FIGURE D-8
 AQUEOUS PHASE RELATIVE PERMS
 $N_{CAP} = 10^{-3}$

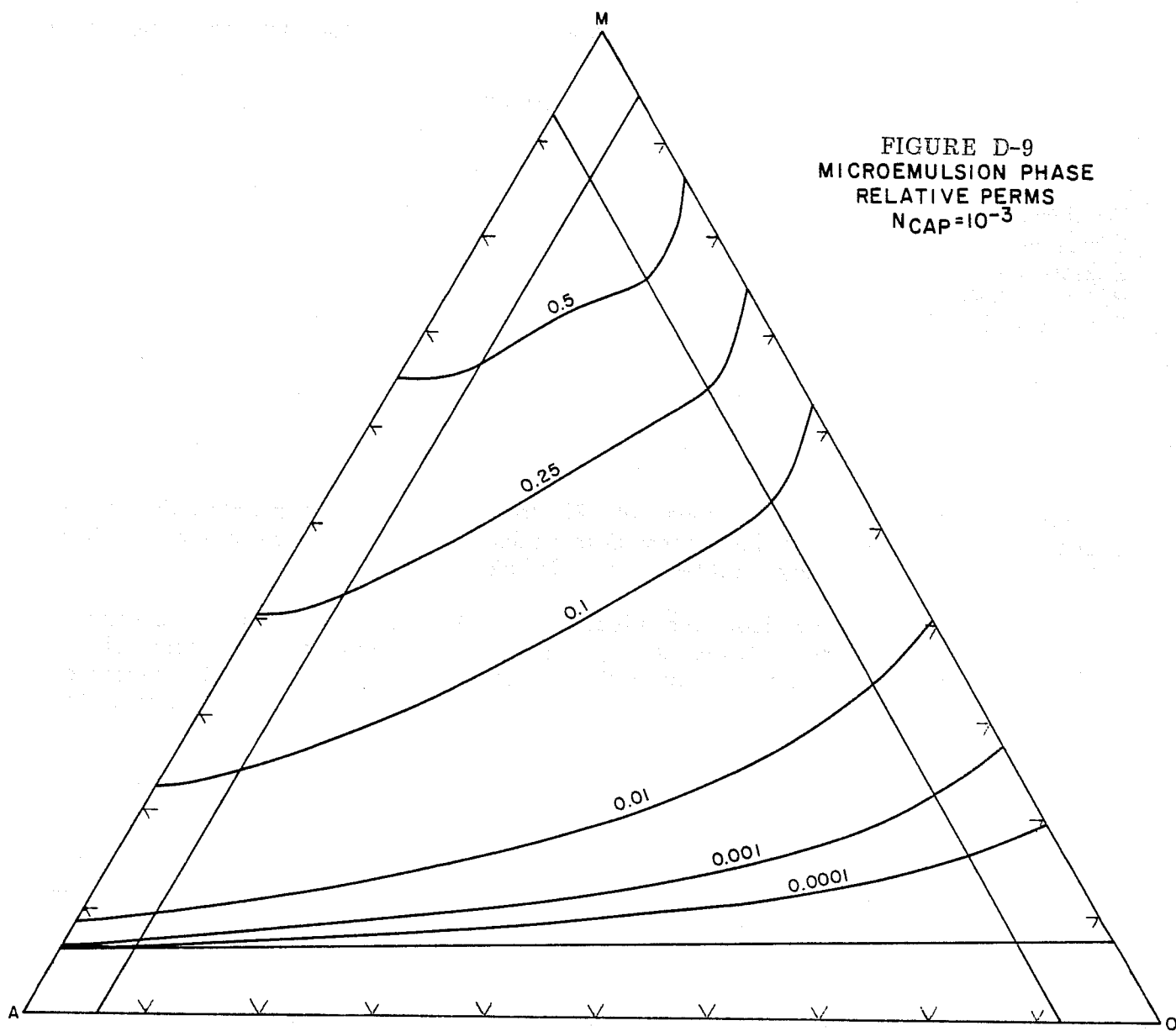


FIGURE D-9
MICROEMULSION PHASE
RELATIVE PERMS
 $N_{CAP}=10^{-3}$

APPENDIX E
CORRESPONDENCE PERTAINING TO
REQUESTS FOR DATA



1201 Dairy Ashford, Suite 200, Houston, Texas 77079, (713) 497-8400 / Cable: INTERCOMP HOUSTON • Telex: 774122

August 1, 1979

Dr. Juris Vairogs
Cities Service Oil Company
Exploration & Production Research Laboratory
P. O. Box 50408
Tulsa, OK 74150

Re: Request for Process Data
El Dorado Numerical Simulation Project

Dear Jerry:

As we discussed over the phone July 27, this letter sets out in detail the status, availability and requests for the process data necessary for simulation of the micellar-polymer flood in the Chesney (No.) lease at El Dorado.

Adequate data are available for injection compositions and volumes of preflush I and II and micellar and polymer slugs, velocity dispersion, relative permeability (capillary number dependence and three-phase relative permeability can be generated from the rock curves), surfactant retention on reservoir rock, cation exchange and polymer buffer viscosity.

There are virtually no data on oil-water-surfactant phase behavior or compositional dependent phase viscosity, both of which are key to the process description.

Core flood and interfacial tension data need supplemental information to be useful. Additional information of interest not found in my review are polymer adsorption on reservoir rock and inaccessible pore volume to polymer.

Specifically, I need the following data:

I. Phase Behavior

What is needed is oil-brine-surfactant equilibrium as a function of salinity (as shown in the attached Figure 1). Ternary diagrams of the type shown in Figure 1 can be generated from rectangular diagrams of the type shown in Figure 2. There are likely many such Figure 2 curves available for El Dorado, inasmuch as Shell developed this means to determine phase behavior. I would like to have a suite of the Figure 2 curves for various surfactant concentrations and oil/brine ratios. This data should of course be for the modified Shell system that was injected at El Dorado.

2. Phase Viscosity

I will also need the viscosity of the flowing phases (oleic-aqueous or oleic-microemulsion-aqueous, depending on salinity) as a function of surfactant, polymer (some polymer was added to the micellar slug) and salt concentration. The viscosity data should span the range of concentrations from the injected values down to a point of dilution where viscosity is independent of composition (essentially pure oil and brine).

3. Core Floods

Figure A-1 (p. 11-4) of the 2nd Annual El Dorado Report gives a curve of oil recovery vs. PV micellar slug in 10" Admire cores. I need the composition of the micellar slug as well as the composition and volumes of the preflush and polymer banks. It was also reported at that time (p. 1-4, 2nd Annual) that a displacement test using the revised Shell design in 1" cores stacked to 40" in length was in progress. If the 40" test was completed it would be preferable for history matching as 10" cores are often affected by capillary end effects and less than fully developed mixing zones. Additional 10" core floods are reported in the 3rd Annual Report and in BETC-79/2 Progress Review No. 17.

4. Interfacial Tension

An IFT map is given in Table A4 (p. 11-5) of the 3rd Annual Report. A copy of that table is attached. I found what appears to be two errors in the table. I calculated the wt. ratio $\text{Na}^+/\text{Ca}^{++}$ as 4.60 rather than the 4.00 value given. Also, it appears that the 0.0078 entry for IFT should be 0.078. I would appreciate your checking these figures.

The major problem with this table, however, is that one does not know which phases the tensions are between: oleic-aqueous, oleic-microemulsion or microemulsion-aqueous. Having the phase behavior discussed in 1) above will help to clarify this point.

Am I correct in assuming the brine/oil volume ratio is constant for all entries in the table? If so, at the very least I need to know the value of the ratio. If there is a functional dependence on brine/oil ratio in this table or if such dependence is available elsewhere, I would like to obtain it. I also need the value of IFT of pure oil against surfactant-free brine.

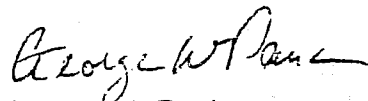
5. Polymer Data

Polymer adsorption (for Abbot biopolymer) on reservoir rock and the inaccessible pore volume to polymer can be obtained from core floods in which polymer concentration was measured in the effluent. Any such data will be needed to accurately characterize the mobility control aspects of the process.

INTERCOMP believes that the El Dorado Micellar-Polymer Project is an important step in EOR technology. For this reason, INTERCOMP wishes to provide an accurate and complete simulation of the process. Therefore, if any data requested is of a confidential nature, INTERCOMP believes it appropriate to request the release of such data from Shell Development Company, and other vendors. INTERCOMP is willing to assist in any way that it can in data solicitation.

If you have any questions regarding the details of my requests, please call me.

Sincerely,

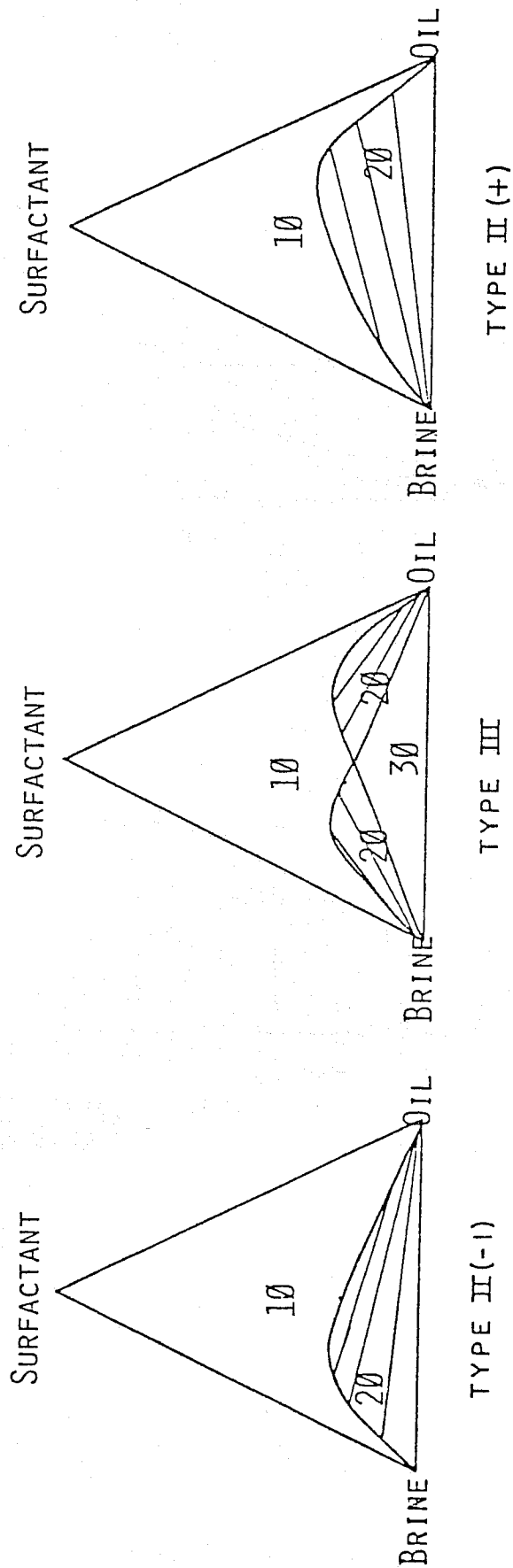


George W. Paul

GWP:vam
Attachments

cc: Mr. R. A. Maier, GURC
Mr. W. D. Howell, DOE

MICELLAR FLOODING TERNARY EQUILIBRIUM



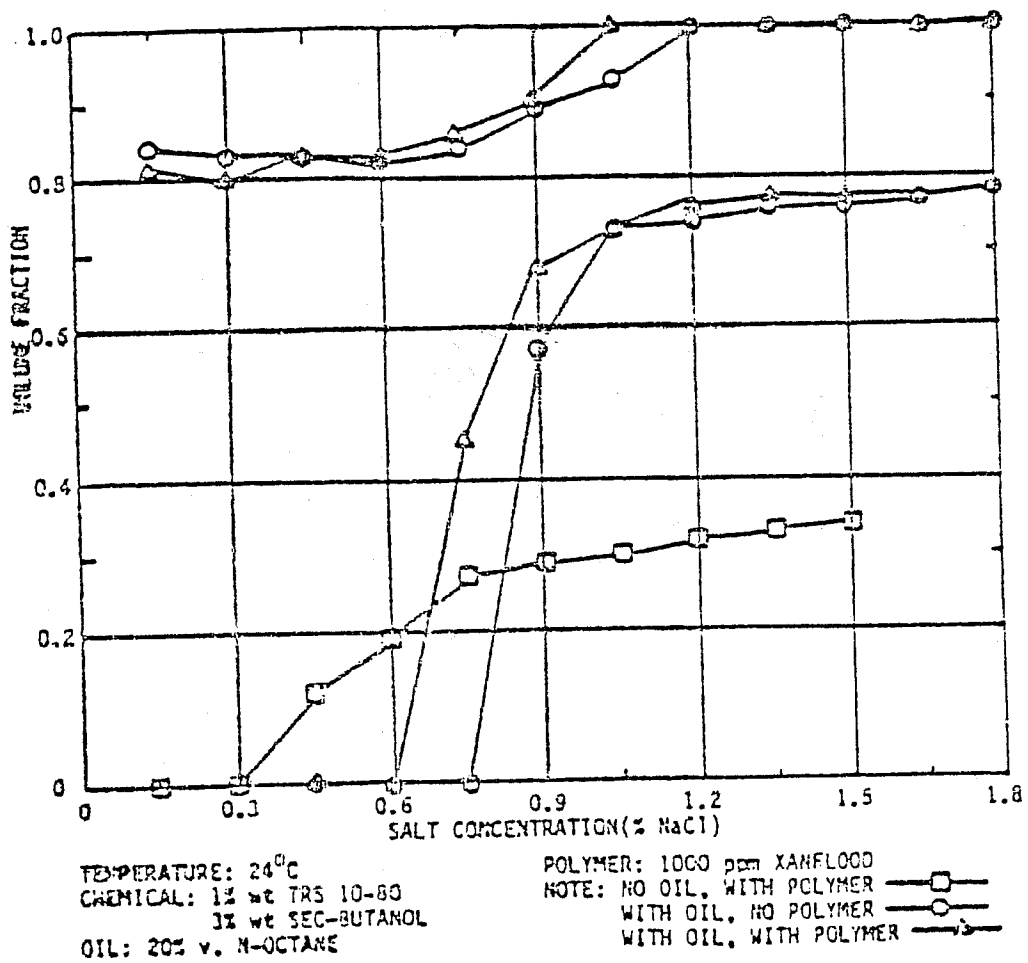


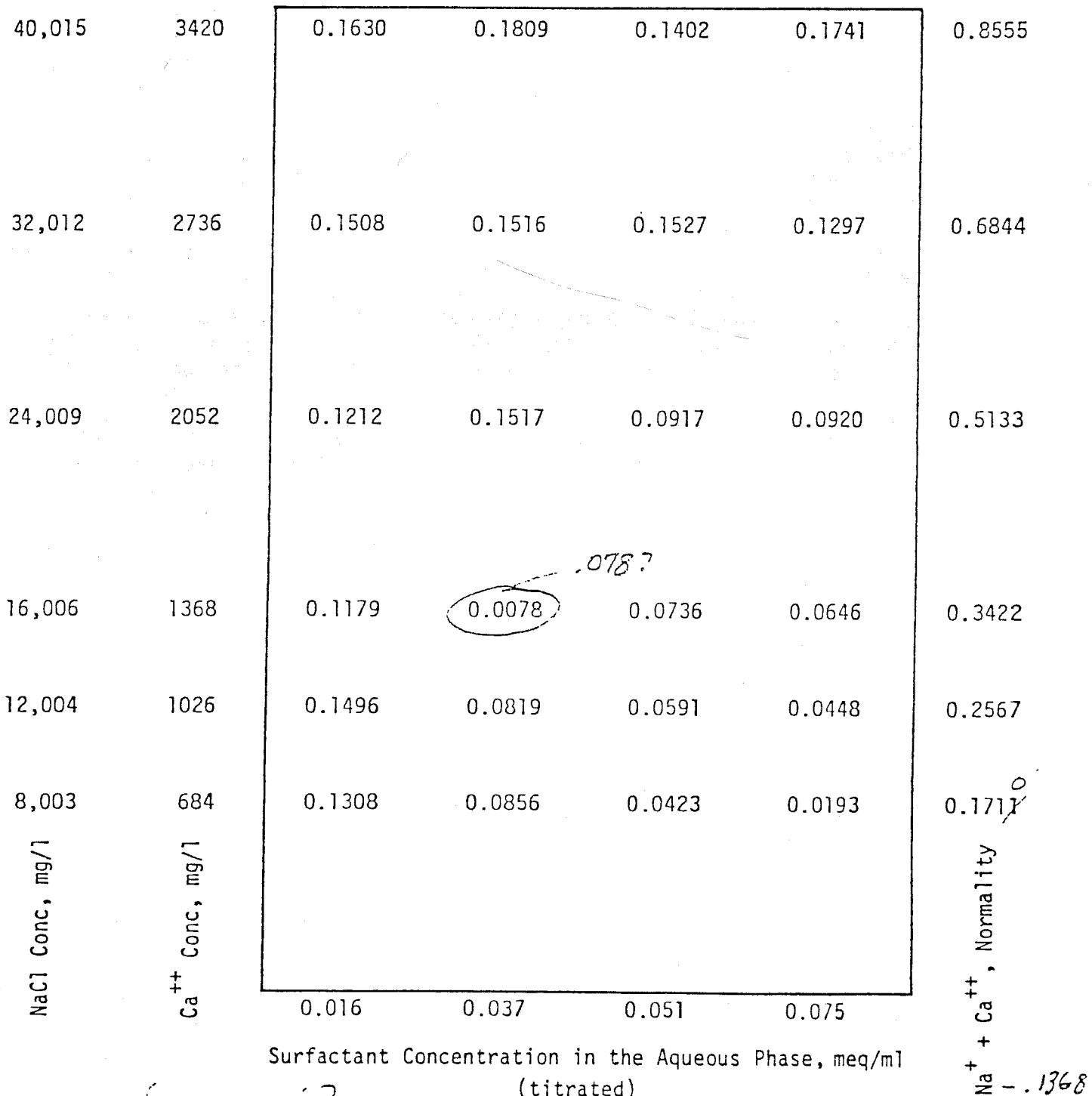
FIGURE 46. TRS 10-80 BEHAVIOR AT 24°C

TABLE A4

INTERFACIAL TENSION MAP FOR MODIFIED MICELLAR SYSTEM DESIGNED FOR THE NORTH PATTERN

Mg⁺⁺ = 0 mg/l (Na⁺)/(Ca⁺⁺) = ~~4.00~~^{4.60} T ≈ 77° F
 4.60 wt/wt

IFT values in dynes/cm Oil phase = Chesney crude oil



phase region?
 w/o int.?

11-5
 227

1N - 12g Ca⁺⁺ = 20g/l ; 1M Ca⁺⁺ = 40g/l
 1N - 12g Na⁺ = 23g/l ; 1M Na⁺ = 23g/l
 1N - 1M NaCl = 23.35g/l = 23.5g/l

Na⁺ + Ca⁺⁺, Normality
 - .1368

RECEIVED
SEP 17 1979



CITIES SERVICE COMPANY
ENERGY RESOURCES GROUP

Exploration & Production Research
Box 50408, Tulsa, Oklahoma 74150
(918) 586-2587

September 13, 1979

Dr. George W. Paul
Intercomp Resource Development
and Engineering, Inc.
1201 Dairy Ashford, Suite 200
Houston, TX 77079

Dear George:

The attached memo from Dr. Kellerhals addresses the five questions raised by you in your August 1, 1979, letter to me. I believe he has answered the questions as well as he can, although his answers may not be what you expected. In particular, we will not have any phase behavior data available for release until later this year. Perhaps Shell can help you in this regard.

Please call me if you want to discuss Dr. Kellerhals' memo or raise additional questions.

Sincerely,

A handwritten signature in cursive script, appearing to read "J. Vairogs".

J. Vairogs
Reservoir Performance Manager

vrn

cc: W. H. Howell
R. A. Maier
G. E. Kellerhals
V. W. Rhoades



INTEROFFICE LETTER

September 11, 1979

TO: Dr. J. Vairogs
FROM: G. E. Kellerhals *GJK*
SUBJECT: Responses to Questions in the Letter to
J. Vairogs (dated August 1, 1979) from
George W. Paul (Intercomp)

1) Phase Behavior

Shell has some data of this type for either the original design or the modified designs. However, any of these data developed by Shell are confidential, and we may not release them. Therefore, Intercomp (or GURC) should contact Shell directly for this information. We have recently been obtaining data of this type. When our work is sufficiently complete to report internally, we shall also report it to the Department of Energy. Using this normal report method, our data will be available in the regular government project reports (monthly and/or annual technical reports).

2) Phase Viscosity

We do not know with certainty the viscosities of the flowing phases as a function of surfactant, polymer, and salt concentration. The viscosity of the surfactant slug (contains polymer) is about 2-4 centipoise (at a shear rate of 7.3 sec^{-1}) higher than the same solution without surfactant. At 7.3 sec^{-1} shear rate the injected surfactant slug had a typical (design) viscosity of 32 centipoise. As the slug is diluted its viscosity declines in such a manner that the curve is parallel to (and slightly higher) a typical or normal concentration versus viscosity curve for biopolymer (Xanthan gum) solution.

Viscosity of Abbott biopolymer solution as a function of concentration and shear rate is given in Table A-6 of the Third Annual Report.

3) Core Floods

The composition of the surfactant slugs and volumes of preflush and polymer banks for the tests reported in Figure A-1 (p. 11-4) of the Second Annual El Dorado Report are available and can be transmitted to you except for the surfactant slug composition which has not been cleared. However, the data of Figure A-1 is for the original chemical formulation using the modified design (lower concentration of surfactant and polymer).

The composition of the surfactant slug injected into the reservoir is given in the Third Annual Report (Table II, p. 1-12). Oil recovery performance using this system is a 10" El Dorado core stack is given in the Third Annual Report (Table A-5, p. 11-6). Data for oil recovery versus surfactant slug size for the surfactant system injected was not obtained but it is felt that such results would be similar to the results in Figure A-1 (p. 11-4) of the Second Annual Report.

The compositions of the Chesney produced brine and El Dorado raw (lake) water used in the test reported in Table A-5 are:

Composition of Synthetic El Dorado Produced Brine

75.973 g	NaCl
9.161 g	CaCl ₂ ·2H ₂ O
16.256 g	MgCl ₂ ·6H ₂ O

diluted to one liter of solution using deionized or distilled water.

Composition of Synthetic El Dorado Lake Water

0.063 g	NaCl
0.109 g	CaCl ₂ ·2H ₂ O
0.043 g	MgCl ₂ ·6H ₂ O

diluted to one liter of solution using deionized or distilled water.

Experimental difficulties prevented the test in stacked cores (length of 40 inches) to be completed properly and the results were judged to probably not be truly representative.

4) Interfacial Tension

The ratio of equivalents of sodium ion to equivalents of calcium ion for the IFT map is four. The ratio of equivalents is what the ratio represents. The weight ratio of sodium to calcium is 4.6.

All of the IFT's in Table A-4 (Third Annual Report) are between an oleic (Chesney crude oil) phase and an aqueous phase with the salinity indicated by the IFT map. The salinity given by the IFT map represents added salts (NaCl and CaCl₂) and does not include the minor quantities of salts that are present in the commercial surfactants. Furthermore, the surfactant concentrations and salinity given by the map are for the aqueous phase before equilibration with Chesney crude oil.

The ratio of oil and aqueous phase volumes for all of the IFT measurements was one (equal volumes of oil and aqueous phase).

The IFT of Chesney crude oil against Chesney produced brine is approximately 30 dyne/cm.

The 0.0078 entry of Table A-4 was recently measured and the corrected value is 0.1016 dyne/cm.

5) Polymer Data

Neither polymer loss (Abbott biopolymer) data for polymer alone nor for polymer flowing behind the surfactant slug was obtained using El Dorado rock (Admire sandstone). That is, during laboratory flow tests the concentration of polymer in the produced effluent was not measured. Likewise, the inaccessible pore volume to polymer was not determined.

db

cc: H. L. Chang
V. W. Rhoades
G. W. Rosenwald



RECEIVED

NOV 5 1979

Department of Energy
Bartlesville Energy Technology Center
P.O. Box 1398
Bartlesville, Oklahoma 74003

November 2, 1979

Mr. Bob Maier
Gulf Universities Research Consortium
5909 West Loop South
Suite 600
Bellaire, TX 77401

Dear Bob:

Enclosed are the data tables, graphs, and narrative describing the phase volume behavior for the modified Shell system used in the Cities Service north pattern. According to Intercomp, this information is essential to the simulation evaluation task in progress.

As noted, copies have been sent to Walter Dowdle, Intercomp, who will get them to George Paul. This information will appear in the Cities Service September monthly report of progress, but this early release should keep the Intercomp effort from being delayed.

If any questions arise, I am sure that Dr. Chang, Cities Service, would be glad to discuss them with you or George.

Sincerely,

jsj William D. Howell

William D. Howell
Technical Project Officer

Enclosure:
As stated

cc w/encl:
→ Mr. Walter Dowdle
Intercomp
1201 Dairy Ashford
Houston, TX 77079

TABLE 1

PHASE VOLUME DATA FOR A SURFACTANT CONCENTRATION OF 0.075 MEQ/ML

Surfactant concentration: 0.075 meq/ml (no polymer present)

Oil phase: El Dorado crude oil

Temperature: Room temperature (≈ 72 deg F)

Salinity, weight percent
NaCl in the aqueous phase
before equilibration

Phase, volume fraction
present after equilibration
period of seven days

	<u>lowest phase</u>		<u>highest phase</u>	
0.0	0.42			0.58
0.35	0.39	0.05	0.05	0.51
0.40	0.46	0.02		0.52
0.50	0.51			0.49
0.61	0.39	0.07		0.54
0.75	0.39	0.22		0.39
0.85	0.49	0.02		0.48
1.00	0.41	0.09		0.50
1.10	0.11	0.82		0.07
1.50	0.05	0.91		0.05
2.00	0.24	0.42		0.34
2.10	0.23	0.48		0.29
2.20	0.27	0.54		0.19
2.30	0.29	0.70		0.01
2.40	0.32			0.68
2.50	0.33			0.67
2.80	0.38			0.62
3.30	0.41			0.59
3.70	0.36	0.05		0.59
4.00	0.41			0.59
4.50	0.46			0.54
5.00	0.51			0.49

TABLE 2

PHASE VOLUME DATA FOR A SURFACTANT CONCENTRATION OF 0.0375 MEQ/ML

Surfactant concentration: 0.0375 meq/ml (no polymer present)

Oil phase: El Dorado crude oil

Temperature: Room temperature (≈ 72 deg F)

Salinity, weight percent
NaCl in the aqueous phase
before equilibration

Phase, volume fraction
present after equilibration
period of seven days

	<u>lowest phase in vial</u>		<u>highest phase in vial</u>
1.0	0.53		0.47
1.1	0.53		0.47
1.2	0.53		0.47
1.4	0.56		0.44
1.5	0.58		0.42
1.6	0.59		0.41
1.7	0.67		0.33
1.8	0.08	0.61	0.31
1.9	0.29		0.71
2.0	0.26	0.20	0.54
2.3	0.08	0.45	0.47

TABLE 3

PHASE VOLUME DATA FOR A SURFACTANT CONCENTRATION OF 0.01875 MEQ/ML

Surfactant concentration: 0.01875 meq/ml (no polymer present)

Oil phase: El Dorado crude oil

Temperature: Room temperature (≈ 72 deg F)

Salinity, weight percent
NaCl in the aqueous phase
before equilibration

Phase, volume fraction
present after equilibration
period of seven days

	<u>lowest phase in vial</u>	<u>highest phase in vial</u>
0.90	0.50	0.50
0.95	0.50	0.50
1.00	0.50	0.50
1.05	0.50	0.50
1.10	0.50	0.50
1.15	0.50	0.50
1.20	0.50	0.50
1.25	0.50	0.50
1.30	0.50	0.50
1.40	0.50	0.50

TABLE 4

PHASE VOLUME DATA FOR A SURFACTANT CONCENTRATION OF
0.075 MEQ/ML AND 900 PPM POLYMER

Surfactant concentration: 0.075 meq/ml (900 ppm polymer present, no Ca^{++} added)

Oil phase: El Dorado crude oil

Temperature: Room temperature (\approx 72 deg F)

Salinity, weight percent
NaCl in the aqueous phase
before equilibration

Phase, volume fraction
present after equilibration
period of seven days

	<u>lowest phase in vial</u>		<u>highest phase in vial</u>	
	0.00	0.33		
0.35	0.15			0.85
0.40	0.41	0.24		0.35
0.50	0.32	0.05	0.36	0.27
0.61	0.45	0.14		0.41
0.75	0.39	0.35		0.26
0.85	0.36	0.21		0.43
1.00	0.13	0.35		0.52
1.10	0.07			0.93
1.50	0.02	0.05	0.88	0.05
2.00	0.24	0.42		0.34
2.50	0.35			0.65
2.80	0.39			0.61
3.30	0.41			0.59
3.70	0.42			0.58
4.00	0.42			0.58
4.50	0.44			0.56
5.00	0.44			0.56

TABLE 5

PHASE VOLUME DATA FOR A SURFACTANT CONCENTRATION OF
0.075 MEQ/ML, 900 PPM POLYMER, AND Ca^{++}

Surfactant concentration: 0.075 meq/ml (900 ppm polymer present, $Na^+/Ca^{++} = 4.0$
- four equivalents of Na^+ per equivalent of Ca^{++} .)

Oil phase: El Dorado crude oil

Temperature: Room temperature (≈ 72 deg F)

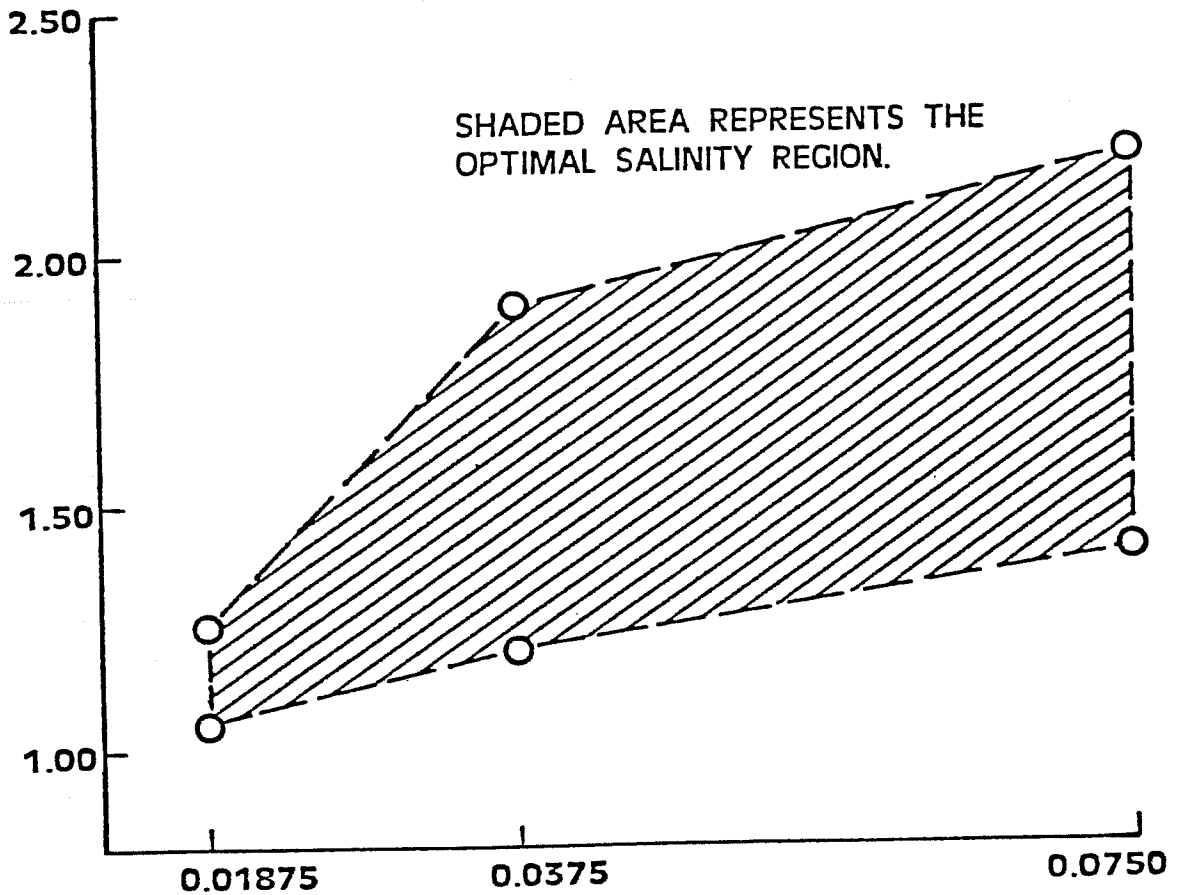
<u>Salinity</u>		<u>Phase, volume fraction present after equilibration period of seven days</u>			
<u>Weight percent NaCl in the aqueous phase before equilibration</u>	<u>ppm Ca^{++} in the aqueous phase before equilibration</u>	<u>lowest phase in vial</u>		<u>highest phase in vial</u>	
0.0	0.0	0.45			0.55
0.06	49	0.27			0.73
0.12	101	0.31			0.69
0.18	149	0.36			0.64
0.24	201	0.31			0.69
0.29	249	0.39	0.38		0.23
0.35	298	0.54	0.05		0.41
0.41	348	0.51	0.04		0.46
0.47	400	0.09	0.41		0.50
0.53	449	0.07	0.47		0.46
0.59	500	0.07	0.39	0.12	0.42
0.88	747	0.33			0.67
1.16	994	0.40			0.60
1.75	1499	0.42			0.58
2.30	1999	0.35	0.12		0.53
3.50	2993	0.29	0.15		0.55
4.67	3999	0.36	0.11		0.53
5.84	4997	0.46			0.54

FIGURE 1

CHESNEY PATTERN SURFACTANT SYSTEM
NO POLYMER PRESENT
NO Ca^{++} ADDED

EQUAL VOLUMES OF CRUDE OIL AND BRINE

SALINITY, WEIGHT PERCENT NaCl IN THE AQUEOUS
PHASE BEFORE EQUILIBRATION



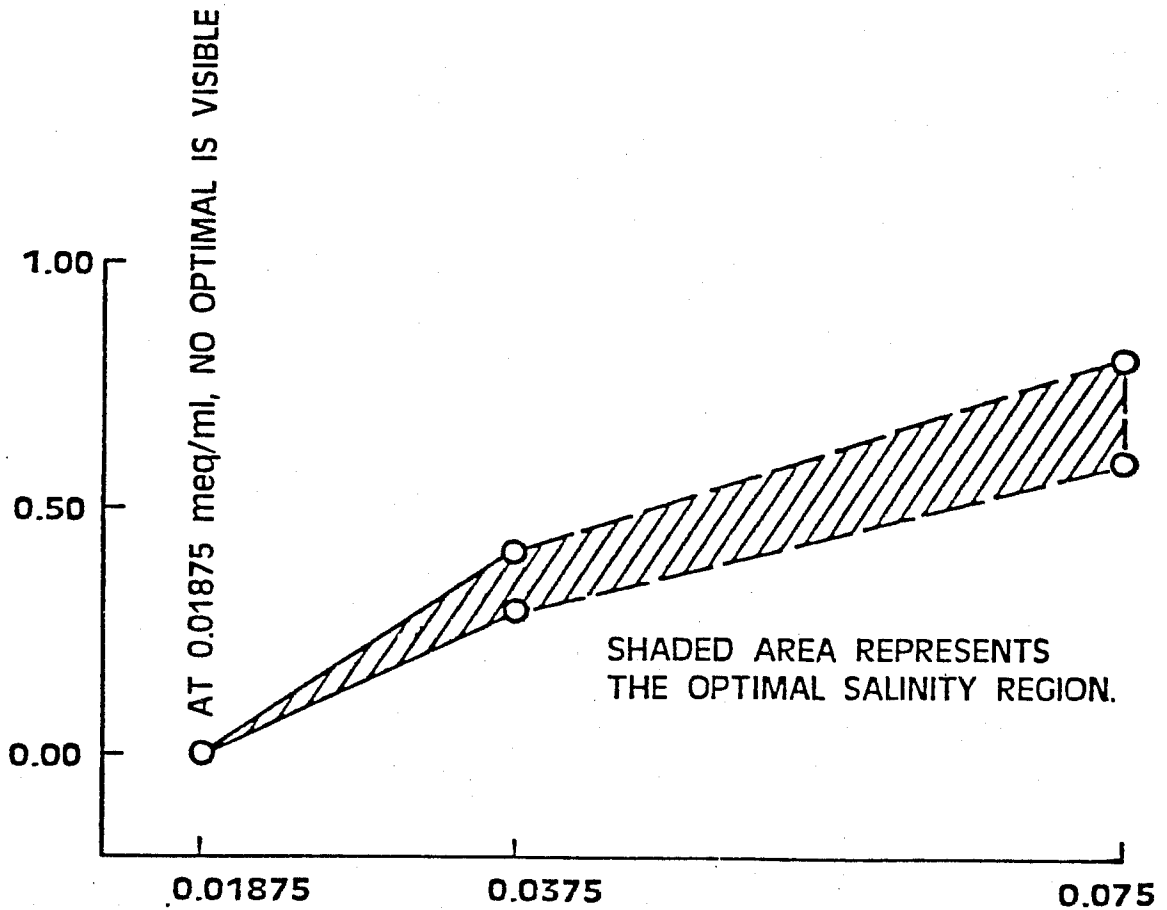
SURFACTANT CONCENTRATION (meq/ml) IN THE
AQUEOUS PHASE BEFORE EQUILIBRATION

FIGURE 2

CHESNEY PATTERN SURFACTANT SYSTEM
NO POLYMER PRESENT $\text{Na}^+/\text{Ca}^{++} = 4.0$

EQUAL VOLUMES OF CRUDE OIL AND BRINE

SALINITY, WEIGHT PERCENT NaCl IN THE AQUEOUS
PHASE BEFORE EQUILIBRATION



SURFACTANT CONCENTRATION (meq/ml) IN THE
AQUEOUS PHASE BEFORE EQUILIBRATION



INTEROFFICE LETTER

October 30, 1979

TO: Mr. R. J. Miller
FROM: G. W. Rosenwald
SUBJECT: El Dorado Micellar-Polymer Project Report,
Summary of Research Activities for September, 1979*

Phase Behavior of North (Chesney) Pattern Surfactant Slug

Phase volume diagrams have been obtained for the north pattern surfactant system for three surfactant concentrations--0.075 meq/ml, 0.0375 meq/ml, and 0.01875 meq/ml. Work was done with and without biopolymer in the surfactant system. Salts used to show the effects of salinity on phase behavior were NaCl and CaCl₂. Equal volumes of El Dorado (Chesney) crude oil and surfactant solution were used in the work.

Assuming the importance of phase behavior in surfactant flooding (published work indicates that this is definitely true), these results indicate the importance of being able to accurately select (predict) the salinity environment throughout the course of the surfactant flood (pre-flush, micellar slug, and polymer drive). In this way, phase behavior results should be useful in predicting (or explaining) laboratory core flood results. Prediction of the salinity environment allows prediction/selection of the optimum phase behavior.

Case I. Phase Behavior; No Polymer Present, No Ca⁺⁺ Added.

The raw phase volume data for this set of conditions are given in Tables 1, 2, and 3. It is evident from the data in these tables that the phase behavior using crude oil is more complex than the "textbook-type" diagrams usually obtained when a pure oil is used. At a surfactant concentration of 0.01875 meq/ml, the phase volume fractions were 0.50 for the range of NaCl concentrations used. The "optimal salinity" (at a surfactant concentration of 0.01875 meq/ml) was from 1.05 to 1.25 percent NaCl. Similar analyses for surfactant concentrations of 0.075 meq/ml and 0.0375 meq/ml resulted in "optimal salinities" of 1.4 to 2.2 percent NaCl and 1.2 to 1.9 percent NaCl, respectively. These salinities refer to the salinity in the aqueous phase before equilibration with crude oil. The data for these surfactant concentrations are summarized in Figure 1.

Case II. Phase Behavior; No Polymer Present, Ca⁺⁺ Present.

To determine the effects of divalent ion on the phase behavior of the surfactant system, a NaCl/CaCl₂ salt mixture was added to the surfactant system. The ratio of equivalents of Ca⁺⁺ was constant and equal to 4.0. Raw data analogous to that in Tables 1, 2, and 3 were obtained at three surfactant concentrations. The results are summarized in Figure 2 where salinity is plotted versus surfactant concentration.

The optimal salinity without adding Ca⁺⁺ is about 0.376 meq/ml, whereas the optimal salinity in the presence of Ca⁺⁺ occurs at a total salinity of about 0.149 meq/ml.

Case III. Phase Behavior; 900 ppm Polymer Present, No Ca⁺⁺ Added.

For these conditions, only one set of vials using a surfactant concentration of 0.075 meq/ml was prepared (see Table 4). The polymer did not appear to alter the optimal salinity appreciably if at all. The optimal salinity in the presence of the polymer was 2.1 to 2.2 weight percent NaCl. However, at a salinity of 1.5 weight percent NaCl, a gel-like lower phase (about 3 percent of the total volume) was present. This phase was not analyzed but is thought to consist mainly of polymer.

Case IV. Phase Behavior; 900 Polymer Present, Ca⁺⁺ Present.

Under these conditions, phase behavior was only investigated for one surfactant concentration, 0.075 meq/ml (see Table 5). With Ca⁺⁺ present, a gel-like lower phase (7 to 9 volume percent of the total) formed at NaCl concentrations from 0.47 weight percent to 0.59 weight percent (Ca⁺⁺ concentrations of 400 to 500 ppm). Again this gel-like phase is thought to consist predominantly of biopolymer. The presence of Ca⁺⁺ (400 to 500 ppm) appears to reduce the salinity at which the gel-like phase appears.

